# BIBLIOGRAPHY

## CHAPTER 1


[1] J. M. Lehn, J. L. Atwood, J. E. D. Davies, D. D. Mac Nicol and F. Vögtle, Eds., Pergamon, Comprehensive Supramolecular Chemistry, Oxford, (**1996**).

[2] E. Fisher, *Ber. Deutch. Chem.* 2, (**1893**), 267.

[3] C. J. Pedersen, Cyclic polyethers and their complexes with metal salts. *J. Am. Chem. Soc.,* 89(26), (**1967**), 7017–7036.

[4] D. J. Cram, Preorganization–from solvents to spherands. *Angew. Chem., Int. Ed. Engl.* 25(12), (**1986**), 1039-1157.

[5] S. Gould and R. C. Scott, 2-Hydroxypropyl-β-cyclodextrin (HP-β-CD): A toxicology review, Food and Chemical Toxicology, 43(10), (**2005**), 1451–1459.

[6] W. Blokzijl and J. B. F. N. Engberts, Hydrophobic effects. Opinions and facts, Angew. Chem. Int. Ed. Engl. 32(11), (**1993**), 1545–1579.

[7] C. B. Aakeröy and K. R. Seddon, The hydrogen bond and crystal engineering, Chem. Soc. Rev. *Chem. Soc. Rev.*, 22, (**1993**), 397-407.

[8] P. Metrangolo and G. Resnati, Halogen bonding: a paradigm in supramolecular chemistry, *Chem. Eur. J.* 7(12), (**2001**), 2511-2519.

[9] R. N. Dsouza, U. Pischel, and W. M. Nau, Fluorescent Dyes and Their Supramolecular Host/Guest Complexes with Macrocycles in Aqueous Solution, *Chem. Rev.* 111, (**2011**), 7941–7980.

[10] D. S. Guo and Y. Liu, Supramolecular Chemistry of p-Sulfonatocalix[n]arenes and Its Biological Applications, *Acc. Chem. Res.* 47, (**2014**), 1925–1934.

[11] X. Song, Y. Wen, J. L. Zhu, F. Zhao, Z. X. Zhang and J. Li, Thermoresponsive Delivery of Paclitaxel by β-Cyclodextrin-Based Poly(N-isopropylacrylamide) Star Polymer via Inclusion Complexation, *Biomacromolecules,* 17, (**2016**), 3957–3963.

[12] A. A. Bagabas, M. Frasconi, J. Iehl, B. Hauser, O. K. Farha, J. T. Hupp, K. J. Hartlieb, Y. Y. Botros and J. F. Stoddart, γ-Cyclodextrin Cuprate Sandwich-Type Complexes, *Inorg. Chem.* 52(6), (**2013**), 2854–2861.

[13] D. V. Talapin and E, V. Shevchenko, Introduction: Nanoparticle Chemistry, Chem. Rev. 116, (**2016**), 10343–10345.

[14] G. Chen, I. Roy, C. Yang, and P. N. Prasad, Nanochemistry and Nanomedicine for Nanoparticle-based Diagnostics and Therapy, *Chem. Rev.* 116(5), (**2016**), 2826–2885.

[15] Guanying Chen, Jangwon Seo, Chunhui Yang and Paras N. Prasad, Nanochemistry and nanomaterials for photovoltaics, *Chem. Soc. Rev.*, 42, (**2013**), 8304-8338.

[16] Z. Liu, W. Jiang, J. Nam, J. J. Moon, and B. Y. S. Kim, Immunomodulating Nanomedicine for Cancer Therapy, *Nano Lett.* 18, (**2018**), 6655–6659.

[17] M. J. Allen, V. C. Tung and R. B. Kaner, Honeycomb carbon: a review of graphene. *Chemical reviews*, *110*(1), (**2010**), 132-145.

[18] S. Kumar, and K. Chatterjee, Comprehensive review on the use of graphene-based substrates for regenerative medicine and biomedical devices. *ACS applied materials & interfaces*, *8*(40), (**2016**), 26431-26457.

[19] A. K. Geim and K. S. Novoselov, The rise of graphene, Nat. Mater. 6, (**2007**) 183–191.

[20] K. S. Novoselov, A. K. Geim, S. V. Morozov, D. Jiang, Y. Zhang, S. V. Dubonos, I. V. Grigorieva and A. A. Firsov, Electric field effect in atomically thin carbon films, Science 306, (**2004**), 666–669.

[21] CNN Wire Staff, Research into Graphene Wins Nobel Prize, October 5, (**2010**). http://www.cnn.com/2010/LIVING/10/05/ sweden.nobel.physics/index.html.

[22] E. M. Del Valle, Cyclodextrins and their uses: a review. *Process biochemistry*, *39*(9), (2004), 1033-1046.

[23] G. Wenz, Cyclodextrins as building blocks for supramolecular structures and functional units. *Angewandte Chemie International Edition in English*, *33*(8), (**1994**), 803-822.

[24] G. Crini, A history of cyclodextrins. *Chemical reviews*, *114*(21), (**2014**), 10940-10975.

[25] M. E. Davis and M. E. Brewster, Cyclodextrin-based pharmaceutics: past, present and future. *Nature reviews Drug discovery*, *3*(12), (**2004**), 1023-1035.

[26] A. V. Baeyer, Ueber die Verbindungen der Aldehyde mit den Phenolen. *Berichte der deutschen chemischen gesellschaft*, *5*(1), (**1872**), 280-282.

[27] C. D. Gutsche and M. Iqbal, p-tert-Butylcalix [4] arene. *Organic Syntheses*, *68*, (**2003**), 234-234.

[28] H. X. Zhao, D. S. Guo, and Y. Liu, Binding Behaviors of p-Sulfonatocalix[4]arene with Gemini Guests, *J. Phys. Chem. B,* 117, (**2013**), 1978–1987.

[29] Z. Liu, S. K. M. Nalluri and J. F. Stoddart, Surveying macrocyclic chemistry: from flexible crown ethers to rigid cyclophanes, Chem. Soc. Rev., 46(9), (**2017**), 2459-2478.

[30] J. S. Bradshaw and R. M. Izatt, Crown ethers: the search for selective ion ligating agents, Acc. Chem. Res., 30(8), (**1997**), 338–345.

[31] G. W. Gokel, W. M. Leevy and M. E. Weber, Crown ethers: sensors for ions and molecular scaffolds for materials and biological models, *Chem. Rev.,* 104, (**2004**), 2723–2750.

[32] W. M. Nau, M., Florea, and K. I. Assaf, Deep inside cucurbiturils: physical properties and volumes of their inner cavity determine the hydrophobic driving force for host–guest complexation. *Israel Journal of Chemistry*, *51*(5-6), (**2011**), 559-577.

[33] F. Biedermann, V. D. Uzunova, O. A. Scherman, W. M. Nau, and A. De Simone, Release of high-energy water as an essential driving force for the high-affinity binding of cucurbit [n] urils. *Journal of the American Chemical Society*, *134*(37), (**2012**), 15318-15323.

[34] D. S. Guo, and Y. Liu, Supramolecular chemistry of p-sulfonatocalix [n] arenes and its biological applications. *Accounts of chemical research*, *47*(7), (**2014**), 1925-1934.

[35] I. Roy, A. Garci, Y. Beldjoudi, R. M. Young, D. J. Pe, M. T. Nguyen, P. J. Das, M. R. Wasielewski, and J. F. Stoddart, Host–Guest Complexation-Mediated Supramolecular Photon Upconversion, *J. Am. Chem. Soc.,* 142, (**2020**), 16600−16609.

[36] I. Roy, S. Bobbala, J. Zhou, M. T. Nguyen, S. K. M. Nalluri, Y. Wu, D. P. Ferris, E. A. Scott, M. R. Wasielewski, and J. F. Stoddart, ExTzBox: a glowing cyclophane for live-cell imaging. *Journal of the American Chemical Society*, *140*(23), (**2018**), 7206-7212.

[37] J. C. Barnes, M. Jurícek, N. L. Strutt, M. Frasconi, S. Sampath, M. A. Giesener, P. L. McGrier, C. J. Bruns, C. L. Stern, A. A. Sarjeant and J. F. Stoddart, ExBox: A Polycyclic Aromatic Hydrocarbon Scavenger, *J. Am. Chem. Soc.* 135, (**2013**), 183−192.

[38] J. M. Lehn, Supramolecular chemistry-scope and perspectives molecules, supermolecules, and molecular devices (Nobel Lecture), *Angewandte Chemie International Edition in English*, *27*(1), (**1988**), 89-112.

[39] S. Y. Zhou, S. X. Ma, H. L. Cheng, L. J. Yang, W. Chen, Y. Q. Yin, Y. M. Shi and X. D. Yang, Host–guest interaction between pinocembrin and cyclodextrins: Characterization, solubilization and stability. *Journal of Molecular Structure*, 1058, (**2014**), 181-188.

[40] C. S. Mangolim, C. Moriwaki, A. C. Nogueira, F. Sato, M. L. Baesso, A. M. Neto and G. Matioli, Curcumin–β-cyclodextrin inclusion complex: stability, solubility, characterisation by FT-IR, FT-Raman, X-ray diffraction and photoacoustic spectroscopy, and food application. *Food chemistry*, *153*, (**2014**), 361-370.

[41] N. Roy, P. Bomzan and M. N. Roy, Probing Host-Guest inclusion complexes of Ambroxol Hydrochloride with α-& β-Cyclodextrins by physicochemical contrivance subsequently optimized by molecular modeling simulations. *Chemical Physics Letters*, (**2020**), 137372.

[42] J. Li, M. Zhang, J. Chao, S. Shuang, Preparation and characterization of the inclusion complex of Baicalin (BG) with β-CD and HP-β-CD in solution: an antioxidant ability study. *Spectrochimica Acta Part A: Molecular and Biomolecular Spectroscopy*, *73*(4), (**2009**), 752-756.

[43] N. Qiua, X. Cheng, G. Wang, W. Wang, J. Wen, Y. Zhang, H. Song, L. Ma, Y. Wei, A. Peng and L. Chen, Inclusion complex of barbigerone with hydroxypropyl-β-cyclodextrin: Preparation and in vitro evaluation, *Carbohydrate polymers* 101, (**2014**), 623-630.

[44] W. Chen, L. J. Yang, S. X. Ma, X. D. Yang, B. M. Fan and J. Lin, Crassicauline A/-cyclodextrin host–guest system: Preparation, characterization, inclusion mode, solubilization and stability, *Carbohydrate Polymers*, *84*(4), (**2011**), 1321-1328.

[45] M. V. Rekharsky and Y. Inoue, Complexation thermodynamics of cyclodextrins, Chem. Rev. 98, (**1998**), 1875–1918.

[46] Y. Liu, B. H. Han and Y. T Chen, Inclusion Complexation of Acridine Red Dye by Calixarenesulfonates and Cyclodextrins: Opposite Fluorescent Behavior, *J. Org. Chem.* 65(19), (**2000**), 6227–6230.

[47] A. K. Geim and K. S. Novoselov, The rise of graphene, Nat. Mater. 6, (**2007**), 183–191.

[48] H. C. Lee, W. W. Liu, S. P. Chai, A. R. Mohamed, A. Aziz, C. S. Khe, N. M. Hidayah and U. Hashim, Review of the synthesis, transfer, characterization and growth mechanisms of single and multilayer graphene. *RSC advances*, *7*(26), (**2017**), 15644-15693.

[49] K. Bolotin, K. Sikes and Z. Jiang, Ultrahigh electron mobility in suspended graphen. *Solid state communications*, *146*(9-10), (**2008**), 351-355.

[50] J. Pan, Y. Yang, W. Fang, W. Liu, K. Le, D. Xu, and X. Li, Fluorescent Phthalocyanine–Graphene Conjugate with Enhanced NIR Absorbance for Imaging and Multi-Modality Therapy, *ACS Appl. Nano Mater.* 1, (**2018**), 2785–2795.

[51] W. Hu, C. Peng, W. Luo, M. Lv, X. Li, D. Li, Q. Huang and C. Fan, Graphene-based antibacterial paper. *ACS nano*, *4*(7), (**2010**), 4317-4323.

[52] J. Kuchlyan, N. Kundu, D. Banik, A. Roy, and N. Sarkar, Spectroscopy and Fluorescence Lifetime Imaging Microscopy To Probe the Interaction of Bovine Serum Albumin with Graphene Oxide, *Langmuir,* 31, (**2015**), 13793–13801.

[53] T. Phatthanakittiphong and G. Seo, Characteristic Evaluation of Graphene Oxide for Bisphenol A Adsorption in Aqueous Solution. *Nanomaterials,* 6(7), (**2016**), 128.

[54] D. Bitounis, H. Ali-Boucetta, B. H. Hong, D. H. Min, and K. Kostarelos, Prospects and Challenges of Graphene in Biomedical Applications, Adv. Mater. *Advanced Materials*, *25*(16), (**2013**), 2258-2268.

[55] Y. Zhang, J. W. Liu, X. W. Chen and J. H. Wang, A three-dimensional amylopectin-reduced graphene oxide framework for efficient adsorption and removal of haemoglobin, J. Mater. Chem. B, 3(6), (**2015**), 983-989.

[56] S. A. Hodge, M. K. Bayazit, K. S. Coleman and M. S. P. Shaffer, Unweaving the rainbow: a review of the relationshipbetween single-walled carbon nanotube molecular structures and their chemical reactivity, *Chem. Soc. Rev.,* 41(12), (**2012**) 4409–4429.

[57] S. Hong and S. Myung, Nanotube Electronics: A flexibleapproach to mobility, Nat. Nanotechnol., 2(4), (**2007**) 207–208.

[58] G. J. Brady, A. J. Way, N. S. Safron, H. T. Evensen,P. Gopalan and M. S. Arnold, Quasi-ballistic carbon nanotubearray transistors with current density exceeding Siand GaAs, *Sci. Adv.,* 2(9), (**2016**) 1601240.

[59] D. Janas, A. P. Herman, S. Boncel and K. K. K. Koziol,Iodine monochloride as a powerful enhancer of electricalconductivity of carbon nanotube wires, Carbon, 73, (**2014**) 225–233.

[60] L. Yu, C. Shearer and J. Shapter, Recent Development of Carbon Nanotube Transparent Conductive Films, Chem.Rev., 116(22), (**2016**) 13413–13453.

[61] J. Yadav, Fullerene: properties, synthesis and application. Research and Reviews: Journal of Physics. 6 (3), (**2018**), 1-6.

[62] K. Ala'a, Isolation, separation and characterization of the fullerenes C60 and C70: The third form of carbon. *Journal of the Chemical Society, Chemical Communications*, 20, (**1990**), 1423-1425.

[63] E. Castro, A. H. Garcia, G. Zavala, and L. Echegoyen, "Fullerenes in biology and medicine." *Journal of Materials Chemistry, 5*(32), (**2017**), 6523-6535.

[64] S. Lijima, Helical Microtubules of Graphitic Carbon. Nature, 354(568), (**1991**), 56-58.

[65] S. Kumar, R. Rani, N. Dilbaghi, K. Tankeshwar and K. H. Kim, Carbon nanotubes: a novel material for multifaceted applications in human healthcare, *Chem. Soc. Rev.,* 46(1), (**2017**), 158–196.

[66] S. Iijima, Helical microtubules of graphitic carbon, *Nature,* 354 (6348) (**1991**), 56-5

[67] R. Andrews, D. Jacques, D. Qian, and T. Rantell, Multiwall Carbon Nanotubes: Synthesis and Application, *Acc. Chem. Res.* 35(12), (**2002**), 1008–1017

[68] D. Tasis, N. Tagmatarchis, A. Bianco and M. Prato, Chemistry of carbon nanotubes, *Chem. Rev.* 106(3), (**2006**), 1105–1136.

[69] S. Chaudhuri, M. Verderame, T. L. Mako, Y. M. Nuwan D. Y. Bandara, A. I. Fernando, and M. Levine, Synthetic-Cyclodextrin Dimers for Squaraine Binding: Effect of Host Architecture on Photophysical Properties, Aggregate Formation and Chemical Reactivity, *Eur. J. Org. Chem.* (**2018**), 1964–1974.

[70] L. Hua, H. Zhang, W. Song, D. Gu and Q. Hu, Investigation of inclusion complex of cilnidipine with hydroxypropyl-β-cyclodextrin, *Carbohydrate Polymers,* 90 (**2012**) 1719–1724.

[71] Z. Huang, S. Tian, X. Ge, J. Zhang, S. Li, M. Li, J. Cheng and H. Zheng, Complexation of chlorpropham with hydroxypropyl-β-cyclodextrin and its application in potato sprout inhibition, *Carbohydrate Polymers,* 107 (**2014**) 241–246.

[72] Y. Wei, J. Zhang, Yan Zhou Weiya Bei Yuan Li Qipeng Yuan Hao Liang, Characterization of Glabridin/hydroxypropyl-β-cyclodextrin Inclusion Complex with Robust Solubility and Enhanced Bioactivity, *Carbohydrate polymers*, *159*, (**2017**), 152-160.

[73] Y. Li, Y. Dong, X. Miao, Y. Ren, B. Zhang, P. Wang, Y. Yu, B. Li, L. Isaacs and L. Cao, Shape-Controllable and Fluorescent Supramolecular Organic Frameworks Through Aqueous Host–Guest Complexation, *Angewandte Chemie*, *130*(3), (**2018**), 737-741.

[74] G. Floresta, C. Talotta, C. Gaeta, M. D. Rosa, U. Chiacchio, P. Neri, and A. Rescifina, γ-Cyclodextrin as a Catalyst for the Synthesis of 2-Methyl-3,5-diarylisoxazolidines in Water, *J. Org. Chem.* 82,(9), (**2017**), 4631–4639.

[75] P. Farras, H. Waller, and A. C. Benniston, Enhanced Photostability of a Ruthenium(II) Polypyridyl Complex under Highly Oxidizing Aqueous Conditions by Its Partial Inclusion into a Cyclodextrin, *Chemistry–A European Journal*, *22*(3), (**2016**), 1133-1140.

[76] I. Roy, S. Bobbala, R. M. Young, Y. Beldjoudi, M. T. Nguyen, M. M. Cetin, J. A. Cooper, S. Allen, O. Anamimoghadam, E. A. Scott, M. R. Wasielewski, and J. F. Stoddart, A Supramolecular Approach for Modulated Photoprotection, Lysosomal Delivery, and Photodynamic Activity of a Photosensitizer, *J. Am. Chem. Soc.* 141, (**2019**), 12296−12304.

[77] J. Jing, A. Szarpak-Jankowska, R. Guillot, I. P. Paintrand, C. Picart, and R. Auzely-Velty, Cyclodextrin/Paclitaxel Complex in Biodegradable Capsules for Breast Cancer Treatment, *Chemistry of Materials*, 25(19), (**2013**), 3867-3873.

[78] P. Farras, H. Waller, and Andrew C. Benniston, Enhanced Photostability of a Ruthenium(II) Polypyridyl Complex under Highly Oxidizing Aqueous Conditions by Its Partial Inclusion into a Cyclodextrin, *Chem. Eur. J.* 22, (**2016**), 1133–1140.

[79] M. Nurunnabi, Z. Khatun, G. R. Reeck, D. Y. Lee and Y. K. Lee, Photoluminescent Graphene Nanoparticles for Cancer Phototherapy and Imaging, *ACS Appl. Mater. Interfaces*, 6, (**2014**), 12413−12421.

[80] G. Nafie, G. Vitale, L. C. Ortega, and N. N. Nassar, Nanopyroxene Grafting with β-Cyclodextrin Monomer for Wastewater Applications, *ACS Appl. Mater. Interfaces,* 9, (**2017**), 42393–42407.

[81] K. Li, Z. Bo, J. Yan and K. Cen, Solid-state NMR Study of Ion Adsorption and Charge Storage in Graphene Film Supercapacitor Electrodes, *Scientific reports*, *6*(1), (**2016**), 1-9.

[82] P. Wang, C. Huang, Y. Xing, W. Fang, J. Ren, H. Yu, and Guojie Wang, NIR-Light- and pH-Responsive Graphene Oxide Hybrid Cyclodextrin Based Supramolecular Hydrogels, *Langmuir* 35, (**2019**), 1021–1031.

## CHAPTER 2

[1] Z. Singh, Applications and toxicity of graphene family nanomaterials and their composites. *Nanotechnol Sci Appl.,* 16(9), (**2016**), 15–28

[2] D. J. Cram, J. M. Cram, Container Molecules and Their Guests, *Royal Society of Chemistry*, 4, (**1997**).

[3] Y. Wei, B. Wang, J. Wu, R. Yang, M. L. Dunn, Bending rigidity and Gaussian bending stiffness of single-layered graphene. Nano Letter, 13(1), (**2013**), 26–30.

[4] M.D. Stoller, S. Park, Y. Zhu, J. An and R. S. Ruoff, Graphene-based ultracapacitors, Nano Letter, 8, (**2008**), 3498–3502.

[5] S. Alwarappan, A. Erdem, C. Liu and C. Z. Li, Probing the electrochemical properties of graphene nanosheets for biosensing applications, *J. Phys. Chem. C*, 113, (**2009**), 8853–8857.

[6] G. Zhang, X. Zeng and L. Ping, Nanomaterials in cancer-therapy drug delivery system. *J Biomed Nanotechnol.,* 9, (**2013**), 741–750.

[7] E. Fisher, Ber. Deutch. Chem. 2, (**1893**), 267.

[8] J. Li, X. Li, Z. Zhou, X. Ni and K. W. Leong, Formation of supramolecular hydrogels induced by inclusion complexation between pluronics and α-cyclodextrin, Macromolecules, 34, (2001), 7236–7237.

[9] F. Hapiot, S. Tilloy, and E. Monflier, Cyclodextrins as Supramolecular Hosts for Organometallic Complexes, *Chemical reviews*, *106*(3), (**2006**), 767-781.

[10] T. Kakuta, Y. Takashima, T. Sano, T. Nakamura, Y. Kobayashi, H. Yamaguchi and A. Harada, Adhesion between semihard polymer materials containing cyclodextrin and adamantane based on host–guest interactions, *Macromolecules,* 48, (**2015**), 732–738.

[11] M. Nakahata, Y. Takashima, H. Yamaguchi, and A. Harada, Redox-responsive self-healing materials formed from host–guest polymers, *Nat. Commun.,* 2, (**2011**), 1-6.

[12] C. J. Pedersen, Cyclic polyethers and their complexes with metal salts. *J Am Chem Soc 89*, (**1967**), 7017–7036

[13] F. Cramer, Occlusion compounds of cyclodextrin, *Angew. Chem.* 64, (**1952**), 136.

[14] F. Cramer, Über Einschlußverbindungen, V. Mitteil.: Basenkatalyse durch innermolekulare Hohlräume, Chem. Ber. Recl. 86, (**1953**), 1576.

[15] B. Tian and J. Liu, The classification and application of cyclodextrin polymers: a review, *New Journal of Chemistry,* 44, (**2020**), 9137-9148.

[16] A. Alsbaiee, B. J. Smith, L. Xiao, Y. Ling, D. E. Helbling and W. R. Dichtel, *Nature,* 529, (**2016**), 190–194.

[17] G. Liu, Q. Yuan, G. Hollett, W. Zhao, Y. Kang and J. Wu, Cyclodextrin-based host–guest supramolecular hydrogel and its application in biomedical fields, *Polym. Chem.,* 9, (**2018**), 3436.

[18] A. Harada, J. Li and M. Kamachi, Preparation and properties of inclusion complexes of polyethylene glycol with alpha-cyclodextrin, *Macromolecules,* 26, (**1993**), 5698–5703.

[19] S. Saha, A. Roy, and M. N. Roy, Mechanistic Investigation of Inclusion Complexes of a Sulfa Drug with α- and β-Cyclodextrins, *Ind. Eng. Chem. Res,* 56, (**2017**), 11672–11683.

[20] W. Su, Y. Liang, Z. Meng, X. Chen, M. Lu, X. Han, X. Deng, Q. Zhang, H. Zhu, and T. Fu, Inhalation of Tetrandrine-hydroxypropyl-β-cyclodextrin Inclusion Complexes for Pulmonary Fibrosis Treatment, *Mol. Pharmaceutics,* 17, (**2020**), 1596−1607.

[21] Y. Wang, S. Zhuo, J. Hou, W. Li, and Y. Ji, Construction of β-Cyclodextrin Covalent Organic Framework-Modified Chiral Stationary Phase for Chiral Separation, *ACS Appl. Mater. Interfaces* 11, (**2019**), 48363−48369.

[22] J. A. Kent, Handbook of Industrial Chemistry and Biotechnology. New York: Springer; 12, (**2012**).

[23] R. K. Singh, R. Kumar and D. P. Singh, Graphene oxide: strategies for synthesis, reduction and frontier applications, RSC Adv., 6, (**2016**), 64993.

[24] S. Bahadorikhalili, L. Ma'mani, H. Mahdavi and A. Shafiee, Copper supported β-cyclodextrin functionalized PEGylated mesoporous silica nanoparticle - graphene oxide hybrid: An efficient and recyclable nano-catalyst for straightforward synthesis of 2-arylbenzimidazoles and 1,2,3-triazoles, *Microporous and Mesoporous Materials*, *262*, (**2018**), 207-216.

[25] D. Y. Zhang, Y. Zheng, C. P. Tan, J. H. Sun, W. Zhang, L. N. Ji, and Z. W. Mao, Graphene Oxide Decorated with Ru(II)−Polyethylene Glycol Complex for Lysosome-Targeted Imaging and Photodynamic/Photothermal Therapy, *ACS Appl. Mater. Interfaces,* 9, (**2017**), 6761−6771.

[26] Y. A. Cheon, J. H. Bae and B. G. Chung, Reduced graphene oxide nanosheet for chemo-photothermal therapy, *Langmuir*, *32*(11), (**2016**), 2731-2736.

[27] A. Sinha and N. R. Jana, Separation of Microcystin-LR by Cyclodextrin-Functionalized Magnetic Composite of Colloidal Graphene and Porous Silica, *ACS Appl. Mater. Interfaces,* 7, (**2015**), 9911−9919.

[28] Y. Choi, A. Sinha, J. Im, H. Jung, and J. Kim, Hierarchically Porous Composite Scaffold Composed of SBA-15 Microrods and Reduced Graphene Oxide Functionalized with Cyclodextrin for Water Purification, *ACS Appl. Mater. Interfaces,* 11, (**2019**), 15764−15772.

[29] S. Navalon, A. Dhakshinamoorthy, M. Alvaro and H. Garcia, Carbocatalysis by graphene-based materials, Chem. Rev. 114, (**2014**), 6179–6212.

[30] A. Emami, H. Ghafuri, M. K. Kenari, and A. Malek, Investigating the Catalytic Performance of Graphene Oxide–Polyaniline–Lignosulfonate Nanocomposite in the Synthesis of Polysubstituted Pyridines via a Four-Component Reaction, *ChemistrySelect*, 3, (**2018**), 6349–6357.

[31] Y. Y. Zhou, J. Yang, M. Liu, S. F. Wang and Qin Lu, A novel fluorometric determination of melamine using cucurbit[7]uril, *Journal of Luminescence,* 130, (**2010**), 817–820.

[32] A. G. Tanwar, P. B. Date, and D. P. Ottoor, In Vitro Investigation of Controlled Release of Ciprofloxacin and Its β-Cyclodextrin Inclusion Complex from Gelatin Grafted Poly(vinyl alcohol) (GPVA) Nanoparticles, *ChemistrySelect,* 4, (**2019**), 11337–11345.

[33] Y. Wei, J. Zhang, Y. Zhou, W. Bei, Y. Li, Q. Yuan and H. Liang, Characterization of Glabridin/hydroxypropyl-β-cyclodextrin Inclusion Complex with Robust Solubility and Enhanced Bioactivity, *Carbohydrate polymers*, 159, (**2017**), 152-160.

[34] B. K. Barman, B. Rajbanshi, A. Yasmin and M. N. Roy, Exploring inclusion complexes of ionic liquids with α- and β-cyclodextrin by NMR, IR, mass, density, viscosity, surface tension and conductance study, *Journal of Molecular Structure,* 1159, (**2018**), 205-215.

[35] Wen Chen, Li-Juan Yang, Shui-Xian Ma, Xiao-Dong Yang, Bao-Min Fan, Jun Lin, Crassicauline A/-cyclodextrin host–guest system: Preparation, characterization, inclusion mode, solubilization and stability, *Carbohydrate Polymers,* 84, (**2011**), 1321–1328.

[36] K. Das, B. Sarkar, P. Roy, C. Basak, R. Chakraborty and R. L. Gardas, Physicochemical investigations of amino acid ionic liquid based inclusion complex probed by spectral and molecular docking techniques, *Journal of Molecular Liquids*, 291, (**2019**), 111255.

[37] S. Barman, B. K. Barman and M. N. Roy, Preparation, characterization and binding behaviors of host-guest inclusion complexes of metoclopramide hydrochloride with α- and β-cyclodextrin molecules, Journal of Molecular Structure, 1155, (**2018**), 503-512.

[38] J. Q. Zhang, D. Wu, K. M. Jiang, D. Zhang, X. Zheng, C. P. Wan, H. Y. Zhu, X. G. Xie, Y. Jin and J. Lin, Preparation, spectroscopy and molecular modelling studies of the inclusion complex of cordycepin with cyclodextrins, *Carbohydrate Research,* 406, (**2015**), 55-64.

[39] P. Dandawatea, K. Vemuri, E. M. Khana, M. Sritharanb and S. Padhye, Synthesis, characterization and anti-tubercular activity of ferrocenyl hydrazones and their -cyclodextrin conjugates, *Carbohydrate Polymers,* 108, (**2014**), 135–144.

[40] Y. Deng, Y. Pang, Y. Guo, Y. Ren, F. Wang, X. Liao and Bo Yang, Host-guest inclusion systems of daidzein with 2-hydroxypropyl-bcyclodextrin (HP-β-CD) and sulfobutyl ether-b-cyclodextrin (SBE-β-CD): Preparation, binding behaviors and water solubility, *Journal of Molecular Structure*, 1118, (**2016**), 307-315.

## CHAPTER 3

[1] J. M. Grange and N. J. C. Snell, Activity of Bromhexine and Ambroxol, semi synthetic derivatives of vasicine from the Indian shrub Adhatoda Vasica, against Microbacterium tuberculosis in vitro, Journal of Ethnopharmacology, 50 (**1996**) 49-53.

[2] J. Peralta, J. J. Poderoso, C. Corazza, M. Fernandez, R. B. Guerreiro and J. C. M. Wiemeyer, Ambroxol Plus Amoxicillin in the Treatment of Exacerbations of Chronic-Bronchitis. Arzneim.-Forsch. 37(8) (**1987**) 969–971.

[3] J. Mo and L. P. Yuan, Compatibility And Thermal Stability Studies Between Omeprazole And Ambroxol Hydrochloride, *Int. Res. J. Pharm.* 8 (3) (**2017**), 56-61.

[4] J. Madsen, I. Canton, N. J. Warren, E. Themistou, A. Blanazs, B. Ustbas, X. Tian, R. Pearson, G. Battaglia, A. L. Lewis, Steven P. Armes and S. P. Nile Blue-Based Nanosized pH Sensors for Simultaneous Far-Red and Near-Infrared Live Bioimaging. *J. Am. Chem. Soc.* 135(39) **(2013)** 14863-14870,

[5] B. Wang, J. Fan, X. Wang, H. Zhu, J. Wang, H. Mu and X. Peng, A Nile blue based infrared fluorescent probe: imaging tumors that over-express cyclooxygenase-2, *Chem. Commun*. 51 **(2015**) 792-795.

[6] J. Mishkinsky, B. Joseph and F. G. Sulman, Hypoglycaemic effect of trigonelline, *Lancet* 2 (**1967**) 1311–1312.

[7] A. E. van Dijk, M. R. Olthof, J. C. Meeuse, E. Seebus , R. J. Heine and R. M. van Dam, Acute effects of decaffeinated coffee and the major coffee components chlorogenic acid and trigonelline on glucose tolerance, *Diabetes Care*, 32, (**2009**), 1023–1025.

[8] T. Tanigawa, R. Pai, T. Arakawa and A. S. Tarnawski, Rebamipide inhibits gastric cancer cell growth. *Digestive,* Digestive diseases and sciences. 52 (**2007**) 240-247.

[9] S. J. Moon, Y. J. Woo, J. H. Jeong, M. K. Park, H. J. Oh, J. S. Park, E. K. Kim, M. L. Cho, S. H. Park, H. Y. Kim and J. K. Min, Rebamipide attenuates pain severity and cartilage degeneration in a rat model of osteoarthritis by downregulating oxidative damage and catabolic activity in chondrocytes, Osteoarthritis and Cartilage. 20 (**2012**) 1426-1438.

[10] J. Kockler, M. Oelgemöller, S. Robertson and B. D. Glass, Photostability of sunscreens, *13*(1) (**2012**) 91-110.

[11] C. Stiefel, T. Schubert, G. E. Morlock, Bioprofiling of Cosmetics with Focus on Streamlined Coumarin Analysis, ACS Omega, 2 (**2017**) 5242−5250.

[12] G. Liu, Q. Yuan, G. Hollett, W. Zhao, Y. Kang and J. Wu, Cyclodextrin-based host–guest supramolecular hydrogel and its application in biomedical fields, *Polym. Chem.,* 9 (**2018**), 3436-3449.

[13] B. Tian and J. Liu, The classification and application of cyclodextrin polymers: a review, *New J. Chem.,* 44, (**2020**), 9137-9148.

[14] F. Hapiot, S. Tilloy, and E. Monflier, Cyclodextrins as Supramolecular Hosts for Organometallic Complexes, *Chemical Reviews,* 3 (**2006**) 767-781.

[15] G. Crini, Review: A History of Cyclodextrins, *Chem. Rev.* 114, (**2014**), 10940–10975.

[16] J. Szejtli, Introduction and General Overview of Cyclodextrin Chemistry, *Chem. Rev.* 98, (**1998**), 1743–1753

[17] K. Uekama, F. Hirayama and T. Irie, Cyclodextrin Drug Carrier Systems, *Chem. Rev.* 98, (**1998**), 2045–2076.

[18] S. Saha, A. Roy and M. N. Roy, Mechanistic Investigation of Inclusion Complexes of a Sulfa Drug with α- and β-Cyclodextrins, *Ind. Eng. Chem. Res.* 56, (**2017**), 11672–11683.

[19] R. L. Abarca, F. J. Rodríguez, A. Guarda, M. J. Galotto and J. E. Bruna, Characterization of beta-cyclodextrin inclusion complexes containing an essential oil component, *Food Chemistry,* 196, (**2016**), 968–975.

[20] W. Su, Y. Liang, Z. Meng, X. Chen, M. Lu, X. Han, X. Deng, Q. Zhang, H. Zhu, and T. Fu, Inhalation of Tetrandrine-hydroxypropyl-β-cyclodextrin Inclusion Complexes for Pulmonary Fibrosis Treatment, *Mol. Pharmaceutics,* 17, (**2020**), 1596–1607.

[21] P. Bomzan, N. Roy, A Sharma, V. Rai, S. Ghosh, A Kumar and M. N. Roy, Molecular encapsulation study of indole-3-methanol in cyclodextrins: Effect on antimicrobial activity and cytotoxicity, *Journal of Molecular Structure,* 1225, (**2021**), 129093.

[22] A. Yasmin, B. K. Barman, N. Roy and M. N. Roy, Synthesis and Characterization of Host Guest Inclusion Complexation of Cyclic Oligosaccharide with Industrially Potent Dye in Different Phases by Physicochemical Contrivance, *ChemistrySelect*, 5, (**2020**), 1803–1808.

[23] A. Dutta, N. Roy, K. Das, D. Roy, R. Ghosh and M. N. Roy, Synthesis and Characterization of Host Guest Inclusion Complexes of Cyclodextrin Molecules with Theophylline by Diverse Methodologies, *Emerging Science Journal,* 4, (**2019**), 52-72.

[24] D. C. Marcano, D. V. Kosynkin, J. M. Berlin, A. Sinitskii, Z. Sun, A. Slesarev, L. B. Alemany, W. Lu and J. M. Tour, Improved Synthesis of Graphene Oxide. *ACS nano,* 4(8), (**2010**), 4806-4814.

[25] R. K. Singh, R. Kumar and D. P. Singh, Graphene oxide: strategies for synthesis, reduction and frontier applications, *RSC Adv.,* 6, (**2016**), 64993-65011.

[26] H. Zhao, L. Yang, Y. Li, X. Ran, H. Ye, G. Zhao, Y. Zhang, F. Liu and C. Li, A comparison study of macrocyclic hosts functionalized reduced graphene oxide for electro chemical recognition of tadalafil. *Biosensors and Bioelectronics,* 89, (**2017**), 361-369.

[27] Y. Deng, Y. Pang, Y. Guo, Y. Ren, F. Wang, X. Liao and B. Yang, Host-guest inclusion systems of daidzein with 2-hydroxypropyl-bcyclodextrin (HP-β-CD) and sulfobutyl ether-b-cyclodextrin (SBE-β-CD): Preparation, binding behaviors and water solubility, *Journal of Molecular Structure* 1118, (**2016**), 307-315.

## CHAPTER 4

[1] Y. Wang and C. Wu, Site-Specific Conjugation of Polymers to Proteins, *Biomacromolecules,* 19 (**2018**) 1804–1825.

[2] J. M. Grange and N. J. C. Snell, Activity of Bromhexine and Ambroxol, semi synthetic derivatives of vasicine from the Indian shrub Adhatoda Vasica, against Microbacterium tuberculosis in vitro, *Journal of Ethnopharmacology*, 50 (**1996**) 49-53.

[3] J. Peralta, J. J. Poderoso, C. Corazza, M. Fernandez, R. B. Guerreiro and J. C. M. Wiemeyer, Ambroxol Plus Amoxicillin in the Treatment of Exacerbations of Chronic-Bronchitis. *Arzneim.-Forsch.* 37(8) (**1987**) 969–971.

[4] J. Mo and L. P. Yuan, Compatibility And Thermal Stability Studies Between Omeprazole And Ambroxol Hydrochloride, *Int. Res. J. Pharm.* 8 (3) (**2017**).

[5] F. Tewes, K. J. Paluch, L. Tajber, K. Gulati, D. Kalantri, C. Ehrhardt and A. Marie, HealySteroid/mucokinetic hybrid nanoporous microparticles for pulmonary drug delivery, *Eur. J. Pharm. Biopharm.* 85(3) (**2013**) 604-613.

[6] A. Das, R. Thakur, A. Dagar and A. Chakraborty, A spectroscopic investigation and molecular docking study on the interaction of hen egg white lysozyme with liposomes of saturated and unsaturated phosphocholines probed by an anticancer drug ellipticine, *Phys. Chem. Chem. Phys.,* 16 (**2014**) 5368.

[7] G. Ambrosi, C. Ghezzi, R. Zangaglia, G. Levandis, C. Pacchetti and F. Blandini, Ambroxol-induced rescue of defective glucocerebrosidase is associated with increased LIMP-2 and saposin C levels in GBA1 mutant Parkinson's disease cells, *Neurobiology of Disease,* 82 (**2015**) 235–242,

[8] O. Gyulai, P. Szabo-Revesz and Z. Aigner, Comparison Study of Different Spherical Crystallization Methods of Ambroxol Hydrochloride, *Crystal Growth & Design,* 17 (**2017**) 5233-5241,

[9] J. Magalhaes, M. E. Gegg, A. Migdalska-Richards and A. H. Schapira, Effects of ambroxol on the autophagy-lysosome pathway and mitochondria in primary cortical neurons, *Scientific Reports,* 8 (**2018**) 1385,

[10] V. R. R. Thummala, M. R. Ivaturi and S. R. Nittala, Identification, and Characterization of One Degradation Product in Ambroxol by HPLC-Hyphenated Techniques, *Sci Pharm.* 82 (**2014**) 247–263.

[11] I. B. Bar, G. Maor, M. Filocamo and M. Horowitz, Ambroxol as a pharmacological chaperone for mutant glucocerebrosidase, *Blood Cells, Molecules and Diseases,* 50 (**2013**) 141–145.

[12] D. Sharma, M. Singh, D. Kumar and G. Singh, Simultaneous Estimation of Ambroxol Hydrochloride and Cetirizine Hydrochloride in Pharmaceutical Tablet Dosage Form by Simultaneous Equation Spectrophotometric Method: A Quality Control Tool for Dissolution Studies, *International Scholarly Research Notices,* (**2014**).

[13] L. Szente and J. Szeman, Cyclodextrins in Analytical Chemistry: Host–Guest Type Molecular Recognition, *Anal. Chem.* 85 (**2013**) 8024–8030.

[14] B. V. K. J. Schmidt and C. B. Kowollik, Dynamic Macromolecular Material Design-The Versatility of Cyclodextrin-Based Host–Guest Chemistry, *Angew. Chem. Int. Ed.* 56 (**2017**) 8350–8369.

[15] A. P. Sherje, F. Patel, M. Murahari, V. Suvarna and K. Patel, Study on effect of L-arginine on solubility and dissolution of Zaltoprofen: Preparation and characterization of binary and ternary cyclodextrin inclusion complexes, *Chemical Physics Letters*, 694 (**2018**) 120–128.

[16] C. S. Mangolim, C. Moriwaki, A. C. Nogueira, F. Sato, M. L. Baesso, A. M. Neto and G. Matioli, Curcumin-β-cyclodextrin inclusion complex: Stability, solubility, characterisation by FT-IR, FT-Raman, X-ray diffraction and photoacoustic spectroscopy, and food application, *Food Chemistry,* 153 (**2014**) 361–370.

[17] W. Chena, L. J. Yang, S. X. Ma, X. D. Yang, B. M. Fan and J. Lin, Crassicauline A/β-cyclodextrin host–guest system: Preparation, characterization, inclusion mode, solubilization and stability, *Carbohydrate Polymers,* 84 (**2011**) 1321–1328.

[18] L. M. M. Gomes, N. Petito, V. G. Costa, D. Q. Falcão and K. G. de Lima Araújo, Inclusion complexes of red bell pepper pigments with β-cyclodextrin: Preparation, characterisation and application as natural colorant in Yogurt, Food Chemistry, 148 (**2014**) 428–436.

[19] M. S. Mokhtar, F. O. Suliman and A. A. Elbashir, Atrazine and ametryne inclusion complexes with 2-hydroxypropyl-b/g-cyclodextrin: Spectroscopic studies and molecular dynamics simulation. *Journal of Molecular Structure,* 1179 (**2019**) 161-170.

[20] M. S. Mokhtar, F. O. Suliman, A. A. Elbashir. The binding interaction of imazapyr with cucurbit[n]uril (n = 6–8): Combined experimental and molecular modeling study. *Spectrochimica Acta Part A: Molecular and Biomolecular Spectroscopy,* 194 (**2018**) 67–75.

[21] A. Abdolmaleki, F. Ghasemi, J. B. Ghasemi, Computer-aided drug design to explore cyclodextrin therapeutics and biomedical applications, *Chem Biol Drug Des,* 89 (**2017**) 257–268.

[22] T. M. C. Babu, S. S. Rajesh, B. V. Bhaskar, S. Devi, A. Rammohan, T. Sivaraman, W. Rajendra, Molecular docking, molecular dynamics simulation, biological evaluation and 2D QSAR analysis of flavonoids from Syzygium alternifolium as potent anti-Helicobacter pylori agents. *RSC Adv.,* 7 (**2017**) 18277.

[23] M. O. Radwan, S. Sonoda, T. Ejima, Zinc-mediated binding of a low-molecular-weight stabilizer of the host anti-viral factor apolipoprotein B mRNA-editing enzyme, catalytic polypeptide-like 3G. *Bioorg Med Chem.* 24 (18) (**2016**) 4398–4405.

[24] J. S. Renny, L. L. Tomasevich, E. H. Tallmadge, D. B. Collum, Method of Continuous Variations: Applications of Job Plots to the Study of Molecular Associations in Organometallic Chemistry, *Angew. Chem. Int. Ed.* 52 (**2013**) 11998–12013.

[25] H. A**.** Benesi, J. H. Hildebrand**,** A Spectrophotometric Investigation of the Interaction of Iodine with Aromatic Hydrocarbons, *Journal of the American Chemical Society* 71 (**1949**) 2703-2707.

[26] Y. Liao, X. Zhang, C. Li, Y. Huang, M. Lei, M. Yan, Y. Zhou, C. Zhao, Inclusion complexes of HP-β-cyclodextrin with agomelatine: Preparation, characterization, mechanism study and in vivo evaluation. *Carbohydrate Polymers*, 147 (**2016**) 415–425.

[27] W. Chen, L. J. Yang, S. X. Ma, X. D. Yang, B. M. Fan, J. Lin. Crassicauline A/β-cyclodextrin host–guest system: Preparation, characterization, inclusion mode, solubilization and stability. *Carbohydrate Polymers,* 84 (**2011**) 1321–1328.

[28] M. V. Ol'khovicha, A. V. Sharapova, S. V. Blokhina, S. Y. Skachilova, O. G. Kesarevb, G. L. Perlovich. Physicochemical characteristics of the inclusion complexes of biologically active compounds with 2-hydroxypropyl-β-cyclodextrin. *Thermochimica Acta,* 639 (**2016**) 1–9.

[29] G. M. Kumar, S. H. Cheruvu, D. Sujatha, S. Sampathi, Formulation and Characterization of Ambroxol Hydrochloride Loaded Ethyl Cellulose Microparticles for Sustained Release, *Journal of Biomaterials and Tissue Engineering,* 4(9) (**2014**) 669-678.

[30] D. Sharma, M. Singh, D. Kumar, G. Singh, M. S. Rathore, Formulation Development and Evaluation of Fast Disintegrating Tablets of Ambroxol Hydrochloride for Pediatrics- A Novel Approach for Drug Delivery, *Indian Journal of Pharmaceutical Education and Research,* 48 (2014) (supplement)

[31] G. Ramana, O. Sravanthi, G. Sahithi, Naga V. Sindhu, G. Priyanka, Formulation and Evaluation of Controlled Release Hydrophilic Matrices of Ambroxol Hydrochloride by Melt Granulation Technique, *American-Eurasian Journal of Scientific Research,* 7(4) (**2012)** 150-159.

[32] M. I. Sancho, S. Andujar, R. D. Porasso, R. D. Enriz, Theoretical and Experimental Study of Inclusion Complexes of β-Cyclodextrins with Chalcone and 2′,4′-Dihydroxychalcone, *J. Phys. Chem. B,* 120 (**2016**) 3000−3011.

[33] F. Xie, G. Ouyang, L. Qin, M. Liu, Supra-dendron Gelator Based on Azobenzene–Cyclodextrin Host–Guest Interactions: Photoswitched Optical and Chiroptical Reversibility, *Chem. Eur. J.* 22(50) (**2016**) 18208–18214.

[34] Q. Tang, C. H. Wang, Y. Y. Xi, Y. Huang and Z. Tao, Host-Guest Complexes of l-Borneol with Cucurbituril and Cyclodextrin and Its Potential Use in Analysis of Drugs, *ChemistrySelect,* 4 **(2019**) 6924 –6929.

[35] L. Wang, J. Yan, Y. Li, K. Xu, S. Li, P. Tang, H. Li, The influence of hydroxypropyl-β-cyclodextrin on the solubility, dissolution, cytotoxicity, and binding of riluzole with human serum albumin, *Journal of Pharmaceutical and Biomedical Analysis,* 117 (**2016**) 453–463.

[36] A. Raza, H. Sun, S. Bano, Y. Zhao, X. Xu, J. Tang, Preparation, characterization, and in vitro anti-inflammatory evaluation of novel water soluble kamebakaurin/hydroxypropyl-β-cyclodextrin inclusion complex. *Journal of Molecular Structure,* 1130 (**2017**) 319-326.

[37] L. Wang, S. Li, P. Tang, J. Yan, K. Xu, H. Li, Characterization and evaluation of synthetic riluzole with β-cyclodextrin and 2,6-di-O-methyl-β-cyclodextrin inclusion complexes, *Carbohydrate Polymers,* 129 (**2015**) 9–16.

[38] P. Dandawate, K. Vemuri, E. M. Khan, M. Sritharan, S. Padhye, Synthesis, characterization and anti-tubercular activity of ferrocenyl hydrazones and their β-cyclodextrin conjugates, *Carbohydrate Polymers,* 108 (**2014**) 135–144.

[39] M. I. Sancho, M. G. Russo, M. S. Moreno, E. Gasull, S. E. Blanco, G. E. Narda, Physicochemical Characterization of 2-Hydroxybenzophenone with β-Cyclodextrin in Solution and Solid State, *J. Phys. Chem. B,* 119 (**2015**) 5918–5925.

[40] P. Tang, X. Ma, D. Wu, S. Li, K. Xu, B. Tang, H. Li, Posaconazole/ hydroxypropyl-β-cyclodextrin host-guest system: Improving dissolution while maintaining antifungal activity, *Carbohydrate Polymers,* 142 (**2016**) 16–23.

[41] Y. Hayashino, M. Sugita, H. Arima, T. Irie, T. Kikuchi, F. Hirata, Predicting the Binding Mode of 2-Hydroxypropyl-β-cyclodextrin to Cholesterol by Means of the MD Simulation and the 3D-RISM-KH Theory, *J. Phys. Chem. B,* 122(21) (**2018**) 5716–5725.

[42] H. Zhang, C. Ge, D. V. der Spoel, W. Feng, T. Tan, Insight into the Structural Deformations of Beta-Cyclodextrin Caused by Alcohol Cosolvents and Guest Molecules, *J. Phys. Chem. B,* 116 (**2012**) 3880–3889.

[43] R. Onnainty, E. M. Schenfeld, M. A. Quevedo, M. A. Fernandez, M. R. Longhi and G. E. Granero, Characterization of the Hydrochlorothiazide: β-Cyclodextrin Inclusion Complex. Experimental and Theoretical Methods, *J. Phys. Chem. B,* 117 (**2013**) 206–217.

[44] Y. Akae, Y. Koyama, H. Sogawa, Y. Hayashi, S. Kawauchi, S. Kuwata and T. Takata, Structural Analysis and Inclusion Mechanism of Native and Permethylated a-Cyclodextrin-Based Rotaxanes Containing Alkylene Axles, *Chem. Eur. J.* 22(15) (**2016**) 5335–5341.

[45] A. P. Sherje, V. Kulkarni, M. Murahari, U. Y. Nayak, P. Bhat, V. Suvarna and B. Dravyakar, Inclusion Complexation of Etodolac with Hydroxypropyl-betacyclodextrin and Auxiliary Agents: Formulation Characterization and Molecular Modeling Studies, *Mol. Pharmaceutics,* 14(4) (**2017**) 1231–1242.

[46] M. P. Vargas and A. M. Castro, Metal containing cryptands as hosts for anions: evaluation of Cu(I)X and pX interactions in halide–tricopper(I) complexes through relativistic DFT calculations, *Phys. Chem. Chem. Phys.,* 17(28) (**2015**) 18677.

[47] A. O. Ortolan, I. Østrøm, G. F. Caramori, R. L. T. Parreira, A. M. Castro and F. Matthias Bickelhaupt, Anion Recognition by Organometallic Calixarenes: Analysis from Relativistic DFT Calculations, *Organometallics,* 37(13) (**2018**) 2167−2176.

[48] M. I. Sancho, S. Andujar, R. D. Porasso and R. D. Enriz, Theoretical and Experimental Study of Inclusion Complexes of β-Cyclodextrins with Chalcone and 2′,4′-Dihydroxychalcone, *J. Phys. Chem. B,* 120 (12) (**2016**) 3000−3011.

[49] M. P. Vargas, and A. M. Castro, Tiara-like Complexes acting as Iodine Encapsulating Agents: The Role of M···I Interactions in [M(μ-SCH2CO2Me)2]8⊂I2 (M = Ni, Pd, Pt) Inclusion Compounds, *J. Phys. Chem. C* 2016, 120 (41) (**2016**) 23441−23448.

[50] A. O. Ortolan, I. Østrøm, G. F. Caramori, R. L. T. Parreira, A. M. Castro and F. Matthias Bickelhaupt, Anion Recognition by Organometallic Calixarenes: Analysis from Relativistic DFT Calculations, *J. Phys. Chem. A* 37(13) (**2018**) 2167-2176.

[51] U. Chaube, D. Chhatbar and H. Bhatt, molecular dynamics simulations and molecular docking studies of benzoxazepine moiety as mTOR inhibitor for the treatment of lung cancer, *Bioorganic & Medicinal Chemistry Letters,* 26(3) (**2016**) 864-874.

[52] I. Daoud, N. Melkemi, T. Salah and S. Ghalem, molecular docking and molecular dynamics study on new Acetylcholinesterase and Butyrylcholinesterase inhibitors, *Computational Biology and Chemistry,* 74 (**2018**) 304–326.

# CHAPTER 5

[1] J. Pan, Y. Yang, W. Fang, W. Liu, K. Le, D. Xu and X. Li, Fluorescent Phthalocyanine–Graphene Conjugate with Enhanced NIR Absorbance for Imaging and Multi-Modality Therapy. *ACS Appl. Nano Mater.* 1(6) **(2018)** 2785–2795.

[2] Z. Tong, G. Singh and A. J. Rainbow, Extreme Dark Cytotoxicity of Nile Blue A in Normal Human Fibroblasts. *Photochemistry and Photobiology.* 74(5) **(2001)** 707–711.

[3] J. Madsen, I. Canton, N. J. Warren, E. Themistou, A. Blanazs, B. Ustbas, X. Tian, R. Pearson, G. Battaglia, A. L. Lewis, Steven P. Armes and S. P. Nile Blue-Based Nanosized pH Sensors for Simultaneous Far-Red and Near-Infrared Live Bioimaging. *J. Am. Chem. Soc.* 135(39) **(2013)** 14863-14870.

[4] B. Wang, J. Fan, X. Wang, H. Zhu, J. Wang, H. Mu and X. Peng, A Nile blue based infrared fluorescent probe: imaging tumors that over-express cyclooxygenase-2, *Chem. Commun*. 51 **(2015**) 792.

[5] A. L. Bastos and D. Marques, Nile Blue Inducible Fluorescence of Tumour Cells, *Zeitschrift für Naturforschung B*, 27(11) **(1992)** 1395–1398.

[6] M. Wainwright, Non-porphyrin Photosensitizers in Biomedicine. *Chem. Soc. Rev.* **1996 25**(5) (1996) 351-359.

[7] H. J. VAN, Staveren, O. C. Speelman, M. J. H. Witjes, L. Louis Cincotta and W. M. Star, Fluorescence Imaging and Spectroscopy of Ethyl Nile Blue A in Animal Models of (Pre) malignancies, *Photochemistry and Photobiology,* 73(1) **(2001)** 32–38.

[8] C. W. Lin, J. R. Janine R. Shulok, S. D. Kirley, L. Cincotta and J. W. Foley, Lysosomal Localization and Mechanism of Uptake of Nile Blue Photosensitizers in Tumor Cells. *CANCER RESEARCH*, 51(10) **(1992)** 2710-2719.

[9] H. R. Thomas, S. P Day, W. E. Woodruff, C. Valles, R. J. Young, Kinloch, I. A. Kinloch, G. W. Morley, J. V. Hanna, N. R. Wilson and J. P. Rourke,

Deoxygenation of Graphene Oxide: Reduction or Cleaning?. *Chem. Mater.* 25(18) (**2013**) 3580-3588.

[10] M. Khandelwal and A. Anil Kumar, One-step chemically controlled wet synthesis of graphene nanoribbons from graphene oxide for high performance supercapacitor applications. *J. Mater. Chem. A* 3 (45), **(2015)** 22975-22988.

[11] T. S. H. Pham, L. Fu, P. Mahon, G. Lai and A. Yu, Fabrication of β-Cyclodextrin-Functionalized Reduced Graphene Oxide and Its Application for Electrocatalytic Detection of Carbendazim *Electrocatalysis,* 7(5) **(2016)** 411–419.

[12] P. Zheng and N. Wu, Fluorescence and Sensing Applications of Graphene Oxide and Graphene Quantum Dots: A Review, *Chem. Asian J.* 12(18) (**2017**) 2343–2353.

[13] B. Rajbanshi, S. Saha, K. Das, B. K. Barman, S. Sengupta, A. Bhattacharjee and M. N. Roy, Study to probe subsistence of host-guest inclusion complexes of α and β-cyclodextrins with biologically potent drugs for safety regulatory dischargement. *Scientific reports 8* (1) (**2018**) 1-20.

[14] M. N. Roy, A. Roy and S. Saha, Probing inclusion complexes of cyclodextrins with amino acids by physicochemical approach. *Carbohydrate polymers*, *151* (**2016**) 458-466.

[15] S. Saha, T. Ray, S. Basak and M. N. Roy, NMR, surface tension and conductivity studies to determine the inclusion mechanism: thermodynamics of host–guest inclusion complexes of natural amino acids in aqueous cyclodextrins. *New Journal of Chemistry*, *40*(1) (**2016**) 651-661.

[16] T. H. Fenger, J Bjerre and M. Bols, Cyclodextrin Aldehydes are Oxidase Mimics. *Chem Bio Chem*, 10(15) (**2009**) 2494–2503.

[17] Y. Liu, Y. Song, Y. Chen, X. Q. Li, F. Ding and R .Q. Zhong, Biquinolino-Modified β-Cyclodextrin Dimers and Their Metal Complexes as Efficient Fluorescent Sensors for the Molecular Recognition of Steroids. *Chem. Eur. J.* 10(15) (**2004**) 3685-3696.

[18] K. Kanagaraj and K. Pitchumani, Per-6-amino-β-cyclodextrin as a Chiral Base Catalyst Promoting OnePot Asymmetric Synthesis of 2-Aryl-2, 3-dihydro-4-quinolones*. J. Org. Chem.* 78(2) **(2013)** 744–751.

[19] F. O'Keeffe, A. Shamsi, R. Darcy, P. Schwinté and I. M. Warner, A Persubstituted Cationic β-Cyclodextrin for Chiral Separations. *Anal. Chem.* 69 (23) **(1997**) 4773-4782.

[20] P. Liu, S. Sun, X. Guo, X. Yang, J. Huang, K. Wang, Q. Wang, J. Liu and L. He, Competitive Host–Guest Interaction between β-Cyclodextrin Polymer and Pyrene-Labeled Probes for Fluorescence Analyses. *Anal. Chem.* 87(5) **(2015**) 2665-2671.

[21] R. Banerjee, R. Riya Sinha and P. Purkayastha, β-Cyclodextrin Encapsulated Coumarin 6 on Graphene Oxide Nanosheets: Impact on Ground-State Electron Transfer and Excited-State Energy Transfer. *ACS Omega* 4(14) (**2019**) 16153−16158.

[22] A. Ray, S. Das and N. Nitin Chattopadhyay, Aggregation of Nile Red in Water: Prevention through Encapsulation in β-Cyclodextrin. *ACS Omega* 4(1) **(2019)** 15−24.

[23] D. C. Marcano, D. V. Kosynkin, J. M. Berlin, A. Sinitskii, Z. Sun, A. Slesarev, L. B. Alemany, W. Lu and J. M. Tour, Improved Synthesis of Graphene Oxide. *ACS nano* 4(8), (**2010**) 4806-4814.

[24] H. Zhao, L. Yang, Y. Li, X. Ran, H. Ye, G. Zhao, Y. Zhang, F. Liu and C. A. Li, A comparison study of macrocyclic hosts functionalized reduced graphene oxide for electro chemical recognition of tadalafil. *Biosensors and Bioelectronics,* 89, (**2017**), 361-369.

[25] M. Khandelwal and A. Kumar, One-step chemically controlled wet synthesis of graphene nanoribbons from graphene oxide for high performance supercapacitor applications. *J. Mater. Chem. A*. 3(45) (**2015**) 22975-22988,

[26] T. S. H. Pham, L. Fu, P. Mahon, G. Lai and A. Yu, Fabrication of β-Cyclodextrin-Functionalized Reduced Graphene Oxide and Its Application for

Electrocatalytic Detection of Carbendazim. *Electrocatalysis* , 7(5) (**2016**) 411–419,

[27] S. K. Cushing, M. Li, F. Huang and N. Wu, Origin of Strong Excitation Wavelength Dependent Fluorescence of Graphene Oxide. *ACS Nano* 8 (1) (**2014**) 1002-1013,

[28] M. Li, S. K. Cushing, X. Cushing, S. Guo and N. Wu, Fingerprinting photoluminescence of functional groups in graphene oxide. *J. Mater. Chem.* 22(44) (**2012**,) 23374-23379,

[29] P. Zheng and N. Wu, Fluorescence and Sensing Applications of Graphene Oxide and Graphene Quantum Dots: a Review. *Chem. Asian J.* 12(18) (**2017**) 2343–2353.

[30] D. Kozawa, Y. Miyauchi, S. Mouri and K. Matsuda, Exploring the Origin of Blue and Ultraviolet Fluorescence in Graphene Oxide. *J. Phys. Chem. Lett.* 4(12) (**2013**) 2035–2040,

[31] J. P. Rourke, P. A. Pandey, J. J. Moore, M. Bates, I. A. Kinloch, R. J. Young and N. R. Wilson, The Real Graphene Oxide Revealed: Stripping the Oxidative Debris from the Graphene-like Sheets. *Angew. Chem. Int. Ed.* 50(14) (**2011**) 3173–3177.

[32] S. Wang, Y. Li, X. Fan, F. Zhang and G. Zhang, β-Cyclodextrin functionalized graphene oxide: an efficient and recyclable adsorbent for the removal of dye pollutants, *Frontiers of Chemical Science and Engineering, 9*(1), (**2015**), 77-83.

[33] C. Xu, J. Wang, L. Wan, J. Lin and X. Wang, Microwave-assisted covalent modification of graphene nanosheets with hydroxypropyl-b-cyclodextrin and its electrochemical detection of phenolic organic pollutants. *J. Mater. Chem.* 21 (28) (**2011**) 10463-10471.

[34] S. R. Pour, M. Dinari and A. Abdolmaleki, Monochlorotriazinyl-β-cyclodextrin Grafted on Graphene Oxide as an Attractive Green Heterogeneous Nanoreactor for Selective Oxidation Reaction with NBS in Wate., *Chemistry Select* **,** 4(20) (**2019**) 6390–6396.

[35] F. Liu, S. Chung, G. Oh and T. S. Seo, Three-Dimensional Graphene Oxide Nanostructure for Fast and Efficient Water-Soluble Dye Removal. *ACS Appl. Mater. Interfaces* 4(2) (**2012**) 922–927.

[36] A. Heydariab and H. Sheiban, Facile polymerization of b-cyclodextrin functionalized graphene or graphene oxide nanosheets using citric acid crosslinker by in situ melt polycondensation for enhanced electrochemical performance. *RSC Adv.* 6(12) (**2016**) 9760 -9771.

[37] S. Liu, T. H. Zeng, M. Hofmann, E. Hofmann, J. Wei, R. Jiang, J. Kong and Y. Chen, Antibacterial Activity of Graphite, Graphite Oxide, Graphene Oxide, and Reduced Graphene Oxide: *Membrane and Oxidative Stress. ACS nano,* 5(9), (**2011**) 6971–6980.

[38] B. R. Coleman, T. Knight, V. Gies, Z. J. Jakubek and S. Zou, Manipulation and Quantification of Graphene Oxide Flake Size: Photoluminescence and Cytotoxicity. *ACS Appl. Mater. Interfaces* 9(34) (**2017**) 28911–28921.

[39] A. Mallick, A. Nandi and S. Basu, Polyethylenimine Coated Graphene Oxide Nanoparticles for Targeting Mitochondria in Cancer Cells. *ACS Appl. Bio. mater.* 2(1) (**2018)** 14-19.

[40] J. M. Tijerina, D. Venkataramani, C. P. Aichele, C. S. Tiwary, J. E. Smay, A. Mathkar, P. Chang and P. M. Ajayan, Quantifi cation of the Particle Size and Stability of Graphene Oxide in a Variety of Solvents. Part. Part. Syst. Charact. 32(3) (**2015**) 334–339.

[41] B. Konkena and S. Vasudevan, Covalently Linked, Water-Dispersible, Cyclodextrin: Reduced-Graphene Oxide Sheets. *Langmuir* 28(34) (**2012**) 12432–12437.

[42] C. K. Chun Kiang Chua and M. Pumera, Monothiolation and Reduction of Graphene Oxide via One-Pot Synthesis: Hybrid Catalyst for Oxygen Reduction. *ACS Nano***,** 9(4) (**2015**) 4193-4199.

[43] C. Xu, X. Wang, J. Wang, H. Hu and L. Wan, Synthesis and photoelectrical properties of b-Cyclodextrin functionalized graphene materials with high

bio-recognition capability. *Chemical Physics Letters,* 498(1-3) (**2010**) 162-167.

[44] L. Yang, H. Zhao, Y. Li, X. Ran, G. Deng, X. Xie and C. P. Li, Fluorescent Detection of Tadalafil Based on Competitive Host–Guest Interaction Using p-Sulfonated Calix[6]arene Functionalized Graphene. *ACS Appl. Mater. Interfaces***,** 7(48) (**2015**) 26557-26565.

[45] A. Yasmin, B. K. Barman, N. Roy and M. N. Roy, synthesis and Characterization of Host Guest Inclusion Complexation of Cyclic Oligosaccharide with Industrially Potent Dye in Different Phases by Physicochemical Contrivance, *Chemistry Select* 5(5) (**2020**) 1803-1808.

[46] K. Pal, S. Mallick and A. L. Koner, Complexation induced fluorescence and acid–base properties of dapoxyl dye with c-cyclodextrin: a drug-binding application using displacement assays. *Phys. Chem. Chem. Phys.* 17(24) (**2015**) 16015-16022.

[47] S. Mohandoss and T. Stalin, Photochemical and computational studies of inclusion complexes between β-cyclodextrin and 1,2-dihydroxyanthraquinones. *Photochem. Photobiol. Sci.*16(4) (**2017**) 476-488.

[48] R. Kurapati, F. Bonachera, J. Russier, A. R. Sureshbabu, C. Ménard-Moyon, K. Kostarelos, and A. Bianco, Covalent chemical functionalization enhances the biodegradation of graphene oxide. *2D Materials*, *5*(1) (**2017**) 015020.

[49] X. L. Wang, R. Sun, W. J. Zhu, X. L. Sha and J. F. Ge, Reversible Absorption and Emission Responses of Nile Blue and Azure A Derivatives in Extreme Acidic and Basic Conditions. *J. Fluorescence, 27(3)* (***2017***) *819-827.*

[50] J. Jose, Y. Ueno and K. Burgess, Water-Soluble Nile Blue Derivatives: Syntheses and Photophysical Properties. *Chem. Eur. J.* 15(2) (**2009**) 418-423.

[51] J. Fan, H. Dong, M. Hu, J. Wang, H. Zhang, H. Zhu, W. Suna and X. Peng, Fluorescence imaging lysosomal changes during cell division and apoptosis observed using Nile Blue based near-infrared emission. *Chem. Commun.* 50(7) **2013** 882-884.

[52] V. H. Frade, M. S. T. Goncalves, P. J. Coutinho and J. C. Moura, Synthesis and spectral properties of long-wavelength fluorescent dyes. *Journal of Photochemistry and Photobiology A: Chemistry.* 185(2-3) (***2007***) 220–230.

[53] V. Martinez and M. Henary, Nile Red and Nile Blue: Applications and Syntheses of Structural Analogues, *Chem. Eur. J.* 22(39) (**2016**) 13764-13782,

[54] Z. Yang, Y. He, J. H. Lee, W.S. Chae, W. X. Ren, J. H. Lee, C. Kang and J. S. Kim, A Nile Red/BODIPY-based bimodal probe sensitive to changes in the micropolarity and microviscosity of the endoplasmic reticulum. *Chem. Commun.* 50(79) (**2014**) 11672-11675,

[55] M. Kubinyi, J. Brátán, A. Grofcsik, L. Biczók, B. Poór, I. Bitter, A. Grün, B.; Bogáti and K. Tóth, Proton transfer and supramolecular complex formation between Nile Blue and tetraundecylcalix[4]resorcinarene-a fluorescence spectroscopic study, *J. Chem. Soc., Perkin Trans.*2(10) (**2002**) 1784–1789,

[56] A. Yadigarli, Q. Song, S. I. Druzhinin, and H. Schönherr, Probing of local polarity in poly(methyl methacrylate) with the charge transfer transition in Nile red, *Beilstein J. Org. Chem. 15(1)* (**2019**) 2552–2562,

[57] W. Li, L. Li, H. Xiao, R. Qi, Y. Huang, Z. Xie and H. Zhang, Iodo-BODIPY: a visible-light-driven, highly efficient and photostable metal-free organic photocatalyst. *RSC advances*, *3*(32)( **2013**) 13417-13421,

[58] J. Jose and K. Kevin Burgess, Syntheses and Properties of Water-Soluble Nile Red Derivatives. *J. Org. Chem. 71(20)*, *(***2006**) 7835-7839.

[59] A. M. Brouwer, Standards for photoluminescence quantum yield measurements in solution (IUPAC Technical Report). *Pure and Applied Chemistry*, *83*(12) (**2011**) 2213-2228.

## CHAPTER 6

[1] R. Moorthy, K. Prabhu and P. Murthy, Studies on the isolation and effect of an orally active hypoglycemic principle from the seeds of fenugreek (*Trigonella foenum graecum*), *Diabetes Bull.* 9 (**1989**) 69–72,

[2] J. Mishkinsky, B. Joseph and F. G. Sulman, Hypoglycaemic effect of trigonelline, *Lancet* 2 (**1967**) 1311–1312.

[3] A. E. van Dijk, M. R. Olthof, J. C. Meeuse, E. Seebus, R. J. Heine and R. M. van Dam, Acute effects of decaffeinated coffee and the major coffee components chlorogenic acid and trigonelline on glucose tolerance, *Diabetes Care*, 32, (**2009**), 1023–1025.

[4] M. R. Olthof, A. E. van Dijk, C. F. Deacon, R. J. Heine, R. M. van Dam, Acute effects of decaffeinated coffee and the major coffee components chlorogenic acid and trigonelline on incretin hormones, *Nutr. Metab.* (Lond) 8 (**2011**) 10.

[5] J. Zhou and S. Zhou, Protection of Trigonelline on Experimental Diabetic Peripheral Neuropathy. Evidence-Based Complementary and Alternative Medicine, vol. 2012, Article ID 8 (**2012**) 164219.

[6] J. Zhou, Trigonelline: a plant alkaloid with therapeutic potential for diabetes and central nervous system disease, *Current Medicinal Chemistry,* 19 (**2012**) 3523-3531,

[7] J. Zhou, S. Zhou and S. Zeng, Experimental diabetes treated with Trigonelline: Effect on β-cell and pancreatic oxidative parameters. Fundamental & Clinical Pharmacology. In press.

[8] Jozsef Szejtli, Introduction and General Overview of Cyclodextrin Chemistry, *Chem. Rev.* 98 (**1998**) 1743-1753,

[9] X. Ge, Z. Huang, S. Tian, Y. Huang and C. Zeng, Complexation of carbendazim with hydroxypropyl-β-cyclodextrin to improve solubility and fungicidal activity, *Carbohydrate Polymers* 89 (**2012**) 208–212.

[10] K. Srinivasan, K. Sivakumar and T. Stalin, 6-Dinitroaniline and β-cyclodextrin inclusion complex properties studied by different analytical methods, *Carbohydrate Polymers,* 113 (**2014**) 577–587.

[11] Y. Yao, Y. Xieb, C. Hong, G. Lic, H. Shen and G. Ji, Development of a myricetin/hydroxypropyl-Î²-cyclodextrin inclusion complex: Preparation, characterization, and evaluation, *Carbohydrate Polymers* 110 (**2014**) 329–337.

[12] G. Corti, M. Cirri, F. Maestrelli, N. Mennini and P. Mura, Sustained-release matrix tablets of metformin hydrochloride in combination with triacetyl-β-cyclodextrin, *European Journal of Pharmaceutics and Biopharmaceutics* 68 (**2008**) 303–309.

[13] S. Ma, W. Chen, X. Yang, N. Zhang, S. Wang, L. Liu and L. Yang, Alpinetin/hydroxypropyl-β-cyclodextrin host–guest system: Preparation, characterization, inclusion mode, solubilization and stability, *Journal of Pharmaceutical and Biomedical Analysis*, 67–68 (**2012**) 193–200.

[14] L. Szente and J. Szejtli, Highly soluble cyclodextrin derivatives: chemistry, properties, and trends in development, Advanced Drug Delivery Reviews 36 (**1999**) 17–28.

[15] M. e. Brewster and T. Loftsson, Cyclodextrins as pharmaceutical solubilizers, *Advanced Drug Delivery Reviews* 59 (**2007**) 645–666.

[16] P. Tang, X. Ma, D. Wu, S. Li, K. Xu, B. Tang and H. Li, Posaconazole/hydroxypropyl-β-cyclodextrin host-guest system: Improving dissolution while maintaining antifungal activity, *Carbohydrate Polymers* 142 (**2016**) 16-23.

[17] L. Hu, H. Zhang, W. Song, D. Gu and Q. Hu, Investigation of inclusion complex of cilnidipine with hydroxypropyl-β-cyclodextrin, *Carbohydrate Polymers* 90 (**2012**) 1719–1724.

[18] L. Hu, H. Zhang, W. Song, D. Gu and Q. Hu, Investigation of inclusion complex of cilnidipine with hydroxypropyl-β-cyclodextrin, *Carbohydrate Polymers* 90 (**2012**) 1719–1724.

[19] S. Barman, D. Ekka, S. Saha and M. N. Roy, NMR, surface tension and conductance study to investigate host–guest inclusion complexes of three sequential ionic liquids with β-cyclodextrin in aqueous media, *Chemical Physics Letters* 658 (**2016**) 43–50.

[20] Y. Liao, X. Zhang, C. Li, Y. Huang, M. Lei, M. Yan, Y. Zhou and C. Zhao, Inclusion complexes of HP-β-cyclodextrin with agomelatine: Preparation,

characterization, mechanism study and in vivo evaluation, *Carbohydrate Polymers,* 147 (**2016**) 415-425.

[21] Z. Huanga, S. Tiana, X. Gea, J. Zhanga, S. Lia, M. Lia, J. Chenga and H. Zheng, Enhancing exopolysaccharide antioxidant formation and yield from *Phellinus* species through medium optimization studies, *Carbohydrate Polymers* 107 (**2014**) 241–246.

[22] Y. Yao, Y. Xie, C. Hong, G. Li, H. Shen and G. Ji, Development of a myricetin/hydroxypropyl-β-cyclodextrin inclusion complex: Preparation, characterization, and evaluation, *Carbohydrate Polymers* 110 (**2014**) 329–337.

[23] P. J. Salústio, P. Pontes, C. Conduto, I. Sanches, C. Carvalho, J. Arrais and H. M. Cabral Marques Advanced Technologies for Oral Controlled Release: Cyclodextrins for Oral Controlled Release, *AAPS PharmSciTech,* 12(4) (**2011**) 1276-1292.

[24] W. Misiuk and M. Zalewska, Investigation of inclusion complex of trazodone hydrochloride with hydroxypropyl-b-cyclodextrin, *Carbohydrate Polymers* 77 (**2009**) 482–488.

[25] S. Saha, A. Roy, K. Roy and M. N. Roy, Study to explore the mechanism to form inclusion complexes of *β*-cyclodextrin with vitamin molecules, *Scientific reports* 6 (**2016**) 35764.

[26] P. Tang, X. Ma, D. Wu, S. Li, K. Xu, B. Tang and H. L, Posaconazole/hydroxypropyl-β-cyclodextrin host–guest system: Improving dissolution while maintaining antifungal activity, *Carbohydrate Polymers* 142 (**2016**) 16–23.

[27] P. D. Ross and S. Subramanian, Thermodynamics of protein association reactions: forces contributing to stability, *Biochemistry*, 20 (11) (**1981**) 3096–3102.

[28] Y. Wei, J. Zhang, Y. Zhou, W. Bei, Y. Li, Q. Yuan and H. Liang, Characterization of glabridin/hydroxypropyl-β-cyclodextrin inclusion complex with robust

solubility and enhanced bioactivity, *Carbohydrate Polymers* 159 (**2017**) 152–160.

[29] S. Jiang, H. Liu, W. Cai, A. Bai, Y. Ouyang and Y. Hu, Quasi-spherical silver nanoparticles with high dispersity and uniform sizes: preparation, characterization and bioactivity in their interaction with bovine serum albumin, *Luminescence* (**2016**).

[30] M. Ahumada, E. Lissi, A. M. Montagut, F. V. Henríquez, N. L. Pacioni and E. I. Alarcon, Association models for binding of molecules to nanostructures, *The Analyst,* 142 (**2017**) 2067-2089.

[31] H. Yisak, M. R. Abshiro and B. S. Chandravanshi, New fluorescence spectroscopic method for the simultaneous determination of alkaloids in aqueous extract of green coffee beans, *Chemistry Central Journal,* 12(1) (**2018**) 1-7.

[32] M. N. Roy, M. C. Roy and K. Roy, Investigation of Inclusion Complex formed by Ionic Liquid and β-Cyclodextrin through Hydrophilic and Hydrophobic Interactions *RSC Adv., 5*(70) (**2015**) 56717-56723.

[33] L. A. Soares, A. F. Vasconcelos Borges Leal, L. F. Fraceto, E. Rose Maia, I. Sabioni Resck, M. J. Kato, E. de Sousa Gil, A. Ribeiro de Sousa, L. Carlos da Cunha and K. Rocha Rezende, Inclusion complexes of γ-cyclodextrin and carboxyl-modified γ-cyclodextrin with C60: Synthesis, characterization and controlled release application via microgels, *J. Incl. Phenom. Macrocycl. Chem.* 64 (**2009**) 23–35.

[34] C. Yuan, Z. Jin, X. Xu, H. Zhuang and W. Shen, Inclusion complex of astaxanthin with hydroxypropyl-β-cyclodextrin: UV, FTIR, $^{1}$H NMR and molecular modeling studies, *Carbohydrate Polymers* 89 (**2012**) 492–496.

[35] J. Wang, Y. Cao, B. Sun and C. Wang, Characterisation of inclusion complex of *trans*-ferulic acid and hydroxypropyl-β-cyclodextrin, *Food Chemistry* 124 (**2011**) 1069–1075.

[36] R. Ghosh, D. Ekka, B. Rajbanshi, A. Yasmin and M. N. Roy, Synthesis, characterization of 1-butyl-4-methylpyridinium lauryl sulfate and its

inclusion phenomenon with β-cyclodextrin for enhanced applications, *Colloids and Surfaces A: Physicochemical and Engineering Aspects* 548 (**2018**) 206-217,

## CHAPTER 7

[1] T. Tanigawa, R. Pai, T. Arakawa and A. S. Tarnawski, Rebamipide inhibits gastric cancer cell growth, Digestive diseases and sciences. 52 (**2007**) 240-247.

[2] S. J. Moon, Y. J. Woo, J. H. Jeong, M. K. Park, H. J. Oh, J. S. Park, E. K. Kim, M. L. Cho, S. H. Park, H. Y. Kim and J. K. Min, Rebamipide attenuates pain severity and cartilage degeneration in a rat model of osteoarthritis by downregulating oxidative damage and catabolic activity in chondrocytes, Osteoarthritis and Cartilage. 20 (**2012**) 1426-1438.

[3] T. Izawa, I. R. Hutami and E. Tanaka, Potential role of rebamipide in osteoclast differentiation and mandibular condylar cartilage homeostasis, Current rheumatology reviews. **14** (**2018**) 62-69.

[4] T. Arakawa, K. Higuchi, Y. Fujiwara, T. Watanabe, K. Tominaga, E. Sasaki, N. Oshitani, T. Yoshikawa and A. S. Tarnawski. 15th anniversary of rebamipide: looking ahead to the new mechanisms and new applications, Digestive diseases and sciences. 50(1) (**2005**) S3-S11.

[5] S. Kinoshita, S. Awamura, K. Oshiden, N. Nakamichi, H. Suzuki and N. Yokoi, Rebamipide (OPC-12759) in the treatment of dry eye: a randomized, double-masked, multicenter, placebo-controlled phase II study, Ophthalmology. 119 (12) (**2012**) 2471-2478.

[6] P. K. Babu, M. R. Bodireddy, R. C. Puttaraju, D. Vagare, R. Nimmakayala, N. Surineni, M. R. Gajula and P. Kumar, Magic Bullet! Rebamipide, a Superior Anti-ulcer and Ophthalmic Drug and Its Large-Scale Synthesis in a Single Organic Solvent via Process Intensification Using Krapcho Decarboxylation, *Org. Process Res. Dev.* 22 (7) (**2018**) 773–779,

[7] B. K. Barman, K. Roy and M. N. Roy, Probing Inclusion Complexes of Pentoxifylline and Pralidoxim inside Cyclic Oligosaccharides by Physicochemical Methodologies, Z. Phys. Chem, 233 (8) (**2019**) 1109-1127.

[8] M. N. Roy, S. Barman and S. Saha, Probing Inclusion Complex Formation of Amantadine Hydrochloride with 18-Crown-6 in Methanol by Physicochemical Approach, Z. Phys. Chem. 231 (**2017**) 1111-1126,

[9] K. Roy, S. Saha, B. Datta, L. Sarkar and M. N. Roy, Study on Host-Guest Inclusion Complexation of a Drug in Cucurbit [6] uril, Z. Phys. Chem, 232 (2) (**2018**) 281-293.

[10] M. R. Infante, L. Perez, A. Pinazo, P. Clapes, M. C. Moran and K. Holmberg, Edited*;* Surfactant science series 114; Marcel Dekker, Inc.: New York, (**2003**) 193-216.

[11] X. J. Loh, Supramolecular host–guest polymeric materials for biomedical applications, Materials Horizons. 1(2) (**2014**) 185-195.

[12] Z. Sebestyén, A. B. Barcza and J. Rohonczy, Inhibition and disintegration of insulin amyloid fibrils: a facile supramolecular strategy with p-sulfonatocalixarenes, Journal of Inclusion Phenomena and Macrocyclic Chemistry, 73(1-4) (**2012**) 199-210.

[13] K. S. Sharma, S. R. Patil, A. K. Rakshit, K. Glenn, M. Doiron, R. M. Palepu and P. A. Hassan, Self-aggregation of a cationic– nonionic surfactant mixture in aqueous media: tensiometric, conductometric, density, light scattering, potentiometric, and fluorometric studies, J. Phys. Chem. 108 (**2004**) 12804-12812.

[14] M. Prasad, S. P. Moulic and R. Palepu, Journal of colloid and interface science. 284(2) **(2005**) 658-666.

[15] C. Das, T. Chakraborty, S. Gosh and B. Das, Mixed micellization of anionic–nonionic surfactants in aqueous media: a physicochemical study with theoretical consideration, Colloid and Polymer. Science, 286 (**2008**) 1143.

[16] S. Gosh and S. P. Moulik, Interfacial and micellization behaviors of binary and ternary mixtures of amphiphiles (Tween-20, Brij-35, and sodium dodecyl

sulfate) in aqueous medium, Journal of Colloid and Interface Science, 208 (**1998**) 357.

[17] S. Ikeda and K. Fujio, The salt-induced sphere-rod transition of micelles of dodecylpyridinium iodide in aqueous NaI solutions, Colloid & Polymer Science, 270 (**1992**) 1009.

[18] S. Backlund, H. Hoiland, O. J. Kvammea and E. Ljosland, Acta Chem. Scand. 36A (**1982**) 697.

[19] A. M. Bolkhus, H. Høiland, E. Gilje and S. Backlund, The effect of inorganic salt on the solubilization of alcohols in aqueous surfactant solutions, Journal of colloid and interface science. 124 (1) (**1988**) 125-129.

[20] P. Job. Formation and stability of inorganic complexes in solution, Ann Chim. 9, (**1928**), 113-203.

[21] Y. Liao, X. Zhang, C. Li, Y. Huang, M. Lei, M. Yan, Y. Zhou and C. Zhao, Inclusion complexes of HP-β-cyclodextrin with agomelatine: preparation, characterization, mechanism study and in vivo evaluation, Carbohydrate Polymers. 147 (**2016**) 415-425.

[22] S. Tasneem, Hydration and Solvation Effect of Glycine and Glycylglycine Molecules with β-Cyclodextrin in Aqueous Media. A Thermodynamic Characteristic of Interaction, Zeitschrift fur Physikalische Chemie, 231 (11-12) (**2017**) 1831-1847.

[23] B. Rajbanshi, S. Saha, K. Das, B. K. Barman, S. Sengupta, A. Bhattacharjee and M. N. Roy, Study to probe subsistence of host-guest inclusion complexes of α and β-cyclodextrins with biologically potent drugs for safety regulatory dischargement, Scientific reports. 8, (1) (**2018**) 13031.

[24] Y. Yao, Y. Xie, C. Hong, G. Li, H. Shen and G. Ji, Development of a myricetin/hydroxypropyl-β-cyclodextrin inclusion complex: Preparation, characterization, and evaluation, Carbohydrate Polymers. 110 (**2014**) 329–337.

[25] S. Chakraborty, S. Basu, A. Lahiri and S. Basak, Inclusion of chrysin in β-cyclodextrin nanocavity and its effect on antioxidant potential of chrysin: A

spectroscopic and molecular modeling approach, Journal of Molecular Structure. 977 (**2010**) 180–188.

[26] Y. Wei, J. Zhang, Y. Zhou, W. Bei, Y. Li, Q. Yuan and H. Liang, Characterization of glabridin/hydroxypropyl-β-cyclodextrin inclusion complex with robust solubility and enhanced bioactivity, Carbohydrate Polymers. 159 (**2017**) 152-160.

[27] R. L. Abarca, F. L. Rodríguez, A. Guarda, M. Galotto and J. E. Bruna, Food Chemistry. 196 **(2016**) 968–975.

[28] C. Yuan, Z. Jin and X. Xu, Inclusion complex of astaxanthin with hydroxypropyl-β-cyclodextrin: UV, FTIR, 1H NMR and molecular modeling studies, Carbohydrate Polymers. 89 (**2012**) 492–496.

[29] S. Ma, W. Chen, X. Yang, N. Zhang, S. Wang, L. Liu and L. Yang, Alpinetin/hydroxypropyl-β-cyclodextrin host–guest system: Preparation, characterization, inclusion mode, solubilization and stability, Journal of Pharmaceutical and Biomedical Analysis. 67 (**2012**) 193–200.

[30] P. Tang, S. Li, L. Wang, H. Yang, J. Yan and H. Li, Inclusion complexes of chlorzoxazone with β-and hydroxypropyl-β-cyclodextrin: characterization, dissolution, and cytotoxicity, Carbohydrate Polymers. 131 (**2015**) 297–305.

[31] L. Szente and J. Szejtli, Highly soluble cyclodextrin derivatives: chemistry, properties, and trends in development, Advanced Drug Delivery Reviews. 36 (**1999**) 17–28.

[32] H. Qu, L. Yang, J. Yu, T. Dong, M. Rong, J. Zhang, H. Xing, Wang, L. Pan and H. Liu. A redox responsive controlled release system using mesoporous silica nanoparticles capped with Au nanoparticles, RSC Advances, 7(57) (**2017**) 35704-35710,

## CHAPTER 8

[1] J. Kockler, M. Oelgemöller, S. Robertson and B. D. Glass, Photostability of sunscreens, *Journal of Photochemistry and Photobiology C: Photochemistry Reviews, 13*(1), (**2012**), 91-110.

[2] S. Afonso, K. Horita, J.P. Sousa e Silva, I.F. Almeida, M.H. Amaral, P.A. Lobão, P.C. Costa, Margarida S. Miranda, Joaquim C.G. Esteves da Silva and J.M. Sousa Lobo, Photodegradation of avobenzone: Stabilization effect of antioxidants, *Journal of Photochemistry and Photobiology B: Biology*, 140, (**2014**) 36-40.

[3] C. Stiefel, T. Schubert and G. E. Morlock, Bioprofiling of Cosmetics with Focus on Streamlined Coumarin Analysis, *ACS Omega,* 2, (**2017**), 5242−5250.

[4] R. Wang, X. Wang, Y. Zhan, Z. Xu, Z. Xu, X. Feng, S. Li and H. Xu, A Dual Network Hydrogel Sunscreen Based on Poly-γ-glutamic Acid/Tannic Acid Demonstrates Excellent Anti-UV, Self-Recovery, and Skin-Integration Capacities, *ACS Appl. Mater. Interfaces,* 11, (**2019**), 37502−37512.

[5] M. Morsella, N. D. Alessandro, A. E. Lanterna and J. C. Scaiano, Improving the Sunscreen Properties of TiO2 through an Understanding of Its Catalytic Properties, ACS Omega, 1, (**2016**), 464−469.

[6] N. Ž. Knezević, N. Ilic, V. Đokic, R. Petrovic, Đ. Janackovic and M. Silica, Organosilica Nanomaterials as UV-Blocking Agents, *ACS Appl. Mater. Interfaces,* 10, (**2018**), 20231−20236.

[7] D. Li, L. Qian, Y. Feng, J. Feng, P. Tang and L. Yang, Co-intercalation of Acid Red 337 and a UV Absorbent into Layered Double Hydroxides: Enhancement of Photostability, ACS Appl. Mater. Interfaces 6 (**2014**) 20603−20611.

[8] L. Yang, L. Qian, Y. Feng, P. Tang and D. Li, Acid Blue 129 and Salicylate Cointercalated Layered Double Hydroxides: Assembly, Characterization, and Photostability, *Ind. Eng. Chem. Res.* 53 (**2014**) 17961−17967.

[9] V. Leandri, J. M. Gardner and M. Jonsson, Coumarin as a Quantitative Probe for Hydroxyl Radical Formation in Heterogeneous Photocatalysis, *J. Phys. Chem. C,* 123 (**2019**) 6667−6674.

[10] C. M. Krauter, J. Mohring, T. Buckup, M. Pernpointner and M. Motzkus, Ultrafast branching in the excited state of coumarin and umbelliferone, Phys. Chem. Chem. Phys., 15 (**2013**) 17846.

[11] V. Kumar, F. A. Al-Abbasi, A. Verma, M. Mujeeb and F. Anwar, Umbelliferone β-D-galactopyranoside Exerts Anti-inflammatory Effect by Attenuating COX-1 and COX-2, *Toxicological Research,* 4(4), (**2015**), 1072-1084.

[12] D. R. Telangea, S. B. Nirgulkara, M, J. Umekara, A, T. Patila, A. M. Petheb and N.R. Bali, Enhanced transdermal permeation and anti-inflammatory potential of phospholipids complex-loaded matrix film of umbelliferone: Formulation development, physico-chemical and functional characterization, *European Journal of Pharmaceutical Sciences,* 131, (**2019**), 23-38.

[13] L. Pan, X. Z. Li, Z.Q. Yan, H. R. Guo and B. Qin, Phytotoxicity of umbelliferone and its analogs: Structureeactivity relationships and action mechanisms, *Plant Physiology and Biochemistry* 97, (**2015**), 272-277.

[14] O. Mazimba, Umbelliferone: Sources, chemistry and bioactivities review, *Bulletin of Faculty of Pharmacy, Cairo University*, *55*(2) (**2017**) 223-232.

[15] F. Anwar, F. A. Al-Abbasi, N. Sethi and V. Kumar, Umbelliferone β-D-galactopyranoside inhibits chemically induced renal carcinogenesis via alteration of oxidative stress, hyperproliferation and inflammation: possible role of NF-kB, *Toxicology Research*, *4*(5) (**2015**) 1308-1323.

[16] V. Leandri, J. M. Gardner and M. Jonsson, Coumarin as a Quantitative Probe for Hydroxyl Radical Formation in Heterogeneous Photocatalysis, *J. Phys. Chem. C,* 123 (**2019**) 6667−6674.

[17] A. Nagarsenkar, L. Guntuku, S. K. Prajapti, S. D. Guggilapu, R. Sonar, G. M. N. Vegi and B. N. Babu, Umbelliferone–oxindole hybrids as novel apoptosis inducing agents, *New J. Chem.,* 41 (**2017**) 12604.

[18] M. N. Roy, S. Saha, S. Barman and D, Ekka, Host–guest inclusion complexes of RNA nucleosides inside aqueous cyclodextrins explored by physicochemical and spectroscopic methods, *RSC Adv.,* 6 (**2016**) 8881-8891.

[19] B. K. Barman, S. Barman and M. N. Roy, Inclusion complexation between tetrabutylphosphonium methanesulfonate as guest and α- and β-

cyclodextrin as hosts investigated by physicochemical methodology, *Journal of molecular liquids,* 264 (**2018**) 80-87.

[20] R. Ghosh, K. Roy, A. Subba, P. Mandal, S. Basak, M. Kundu and M. N. Roy, Case to case study for exploring inclusion complexes of an anti-diabetic alkaloid with α and β cyclodextrin molecules for sustained Dischargement, *Journal of Molecular Structure,* 1200, **(2020),** 126988.

[21] T. Mori, R. Tsuchiya, M. Doi, N. Nagatani and T. Tanaka, Solubilization of ultraviolet absorbers by cyclodextrin and their potential application in cosmetics, *Journal of Inclusion Phenomena and Macrocyclic Chemistry,* 93 (1-2) (**2019**) 91-96.

[22] G. M. Metilda and J. P. Kumari, Preparation and Characterization of Umbelliferone and Hydroxy Propyl α-Cyclodextrin Inclusion Complex, 5(5) (**2015**) 158-160.

[23] E. Wang, G. Chen and C. Han, Crystal Structures of β-Cyclodextrin Inclusion Complexes with 7-Hydroxycoumarin and 4-Hydroxycoumarin and Substituent Effects on Inclusion Geometry, *Chin. J. Chem.* 29 (**2011**) 617-622.

[24] H. Rahaman, N. Roy, A. Roy, S. Ray and M. N. Roy, Exploring Existence of Host-Guest Inclusion Complex of β-Cyclodextrin of a Biologically Active Compound with the Manifestation of Diverse Interactions, *Emerging Science Journal,* 2(5) (**2018**) 251-260.

[25] Q. Geng, T. Li, X. Wang, W. Chu, M. Cai, J. Xie and H. Ni, The mechanism of bensulfuronmethyl complexation with β-cyclodextrin and 2-hydroxypropyl-β-cyclodextrin and effect on soil adsorption and bio-activity, *Scientific reports, 37*(8) (**1998**) 1547-1555.

[26] O. Adeoye, J. Conceição, P. A. Serra, A. B. da Silva, N. Duarte, R. C. Guedes, M. C. Corvo, A. A. Ricardo, L. Jicsinszky, T. Casimiro and H. C. Marques, Cyclodextrin solubilization and complexation of antiretroviral drug lopinavir: In silico prediction; Effects of derivatization, molar ratio and preparation method, *Carbohydrate Polymer, 227,* (**2020**), 115287

[27] Y. Deng, Y. Pang, Y. Guo, Y. Ren, F. Wang, X. Liao and B. Yang, Host-guest inclusion systems of daidzein with 2-hydroxypropyl-bcyclodextrin (HP-β-CD) and sulfobutyl ether-b-cyclodextrin (SBE-β-CD): Preparation, binding behaviors and water solubility, *Journal of Molecular Structure,* 1118, (**2016**), 307-315.

[28] P. H. Shan, J. Zhao, X. Y. Deng, R. L. Lin, B. Bian, Z. Tao, X. Xiao and J. X. Liu, Selective recognition and determination of phenylalanine by a fluorescent probe based on cucurbit[8]uril and palmatine, *Analytica Chemica Acta,* 1104 (**2020**) 164-171.

[29] A. Favrelle, G. Gouhier, F. Guillen, C. Martin, N. Mofaddel, S. Petit, K. M. Mundy, S. P. Pitre and B. D. Wagner, Structure−Binding Effects: Comparative Binding of 2-Anilino-6-naphthalenesulfonate by a Series of Alkyl- and Hydroxyalkyl-Substituted β-Cyclodextrins, *J. Phys. Chem. B,* 119 (**2015**) 12921−12930.

[30] T. Kida, T. Iwamoto, Y. Fujino, N. Tohnai, M. Miyata and M. Akashi, Strong Guest Binding by Cyclodextrin Hosts in Competing Nonpolar Solvents and the Unique Crystalline Structure, *Organic Letters, 13* (17) (**2011**) 4570-4573.

[31] N. Roy, R. Ghosh, K. Das, D. Roy, T. Ghosh and M. N. Roy, Study to synthesize and characterize host-guest encapsulation of antidiabetic drug (TgC) and hydroxy propyl-b-cyclodextrin augmenting the antidiabetic applicability in biological system, *Journal of Molecular Structure,* 1179 (**2019**) 642-650.

[32] M. Natha, R. Jairath, G. Eng, X. Song and A. Kumar, New diorganotin(IV) derivatives of 7-hydroxycoumarin (umbelliferone) and their adducts with 1,10-phenanthroline, *Spectrochimica Acta Part A: Molecular and Biomolecular Spectroscopy*, *61* (13-14), (**2005**) 3155-3161.

[33] D. R. Telangea, S. B. Nirgulkara, M. J. Umekara, A. T. Patila, A. M. Petheb and N. R. Bali, Enhanced transdermal permeation and anti-inflammatory potential of phospholipids complex-loaded matrix film of umbelliferone: Formulation development, physico-chemical and functional characterization, *European Journal of Pharmaceutical Sciences,* 131 (**2019**) 23-28.

[34] A. Dutta, N. Roy, K. Das, D. Roy, R. Ghosh and M. N. Roy, Synthesis and Characterization of Host Guest Inclusion Complexes of Cyclodextrin Molecules with Theophylline by Diverse Methodologies, *Emerging Science Journal,* 4(1) (**2020**) 52-72.

[35] R. G. dos Santos, J. C. M. Bordado and M. M. Mateus. "1H-NMR dataset for hydroxycoumarins–Aesculetin, 4-Methylumbelliferone, and umbelliferone." *Data in brief,* 8 (**2016**) 308-311.

[36] C. R. Arza, P. Froimowicz and H. Ishida, Smart chemical design incorporating umbelliferone as natural renewable resource toward the preparation of thermally stable thermosets materials based on benzoxazine chemistry, *RSC Adv.,* 5, (**2015**), 97855.

[37] B. Rajbanshi, A. Dutta, B. Mahato, D. Roy, D, K. Maiti, S. Bhattacharyya and M. N. Roy, Study to explore host guest inclusion complexes of vitamin $B_1$ with CD molecules for enhancing stability and innovative application in biological system, *Journal of Molecular Liquids,* 298 **(2020**) 111952.

[38] P. Froimowicz, C. R. Arza, S. Ohashi and H. Ishida, Tailor-Made and Chemically Designed Synthesis of Coumarin-Containing Benzoxazines and Their Reactivity Study Toward Their Thermosets, *Journal of Polymer Science Part A*, 54(10), (**2015**), 1428-1435.

[39] I. Lacatusu, N. Badea, A. Murariu, O. Oprea, D. Bojin and A. Meghea, Antioxidant Activity of Solid Lipid Nanoparticles Loaded with Umbelliferone, *Soft Materials,* 11(1), (**2013**), 75-84.

[40] K. Das, B. Datta, B. Rajbanshi and M. N. Roy, Evidences for Inclusion and Encapsulation of an Ionic liquid with β-CD and 18-C-6 in Aqueous Environments by Physicochemical Investigation, *J. Phys. Chem. B,* 122( 5) (**2018**) 1679-1694.

[41] C. Stiefel, T. Schubert and G. E. Morlock, Bioprofiling of Cosmetics with Focus on Streamlined Coumarin Analysis, *ACS Omega,* 2 (**2017**) 5242−5250.

[42] N. Roy, P. Bomzan and M. N. Roy, Probing Host-Guest inclusion complexes of Ambroxol Hydrochloride with α- & β-Cyclodextrins by physicochemical

contrivance subsequently optimized by molecular modeling simulations, *Chemical Physics Letters,* 748 (**2020**) 137372.

[43] G. Nafie, G. Vitale, L. C. Ortega and N. N. Nassar, Nanopyroxene grafting with β-Cyclodextrin monomer for wastewater applications, *ACS Applied Materials & Interfaces,* 9(48) (**2017**) 42393-42407.

[44] L. Ismahan, N. Leila, M. Fatiha, G. Abdelkrim, C. Mouna, B. Nada, H. Brahim, Computational study of inclusion complex of l-Glutamine/beta-Cycldextrin: Electronic and intermolecular interactions investigations, *Journal of Molecular Structure,* 1206 (**2020**) 127740.

[45] Y. Akae, Y. Koyama, H. Sogawa, Y. Hayashi, S. Kawauchi, S. Kuwata and T. Takata, Structural Analysis and Inclusion Mechanism of Native and Permethylated aCyclodextrin-Based Rotaxanes Containing Alkylene Axles, *Chem. Eur. J.* 22 (**2016**) 5335–5341.

[46] U. Chaube, D. chhatbar and H. Bhatt, 3D-QSAR, molecular dynamics simulations and molecular docking studies of benzoxazepine moiety as mTOR inhibitor for the treatment of lung cancer, *Bioorganic & Medicinal Chemistry Letters*, 26(3), (**2016**), 864-874.

[47] I. Daoud, N. Melkemi, T. Salah and S. Ghalem, Combined QSAR, molecular docking and molecular dynamics study on new Acetylcholinesterase and Butyrylcholinesterase inhibitors, *Computational biology and chemistry*, 74, (**2018**), 304-326.

# INDEX

ACS OMEGA

http://pubs.acs.org/journal/acsodf

Article

# Exploring the Inclusion Complex of a Drug (Umbelliferone) with α-Cyclodextrin Optimized by Molecular Docking and Increasing Bioavailability with Minimizing the Doses in Human Body

Niloy Roy, Biswajit Ghosh, Debadrita Roy, Biswajit Bhaumik, and Mahendra Nath Roy*

Cite This: https://dx.doi.org/10.1021/acsomega.0c04716

Read Online

ACCESS | Metrics & More | Article Recommendations | Supporting Information

**ABSTRACT:** In this study, umbelliferone and α-cyclodextrin host molecules have been mixed up through a coprecipitation method to prepare a supramolecular complex to provide physical insights into the formation and stability of the inclusion complex (IC). The prepared hybrid was characterized by $^1$H nuclear magnetic resonance ($^1$H NMR), Fourier transform infrared (FTIR) spectroscopy, electrospray ionization (ESI) mass spectrometry, DSC, and fluorescence spectroscopic studies. Job's plot provides a stoichiometric ratio of 1:1 and the Benesi−Hildebrand double reciprocal plot gives binding constant values using fluorescence spectroscopic titrations and the ESI mass data support the experimental observations. The results of molecular modeling were systematically analyzed to validate the inclusion complexation. In preliminary computational screening, α-cyclodextrin IC of umbelliferone was found to be quite stable based on the docking score, binding free energies, and dynamic simulations. In addition, the results obtained from $^1$H NMR and FTIR spectroscopy studies supported the inclusion complexation phenomenon. The results obtained from computational studies were found to be consistent with the experimental data to ascertain the encapsulation of umbelliferone into α-cyclodextrin.

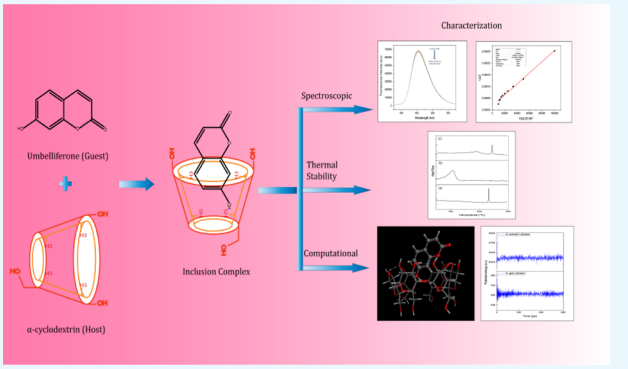


## 1. INTRODUCTION

In recent years, skin allergy and different cancers, such as basal and squamous cell carcinomas and malignant melanoma have become some of the most important health issues because of extensive exposure to sunlight as well as ultraviolet (UV) radiation.[1,2] To tackle this problem, various UV-absorbing agents have been introduced as the formulations in cosmetic industries.[3] It is important to keep in mind that the overall impact of biologically active ingredients through cosmetics with multiple product usage over a day in the skin has to be sufficiently low with a minimum side effect. Nowadays, sunscreen ingredients are produced by various metal nanoparticles (predominantly ZnO and $TiO_2$ nanoparticles) for active UVA and UVB protection of skin, which absorb, reflect, and scatter UV radiation, along with other organic molecules as UV absorbers, for example, avobenzone and sulisobenzone.[4,5] However, there is an increasing concern regarding the adverse health and environmental effects of these sunscreen ingredients and, therefore, various researchers already have started to find safer alternatives, for example, by surface coating of hazardous nanomaterials with silica layers or by enclosing different organic UV absorbers within the framework of organosilica nanoparticles.[6] The loaded UV filter molecules encapsulated in a supramolecular matrix could easily be synthesized and dispersed so that they can be shielded from constant damage by an external mechanical force.[7]

Owing to their wide range of photostability, excellent photosensitivity, and high color strength, organic dyes have attracted significant interest and been widely used in textiles, paints, inks, electronic devices, and metal oxide ($TiO_2$) photocatalysis.[8,9] Coumarin belongs to a chemical class of benzopyrones, which include further naturally occurring derivatives, such as umbelliferone (UMB) (7-hydroxycoumarin), aesculetin (6,7-dihydroxycoumarin), or herniarin (7-methoxycoumarin), showing a wide variety of potential biological activities, for example, lipid-lowering ability, anticarcinogenic activity, and HIV-inhibition activity.[10,11] The odor-fixing properties and sweet, warm, and vanilla-like scent of coumarin make it a promising synthetic fragrance component or a natural ingredient of various essential oils and plant extracts, such as sweet woodruff, Tonka, or lavender, in a large number of cosmetic products.[12,13]

Received: September 25, 2020
Accepted: November 4, 2020

Scheme 1. Two-Dimensional Structure of (a) UMB and (b) α-Cyclodextrin

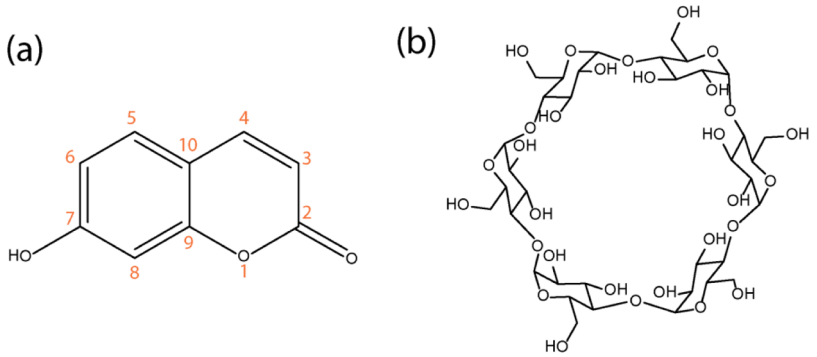


UMB, a coumarin-based molecule, has been extensively used as a sunscreen agent in cosmetics and optical brighteners in textiles.[14] UMB is a 7-hydroxycoumarin that is a pharmacologically active agent and shows antidiabetic, antihyperlipidemic, antioxidant, anti-inflammatory, and free radical-scavenging activities.[15,16] UMB has been generally introduced as the initial starting material for the preparation of more complex coumarin derivatives and is widely used as a synthon for a wider variety of coumarin-heterocycles with potential biological activity.[17]

Cyclodextrins are well-known cyclic oligosaccharides consisting of six, seven, or eight α-(1 → 4)-D-glucoside moieties, giving rise to α-, β-, and γ-CDs, respectively.[18−20] Owing to their nontoxic nature and complexation ability, CDs are generally regarded as safe and have received widespread attention for application in food, agriculture, cosmetics, and pharmaceutical industries.[21−23] Recently, various works have been carried out with different organic UV-absorbing agents with cyclodextrins, for example, Mori et al.[24] shown that octylmethoxy cinnamate and avobenzone have been formulated with different cyclodextrins into cosmetic sunscreens. These kinds of chemical modifications through supramolecular complexation possibly will enhance the substance concentration in the upper skin layers by reducing its percutaneous penetration. Previously, a similar kind of inclusion complexation studies has been done by Meltida and Kumari and Wang et al. with UMB and βCD as well as HP-α-CD.[25,26] Herein, we have designed three different inclusion complexes and, thereafter, different kinds of characterization techniques have been applied to check the formation of the inclusion complex. In this study, we report the synthesis and characterization of the UMB + αCD inclusion complex and our main objective was to determine the influence of complexation with αCD in improving thermal stability as well as photostability (Scheme 1).

## 2. EXPERIMENTAL SECTION

**2.1. Materials.** Both UMB and α-cyclodextrin were obtained from Sigma-Aldrich Pvt. Ltd. (India). All reagents were of analytical reagent grade and were used without further purification (Table S1). Doubly distilled water was used in all experiments.

**2.2. Instruments.** All the fluorescence titrations were carried out on a bench top spectrofluorimeter from Photon Technologies International (PTI) QuantaMaster-40, USA. Solution-state nuclear magnetic resonance (NMR) experiments were performed on a Bruker AVANCE DRX 400 NMR spectrometer operating at 400 MHz for obtaining the $^1$H NMR spectra. Fourier transform infrared (FTIR) spectra were obtained using a PerkinElmer spectrometer with a resolution of 4 cm$^{-1}$. All DSC spectra were recorded using a PerkinElmer Pyris DSC 6 with 1.2 mg of the sample in all cases by heating in the range of 30−300 °C at a rate of 10 °C/min under a $N_2$ gas flow of 40 mL/min. All samples were prepared with spectroscopic grade KBr, which constituted a 100:1 ratio with respect to the total sample.

**2.3. Sample Preparation.** The inclusion complexation of UMB with αCD was prepared by applying the coprecipitation method.[27] A solution of αCD (1.38 g) and UMB (0.2 g) was prepared in 25 mL of double-distilled water in a 1:1 molar ratio and stirred at 55 °C for 48 h. The resulting clear solution was evaporated to dryness. Then, the white precipitate was filtered cautiously and washed with ethanol and water four times to eliminate uncomplexed UMB and αCD. The resulting precipitate was then dried in a hot air oven at 50 °C for 12 h. The obtained inclusion complex was kept in a desiccator prior to analysis.

**2.4. Preparation of 3D-Structures of UMB and α-Cyclodextrin.** The crystal structures of UMB (CCDC code: 1139276) and αCD (CCDC code: 125105) were collected from Cambridge Crystallographic Data Center (CCDC). The missing hydrogen atoms and atomic charges to CDs as well as UMB were added and energy minimization was carried out with force field MMFF94x and gradient 0.05 kcal·mol$^{-1}$·Å$^{-1}$ using MOE.2015 software.[28] These structures were used as a starting point to perform the computational studies.

**2.5. Molecular Docking and Simulations.** In supramolecular chemistry, molecular docking is a computational process of searching for a guest that is able to fit both geometrically and energetically in the cavity of the host moiety.[28,29] This is a process by which two molecules fit together in 3D space. The aim of docking is to predict the predominant binding mode for a guest with a host of a known three-dimensional structure. An established docking protocol for host−guest system implemented in MOE was applied. The docking was carried out with the default parameters, that is, with the triangle matcher method and ordered with the London ΔG scoring function. The top five produced poses were ranked as per their docking scores and saved in a separate database file in a .mdb format. The build-in scoring function of MOE, S-score, was used to predict the binding affinity (kcal·mol$^{-1}$) of the optimized structure of the inclusion complex.

## 3. RESULTS AND DISCUSSION

**3.1. Job's Plot.** A very reliable continuous variation method also known as Job's plot was performed in order to


https://dx.doi.org/10.1021/acsomega.0c04716
ACS Omega XXXX, XXX, XXX−XXX

validate the stoichiometry of the inclusion complex.[30] The sum of the concentrations of both components was kept constant ([UMB] + [αCD] = $1.0 \times 10^{-4}$ M) and the molar fraction of UMB ($R$ = [UMB]/([UMB] + [αCD])) varied from 0.0 to 1.0 (Table S2). In order to calculate the stoichiometry, the fluorescence emission intensity variations ($F$) of UMB were plotted versus the molar fraction ($R$).[31] Figure 1 illustrates the continuous variation spectra of the αCD/UMB system examined by fluorescence titrations.

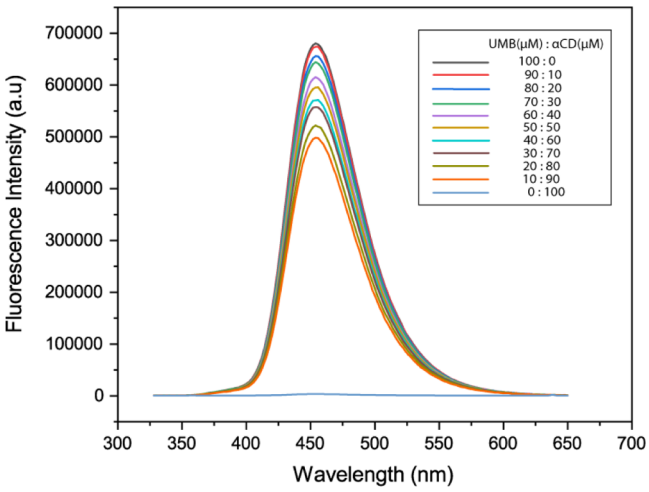


**Figure 1.** Fluorescence emission spectra of UMB by varying both host and guest such that the sum of the concentrations of both components was kept constant ([UMB] + [αCD] = $1.0 \times 10^{-4}$ M).

The plot observed in Figure 2 showed the maximum at a molar fraction of about 0.5, indicating that the stoichiometry of

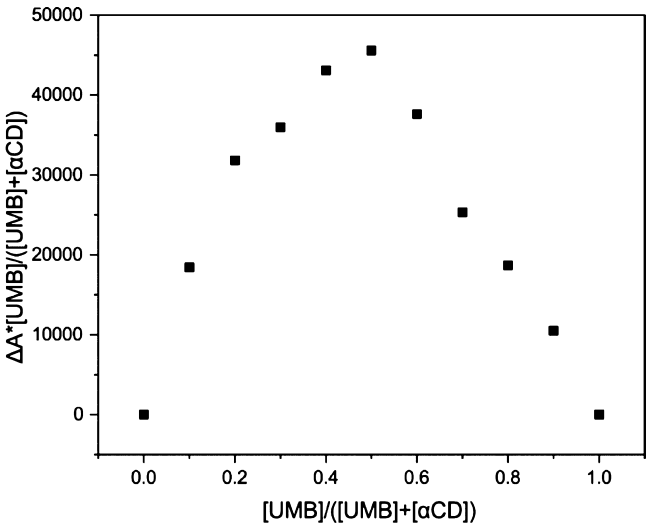


**Figure 2.** Job's plot of the UMB/αCD inclusion complex using fluorescence emission spectroscopy.

the complex UMB + αCD was 1:1 in agreement with the linear plot obtained from the Benesi–Hildebrand method.

**3.2. Association Constant Calculations.** The stoichiometry and formation constant of the UMB and αCD complex was studied by using fluorescence emission titration.[32] Association constants ($K_a$) of host–guest inclusion complexes were calculated using the modified Benesi–Hildebrand equation (eq 1) from the fluorescence experimental data. The addition of α-cyclodextrin to an aqueous solution of UMB resulted in a decrease of the measured fluorescence intensity. The fluorescence signal of UMB is highly sensitive to the addition of the αCD solution.

$$\frac{1}{F_o - F} = \frac{1}{(F_o - F_{max}) \times K_a \times [CD]^n} + \frac{1}{F_o - F_{max}} \quad (1)$$

where $F$ and $F_o$ denote the fluorescence intensity of UMB on adding αCD and pure UMB, respectively. $F_{max}$ is the saturation fluorescence intensity. $K_a$ is the association constant obtained by dividing the intercept by the slope. $n$ is the binding stoichiometry between αCD and UMB.

The binding constant of the complexes assumed with the use of eq 1 can be verified by plotting the double reciprocal plot of $1/(F_o - F)$ versus $1/[\alpha CD]$ (Table S3); this plot will be linear in the case of 1:1 complexation, but will be curved if higher-order complexes occur.[33] Figure 3 shows the double reciprocal plot, demonstrating the highly linear plot, with $R^2$ = 0.9992, confirming 1:1 complexation for this αCD.

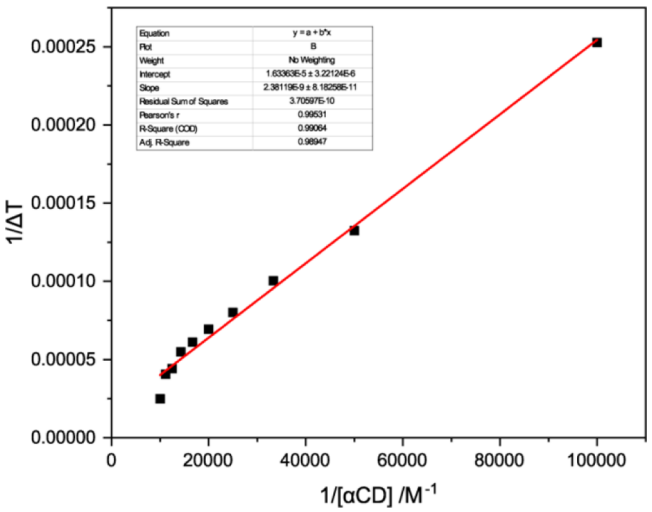


**Figure 3.** Double reciprocal Benesi–Hildebrand plot of $1/(F_o - F)$ vs $1/[\alpha CD]$ at 298.15 K.

Figure 4 depicts the fluorescence spectra of UMB with increasing concentration of αCD. There is a decrease in the fluorescence intensity of UMB with αCD addition, indicating the formation of an inclusion complex between UMB and αCD. From this fluorescence titration, we had estimated the binding constant shown in Table 1, using the intercept and slope, it was found to be $6.86 \times 10^3$ $M^{-1}$ at 298.15 K and Gibbs free energy was −5.21 kcal·mol$^{-1}$.

**3.3. FTIR Spectral Analysis.** The solid inclusion complex formation is analyzed by FTIR spectroscopy. FTIR spectroscopy is used to confirm the formation of the solid inclusion complex by considering the deviation of the peak shape position and intensity.[34] Figure 5 depicts all the spectra of pure UMB, αCD, and the UMB + αCD inclusion complex. The FTIR spectrum of pure UMB disclosed typical absorption bands at 3177 cm$^{-1}$ for phenolic (−O−H stretching), 1603 cm$^{-1}$ for (C═O stretching), 1684, 1567, and 1510 cm$^{-1}$ for (aromatic C═C stretching), and 1319 and 1135 cm$^{-1}$ for (C−O−C stretching).[35] In the case of αCD, stretching vibration of O−H at 3398 cm$^{-1}$, stretching vibration of −C−H from $-CH_2$ at 2926 cm$^{-1}$, bending vibration of −C−H from $-CH_2$, and


https://dx.doi.org/10.1021/acsomega.0c04716
ACS Omega XXXX, XXX, XXX−XXX

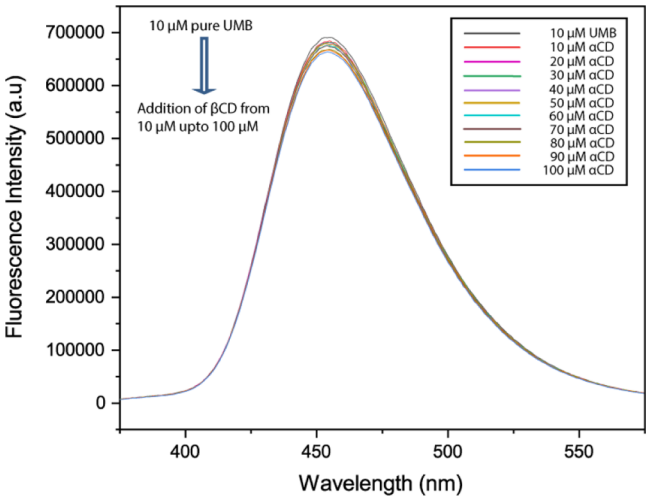


**Figure 4.** Fluorescence spectra of UMB in the absence and presence of various concentrations of $\alpha$CD at 298.2 K, where the initial concentration of UMB was 10 $\mu$M and the concentration of $\alpha$CD was varied from 10, 20, 30 $\mu$M upto 100 $\mu$M.

**Table 1. Stability Constant ($K_a$ and log $K_a$) and Gibbs Free Energy Change ($\Delta G$) at 298.15 K for the Inclusion Complexation of CDs with UMB Guest in Water (1 kcal = 4.2 kJ)**

| host | guest | $K_a$ ($M^{-1}$) | log $K_a$ | $\Delta G°$/kcal $mol^{-1}$ |
|---|---|---|---|---|
| $\alpha$CD | UMB | 6860 | 3.83 | −5.21 |

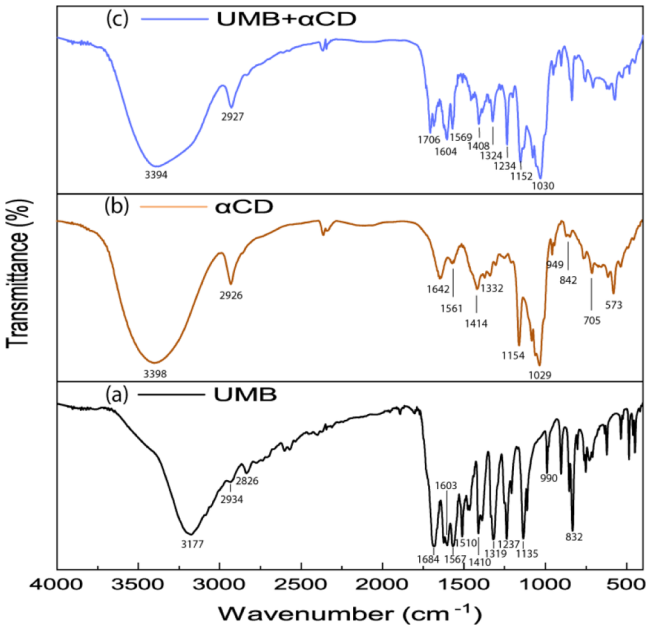


**Figure 5.** FTIR spectra of (a) UMB, (b) $\alpha$CD, and (c) UMB + $\alpha$CD inclusion complex.

bending vibration of O−H and C−O−C at 1416 and 1154 $cm^{-1}$, respectively, were found. Stretching vibration of C−C−O and skeletal vibration involving $\alpha$-1,4 linkage at 949 $cm^{-1}$ appeared at 1129 $cm^{-1}$.[36] When, the UMB + $\alpha$CD inclusion complex is formed, −O−H bond-stretching frequency of the hydroxyl group of cyclodextrin was observed at 3394 $cm^{-1}$, the C═O group of lactone moiety got shifted to 1706 $cm^{-1}$, the phenolic O−H part of UMB observed in pure guest at 3177 $cm^{-1}$ has been diminished, and aromatic C═C stretching vibrations that appeared at 1684, 1567, and 1510 $cm^{-1}$ in pure UMB are absent after inclusion complexation (Table S4). From the above data, it can be concluded that the aromatic part of UMB has been inserted into the cavity of $\alpha$-cyclodextrin.

**3.4. $^1$H NMR Studies.** The $^1$H NMR spectra of UMB, $\alpha$CD, and the inclusion complex (in $D_2O$) are shown in Figure 6. In the spectrum of the UMB + $\alpha$CD inclusion complex, appreciable chemical shift changes were observed for protons of UMB as well as $\alpha$CD in the inclusion complex with respect to the spectra of the free UMB and $\alpha$CD, respectively. The chemical shifts of the $\alpha$CD protons in the absence and presence of UMB are listed in Table 2. From the spectra, it is observed that changes in the signals of H-1, H-2, and H-4 protons on the outer surface of $\alpha$CD are negligible with $\Delta\delta$ values of −0.00, −0.03, and −0.04, respectively. However, complexation of a hydrophobic guest causes significant chemical shift changes of H-3 and H-5 protons that are present in the inner cavity of $\alpha$CD,[37,38] and in this case it was found to be an upfield shift of −0.10 and −0.06 ppm for H-3 and H-5 protons, respectively. It is to be mentioned that the chemical shift variation for H-3 was higher than that for H-5 after the formation of the inclusion complex.

To further explore the possible inclusion mode of UMB + $\alpha$CD, we compared the $^1$H NMR spectrum of UMB in the absence and presence of $\alpha$CD.[39] Chemical shift changes for different protons in UMB with the inclusion complex are listed in Table 2. Here, it is observed that aromatic protons such as H-5, H-6, and H-8 are highly upfield shifted and found to be −0.09, −0.011, and −0.07 respectively. Based on these $^1$H NMR results, we deduced the aromatic group of UMB deeply inserted into the cavity of $\alpha$CD and the possible inclusion modes for the UMB + $\alpha$CD complex are illustrated in Scheme 2.

**3.5. DSC Analysis.** A further insight into the interaction of host, guest, and complexed state can be assigned via the DSC study.[40] A shift or change in the intensity of the peak or disappearance of melting, boiling, and sublimation points is observed in DSC curves because of the inclusion of a drug in cyclodextrin. Thermogram of pure UMB {Figure 7a} exhibited a single endothermic peak in the temperature range of 30−300 °C.[41,42] The peak appeared at around 233 °C was sharp and strong. Formation of this peak indicates the purity as well as crystalline character of UMB. Whereas, in the case of $\alpha$CD, an endothermic peak appeared at around 108 °C, which corresponds to the release of water molecules bound with different energy in the cavity of cyclodextrin {Figure 7b}. When the inclusion complex was formed, the peak appeared at 233 °C in pure UMB got slightly shifted to a higher temperature of 244 °C {Figure 7c}. Therefore, from the comparison of the above three thermograms and their shifted peaks, it was elucidated that some weak interactions, which could be hydrogen bonding, van der Waals, or electrostatic interactions, occurred between UMB and $\alpha$CD.

**3.6. ESI-MS Studies.** A suitable estimation of the relative gas-phase stabilities of the inclusion complex was evaluated by electrospray ionization mass spectrometry (ESI-MS).[43] In Figure S1, the peaks observed at $m/z$ 681.56, 1135.96, and 1157.99 are related to the molecular ions, [UMB + $\alpha$CD + H]$^+$, and [UMB + $\alpha$CD + Na]$^+$, respectively.[44] As can be seen from this figure, in the positive mode there are peaks centered at $m/z$ 1157.99 (Table 3, Figure S1), which clearly denote the


https://dx.doi.org/10.1021/acsomega.0c04716
ACS Omega XXXX, XXX, XXX−XXX

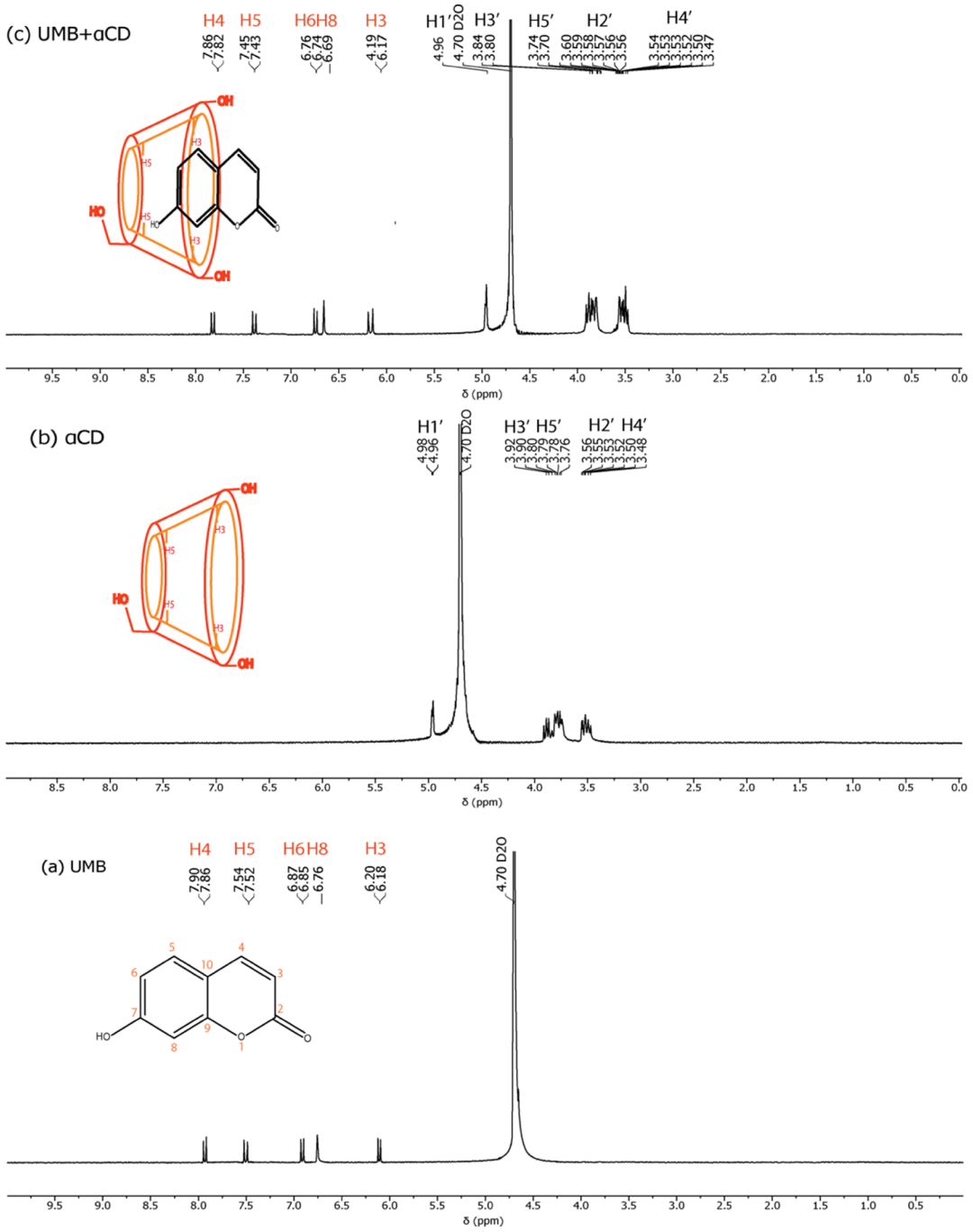


**Figure 6.** $^{1}$H NMR spectra of (a) UMB, (b) $\alpha$CD, and (c) UMB + $\alpha$CD inclusion complex.

**Table 2. $^{1}$H NMR Data for UMB in the UMB + $\alpha$CD Complex in $D_2O$**

| guest | position of protons | pure guest chemical shift (ppm) | inclusion complex chemical shift (ppm) (IC) | change in chemical shift $\Delta\delta = (\delta_{IC} - \delta_{pure})$ |
|---|---|---|---|---|
| UMB | H-3 | 6.18−6.20 (1H, d, $J$ = 8 Hz) | 6.17−6.19 (1H, d, $J$ = 8 Hz) | −0.01 |
| | H-4 | 7.86−7.90 (1H, d, $J$ = 16 Hz) | 7.82−7.86 (1H, d, $J$ = 16 Hz) | −0.04 |
| | H-5 | 7.52−7.54 (1H, d, $J$ = 8 Hz) | 7.43−7.45 (1H, d, $J$ = 8 Hz) | −0.09 |
| | H-6 | 6.85−6.87 (1H, d, $J$ = 8 Hz) | 6.74−6.76 (1H, d, $J$ = 8 Hz) | −0.11 |
| | H-8 | 6.76 (1H, s) | 6.69 (1H, s) | −0.07 |
| $\alpha$CD | H-3′ | 3.90−3.92 (6H, m) | 3.80−3.84 (6H, m) | −0.10 |
| | H-5′ | 3.76−3.80 (6H, m) | 3.70−3.74 (6H, m) | −0.06 |

formation of the singly charged ions of the [UMB + $\alpha$CD + Na]$^{+}$ complex.

**3.7. Molecular Docking Studies.** In recent years, the molecular docking has been extensively used to predict the



https://dx.doi.org/10.1021/acsomega.0c04716
ACS Omega XXXX, XXX, XXX−XXX

**Scheme 2. Schematic Illustration of the UMB + αCD Inclusion Complex**

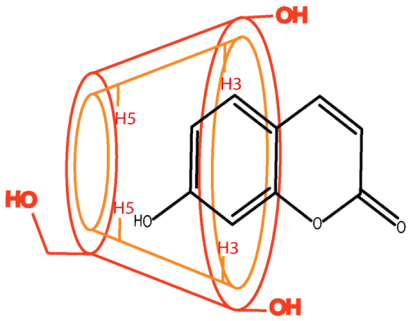


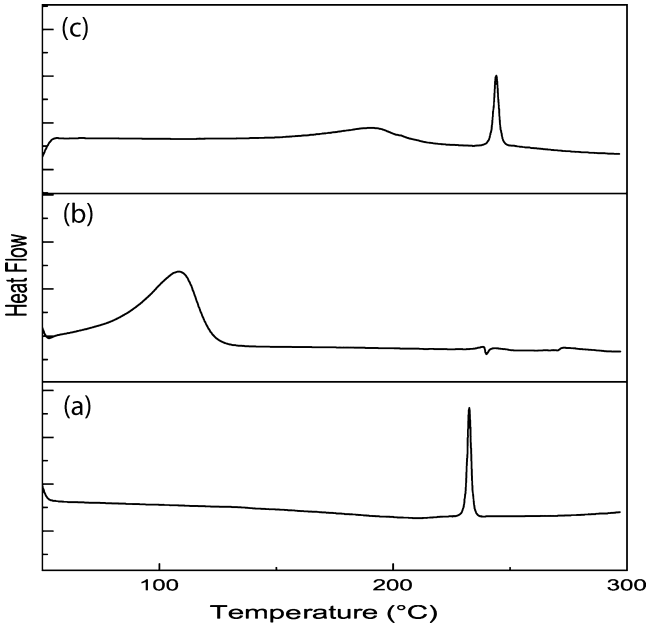


**Figure 7.** DSC thermograms of (a) UMB, (b) αCD, and (c) UMB + αCD inclusion complex.

**Table 3. ESI-MS Analysis of the Complexes with Calculated as Well as Experimental Mass Values**

| name of the complexes | calculated mass (a.u.) | experimental mass (a.u.) |
|---|---|---|
| $[UMB + \alpha CD + H]^+$ | 1134.98 | 1135.96 |
| $[UMB + \alpha CD + Na]^+$ | 1157.98 | 1157.99 |

bound conformations of CD and various drug molecules.[45] The docking has been carried out for five different poses as shown in Figure 8. Docking results revealed the structural orientation of UMB inside the cavity of αCD as well as the lowest energy structure of the UMB + αCD inclusion complex.[46]

The computationally calculated binding affinities of the first five energy conformers of the UMB + αCD inclusion complex were −3.60, −3.59, −3.47, −3.42, and −3.42 kcal·mol$^{-1}$, respectively, which were very near to the experimentally measured values (Table 4). Docking results demonstrate that the UMB was not completely embedded into the αCD cavities in all poses because of its small cavity size. For the first two poses, that is, Figure 9a,b, the binding affinity was quite similar and the change was about 0.01 kcal·mol$^{-1}$. However, their structural orientation was totally different. In the first pose, the lactone moiety was located at the wider side of the αCD cavities but in the second case, the aromatic part came closer to the wider side of the αCD cavity, which was also supported by various spectroscopic methods, such as $^1$H NMR, FTIR, and so forth. However, in this work, only five conformations of optimized inclusion complexes based on their binding affinity have been studied and showed. If someone closely looks at the five conformations, it can be observed that Figure 8d,e are the conformations with least binding affinity and subsequently are not being encapsulated in the cavity of αCD. Therefore, the molecular docking and free energy calculation results suggested that UMB bound to αCD with both hydrophobic and electrostatic interactions.

**3.8. Potential Energy Calculations of the Inclusion Complex.** Potential energy calculations were carried out in order to obtain some information about the geometry and stability of the host−guest complex and to find the intermolecular interaction in αCD and UMB inclusion complexation.[47] $\Delta E$ of the complexation was calculated for the minimum energy mode according to eq 2 and the data of $E_{Complex}$, $E_{Host} + E_{Guest}$, and $\Delta E$ are listed in Table 4. This potential energy term ($E$) is actually a summation of various different energy terms and can be stated as eq 3.

$$\Delta E = E_{Complex} - (E_{Host} + E_{Guest}) \quad (2)$$

$$E = E_{str} + E_{ang} + E_{stb} + E_{oop} + E_{tor} + E_{vdW} + E_{ele} + E_{sol} \quad (3)$$

where, $E_{str}$, $E_{ang}$, $E_{stb}$, $E_{oop}$, $E_{tor}$, $E_{vdW}$, $E_{ele}$, and $E_{sol}$ are potential energy components for bond stretching, bond angle, stretching bending, out of plane bending, dihedral torsional, van der Waals, electrostatic, and solvation energies, respectively.[48]

The energies of the complex and its different components are summarized in Tables 5 and S5. As seen from the table, all the other energy components are unaltered but it is the van der Waals ($\Delta E_{vdW}$) and electrostatic ($\Delta E_{ele}$) energies that are responsible for the complexation. The host−guest complexation in the gas phase is driven predominantly by vdW interactions. When the inclusion complex is formed, change in vdW energy, that is, $\Delta E_{vdW}$ = −12.186 kcal·mol$^{-1}$ is much lower than $\Delta E_{ele}$ = −7.839 kcal·mol$^{-1}$, indicating the vdW forces play a pivotal role in the formation of UMB/αCD in an aqueous environment.

**3.9. Dynamic Simulations.** In this study, we used molecular dynamics to calculate the stability of the UMB and αCD inclusion complex equilibrium.[49] The rigid microenvironment of the guest inside the host cavity and the stability of the complexes have been discussed using MD simulations based on the potential energy change with time.

Figure 9 shows the plot of potential energy versus time (ps) obtained through MD simulations for the complex structure in the gas phase as well as in the solvent phase. For complex UMB + αCD in the gas phase, we noticed a potential energy change from 586.201 to 385.245 kcal·mol$^{-1}$ during first 100 ps; it also showed a slight variation of potential energy: 385.245 to 387.618 kcal·mol$^{-1}$ in the second part of the interval between 100 and 600 ps. The binary inclusion complex of UMB in the gas phase showed an initial potential energy value and high fluctuations in the potential energy, but latter got stabilized after 100 ps of time. In the solvent phase, we noted that the UMB + αCD complex has a potential energy change from −5021.233 to −6190.101 kcal·mol$^{-1}$ during first 100 ps, we also noticed a variation of potential energy: −6190.101 to −6122.078 kcal·mol$^{-1}$ in the second part of the interval


https://dx.doi.org/10.1021/acsomega.0c04716
ACS Omega XXXX, XXX, XXX−XXX

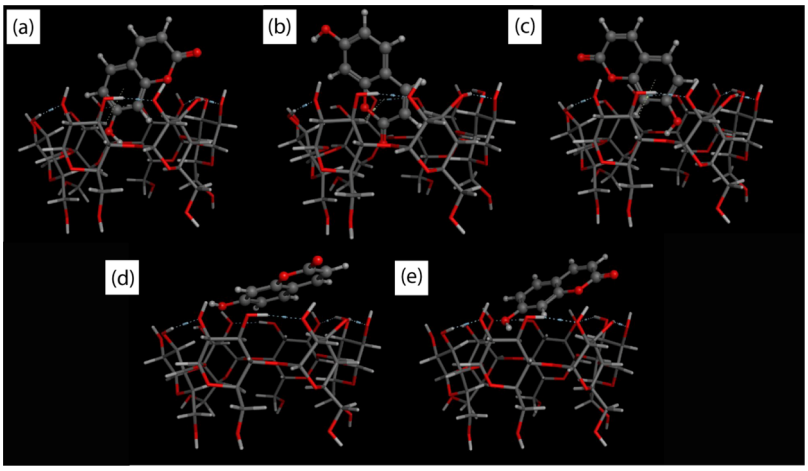


**Figure 8.** Top best five conformational models of the UMB + $\alpha$CD inclusion complex from (a) to (e) based on their binding affinity analyzed using MOE.2015 molecular docking software.

**Table 4. Binding Affinity of UMB + $\alpha$CD in Different Poses Obtained from Molecular Docking**

| ligand with receptor (UMB + $\alpha$CD) | binding affinity($\Delta G$) in kcal·mol$^{-1}$ | rmsd_refine |
|---|---|---|
| pose 1 | −3.60 | 1.96 |
| pose 2 | −3.59 | 0.73 |
| pose 3 | −3.47 | 1.60 |
| pose 4 | −3.42 | 1.80 |
| pose 5 | −3.42 | 1.07 |

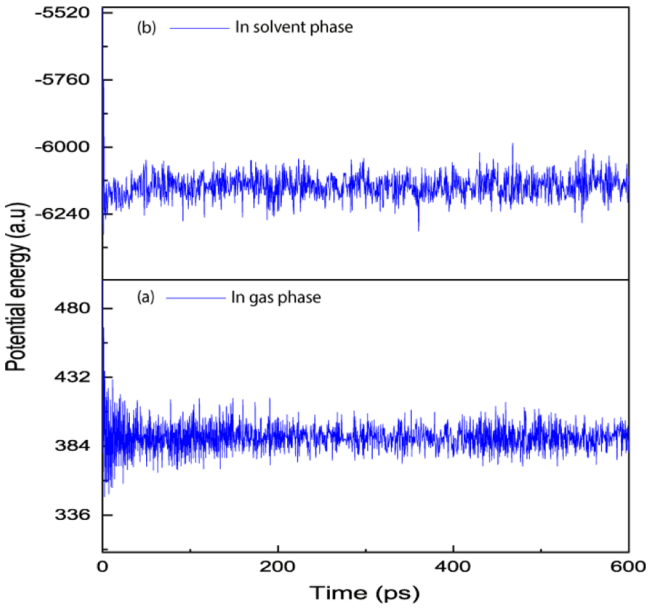


**Figure 9.** Evaluation of potential energy of the complex as a function of time (a) in gas phase (b) in solvent phase.

**Table 5. Potential Energy of $\alpha$CD ($E_{Host}$), UMB ($E_{Guest}$), Inclusion Complex ($E_{Complex}$), and Change in Potential Energy ($\Delta E$)**

| inclusion complex | $E_{Host}$ (kcal·mol$^{-1}$) | $E_{Guest}$ (kcal·mol$^{-1}$) | $E_{Complex}$ (kcal·mol$^{-1}$) | $\Delta E$ (kcal·mol$^{-1}$) |
|---|---|---|---|---|
| UMB + $\alpha$CD | 602.083 | 46.778 | 605.615 | −43.246 |

between 100 and 600 ps.[50] Therefore, we observed that the complex becomes stable after 100 ps in both phases. The potential energy deviance of the complex was less for the inclusion complex in the solvent phase compared to the inclusion complex in the gas phase indicating the better stability of the supramolecular inclusion complex in the solvent phase.

## 4. CONCLUSIONS

In the present study, UMB + $\alpha$CD was designed, synthesized, and characterized by using $^1$H NMR, FTIR, and ESI-MS. Job's plot was used to confirm the stoichiometry of the inclusion complex. From the FTIR and NMR data, it is confirmed that the aromatic part has been inserted into the $\alpha$-cyclodextrin cavity. Differential scanning calorimetric value for the inclusion complex confirms that it is thermally stable upto 244 °C. Thermodynamic parameters like the binding constant have been found to be favorable for stable inclusion complexation. From the molecular docking study, it is observed that when UMB inserted through the aromatic part, it showed the highest binding affinity compared to the rest of the four poses, which confirmed the preferential encapsulation and the geometry of the inclusion complex obtained from $^1$H NMR experiments. Thus, molecular docking as well as dynamic simulations also support the experimental evidence. Thus, the overall study concluded that the UMB-$\alpha$−cyclodextrin supramolecular hybrid could lead to further developments of sunscreen agents.

## ■ ASSOCIATED CONTENT

### Supporting Information

The Supporting Information is available free of charge at https://pubs.acs.org/doi/10.1021/acsomega.0c04716.

Detailed descriptions of all the chemicals used, Job's plot table, association constant data, ESI-MS spectra of the inclusion complexes, and potential energy calculations of both inclusion complexes using computational studies (PDF)

## ■ AUTHOR INFORMATION

### Corresponding Author

**Mahendra Nath Roy** − *Department of Chemistry, University of North Bengal, Darjeeling 734013, India;* orcid.org/



https://dx.doi.org/10.1021/acsomega.0c04716
ACS Omega XXXX, XXX, XXX−XXX

0000-0002-7380-5526; Email: mahendraroy2002@yahoo.co.in

### Authors

**Niloy Roy** − *Department of Chemistry, University of North Bengal, Darjeeling 734013, India*

**Biswajit Ghosh** − *Department of Chemistry, University of North Bengal, Darjeeling 734013, India*

**Debadrita Roy** − *Department of Chemistry, University of North Bengal, Darjeeling 734013, India*

**Biswajit Bhaumik** − *Department of Chemistry, Surya Sen Mahavidyalaya, Jalpaiguri 734004, India*

Complete contact information is available at: https://pubs.acs.org/10.1021/acsomega.0c04716

### Notes

The authors declare no competing financial interest.

## ■ ACKNOWLEDGMENTS

N.R. acknowledges UGC-NFSC for Junior Research fellowship {ref. no. 2219/(CSIR-UGC NET JUNE 2019)}. Corresponding author M.N.R. is very much thankful to UGC for receiving one time Grant of seven lakhs from UGC-BSR (ref. no. F.4-10/2010).

## ■ REFERENCES

(1) Kockler, J.; Oelgemöller, M.; Robertson, S.; Glass, B. D. Photostability of sunscreens. *J. Photochem. Photobiol., C* **2012**, *13*, 91−110.

(2) Afonso, S.; Horita, K.; Sousa e Silva, J. P.; Almeida, I. F.; Amaral, M. H.; Lobão, P. A.; Costa, P. C.; Miranda, M. S.; Esteves da Silva, J. C. G.; Sousa Lobo, J. M. Photodegradation of avobenzone: Stabilization effect of antioxidants. *J. Photochem. Photobiol., C* **2014**, *140*, 36−40.

(3) Stiefel, C.; Schubert, T.; Morlock, G. E. Bioprofiling of Cosmetics with Focus on Streamlined Coumarin Analysis. *ACS Omega* **2017**, *2*, 5242−5250.

(4) Wang, R.; Wang, X.; Zhan, Y.; Xu, Z.; Xu, Z.; Feng, X.; Li, S.; Xu, H. A Dual Network Hydrogel Sunscreen Based on Poly-γ-glutamic Acid/Tannic Acid Demonstrates Excellent Anti-UV, Self-Recovery, and Skin-Integration Capacities. *ACS Appl. Mater. Interfaces* **2019**, *11*, 37502−37512.

(5) Morsella, M.; d'Alessandro, N.; Lanterna, A. E.; Scaiano, J. C. Improving the Sunscreen Properties of TiO2 through an Understanding of Its Catalytic Properties. *ACS Omega* **2016**, *1*, 464−469.

(6) Knežević, N. Ž.; Ilić, N.; Dokić, V.; Petrović, R.; Janaćković, D. Mesoporous Silica and Organosilica Nanomaterials as UV-Blocking Agents. *ACS Appl. Mater. Interfaces* **2018**, *10*, 20231−20236.

(7) Li, D.; Qian, L.; Feng, Y.; Feng, J.; Tang, P.; Yang, L. Co-intercalation of Acid Red 337 and a UV Absorbent into Layered Double Hydroxides: Enhancement of Photostability. *ACS Appl. Mater. Interfaces* **2014**, *6*, 20603−20611.

(8) Yang, L.; Qian, L.; Feng, Y.; Tang, P.; Li, D. Acid Blue 129 and Salicylate Cointercalated Layered Double Hydroxides: Assembly, Characterization, and Photostability. *Ind. Eng. Chem. Res.* **2014**, *53*, 17961−17967.

(9) Leandri, V.; Gardner, J. M.; Jonsson, M. Coumarin as a Quantitative Probe for Hydroxyl Radical Formation in Heterogeneous Photocatalysis. *J. Phys. Chem. C* **2019**, *123*, 6667−6674.

(10) Krauter, C. M.; Möhring, J.; Buckup, T.; Pernpointner, M.; Motzkus, M. Ultrafast branching in the excited state of coumarin and umbelliferone. *Phys. Chem. Chem. Phys.* **2013**, *15*, 17846−17861.

(11) Kumar, V.; Al-Abbasi, F. A.; Verma, A.; Mujeeb, M.; Anwar, F. Umbelliferone β-D-galactopyranoside Exerts Anti-inflammatory Effect by Attenuating COX-1 and COX-2. *Toxicol. Res.* **2015**, *4*, 1072−1084.

(12) Telange, D. R.; Nirgulkar, S. B.; Umekar, M. J.; Patil, A. T.; Pethe, A. M.; Bali, N. R. Enhanced transdermal permeation and anti-inflammatory potential of phospholipids complex-loaded matrix film of umbelliferone: Formulation development, physico-chemical and functional characterization. *Eur. J. Pharm. Sci.* **2019**, *131*, 23−38.

(13) Pan, L.; Li, X.-z.; Yan, Z.-q.; Guo, H.-r.; Qin, B. Phytotoxicity of umbelliferone and its analogs: Structure-activity relationships and action mechanisms. *Plant Physiol. Biochem.* **2015**, *97*, 272−277.

(14) Mazimba, O. Umbelliferone: Sources, chemistry and bioactivities review. *Bull. Fac. Pharm. (Cairo Univ.)* **2017**, *55*, 223−232.

(15) Anwar, F.; Al-Abbasi, F. A.; Bhatt, P. C.; Ahmad, A.; Sethi, N.; Kumar, V. Umbelliferone β-D-galactopyranoside inhibits chemically induced renal carcinogenesis via alteration of oxidative stress, hyperproliferation and inflammation: possible role of NF-kB. *Toxicol. Res.* **2015**, *4*, 1308−1323.

(16) Real, M.; Gámiz, B.; López-Cabeza, R.; Celis, R. Sorption, persistence, and leaching of the allelochemical umbelliferone in soils treated with nanoengineered sorbents. *Sci. Rep.* **2019**, *9*, 9764.

(17) Nagarsenkar, A.; Guntuku, L.; Prajapti, S. K.; Guggilapu, S. D.; Sonar, R.; Vegi, G. M. N.; Babu, B. N. Umbelliferone−oxindole hybrids as novel apoptosis inducing agents. *New J. Chem.* **2017**, *41*, 12604−12610.

(18) Brewster, M. E.; Loftsson, T. Cyclodextrins as pharmaceutical solubilizers. *Adv. Drug Delivery Rev.* **2007**, *59*, 645−666.

(19) Roy, M. N.; Saha, S.; Barman, S.; Ekka, D. Host−guest inclusion complexes of RNA nucleosides inside aqueous cyclodextrins explored by physicochemical and spectroscopic methods. *RSC Adv.* **2016**, *6*, 8881−8891.

(20) Ceborska, M. Interactions of Native Cyclodextrins with Biorelevant Molecules in the Solid State: A Review. *Curr. Org. Chem.* **2014**, *18*, 1878−1885.

(21) Bomzan, P.; Roy, N.; Sharma, A.; Rai, V.; Ghosh, S.; Kumar, A.; Roy, M. N. Molecular Encapsulation Study of Indole-3-methanol in Cyclodextrins: Effect on Antimicrobial Activity and Cytotoxicity. *J. Mol. Struct.* **2021**, *1225*, 129093.

(22) Ghosh, R.; Roy, K.; Subba, A.; Mandal, P.; Basak, S.; Kundu, M.; Roy, M. N. Case to case study for exploring inclusion complexes of an anti-diabetic alkaloid with α and β cyclodextrin molecules for sustained Dischargement. *J. Mol. Struct.* **2020**, *1200*, 126988.

(23) Tian, B.; Hua, S.; Liu, J. Cyclodextrin-based delivery systems for chemotherapeutic anticancer drugs: A review. *Carbohydr. Polym.* **2020**, *232*, 115805.

(24) Mori, T.; Tsuchiya, R.; Doi, M.; Nagatani, N.; Tanaka, T. Solubilization of ultraviolet absorbers by cyclodextrin and their potential application in cosmetics. *J. Inclusion Phenom. Macrocyclic Chem.* **2019**, *93*, 91−96.

(25) Metilda, G. M.; Kumari, J. P. Preparation and Characterization of Umbelliferone and Hydroxy Propyl α-Cyclodextrin Inclusion Complex. *Indian J. Appl. Res.* **2015**, *5*, 158−160.

(26) Wang, E.; Chen, G.; Han, C. Crystal Structures of β-Cyclodextrin Inclusion Complexes with 7-Hydroxycoumarin and 4-Hydroxycoumarin and Substituent Effects on Inclusion Geometry. *Chin. J. Chem.* **2011**, *29*, 617−622.

(27) Rahaman, H.; Roy, N.; Roy, A.; Ray, S.; Roy, M. N. Exploring Existence of Host-Guest Inclusion Complex of β-Cyclodextrin of a Biologically Active Compound with the Manifestation of Diverse Interactions. *Emerg. Sci. J.* **2018**, *2*, 251−260.

(28) Geng, Q.; Li, T.; Wang, X.; Chu, W.; Cai, M.; Xie, J.; Ni, H. The mechanism of bensulfuronmethyl complexation with β-cyclodextrin and 2-hydroxypropyl-β-cyclodextrin and efect on soil adsorption and bio-activity. *Sci. Rep.* **2019**, *9*, 1882.

(29) Adeoye, O.; Conceição, J.; Serra, P. A.; Bento da Silva, A.; Guedes, R. C.; Corvo, M. C.; Aguiar-Ricardo, A.; Jicsinszky, L.; Casimiro, T.; Cabral-Marques, H. Cyclodextrin solubilization and complexation of antiretroviral drug lopinavir: In silico prediction; Effects of derivatization, molar ratio and preparation method. *Carbohydr. Polym.* **2020**, *227*, 115287.

(30) Deng, Y.; Pang, Y.; Guo, Y.; Ren, Y.; Wang, F.; Liao, X.; Yang, B. Host-guest inclusion systems of daidzein with 2-hydroxypropyl-

bcyclodextrin (HP-β-CD) and sulfobutyl ether-b-cyclodextrin (SBE-βCD): Preparation, binding behaviors and water solubility. *J. Mol. Struct.* **2016**, *1118*, 307−315.
(31) Shan, P.-H.; Zhao, J.; Deng, X.-Y.; Lin, R.-L.; Bian, B.; Tao, Z.; Xiao, X.; Liu, J.-X. Selective recognition and determination of phenylalanine by a fluorescent probe based on cucurbit[8]uril and palmatine. *Anal. Chim. Acta* **2020**, *1104*, 164−171.
(32) Favrelle, A.; Gouhier, G.; Guillen, F.; Martin, C.; Mofaddel, N.; Petit, S.; Mundy, K. M.; Pitre, S. P.; Wagner, B. D. Structure−Binding Effects: Comparative Binding of 2-Anilino-6-naphthalenesulfonate by a Series of Alkyl- and Hydroxyalkyl-Substituted β-Cyclodextrins. *J. Phys. Chem. B* **2015**, *119*, 12921−12930.
(33) Kida, T.; Iwamoto, T.; Fujino, Y.; Tohnai, N.; Miyata, M.; Akashi, M. Strong Guest Binding by Cyclodextrin Hosts in Competing Nonpolar Solvents and the Unique Crystalline Structure. *Org. Lett.* **2011**, *13*, 4570−4573.
(34) Roy, N.; Ghosh, R.; Das, K.; Roy, D.; Ghosh, T.; Roy, M. N. Study to synthesize and characterize host-guest encapsulation of antidiabetic drug (TgC) and hydroxy propyl-b-cyclodextrin augmenting the antidiabetic applicability in biological system. *J. Mol. Struct.* **2019**, *1179*, 642−650.
(35) Nath, M.; Jairath, R.; Eng, G.; Song, X.; Kumar, A. New diorganotin(IV) derivatives of 7-hydroxycoumarin (umbelliferone) and their adducts with 1,10-phenanthroline. *Spectrochim. Acta, Part A* **2005**, *61*, 3155−3161.
(36) Telange, D. R.; Nirgulkar, S. B.; Umekar, M. J.; Patil, A. T.; Pethe, A. M.; Bali, N. R. Enhanced transdermal permeation and anti-inflammatory potential of phospholipids complex-loaded matrix film of umbelliferone: Formulation development, physico-chemical and functional characterization. *Eur. J. Pharm. Sci.* **2019**, *131*, 23−38.
(37) Dutta, A.; Roy, N.; Das, K.; Roy, D.; Ghosh, R.; Roy, M. N. Synthesis and Characterization of Host Guest Inclusion Complexes of Cyclodextrin Molecules with Theophylline by Diverse Methodologies. *Emerg. Sci. J.* **2020**, *4*, 52−72.
(38) dos Santos, R. G.; Moura Bordado, J. C.; Mateus, M. M. $^{1}$H-NMR dataset for hydroxycoumarins−Aesculetin, 4-Methylumbelliferone, and umbelliferone. *Data Brief* **2016**, *8*, 308−311.
(39) Arza, C. R.; Froimowicz, P.; Ishida, H. Smart chemical design incorporating umbelliferone as natural renewable resource toward the preparation of thermally stable thermosets materials based on benzoxazine chemistry. *RSC Adv.* **2005**, *5*, 97855−97861.
(40) Rajbanshi, B.; Dutta, A.; Mahato, B.; Roy, D.; Maiti, D. K.; Bhattacharyya, S.; Roy, M. N. Study to explore host guest inclusion complexes of vitamin B1 with CD molecules for enhancing stability and innovative application in biological system. *J. Mol. Liq.* **2020**, *298*, 111952.
(41) Froimowicz, P.; Rodriguez Arza, C.; Ohashi, S.; Ishida, H. Tailor-Made and Chemically Designed Synthesis of Coumarin-Containing Benzoxazines and Their Reactivity Study Toward Their Thermosets. *J. Polym. Sci., Part A: Polym. Chem.* **2016**, *54*, 1428−1435.
(42) Lacatusu, I.; Badea, N.; Murariu, A.; Oprea, O.; Bojin, D.; Meghea, A. Antioxidant Activity of Solid Lipid Nanoparticles Loaded with Umbelliferone. *Soft Mater.* **2013**, *11*, 75−84.
(43) Das, K.; Datta, B.; Rajbanshi, B.; Roy, M. N. Evidences for Inclusion and Encapsulation of an Ionic liquid with β-CD and 18-C-6 in Aqueous Environments by Physicochemical Investigation. *J. Phys. Chem. B* **2018**, *122*, 1679−1694.
(44) Stiefel, C.; Schubert, T.; Morlock, G. E. Bioprofiling of Cosmetics with Focus on Streamlined Coumarin Analysis. *ACS Omega* **2017**, *2*, 5242−5250.
(45) Roy, N.; Bomzan, P.; Nath Roy, M. Probing Host-Guest inclusion complexes of Ambroxol Hydrochloride with α- & β-Cyclodextrins by physicochemical contrivance subsequently optimized by molecular modeling simulations. *Chem. Phys. Lett.* **2020**, *748*, 137372.
(46) Nafie, G.; Vitale, G.; Carbognani Ortega, L.; Nassar, N. N. Nanopyroxene grafting with β-Cyclodextrin monomer for wastewater applications. *ACS Appl. Mater. Interfaces* **2017**, *9*, 42393−42407.
(47) Ismahan, L.; Leila, N.; Fatiha, M.; Abdelkrim, G.; Mouna, C.; Nada, B.; Brahim, H. Computational study of inclusion complex of l-Glutamine/beta-Cycldextrin: Electronic and intermolecular interactions investigations. *J. Mol. Struct.* **2020**, *1206*, 127740.
(48) Akae, Y.; Koyama, Y.; Sogawa, H.; Hayashi, Y.; Kawauchi, S.; Kuwata, S.; Takata, T. Structural Analysis and Inclusion Mechanism of Native and Permethylated aCyclodextrin-Based Rotaxanes Containing Alkylene Axles. *Chem.—Eur. J.* **2016**, *22*, 5335−5341.
(49) Chaube, U.; Chhatbar, D.; Bhatt, H. 3D-QSAR, molecular dynamics simulations and molecular docking studies of benzoxazepine moiety as mTOR inhibitor for the treatment of lung cancer. *Bioorg. Med. Chem. Lett.* **2016**, *26*, 864−874.
(50) Daoud, I.; Melkemi, N.; Salah, T.; Ghalem, S. Combined QSAR, molecular docking and molecular dynamics study on new Acetylcholinesterase and Butyrylcholinesterase inhibitors. *Comput. Biol. Chem.* **2018**, *74*, 304−326.


https://dx.doi.org/10.1021/acsomega.0c04716
*ACS Omega* XXXX, XXX, XXX−XXX

Chemical Physics Letters 748 (2020) 137372

Contents lists available at ScienceDirect

Chemical Physics Letters

journal homepage: www.elsevier.com/locate/cplett

Research paper

# Probing Host-Guest inclusion complexes of Ambroxol Hydrochloride with α- & β-Cyclodextrins by physicochemical contrivance subsequently optimized by molecular modeling simulations

Niloy Roy, Pranish Bomzan, Mahendra Nath Roy*

*Department of Chemistry, University of North Bengal, Darjeeling 734013, India*

## HIGHLIGHTS

- Complexes are well characterized by experimentally as well as theoretically in depth.
- Bond length, dihedral angle changes confirm conformational changes of guest molecules.
- Molecular modeling and dynamic simulations predict inclusion phenomena.
- Spectroscopic methods were used to evaluate various thermodynamic parameters.

## ARTICLE INFO

*Keywords:*
α-Cyclodextrin
β-Cyclodextrin
Conformational change
Supramolecular assembly
Host-guest dynamics

## ABSTRACT

Herein, we report the inclusion of AMB in cyclodextrins leading to host-guest assemblies. The inclusion complexes comprised of Ambroxol Hydrochloride (AMB) with α-cyclodextrin (αCD) and β-cyclodextrin (βCD) have been confirmed by experimental (UV–vis titration, FTIR, ESI-MS, $^{1}$NMR, 2D-NMR) and computational studies (molecular docking, molecular mechanics calculation). The molecular docking studies demonstrate a better insight into geometry and inclusion mode of AMB inside αCD as well as βCD cavity. Formation of inclusion complexes with different cyclodextrins causes some structural changes of guest molecules during the encapsulation process confirmed by bond length, dihedral angle changes and dynamic simulations.

## 1. Introduction

Now-a-days, site specific formulation of a potential drug is very much important for the betterment of the drug in pharmaceutical industry [1]. Although, Ambroxol Hydrochloride (AMB) is a mucolytic drug that reduces the thickness of the sputum [2] and also used to treat conditions with abnormal mucus secretion [3] allowing the patient to breathe freely and deeply by promoting mucus clearance, facilating expectoration and easing productive cough [4,5]. But being soluble in hot water and practically insoluble in dichloro methane and soluble in Methanol [6], a supramolecular assemble of pure Ambroxol Hydrochloride (AMB) with cyclodextrin molecules tagged with a protein or enzyme could make it a potent mucolytic and mucokinetic agent. Some recent studies include the drugs having a role in treatment of Gaucher's disease [7], Parkinson disease [8] and other aging-associated diseases involving dysfunction of autophagy [9].

AMB is a mucolytic drug as a salt form of Ambroxol (Scheme 1), a metabolite of bromohexine [10]. Ambroxol can also be used as a pharmacological chaperone therapy (PCT) for the treatment of Guacher Disease (GD) [11]. Ambroxol Hydrochloride occurs as a white crystalline powder [12]. Due to its poor water solubility, AMB has been used as an oral suspension. The aqueous solubility and dissolution of these drugs are key factors in determining the bioavailability of its oral preparation [13].

Cyclodextrins (CD) are cyclic oligosaccharides widely used for the recognition of various guest molecules give rise to inclusion complex (IC) [14]. CDs are non toxic, biodegradable and biocompatible along with the collective effects of inclusion, size-specificity, controlled release capability and transport properties make it suitable as a host molecule [15,16]. Supramolecular complexation can increase the water solubility as well as bio availability [17,18]. Among different types of cyclodextrins, αCD and βCD (Scheme 1) are taken as host molecules due to both size and solubility matching with the Ambroxol Hydrochloride i.e the guest molecule. Now-a-days, apart from experiments, researchers also perform different molecular simulation studies with guest, host and their inclusion complexes to gather information at a

* Corresponding author.
*E-mail address:* mahendraroy2002@yahoo.co.in (M. Nath Roy).

https://doi.org/10.1016/j.cplett.2020.137372
Received 14 February 2020; Received in revised form 14 March 2020; Accepted 18 March 2020
Available online 20 March 2020

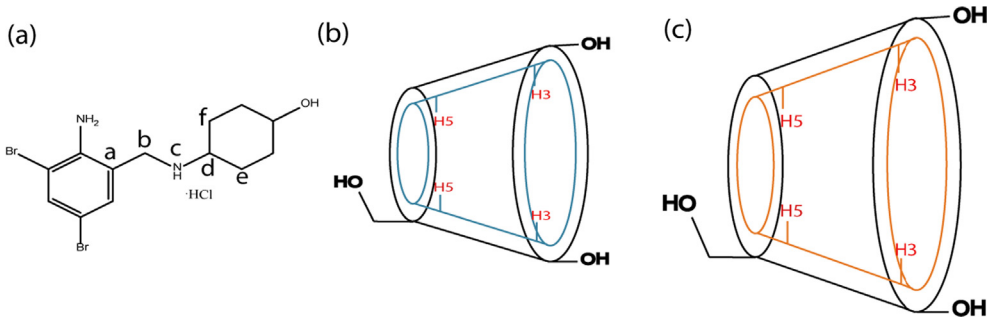


**Scheme 1.** Two dimensional structures of (a) Ambroxol hydrochloride (b) α-cyclodextrin (c) β-cyclodextrin.

molecular level e.g, quantum mechanics, molecular dynamics (MD) and molecular mechanics (MM) approximations [19,20].

The aim of the present study is to evaluate whether host–guest inclusion complex has been formed between the guest Ambroxol Hydrochloride and the two types of hosts cyclodextrins αCD and βCD and also to investigate the different interactions between host and the guest molecules in the inclusion complex. Additionally, molecular modeling study by MOE.2015 software from chemical computing group was performed to validate the change in geometrical configuration of the complex obtained from experimental results [21]. Different physiochemical, spectroscopic techniques for the two inclusion complexes in aqueous solution have been performed to investigate whether the IC formation has taken place as well as to study different interactive forces occurring in the two inclusion complexes.

## 2. Experimental section

### 2.1. Materials and materials

Ambroxol Hydrochloride (M.W = 414.57, Purity > 98.0%) which was used as the guest molecule in our study was purchased from TCI Chemicals (India) Pvt. Ltd & the two hosts required that is βCD (M.W = 1134.98, Purity > 97.0%) and αCD (M.W = 972.84, Purity > 98.0%) were bought from SIGMA- ALDRICH India (Table S1). Double distilled water has been used throughout the experiment.

### 2.2. Methods

Stock solutions of Ambroxol Hydrochloride, βCD and αCD were prepared by mass (Mettler Toledo AG-285 with uncertainty 0.0001 g) and by dilution. The solution of αCD and βCD were prepared by heating it slightly in a water bath. All the $^1$H NMR and 2D-NMR data were plotted with the help of Mestrenova 12. Origin 2018 software has been used for the plotting the entire graphs. All the spectroscopic experiments were carried out in a solution of ethanol/water mixture (3:7, v/v).

### 2.3. UV–visible spectroscopy

UV–vis titration was performed by using Agilent 8453 Spectrophotometer. The temperatures were regulated with a digital thermostat for the association constant measurement. The absorption spectra were recorded at 293 ± 0.15 K, 303 ± 0.15 K, 313 ± 0.15 K respectively.

### 2.4. Fourier transform infrared (FTIR)

FTIR spectra were recorded by a Perkin Elmer FTIR spectrometer by the solid KBr disk technique. KBr disks with 1 mg of solid inclusion complex and 100 mg of KBr were prepared. Measurements were performed in the scanning range of (4000–400 cm$^{-1}$) at the room temperature to record the FT-IR spectral data.

### 2.5. $^1$H NMR and 2D-NMR spectroscopy

All NMR spectra were recorded on a Bruker AVANCE spectrometer at 400 MHz and 25 $^0$C in $D_2O$. The residual HDO line had a line width at a half-height of 2.59 Hz. Two-dimensional (2D) ROESY spectra were acquired at 25 $^0$C with number of scan 8, and a 2048 K time domain in F2 (FID resolution 5.87 Hz) and 460 experiments in F1.

### 2.6. ESI-MS spectrometry

ESI-MS spectra for the both complexes were collected using Agilent, 6460 Triple quad LC/MS, 1200 Infinity series equipped with electrospray ionization (ESI) interface. The gas temperature was 300 $^0$C with flow rate of 5 L min$^{-1}$. The capillary voltage was calibrated at 3.5 kV and injection volume was about 5.00 ml.

### 2.7. Molecular modeling studies

Molecular modeling studies were performed to predict the formation of AMB + αCD and AMB + βCD inclusion complexes and to measure their binding affinity by utilizing MOE.2015 software, which are available in the Chemical Computing Group (CCG). The 3D optimized structure of AMB (ID: 234307), αCD (ID: 125105), βCD (ID: 762697) were taken from Chembridge Crystal data centre (CCDC) as CIF file and used as received. Hydrogen atoms and partial charges were added to the protein. Molecular modeling calculations were carried out with molecular mechanics MMFF94x force field. The hydrogens and charges were fixed, and the RMS gradient was set to 0.005 kcal/mol. Conformations of ligand (CDs) were fitted in the position with the Triangle Matcher method and ordered with the London Δ*G* scoring function. A maximum of 5 conformations of each guest were allowed to be saved in a separate database file as .mdb format. The produced poses were ranked based on their docking scores. Finally, we choose the best energy pose [22,23].

### 2.8 Dynamic simulation

Molecular dynamics and simulations studies are generally performed to obtain the stable structure of inclusion complexes with respect to time, temperature, kinetic energy and potential energy. The forcefield was taken to be MMFF94x. MOE dynamics simulation uses the Nosé-Poincaré-Andersen (NPA) equations of motion. Default steps and protocols of the MD were selected to optimize the systems equilibrium 100 ps and production run was carried out for 500 ps.

### 2.9 Sample preparation of Solid Inclusion Complex of Ambroxol Hydrochloride with Cyclodextrins

To prepare 1:1 a solid Inclusion Complex between Ambroxol Hydrochloride and αCD as well as with βCD, at first, 30 mg of solid guest compound of AMB (which is also pretty much soluble in hot water) was taken in a beaker and amount 40 ml of distilled water was

added to it and placing it in a thermostated water bath at temperature set at 323.15 K with constant stirring in a magnetic stirrer. Next, accurately measured 70.39 mg of αCD and 82.13 mg of βCD were added in solid form in two different beakers slowly in presence of the constant stirring. It was kept in the thermostated water bath for 24–48 h. Thereafter, it was collected and dried in a hot oven & after that inclusion complexes in the solid form were obtained.

## 3. Results and discussions

Ambroxol Hydrochloride guest molecule selected in this investigation was moderately soluble in water. Our aim was to study the formation of inclusion complex between the host and the guest and also to evaluate the interactions and different thermodynamic parameters of the inclusion complex, so all the measurements were done in room temperature and in aqueous-ethanolic solution such as UV–vis Studies etc. However, FTIR Spectroscopy, NMR, SEM analysis were performed by the prepared solid inclusion complex between Ambroxol Hydrochloride and CDs.

### *3.1. Job's plot: Determination of stoichiometry behaviour of cyclodextrins inclusion complex with Ambroxol Hydrochloride*

Job's plot method which is also known as the continuous variation method is a very efficient and successful way to recognize stoichiometry of any host–guest inclusion complexes [24]. So, due to this reason the Job's Plot was applied here by using UV–visible spectroscopy. Here, two sets of solutions were prepared of Ambroxol Hydrochloride with αCD and βCD respectively in 30% ethanolic-aqueous (3:7, v/v) solution, by varying the mole fractions of the guest (Ambroxol) in the range of 0–1. Job's plots of the mentioned sets of solutions were plotted as ΔA × R against R, where ΔA means the difference in absorbance of AMB (Guest) without and with CD and R = [AMB]/([AMB] + [CD]). The absorbance values were obtained at respective $\lambda_{max}$ for each solution by maintaining 298.15 K temperature. The stoichiometry of an inclusion complex is obtained by taking the corresponding value of R at the maximum point on the Job's Plot curve, for example, if the ratio of guest to host is 1:2 for R∽0.33, 1:1 for R∽0.5 and 2:1 for R∽0.66 and so on. Here, in this work we got R∽0.5 as maxima in the plot (Fig. 1), reflecting a 1:1 stoichiometry (Guest:Host) for both the inclusion complexes (Table S2 & S3).

### *3.2. Determination of binding constant of both complexes in aqueous ethanol by UV–vis spectroscopy.*

The binding constant between αCD, βCD and the guest molecule Ambroxol has been calculated via UV–Vis spectroscopy with the help of Benesi–Hildebrand technique which represents one of the most well-known strategies to determine binding constants of the Inclusion Complexes based on absorption spectra of the inclusion complex [25]. Accurate estimation of binding (association) constants of the inclusion complexes under investigation can be obtained by observing changes in the absorption intensity of the AMB at different temperature as a function of the CD's concentration (Table 2) and according to method for 1:1 Inclusion complex between guest and host, the double reciprocal plots have been drawn using equation (1).

$$\frac{1}{[A-A_0]} = \frac{1}{K_a[AMB]_0\Delta\varepsilon} \times \frac{1}{[CD]_0} + \frac{1}{\Delta\varepsilon} \quad \ldots\ldots\ldots (1)$$

For AMB + αCD, Association constant of 1:1 host and guest was found to be 4226 $M^{-1}$, 8993 $M^{-1}$, and 15799 $M^{-1}$ at 293.15 K, 303.15 K and 313.15 K respectively with good correlation factors (Table 1 & Table S4). Double reciprocal plot was calculated using Benesi-Hildebrand to obtain the slope and intercept (Fig. S1, S2 & S3).

Association constant ($k_a$) value for AMB + βCD was calculated by dividing the intercept by the slope of the straight line (Table S6), which was found from the double reciprocal plot (Figure S5, S6, S7) at three different temperatures 293.15 K, 303.15 K & 313.15 K have been found to be 27780 $M^{-1}$, 37333 $M^{-1}$ & 45379 $M^{-1}$ respectively (Table 1 and Figs. 2 and 3 ).

From Table 1, we observe that with the increase in temperature association constant values (Ka) increases for both the system and the Ka values for AMB with βCD system were found to be higher in all three temperatures than the AMB with αCD system. The linear increase in $k_a$ value when increasing the temperature from 293.15 K to 313.15 K clearly indicated the endothermic nature of Inclusion Complexation between Ambroxol Hydrochloride and αCD and βCD and also suggests that βCD forms the complex with better stability.

**Table 1**
Association constant of the Inclusion complex between AMB, αCD & βCD at three different Temperatures; ± sign indicates the standard deviation.

| System | Temperature (K) | Slope | Intercept | Association constant (Ka)/($M^{-1}$) |
|---|---|---|---|---|
| AMB + αCD | 293.15 | 0.000725 | 3.06391 | 4226 ± 1195 |
| | 303.15 | 0.000456 | 4.10125 | 8993 ± 1765 |
| | 313.15 | 0.000447 | 7.08252 | 15799 ± 172 |
| AMB + βCD | 293.15 | 0.000283 | 7.86202 | 27780 ± 2570 |
| | 303.15 | 0.000242 | 9.03459 | 37333 ± 1036 |
| | 313.15 | 0.000239 | 10.84575 | 45379 ± 821 |

### *3.3. Thermodynamic parameters:*

The thermodynamic parameters of the analyzed inclusion processes, enthalpy change (ΔH°) and entropy change (ΔS°) and Gibbs free energy

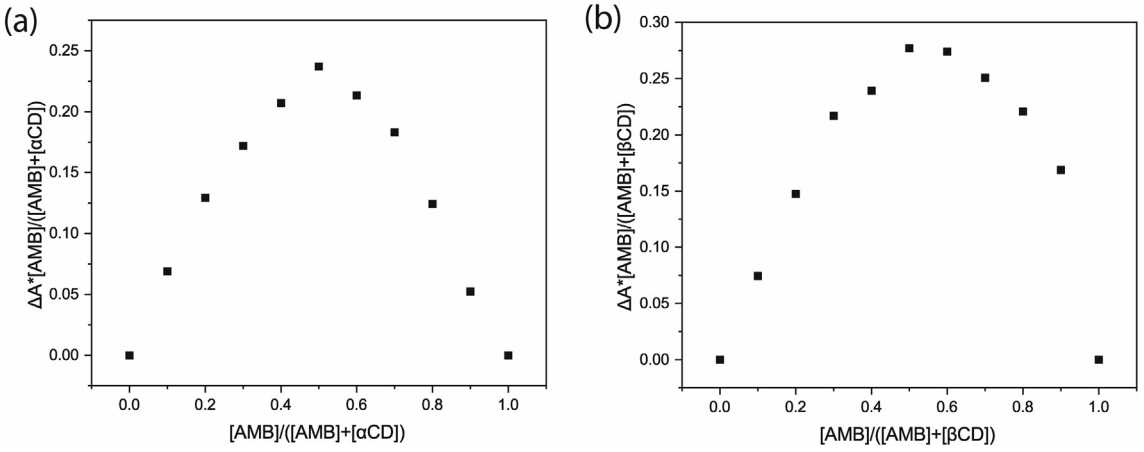


**Fig. 1.** Job's Plot of the (a) AMB + αCD and (b) AMB + βCD system at 298.15 K.

**Table 2**
Various thermodynamic parameters of AMB + αCD and AMB + βCD complex system (1 cal = 4.184 J).

| System | Temp(K) | Ka/$M^{-1}$ | $\Delta H^0$/KJ $mol^{-1}$ | $\Delta S^0$/KJ $mol^{-1}$ $K^{-1}$ | ΔG KJ $mol^{-1}$ | ΔG KCal $mol^{-1}$ |
|---|---|---|---|---|---|---|
| **AMB + αCD** | 293.15 | 4226 | 50.3166 | 0.2411 | −20.3649 | −4.86 |
| | 303.15 | 8993 | | | –22.7760 | −5.44 |
| | 313.15 | 15,799 | | | −25.1871 | −6.01 |
| **AMB + βCD** | 293.15 | 27,780 | 18.7543 | 0.1490 | −24.9483 | −5.96 |
| | 303.15 | 37,333 | | | −26.4391 | −6.31 |
| | 313.15 | 45,379 | | | −28.9299 | −6.91 |

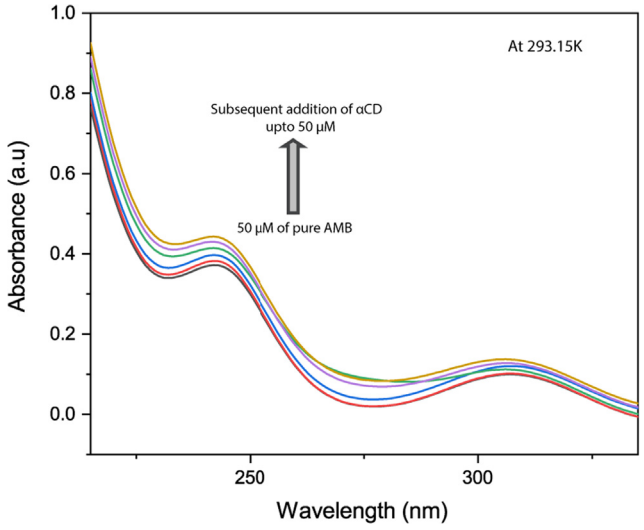


**Fig. 2.** Variation of UV–vis spectra in subsequent addition of αCD in 50 μM aqueous solution of AMB at 293.15 K.

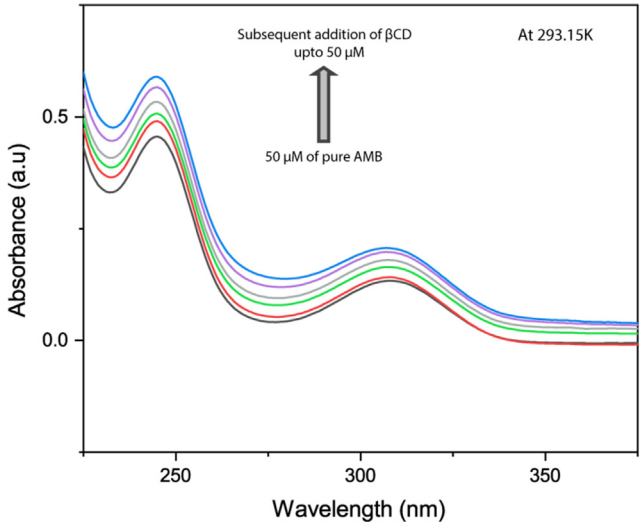


**Fig. 3.** Variation of UV–vis spectra in subsequent addition of βCD in 50 μM aqueous solution of AMB at 293.15 K.

change (ΔG°) can be obtained by means of the classical van't Hoff equation (Eq. (2)): [26]

$$\Delta G^{\circ} = \Delta H^{\circ} - T\Delta S^{\circ} \quad (2)$$

In case of AMB + αCD inclusion complex (Table 2), ΔG° was found to be −4.86 Kcal/mol, −5.44 Kcal/mol, and −6.01 Kcal/mol at 293.15 K, 303.15 K and 313.15 K respectively (Table S5).

However, in case of AMB + βCD inclusion complex, ΔG° was found

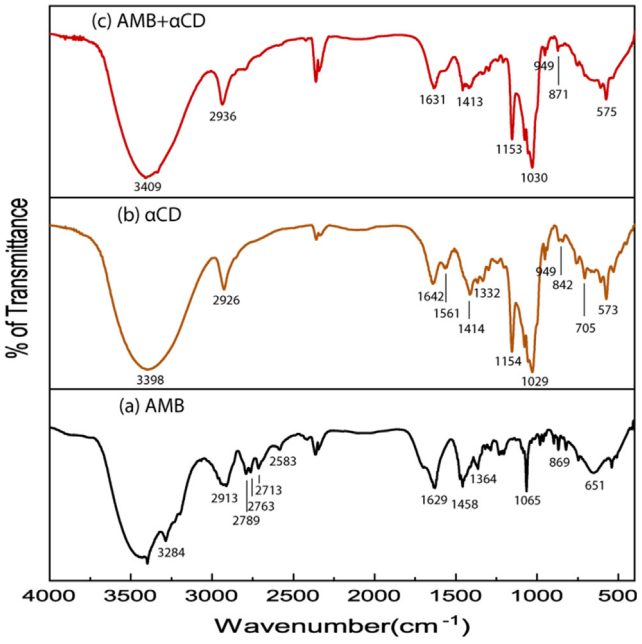


**Fig. 4.** FTIR spectra of (a) pure AMB (b) αCD (c) AMB + αCD inclusion complex.

to be −5.96 Kcal/mol, −6.31 Kcal/mol, and −6.91 Kcal/mol at 293.15 K, 303.15 K and 313.15 K respectively (Table 2 & S7). In both cases, the ΔH° and ΔS° are found to be positive. These values indicate that the inclusion processes are endothermic in nature (entropically favored, and with a nonfavorable enthalpic expression). Thus, these results indicate hydrophobic effects are the main driving forces for the formation of inclusion complexes. In order to approve the above experimental results, a molecular modeling study combining MD simulations was performed.

### 3.4. FTIR spectral analysis

FTIR spectroscopy is an important method to confirm the formation of inclusion complex from the variation in shape, size, shift and intensity of the absorption peak of Guest and Host moiety [27]. There will be broadening, widening, disappearance or change in intensity of the peaks due to complexations [28]. The FTIR spectra of pure AMB, αCD, βCD and the inclusion complexes AMB + αCD and AMB + βCD were recorded and all the peaks were assigned and shown in Figs. 4 & 5.

The infrared spectra of the guest molecule (AMB) showed some few characteristic peaks e.g, a peak at 3193 $cm^{-1}$ was associated with the stretching vibration of aromatic C-H bond [29]. The strong C = C stretching vibrational peak was observed at 1629 $cm^{-1}$, which belongs to the benzene ring [30]. Usually, the vibration of aromatic C-N in $NH_2$ group observed at 1284 $cm^{-1}$. The aliphatic C-N stretching mode was observed at 1458 $cm^{-1}$. The N-H of aromatic amine group showed its stretching vibration at 3300 $cm^{-1}$. However, symmetric stretching mode of aliphatic amine N-H appeared at 3284 $cm^{-1}$ [31].

When inclusion complex is formed, some of the characteristic peaks got disappeared. There are significant differences in the spectra of the inclusion complexes in comparison with the individual drugs. Most of the peaks of the drugs get flattened, indicating a strong intermolecular interaction between the drugs and CDs [32].

For AMB + αCD inclusion complex, the protons belong to the aromatic ring which appeared at 3193 $cm^{-1}$ in pure AMB is diminished in the IR spectra of the complexes. The vibration of aromatic C-N in $NH_2$ group observed at 1284 $cm^{-1}$ and C-N in –NH- group at 1458 $cm^{-1}$ (Fig. 4) has been disappeared possibly due to formation of encapsulation. Therefore, it suggests that probably few portions of the

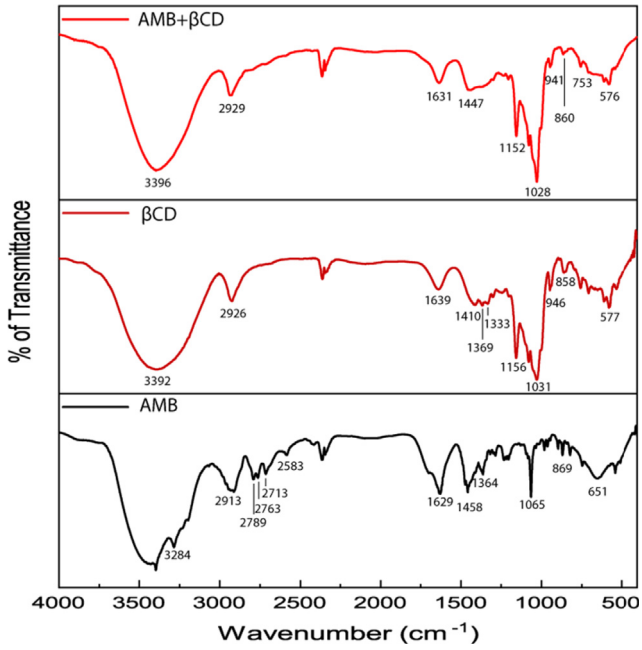


**Fig. 5.** FTIR spectra of (a) pure AMB (b) βCD (c) AMB + βCD inclusion complex.

aromatic part of AMB as well as cyclohexyl part have been encapsulated to the αCD cavity.

For AMB + βCD inclusion complex, the aromatic ring proton which appeared at 3193 $cm^{-1}$ in pure AMB is also diminished in the IR spectra of the complexes (Fig. 5). The vibration of aromatic C-N in $NH_2$ group observed at 1284 $cm^{-1}$ has been shifted to 1206 $cm^{-1}$ whereas, C-N in –NH- group observed at 1458 $cm^{-1}$ has been shifted to 1447 $cm^{-1}$ possibly due to formation of encapsulation. Therefore, it suggests that probably few portions of the aromatic part of AMB as well as cyclohexyl part have been encapsulated to the cyclodextrin cavity.

### 3.5. $^1H$ NMR spectra analysis

The molecular interactions between Host-Guest molecules in inclusion complexes are investigated using $^1H$ NMR [33]. Normally, $^1H$ NMR is used for obtaining the molecular interaction information regarding selective line broadening or chemical shift displacement of host and guest molecules. These chemical shifts are easily observable for protons located at the inner surface (H-3 and H-5) of the cyclodextrins, but it is very difficult to observe the chemical shifts of protons (H-1, H-2 & H-4) located at the outer surface of the Cyclodextrin [34]. It can be observed that these chemical shifts appeared due to inclusion complex development due to the inclusion of Guest into the Host molecule and not because of non-specific correlation between host–guest molecules.

The possible interaction between AMB and αCD for inclusion complex formation was investigated by comparing the $^1H$ NMR spectra of AMB, αCD and the AMB + αCD inclusion complex in $D_2O$ (Fig S9). The chemical shifts of βCD protons with or without AMB were compared in (Table 3a). The chemical shift variations were calculated by the equation: Δ(difference) = Δ(complex)-Δ(free). The positive and negative signs indicate a downfield and upfield shifts, In (Table 3a), upfield shifts are quite evident (-0.04 ppm and −0.01 ppm) observed for the H3′ and H5′ respectively i.e Protons that are located inside the cavity of βCD. But very little to none upfield shifts can be observed of H4′ and H1′ protons could be observed for the protons of βCD that are located outside the cavity.

Inclusion mode of AMB + αCD complex can also be characterized by the chemical shift variation of proton of AMB. Aromatic protons which are designated as H4, H6 when form inclusion complexes chemical shift values have been shifted to downfield (Δδ: H4 0.02, H6 0.03) which indicated that they tend to appear outside the cavity. Whereas, H8, H9 protons belong to the benzyl and secondary NH protons shows significant upfield shift as well as cyclohexane ring protons also show quite good upfield shift (Table 3b). This concludes that apart from aromatic part, rest of the part has been totally inserted into the cavity.

Similarly, $^1H$ NMR spectra of AMB, βCD and the AMB + βCD inclusion complex in $D_2O$ were taken to verify the possible interaction between AMB and βCD for inclusion complex (Fig. S10). The chemical shifts of βCD protons with or without AMB were compared in (Table 4a). Upfield shifts are quite obvious observed for the H3′ and H5′ respectively i.e Protons that are located inside the cavity of βCD. But very little to none upfield shifts can be observed of H4′ and H1′ protons could be observed for the protons of βCD that are located outside the cavity.

It is known that H5′ protons are near the narrow side of the cavity while H3′ protons are near the wide side of the cavity of βCD. In our study of AMB + βCD inclusion complex formation, H3′ possessed reasonably larger chemical shift variation (-0.03 ppm) than H5′ (-0.01 ppm). So it could be proposed that AMB got inserted from wide side of βCD cavity. Moreover, the upfield shifts of H3′ and H5′ protons signify the masking in presence of dense electronic clouds which results in shielding of protons. But in case of protons which are present outside the cavity such as H1′, H4′ H2′ the variation of chemical shifts are little or none.

In Table 4b, the inclusion mode of the AMB + βCD can be further investigated by comparing the 1H NMR spectrum of Ambroxol in the absence and in presence of βCD. As showed in Fig. S10, mostly AMB signals appeared at 1.23–7.70 ppm, which was almost in similar with the βCD protons (2.13–4.98 ppm).Therefore, few AMB protons signals were overlapped specially around (3.4–5.0 ppm) region in the spectra of AMB + βCD complex. It was observed that AMB protons signals were much weaker as compared to βCD due to the less percentage of AMB (Guest) in the inclusion complex with βCD. Moreover, after inclusion in βCD chemical shift changes were also reported for AMB protons signals between free and complexed state (Table 4b). we observed that βCD induced variations in chemical shift occurred in case of few protons but pretty much significant differences as compared to αCD were reported in case of H4, H6 protons (Δδ: H4 −0.03; H6 −0.01), which were characterized by aromatic protons of benzene ring (Fig. S10). However, H12, H14 proton of AMB shows significant variations (Δδ: H12, H14 −0.03). From these findings it can also be proposed that probably the Aromatic ring of Ambroxol.HCl get stabilize outside the βCD cavity.

**Table 3a**
Chemical shift data (in ppm) of protons of free αCD and of AMB + αCD complex and their differences.

| Protons Of αCD | Δδ (Free) (ppm) | Δδ (Complex) (ppm) | Δδ (Difference) (ppm) |
|---|---|---|---|
| H1′ | 4.97–4.96 (d, *J* = 4 Hz) | 4.96 (d, *J* = 4 Hz) | −0.01 |
| H4′ | 3.50–3.47 (t, *J* = 12 Hz) | 3.50–3.47 (t, *J* = 12 Hz) | 0.00 |
| H3′ | 3.91–3.80 (dd, *J* = 8 Hz) | 3.87–3.81 (t, *J* = 8 Hz) | **−0.04** |
| H5′ | 3.79–3.74 (m, *J* = 8 Hz) | 3.79–3.75 (t, *J* = 8 Hz) | **−0.01** |
| H2′ | 3.56–3.52 (dd, *J* = 4 Hz) | 3.56–3.52 (dd ,*J* = 4 Hz) | 0.00 |

**Table 3b**
Chemical shift Data (in ppm) of protons of AMB in Free State and during Inclusion Complexation with αCD.

| PROTONS OF AMB | δ(Free) (ppm) | δ(Complex) (ppm) | δ(Difference) (ppm) |
|---|---|---|---|
| H4 | 7.70 (1H, s) | 7.72 (1H, s) | 0.02 |
| H6 | 7.33 (1H, s) | 7.36 (1H, s) | 0.03 |
| H8 | 2.00–1.97 (1H, d, *J* = 12 Hz) | 2.01–1.97 (1H, d, *J* = 12 Hz) | 0.01 |
| H9 | 2.14–2.12 (1H, d, *J* = 12 Hz) | 2.18–2.16 (1H, d, *J* = 12 Hz) | 0.04 |
| *H*10 | 3.18–3.12 (1H, t, *J* = 12 Hz) | – | 0 |
| H13 | 3.61–3.56 (1H, m, *J* = 4 Hz) | _ | _ |
| H12, H14 | 1.49–1.40 (4H, q, *J* = 12 Hz) | 1.44 (4H, q, *J* = 12 Hz) | −0.05 |
| *H*11, H15 | 1.32–1.23 (4H, q, *J* = 12 Hz) | 1.30 (4H, q, *J* = 12 Hz) | −0.02 |
| H16 | 4.15 (2H, s) | 4.17 (1H, s) | 0.02 |

**Table 4a**
Chemical shift Data (in ppm) of protons of βCD in Free State and during Inclusion Complexation with AMB.

| PROTONS OF βCD | δ(Free) (ppm) | δ(Complex) (ppm) | Δδ(Difference) (ppm) |
|---|---|---|---|
| H1′ | 4.98–4.97 (d, *J* = 4 Hz) | 4.98–4.97 (d, *J* = 4 Hz) | 0 |
| H4′ | 3.49–3.47 (t, *J* = 12 Hz) | 3.49–3.47 (t, *J* = 12 Hz) | 0.00 |
| H3′ | 3.90–3.86 (t, *J* = 8 Hz) | 3.87–3.83 (t, *J* = 8 Hz) | **−0.03** |
| H5′ | 3.79–3.75 (t, *J* = 8 Hz) | 3.78–3.75 (t, *J* = 8 Hz) | **−0.01** |
| H2′ | 3.57–3.54 (dd, *J* = 4 Hz) | 3.57–3.51 (dd ,*J* = 4 Hz) | 0.00 |

### 3.6. 2D-ROESY NMR spectral analysis.

Two-dimensional (2D) NMR spectroscopy provides significant information and conclusive evidence about the spatial proximity between the atoms of host and guest via observations of the intermolecular dipolar cross-correlations [35]. The two protons that are closely located in space within 0.4 nm can produce a nuclear Overhauser effect (NOE) cross-correlation in rotating-frame NOE spectroscopy (ROESY). Here we obtained 2D ROESY spectra of the inclusion complexes of AMB with αCD and βCD to procure more conformational information and encapsulation mechanism. The 2D-ROESY spectrum of the AMB + αCD complex (Fig. S11) showed considerable correlation of the aromatic H-6 and alicyclic H-11/H-15 protons of AMB with the H-5 and H-3 protons of αCD respectively. These results recommends that the AMB molecule was encapsulated within the cavity of αCD via the narrower rim, suggesting half of the aromatic ring containing bulky Br atoms outside the narrower rim and half of the alicyclic ring containing –OH group outside the wider rim. The ROESY spectrum of the AMB + βCD complex (Fig. S12) also showed significant correlations between the aromatic H-6 and alicyclic H-12/H-14 protons of AMB with the H-3 and H-5 protons of βCD respectively. These outcomes, however, suggest that the AMB molecule was included in the βCD cavity via the wider rim, indicating half of the aromatic ring containing bulky Br atoms outside the wider rim. Based on the observation from $^{1}$H NMR and 2D-NMR, a plausible mechanism have been drawn and shown in Scheme 2.

### 3.7. ESI-MS of the inclusion complex analysis:

The formation of the inclusion complexes of AMB with αCD and βCD were examined by ESI-mass spectrometry [36]. The spectra are shown in the Fig. S13 & S14 and the *m/z* values for the observed peaks are enlisted in Table 5. The peaks appeared at *m/z* 1388.58 and 1410.36 corresponds to the $[AMB + \alpha CD + H]^+$ and $[AMB + \alpha CD + Na]^+$ respectively, and the peaks at 1550.65 and 1572.44 corresponds to the $[AMB + \beta CD + H]^+$ and $[AMB + \beta CD + Na]^+$ respectively. These observed peaks in the spectra recommends that AMB is encapsulated inside the cyclodextrin cavity, and the stoichiometric ratio of the host–guest is 1:1.

### 3.8. Scanning electron microscope (SEM) analysis

Scanning electron microscopy (SEM) is a very suitable qualitative analysis technique to visualize the surface texture of different materials [37]. SEM photographs of αCD, βCD, AMB and their inclusion complexes are shown in Fig. 6. Pure AMB shows its amorphous characteristics. The micrographs of βCD presented homogeneous morphology and polyhedral flake like crystals whereas αCD shows its well defined prismatic shape as reported in other literatures [38]. In contrast, the inclusion complex appeared as regular particles in which the original morphology of both components disappeared in both cases and homogeneous plate-like structures with crystal particles were present and it is quite different from the sizes and shapes of αCD, βCD and AMB, which confirms the formation of the inclusion complex.

**Table 4b**
Chemical shift Data (in ppm) of protons of AMB in Free State and during Inclusion Complexation with βCD.

| PROTONS OF AMB | δ(Free) (ppm) | δ(Complex) (ppm) | δ(Difference) (ppm) |
|---|---|---|---|
| **H4** | 7.70 (1H, s) | 7.67 (1H, s) | **−0.03** |
| **H6** | 7.33 (1H, s) | 7.32 (1H, s) | **−0.01** |
| H8 | 2.00–1.97 (1H, d, *J* = 12 Hz) | 2.03–1.99 (1H, d, *J* = 12 Hz) | 0.03 |
| H9 | 2.14–2.12 (1H, d, *J* = 12 Hz) | 2.17–2.14 (1H, d, *J* = 12 Hz) | 0.03 |
| H10 | 3.18–3.12 (1H, t, *J* = 12 Hz) | – | 0 |
| H13 | 3.61–3.56 (1H, m, *J* = 4 Hz) | – | – |
| **H12, H14** | 1.49–1.40 (4H, q, *J* = 12 Hz) | 1.46–1.43 (4H, q, *J* = 12 Hz) | **−0.03** |
| H11, H15 | 1.32–1.23 (4H, q, *J* = 12 Hz) | 1.32–1.25 (4H, q, *J* = 12 Hz) | 0 |
| H16 | 4.15 (2H, s) | 4.15 (1H, s) | 0 |

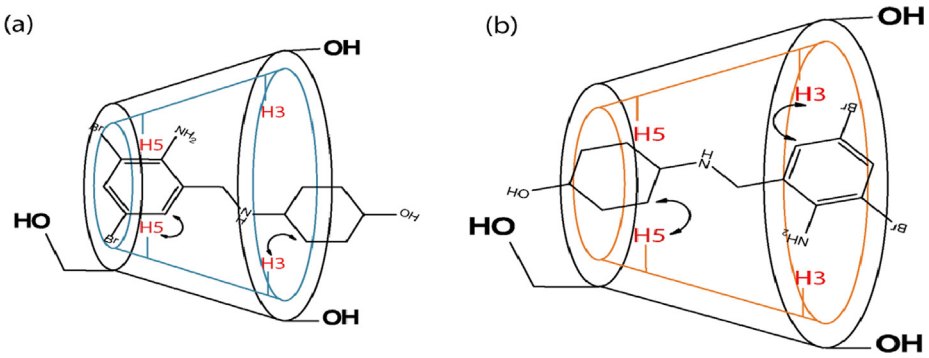


**Scheme 2.** Plausible inclusion mechanism of (a) AMB + αCD inclusion complex (b) AMB + βCD inclusion complex predicted by $^{1}$H NMR and 2D-NMR.

**Table 5**
ESI-MS mass spectra of different inclusion complex.

| Name of the complexes | Calculated mass (a.u) | Experimental mass (a.u) |
|---|---|---|
| [AMB + αCD + H]$^{+}$ | 1388.41 | 1388.58 |
| [AMB + αCD + Na]$^{+}$ | 1410.41 | 1410.36 |
| [AMB + βCD + H]$^{+}$ | 1550.53 | 1550.65 |
| [AMB + βCD + Na]$^{+}$ | 1572.53 | 1572.44 |

### 3.9. Molecular docking results

#### 3.9.1. Prediction of AMB + αCD and AMB + βCD inclusion complexes binding mode

Molecular modelling techniques, such as molecular docking, have been well recognised in predicting the binding modes [39] and interaction profiles of inclusion complexes with different receptor like structures including CDs [40]. Previous studies [41] have confirmed that the most of the guest molecules are usually inserted into CDs via the larger outer rim than that of the smaller one. But in our case, AMB + αCD showed different results (Fig. 7a & b) i.e, AMB has been inserted through narrow rim and aromatic ring was present almost outside, whereas cyclohexane ring was present at wider side of the ring. However, aromatic N-H were connected with $CH_2$-OH group of αCD through bond which make whole complex stabilized and the distance between these two group was found to be 2.13 Å (Table 6). The snapshots of AMB + βCD complexes illustrated in Fig. 7c & d show that AMB enters the nanocavity of the host in such a way that the both the bromine atoms of aromatic part was present outside of the wider rim of the cavity but benzyl carbon i.e, carbon next to the phenyl group attached with secondary group (–$NH_2$-) and whole cyclohexane ring were inserted into the cavity and stabilized at the norrower rim. The distance of secondary N-H group of AMB with the oxygen atom that attached with two glucopyranose rings of βCD was 2.36 Å, which connected by hydrogen bond (Table 6). In most of the previous studies show[42] that if both aromatic part and aliphatic part are present in a molecule, then most of the cases aromatic part got inserted but here, anomalous behaviour happen that may be due to the present of two bulky bromine atoms that present in the aromatic ring.

Moreover, the binding energy ($\Delta G^0$) for the best docking pose of the complexes was also calculated at room temperature (Table 7). The $\Delta G^0$ values of modes AMB + αCD and AMB + βCD in the 1:1 stoichiometry were −3.68 and −4.57 kcal/mol, respectively obtained from the S dock score of MOE database viewer. The results indicated that the complex were stable by good binding energy and drug were completely embedded into the CD cavities and the computational data is quite comparable with our experimental data which is in the range of −4.86 kcal/mol to −6.01 kcal/mol and −5.96 to −6.91 kcal/mol for AMB + αCD and AMB + βCD inclusion complex respectively (Table 2). The findings of this theoretical study are consistent with the results of UV–vis titration, FT-IR, NMR and ESI-MS study.

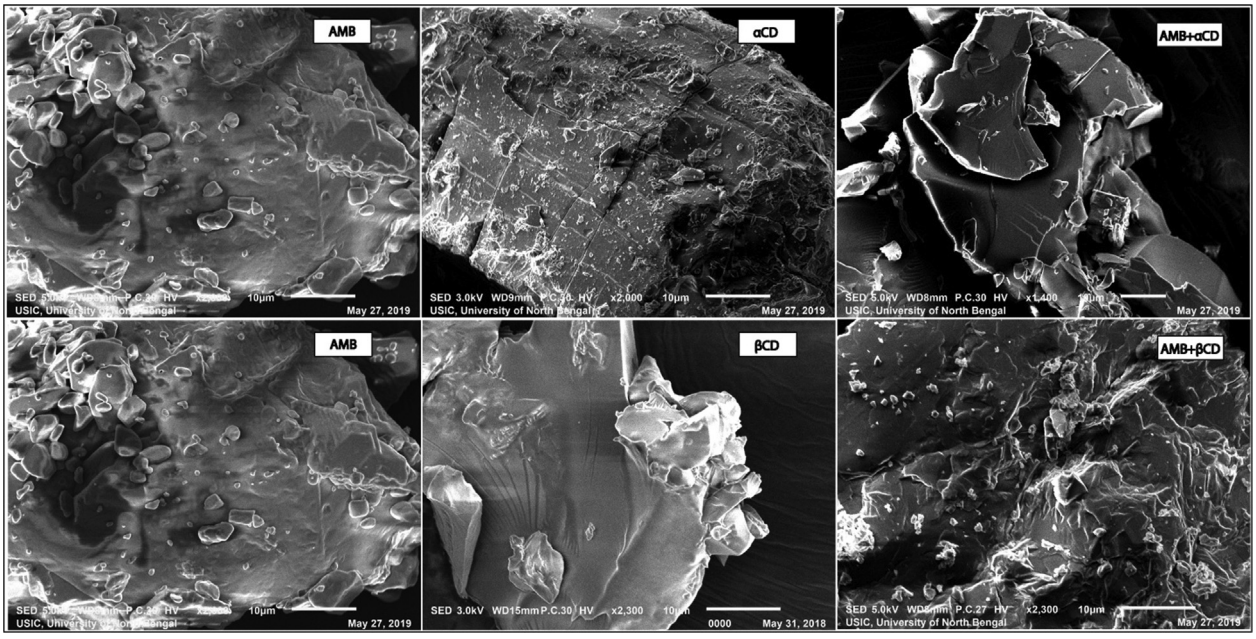


**Fig. 6.** Scanning Electron Microscope microphotograph of AMB, αCD, βCD, AMB + αCD complex and AMB + βCD complex.

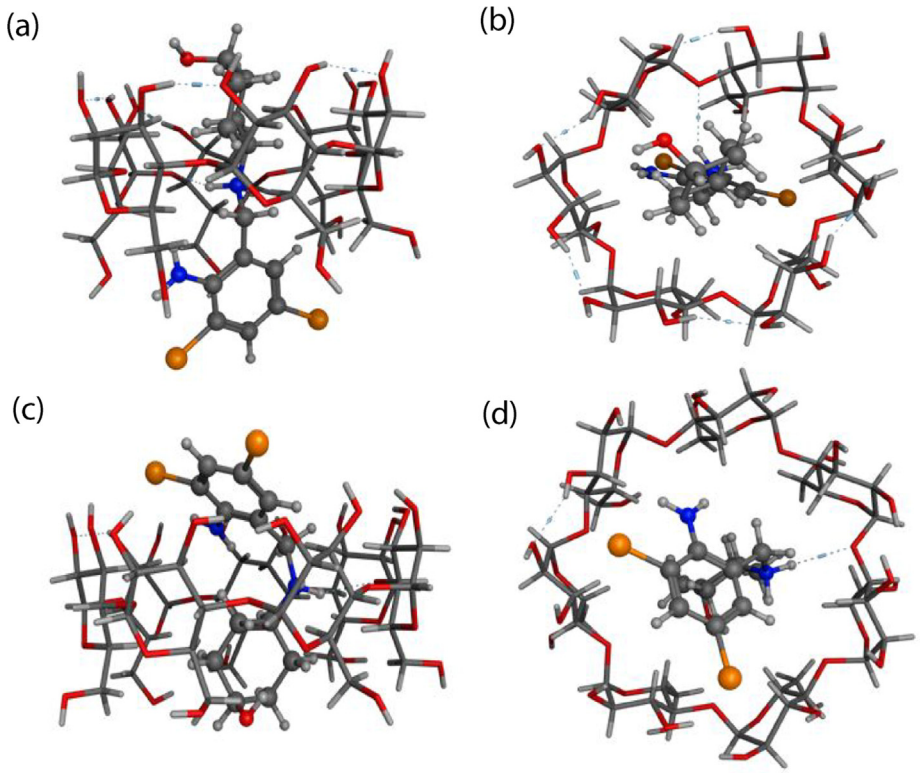


**Fig. 7.** (a) AMB + αCD Side view; (b) AMB + αCD Upper view; (c) AMB + βCD side view; (d) AMB + βCD Upper view; atom designation: gray, carbon; red, oxygen; blue, nitrogen; orange, bromine. (For interpretation of the references to colour in this figure legend, the reader is referred to the web version of this article.)

**Table 6**
Hydrogen bonding distance in AMB + αCD and AMB + βCD Complex from Molecular Docking.

| Receptor atoms | AMB atoms | Distance (Å) |
|---|---|---|
| **αCD ($CH_2$-O)** | **N**(aromatic)-**H** | 2.13 |
| **βCD (pyranose$CH_2$-O-$CH_2$pyranose)** | **N**($SP^3$)-**H** | 2.36 |

**Table 7**
Binding affinity of AMB + αCD and AMB + βCD obtained from Molecular Docking.

| Ligand with receptor | Binding affinity(ΔG)in kcal.$mol^{-1}$ | rmsd_refine |
|---|---|---|
| AMB + αCD | −3.68 | 3.95 |
| AMB + βCD | −4.57 | 2.31 |

*3.9.2. Potential energy calculations of two different inclusion complexes (AMB + αCD and AMB + βCD)*

Changes in Potential energy (ΔE) for both the complexes were also calculated in order to obtain some profound information about the geometry of the host–guest complexes and to find the intermolecular interaction in between host and guest inclusion complexation [43]. ΔE of the complexation was calculated for the minimum energy mode of docked complex according to Eq. (1) and the data of $E_{complex}$, $E_{host}$ + $E_{guest}$, ΔE were listed in Table 8. Solvation energy is zero because the modeling was carried out in gas phase.

$$\Delta E = E_{Complex} - (E_{Host} + E_{Guest}) \quad (1)$$

The results show that the potential energies for the complexes of AMB with αCD and βCD were −174.886 kcal $mol^{-1}$ and −213.260 kcal $mol^{-1}$, respectively, indicating that AMB has stronger affinity for βCD than that for Acd [44]. Electrostatic potential energy surfaces of both the complex show the charge distribution of molecule

**Table 8**
Potential energy calculation of the docked complex without energy minimization.

| Inclusion Complex | $E_{Host}$ (Kcal/mol) | $E_{Guest}$ (Kcal/mol) | $E_{Complex}$ (Kcal/mol) | ΔE (Kcal/mol) |
|---|---|---|---|---|
| AMB + αCD | 511.134 | 254.702 | 590.950 | −174.886 |
| AMB + βCD | 1253.700 | 254.702 | 1295.142 | −213.260 |

three dimensionally (Fig. 8). Sherje et al., [45] in their work, beautifully showed that various potential energy components have overall effect on forming stable inclusion complex. In our case of AMB + αCD inclusion complex (Table S8), Van der walls energy (vdw) was found to be 170.84 kcal/mol and electrostatic interaction energy (ele) was about 172.20 kcal/mol. So, the differential (Del) van der Waals energy was 44.88 kcal/mol, and the Del electrostatic energy was −12.51 kcal/mol. It is the van der Waals energy that makes the inclusion complex stable. However, in case of AMB + βCD inclusion complex (Table S9), Van der walls energy (vdw) was found to be 175.33 kcal/mol and electrostatic interaction energy (ele) was about 268.75 kcal/mol. So, the differential (Del) van der Waals energy was 9.45 kcal/mol, and the Del electrostatic energy was 42.85 kcal/mol. It is the electrostatic interaction energy that makes the inclusion complex stable [46,47].

*3.9.3. Change in the dihedral angle and bond length of AMB after forming inclusion complexes.*

To establish the modification of the structural conformation of AMB upon insertion into αCD and βCD, we have once used MD docking. Sancho et al. [32], showed that change in dihedral angle and bond length could give us strong evidence of conformational changes. After getting the docked pose of all the inclusion complexes, we have measured the dihedral angle of free AMB and the complex encapsulated AMB. The calculated dihedral angles of pure AMB between the carbon atoms labeled as a-b-c-d, b-c-d-e and b-c-d-f were found to be 172.1$^0$,

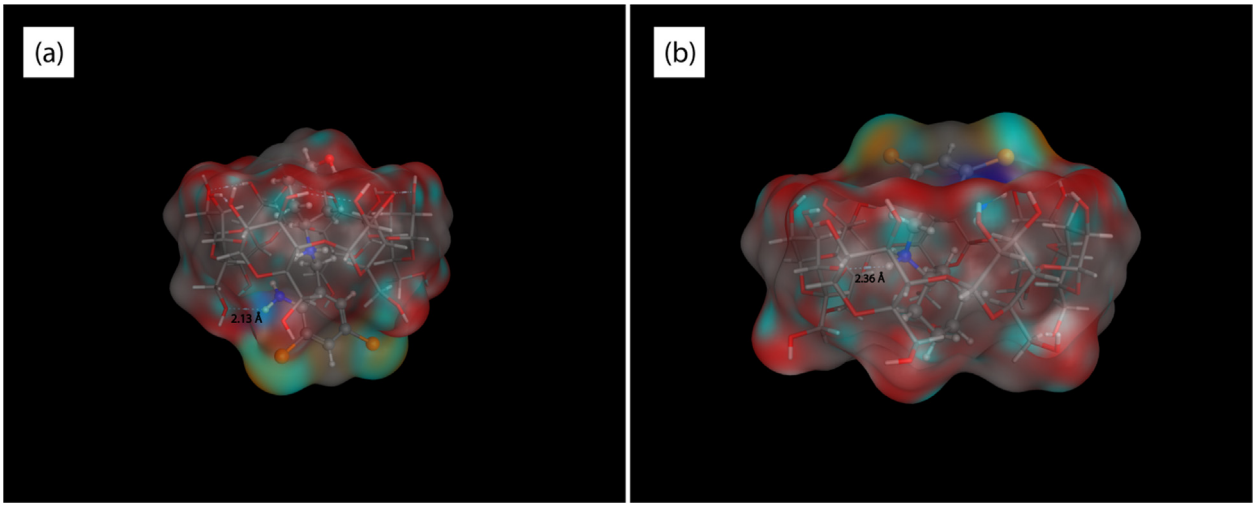


**Fig. 8.** electrostatic potential energy surface of (a) AMB + αCD (b) AMB + βCD inclusion complex.

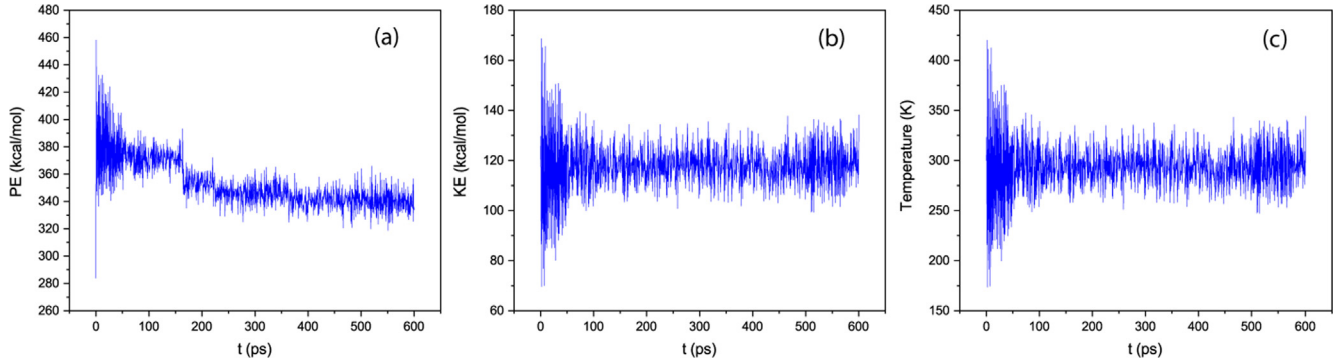


**Fig 9.** Molecular dynamic simulation study of AMB + αCD inclusion complex with respect to (a) time versus kinetic energy (b) time versus potential energy (c) time versus temperature.

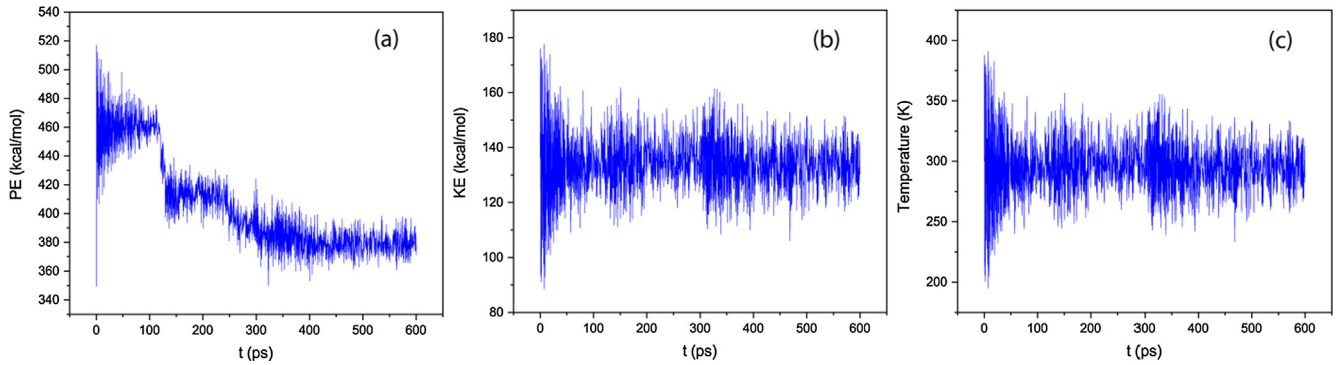


**Fig 10.** Molecular dynamic simulation study of AMB + βCD inclusion complex with respect to (a) time versus kinetic energy (b) time versus potential energy (c) time versus temperature.

$66.4^0$, and $-168.5^0$ respectively (Scheme 1). However, for inclusion complex AMB + αCD, the dihedral angles for the same labelling were found to be $-174.9^0$, $-70.9^0$ and $172.7^0$. It is clear evidence that all the planes were rotated to their opposite direction after forming complex. But in case of AMB + βCD complex, the dihedral angles were found to be $81.8^0$, $152.6^0$ and $-86.8^0$. It suggests that all the planes were getting shifted to get the stability of the complex. Docking poses all supports the conclusion as in encapsulated form, AMB got deformed structure. Change in bond length of guest AMB also confirms structural changes in both the inclusion complexes. In free AMB, Bond length of aromatic amine **N-H** bond is around 0.86 Å. Whereas, aliphatic $\mathbf{N_c}$-$\mathbf{C}H_2$, Ph-$\mathbf{C_b}$-**H** is about 1.45 Å and 0.97 Å respectively. When it forms inclusion complex, aromatic amine **N-H** bond slightly shifted from 0.86 Å to 1.03 Å in case of AMB + αCD due to hydrogen bonding with hydroxyl group of αCD and 0.86 Å to 1.01 Å in case of AMB + βCD due to van der Waals force of attraction. While, aliphatic $\mathbf{N_c}$-$\mathbf{C}H_2$ gets increased from 1.45 Å to 1.47 Å in AMB + αCD and 1.50 Å in case of AMB + βCD. In addition, Ph-$\mathbf{C_b}$-**H** bond length is also increased from 0.97 Å to 1.08 Å in case of AMB + αCD and 1.10 Å in case of AMB + βCD respectively possibly due to the hydrophobic interaction of inner cavity protons.

### *3.9.4. Molecular dynamics (MD) simulations*

Molecular dynamics and simulations (MD/MS) study was performed

on both of the inclusion complexes to check the stability of the host–guest complex with respect to time [48,49]. Optimized Inclusion complexes obtained after docking were simulated in gas phase from 0 picoseconds to 600 picoseconds (100 ps of equilibrium and 500 ps of production) with respect to temperature, potential energy and kinetic energy. Before simulation process, whole complex systems were energy minimized. Simulation study of AMB + αCD inclusion complex revealed that initially potential energy of the complex was found to be 283.90 kcal/mol, with the increase in time energy get decreasing and a mild break point found after 150 ps the whole assemble get stabilized after 150 ps and it stayed stabilised up to 600 ps with 333.81 kcal/mol energy respect to temperature, potential energy and kinetic energy, as shown in Fig. 9(a–c), respectively [50,51]. In case of AMB + βCD complex, initial potential energy was found to be 349.53 kcal/mol. At around 120 ps, potential energy was 454.85 kcal/mol, then, a sharp break in the curve was observed and potential energy drop down to 432.29 kcal/mol and with increase in time potential energy getting decrease and stabilized upto 371.30 kcal/mol at 600 ps Fig. 10(a–c).

## 4. Conclusions

In this paper, we report structural and conformational changes after inclusion of AMB with two different host molecules. The thermodynamic data for two inclusion complexes (AMB + αCD and AMB + βCD) make us understand that AMB has been encapsulated with ease. Despite the structural similarity between these two hosts, their inclusion complexes show interesting differences with respect to their dihedral angle changes and potential energy changes. Inclusion mechanism has been outlined from various spectroscopic methods, e.g, Job's plot, $^{1}$H NMR, 2D-NMR, ESI-MS. Then, it is finally confirmed by molecular docking method and theoretically predicts their binding modes. Potential energy calculation indicates that after inclusion complexation of AMB in β-cyclodextrin give more stabilization than that of in α-cyclodextrin. Molecular docking poses of both the complexes confirm that conformational changes occur after encapsulation. Dynamic simulation also confirms that β-CD-complex after a certain time gives more stabilization than α-CD-complex and their dynamic behaviour with respect to time (ps).

## Declaration of Competing Interest

The authors declare that they have no known competing financial interests or personal relationships that could have appeared to influence the work reported in this paper.

## Acknowledgement

This work was supported by State fellowship (Ref No. 600/R-2018) to NR given by Govt of west Bengal. Co-author PB is very grateful to UGC for getting Junior Research fellowship (Ref No. 222/(CSIR-UGC NET DEC. 2017)). Corresponding author Prof. M. N. Roy is very much thankful to UGC for getting one time Grant of seven lakh from UGC-BSR (Ref. No. F.4-10/2010).

## Appendix A. Supplementary data

Supplementary data to this article can be found online at https://doi.org/10.1016/j.cplett.2020.137372.

## References

[1] Y. Wang, C. Wu, Site-Specific Conjugation of Polymers to Proteins, Biomacromolecules 19 (2018) 1804–1825, https://doi.org/10.1021/acs.biomac.8b00248.
[2] J.M. Grange, N.J.C. Snell, Activity of Bromhexine and Ambroxol, semi synthetic derivatives of vasicine from the Indian shrub Adhatoda Vasica, against Microbacterium tuberculosis in vitro, J. Ethnopharmacol. 50 (1996) 49–53, https://doi.org/10.1016/0378-8741(95)01331-8.
[3] J. Peralta, J.J. Poderoso, C. Corazza, M. Fernandez, R.B. Guerreiro, J.C.M. Wiemeyer, Ambroxol Plus Amoxicillin in the Treatment of Exacerbations of Chronic-Bronchitis, Arzneim.-Forsch. 37–2 (1987) 969–971.
[4] J. Mo, L.P. Yuan, Compatibility And Thermal Stability Studies Between Omeprazole And Ambroxol Hydrochloride, Int. Res. J. Pharm. 8 (3) (2017), https://doi.org/10.7897/2230-8407.080337.
[5] F. Tewes, K.J. Paluch, L. Tajber, K. Gulati, D. Kalantri, C. Ehrhardt, A. Marie, Anne Marie HealySteroid/mucokinetic hybrid nanoporous microparticles for pulmonary drug delivery, Eur. J. Pharm. Biopharm. (2013), https://doi.org/10.1016/j.ejpb.2013.03.020.
[6] A. Das, R. Thakur, A. Dagar, A. Chakraborty, A spectroscopic investigation and molecular docking study on the interaction of hen egg white lysozyme with liposomes of saturated and unsaturated phosphocholines probed by an anticancer drug ellipticine, Phys. Chem. Chem. Phys. 16 (2014) 5368, https://doi.org/10.1039/C3CP54247E.
[7] G. Ambrosi, C. Ghezzi, R. Zangaglia, G. Levandis, C. Pacchetti, F. Blandini, Ambroxol-induced rescue of defective glucocerebrosidase is associated with increased LIMP-2 and saposin C levels in GBA1 mutant Parkinson's disease cells, Neurobiology of Disease 82 (2015) 235–242, https://doi.org/10.1016/j.nbd.2015.06.008.
[8] O. Gyulai, P. Szabo-Revesz, Z. Aigner, Comparison Study of Different Spherical Crystallization Methods of Ambroxol Hydrochloride, Cryst. Growth Des. 17 (2017) 5233–5241, https://doi.org/10.1021/acs.cgd.7b00764.
[9] J. Magalhaes, M.E. Gegg, A. Migdalska-Richards, A.H. Schapira, Effects of ambroxol on the autophagy-lysosome pathway and mitochondria in primary cortical neurons, Sci. Rep. 8 (2018) 1385, https://doi.org/10.1038/s41598-018-19479-8.
[10] V.R.R. Thummala, M.R. Ivaturi, S.R. Nittala, Identification, and Characterization of One Degradation Product in Ambroxol by HPLC-Hyphenated Techniques, Sci Pharm. 82 (2014) 247–263, https://doi.org/10.3797/scipharm.1310-21.
[11] I.B. Bar, G. Maor, M. Filocamo, M. Horowitz, Ambroxol as a pharmacological chaperone for mutant glucocerebrosidase, Blood Cells Mol. Dis. 50 (2013) 141–145, https://doi.org/10.1016/j.bcmd.2012.10.007.
[12] Deepak Sharma, Mankaran Singh, Dinesh Kumar, Gurmeet Singh, Simultaneous Estimation of Ambroxol Hydrochloride and Cetirizine Hydrochloride in Pharmaceutical Tablet Dosage Form by Simultaneous Equation Spectrophotometric Method: A Quality Control Tool for Dissolution Studies, ISRN Analytical Chemistry 2014 (2014) 1–6, https://doi.org/10.1155/2014/236570.
[13] L. Szente, J. Szeman, Cyclodextrins in Analytical Chemistry: Host−Guest Type Molecular Recognition, Anal. Chem. 85 (2013) 8024–8030, https://doi.org/10.1021/ac400639y.
[14] B.V.K.J. Schmidt, C.B. Kowollik, Dynamic Macromolecular Material Design-The Versatility of Cyclodextrin-Based Host-Guest Chemistry, Angew. Chem. Int. Ed. 56 (2017) 8350–8369, https://doi.org/10.1002/anie.201612150.
[15] A.P. Sherje, F. Patel, M. Murahari, V. Suvarna, K. Patel, Study on effect of L-arginine on solubility and dissolution of Zaltoprofen: preparation and characterization of binary and ternary cyclodextrin inclusion complexes, Chem. Phys. Lett. 694 (2018) 120–128, https://doi.org/10.1016/j.cplett.2018.01.025.
[16] C.S. Mangolim, C. Moriwaki, A.C. Nogueira, F. Sato, M.L. Baesso, A.M. Neto, G. Matioli, Curcumin–b-cyclodextrin inclusion complex: Stability, solubility, characterisation by FT-IR, FT-Raman, X-ray diffraction and photoacoustic spectroscopy, and food application, Food Chem. 153 (2014) 361–370, https://doi.org/10.1016/j.foodchem.2013.12.067.
[17] W. Chena, L.J. Yang, S.X. Ma, X.D. Yang, B.M. Fan, J. Lin, Crassicauline A/β-cyclodextrin host–guest system: Preparation, characterization, inclusion mode, solubilization and stability, Carbohydr. Polym. 84 (2011) 1321–1328, https://doi.org/10.1016/j.carbpol.2011.01.031.
[18] L.M.M. Gomes, N. Petito, V.G. Costa, D.Q. Falcão, K.G. de Lima Araújo, Inclusion complexes of red bell pepper pigments with β-cyclodextrin: preparation, characterisation and application as natural colorant in Yogurt, Food Chemistry 148 (2014) 428–436, https://doi.org/10.1016/j.foodchem.2012.09.065.
[19] M.S. Mokhtar, F.O. Suliman, A.A. Elbashir, Atrazine and ametryne inclusion complexes with 2-hydroxypropyl-b/g-cyclodextrin: Spectroscopic studies and molecular dynamics simulation, J. Mol. Struct. 1179 (2019) 161–170, https://doi.org/10.1016/j.molstruc.2018.11.002.
[20] M.S. Mokhtar, F.O. Suliman, A.A. Elbashir, The binding interaction of imazapyr with cucurbit[n]uril (n = 6–8): Combined experimental and molecular modeling study, Spectrochim. Acta Part A Mol. Biomol. Spectrosc. 194 (2018) 67–75, https://doi.org/10.1016/j.saa.2018.01.007.
[21] A. Abdolmaleki, F. Ghasemi, J.B. Ghasemi, Computer-aided drug design to explore cyclodextrin therapeutics and biomedical applications, Chem Biol Drug Des 89 (2017) 257–268, https://doi.org/10.1111/cbdd.12825.
[22] T.M.C. Babu, S.S. Rajesh, B.V. Bhaskar, S. Devi, A. Rammohan, T. Sivaraman, W. Rajendra, Molecular docking, molecular dynamics simulation, biological evaluation and 2D QSAR analysis of flavonoids from Syzygium alternifolium as potent anti-Helicobacter pylori agents, RSC Adv. 7 (2017) 18277, https://doi.org/10.1039/C6RA27872H.
[23] M.O. Radwan, S. Sonoda, T. Ejima, Zinc-mediated binding of a low-molecular-weight stabilizer of the host anti-viral factor apolipoprotein B mRNA-editing enzyme, catalytic polypeptide-like 3G, Bioorg Med Chem. 24 (18) (2016) 4398–4405, https://doi.org/10.1016/j.bmc.2016.07.030.
[24] J.S. Renny, L.L. Tomasevich, E.H. Tallmadge, D.B. Collum, Method of Continuous Variations: Applications of Job Plots to the Study of Molecular Associations in Organometallic Chemistry, Angew. Chem. Int. Ed. 52 (2013) 11998–12013, https://doi.org/10.1002/anie.201304157.

[25] H.A. Benesi, J.H. Hildebrand, A Spectrophotometric Investigation of the Interaction of Iodine with Aromatic Hydrocarbons, J. Am. Chem. Soc. 71 (1949) 2703–2707, https://doi.org/10.1021/ja01176a030.
[26] Y. Liao, X. Zhang, C. Li, Y. Huang, M. Lei, M. Yan, Y. Zhou, C. Zhao, Inclusion complexes of HP-β-cyclodextrin with agomelatine: Preparation, characterization, mechanism study and in vivo evaluation, Carbohydr. Polym. 147 (2016) 415–425, https://doi.org/10.1016/j.carbpol.2016.04.022.
[27] W. Chen, L.J. Yang, S.X. Ma, X.D. Yang, B.M. Fan, J. Lin, Crassicauline A/β-cyclodextrin host–guest system: preparation, characterization, inclusion mode, solubilization and stability, Carbohydr. Polym. 84 (2011) 1321–1328, https://doi.org/10.1016/j.carbpol.2011.01.031.
[28] M.V. Ol'khovicha, A.V. Sharapova, S.V. Blokhina, S.Y. Skachilova, O.G. Kesarevb, G.L. Perlovich, Physicochemical characteristics of the inclusion complexes of biologically active compounds with 2-hydroxypropyl-β-cyclodextrin, Thermochimica Acta 639 (2016) 1–9.
[29] G.M. Kumar, S.H. Cheruvu, D. Sujatha, S. Sampathi, Formulation and Characterization of Ambroxol Hydrochloride Loaded Ethyl Cellulose Microparticles for Sustained Release, Journal of Biomaterials and Tissue Engineering 4 (2014) 1–9, https://doi.org/10.1166/jbt.2014.1228.
[30] D. Sharma, M. Singh, D. Kumar, G. Singh, M.S. Rathore, Formulation Development and Evaluation of Fast Disintegrating Tablets of Ambroxol Hydrochloride for Pediatrics- A Novel Approach for Drug Delivery, Indian Journal of Pharmaceutical Education and Research 48 (supplement) (2014).
[31] G. Ramana, O. Sravanthi, G. Sahithi, Naga V. Sindhu, G. Priyanka, Formulation and Evaluation of Controlled Release Hydrophilic Matrices of Ambroxol Hydrochloride by Melt Granulation Technique, American-Eurasian Journal of Scientific Research 7 (4) (2012) 150–159, https://doi.org/10.5829/idosi.aejsr.2012.7.4.6631.
[32] M.I. Sancho, S. Andujar, R.D. Porasso, R.D. Enriz, Theoretical and Experimental Study of Inclusion Complexes of β-Cyclodextrins with Chalcone and 2′,4′-Dihydroxychalcone, J. Phys. Chem. B 120 (2016) 3000–3011, https://doi.org/10.1021/acs.jpcb.5b11317.
[33] F. Xie, G. Ouyang, L. Qin, M. Liu, Supra-dendron Gelator Based on Azobenzene-Cyclodextrin Host–Guest Interactions: Photoswitched Optical and Chiroptical Reversibility, Chem. Eur. J. 22 (2016) 18208–18214, https://doi.org/10.1002/chem.201603998.
[34] Q. Tang, C.H. Wang, Y.Y. Xi, Y. Huang, Z. Tao, Host-Guest Complexes of l-Borneol with Cucurbituril and Cyclodextrin and Its Potential Use in Analysis of Drugs, ChemistrySelect 4 (2019) 6924–6929, https://doi.org/10.1002/slct.201900913.
[35] L. Wang, J. Yan, Y. Li, K. Xu, S. Li, P. Tang, H. Li, The influence of hydroxypropyl-β-cyclodextrin on the solubility, dissolution, cytotoxicity, and binding of riluzole with human serum albumin, J. Pharm. Biomed. Anal. 117 (2016) 453–463, https://doi.org/10.1016/j.jpba.2015.09.033.
[36] A. Raza, H. Sun, S. Bano, Y. Zhao, X. Xu, J. Tang, Preparation, characterization, and in vitro anti-inflammatory evaluation of novel water soluble kamebakaurin/hydroxypropyl-β-cyclodextrin inclusion complex, J. Mol. Struct. 1130 (2017) 319–326, https://doi.org/10.1016/j.molstruc.2016.10.059.
[37] L. Wang, S. Li, P. Tang, J. Yan, K. Xu, H. Li, Characterization and evaluation of synthetic riluzole with β-cyclodextrin and 2,6-di-O-methyl-β-cyclodextrin inclusion complexes, Carbohydr. Polym. 129 (2015) 9–16, https://doi.org/10.1016/j.carbpol.2015.04.046.
[38] P. Dandawate, K. Vemuri, E.M. Khan, M. Sritharan, S. Padhye, Synthesis, characterization and anti-tubercular activity of ferrocenyl hydrazones and their β-cyclodextrin conjugates, Carbohydr. Polym. 108 (2014) 135–144, https://doi.org/10.1016/j.carbpol.2014.03.006.
[39] M.I. Sancho, M.G. Russo, M.S. Moreno, E. Gasull, S.E. Blanco, G.E. Narda, Physicochemical Characterization of 2-Hydroxybenzophenone with β-Cyclodextrin in Solution and Solid State, J. Phys. Chem. B 119 (2015) 5918–5925, https://doi.org/10.1021/acs.jpcb.5b01742.
[40] P. Tang, X. Ma, D. Wu, S. Li, K. Xu, B. Tang, H. Li, Posaconazole/hydroxypropyl-β-cyclodextrin host-guest system: Improving dissolution while maintaining antifungal activity, Carbohydr. Polym. 142 (2016) 16–23, https://doi.org/10.1016/j.carbpol.2016.01.042.
[41] Y. Hayashino, M. Sugita, H. Arima, T. Irie, T. Kikuchi, F. Hirata, Predicting the Binding Mode of 2-Hydroxypropyl-β-cyclodextrin to Cholesterol by Means of the MD Simulation and the 3D-RISM-KH Theory, J. Phys. Chem. B 122 (2018) 5716–5725, https://doi.org/10.1021/acs.jpcb.8b02098.
[42] H. Zhang, C. Ge, D.V. der Spoel, W. Feng, T. Tan, Insight into the Structural Deformations of Beta-Cyclodextrin Caused by Alcohol Cosolvents and Guest Molecules, J. Phys. Chem. B 116 (2012) 3880–3889, https://doi.org/10.1021/jp300674d.
[43] R. Onnainty, E.M. Schenfeld, M.A. Quevedo, M.A. Fernandez, M.R. Longhi, G.E. Granero, Characterization of the Hydrochlorothiazide: β-Cyclodextrin Inclusion Complex. Experimental and Theoretical Methods, J. Phys. Chem. B 117 (2013) 206–217, https://doi.org/10.1021/jp311274c.
[44] Y. Akae, Y. Koyama, H. Sogawa, Y. Hayashi, S. Kawauchi, S. Kuwata, T. Takata, Structural Analysis and Inclusion Mechanism of Native and Permethylated a-Cyclodextrin-Based Rotaxanes Containing Alkylene Axles, Chem. Eur. J. 22 (2016) 5335–5341, https://doi.org/10.1002/chem.201504882.
[45] A.P. Sherje, V. Kulkarni, M. Murahari, U.Y. Nayak, P. Bhat, V. Suvarna, B. Dravyakar, Inclusion Complexation of Etodolac with Hydroxypropyl-betacyclodextrin and Auxiliary Agents: Formulation Characterization and Molecular Modeling Studies, Mol. Pharmaceutics 14 (2017) 1231–1242, https://doi.org/10.1021/acs.molpharmaceut.6b01115.
[46] M.P. Vargas, A.M. Castro, Metal containing cryptands as hosts for anions: evaluation of Cu(I)X and pX interactions in halide–tricopper(I) complexes through relativistic DFT calculations, Phys. Chem. Chem. Phys. 17 (2015) 18677, https://doi.org/10.1039/c5cp02737c.
[47] A.O. Ortolan, I. Østrøm, G.F. Caramori, R.L.T. Parreira, A.M. Castro, F. Matthias Bickelhaupt, Anion Recognition by Organometallic Calixarenes: Analysis from Relativistic DFT Calculations, Organometallics 37 (2018) 2167–2176, https://doi.org/10.1021/acs.organomet.8b00292.
[48] M.P. Vargas, A.M. Castro, Tiara-like Complexes acting as Iodine Encapsulating Agents: The Role of M···I Interactions in [M(μ-SCH2CO2Me)2]8⊂I2 (M = Ni, Pd, Pt) Inclusion Compounds, J. Phys. Chem. C 120 (2016) 23441–23448, https://doi.org/10.1021/acs.jpcc.6b08643.
[49] A.O. Ortolan, I. Østrøm, G.F. Caramori, R.L.T. Parreira, A.M. Castro, F. Matthias Bickelhaupt, Anion Recognition by Organometallic Calixarenes: Analysis from Relativistic DFT Calculations, J. Phys. Chem. A 122 (2018) 3328–3336, https://doi.org/10.1021/acs.jpca.8b01866.
[50] U. Chaube, D. Chhatbar, H. Bhatt, molecular dynamics simulations and molecular docking studies of benzoxazepine moiety as mTOR inhibitor for the treatment of lung cancer, Bioorg. Med. Chem. Lett. 26 (2016) 864–874, https://doi.org/10.1016/j.bmcl.2015.12.075.
[51] I. Daoud, N. Melkemi, T. Salah, S. Ghalem, molecular docking and molecular dynamics study on new Acetylcholinesterase and Butyrylcholinesterase inhibitors, Comput. Biol. Chem. 74 (2018) 304–326, https://doi.org/10.1016/j.compbiolchem.2018.03.021.

Journal of Molecular Structure 1179 (2019) 642–650

Contents lists available at ScienceDirect

Journal of Molecular Structure

journal homepage: http://www.elsevier.com/locate/molstruc

# Study to synthesize and characterize host-guest encapsulation of antidiabetic drug (TgC) and hydroxy propyl-β-cyclodextrin augmenting the antidiabetic applicability in biological system

Niloy Roy, Raja Ghosh, Koyeli Das, Debadrita Roy, Tulika Ghosh, Mahendra Nath Roy*

*Department of Chemistry, University of North Bengal, Darjeeling 734013, India*

ARTICLE INFO

*Article history:*
Received 26 September 2018
Received in revised form
14 November 2018
Accepted 14 November 2018
Available online 17 November 2018

*Keywords:*
Trigonelline hydrochloride (TgC)
Hydroxypropyl-β-cyclodextrin (HP-β-CD)
Scanning electron microscope (SEM)
Encapsulation
NMR
Fluorescence

ABSTRACT

An inclusion complex of a biologically active alkaloid Trigonelline hydrochloride (TgC) and hydroxypropyl-β-cyclodextrin (HP-β-CD) was prepared and characterized by several physicochemical and spectroscopic methods. The Trigonelline/HP-β-CD inclusion complex was confirmed by UV–vis Job's plot, fluorescence, conductance and SEM. Here, the inclusion mode is described with regard to structural aspect using $^{1}$H NMR, FTIR spectroscopy. Trigonelline hydrochloride (TgC) being an anti diabetic natural product, its inclusion complex was precisely checked for its sustained release by fluorescence spectroscopy.



## 1. Introduction

Fenugreek (*Trigonella foenum graecum*) is one of the most widely used medicinal plants in medicine. Trigonelline hydrochloride (TgC), one of the major alkaloid of fenugreek, has been reported to be responsible for showing immense potential pharmacological activities. It has the ability to reduce blood glucose concentration in rats [1,2] and in human [3,4] which indicate that it has a potential antidiabetic activity. It helps to reduce the total cholesterol (TC) and triglyceride (TG) levels. TgC has antioxidant activities in cell-free systems as well as human colon cell lines [5]. The anti diabetic activity of the fenugreek seeds have been reported [6]. Its protects β-cells of the pancreas and increases insulin sensitivity index as well as insulin content [7]. (see Schemes 1 and 2)

Cyclodextrins (CDs) are cyclic oligo saccharides of α-D-glucose that are formed through glycosidic α-1, 4 bonds [8]. Cyclodextrins (CDs) have been used extensively as additives that can increase the solubility of poorly water-soluble organic compounds, by forming an inclusion complex between the host cyclodextrin and the guest molecules [9]. The resulting inclusion or host–guest complexes having unusual physical, chemical and biological properties can greatly increase the interest in scientific and technological aspect, e.g, inner cavity of Cyclodextrins are hydrophobic whereas outer cavity is hydrophilic in nature [10]. Such noncovalent interactions can actually improve the guest's water solubility, bioavailability as well as stability [11]; they can also be used for controlled release of the guest molecules [12]. Hydroxypropyl-beta-cyclodextrin (HP-β-CD), a hydroxy alkyl derivative, is an alternative to parent CDs, having higher water solubility and may have slightly more toxicologically benign [13]. 2-Hydroxy propyl-β-cyclodextrin is commercialised under the trade name of Molecusol™ and Encapsin™ [14]. It does not have any nephrotoxicity in human body just like beta-cyclodextrin. As the first approved CD derivative by FDA, HP-β-CD has wide applications in food, pharmaceuticals and agriculture etc [15].

In order to show some therapeutic affect on biological system, a drug has to be released from their carrier. Here, cyclodextrin has been used as the drug carrier. From the literature, it is reported that hydroxy propyl-β-cyclodextrin can be used modified or controlled release carrier.

In the present study, HP-β-CD has been used as the host molecule whereas TgC as guest molecule. HP-β-CD can increase the water solubility of pure TgC (50 mg/mL) to up to four times after

* Corresponding author.
*E-mail address:* mahendraroy2002@yahoo.co.in (M.N. Roy).

https://doi.org/10.1016/j.molstruc.2018.11.049
0022-2860/

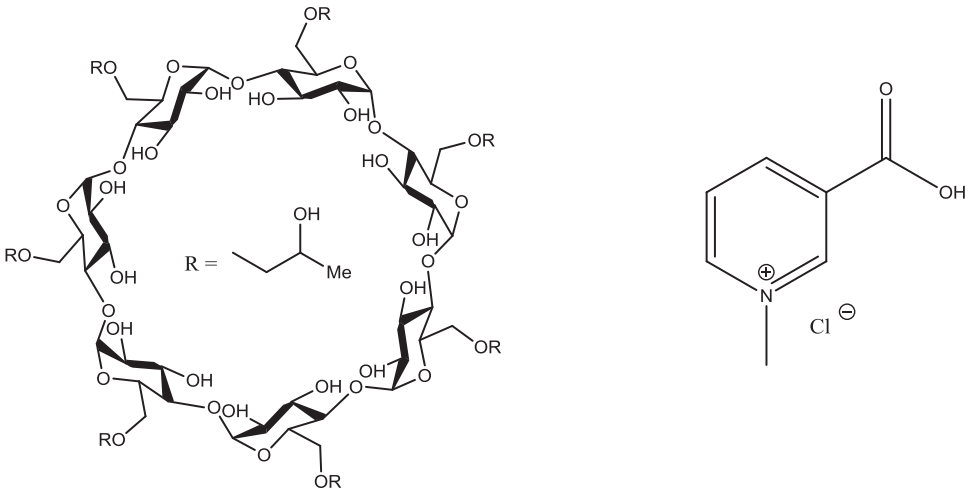


**Scheme 1.** The molecular structures of Hydroxypropyl beta cyclodextrin and Trigonelline hydrochloride.

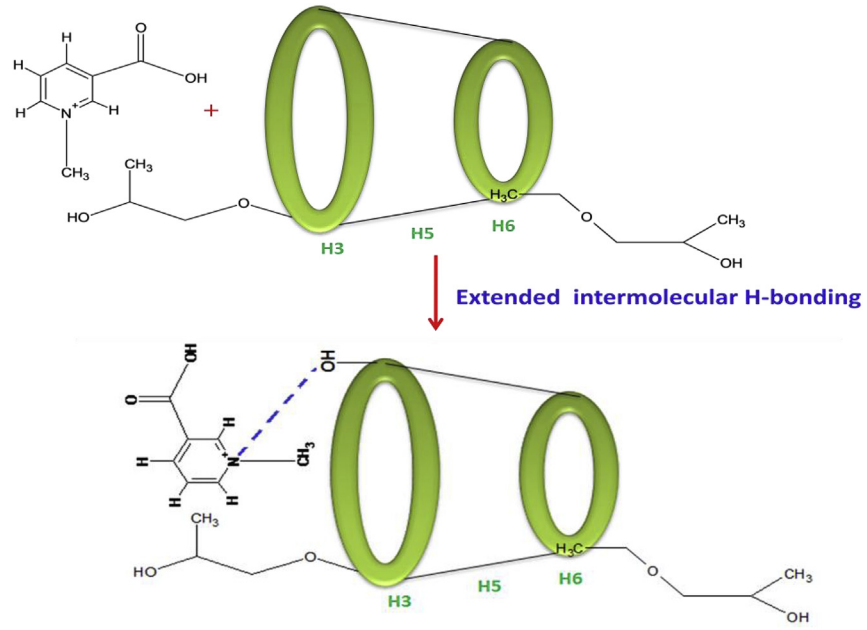


**Scheme 2.** Schematic Representation for encapsulation.

formation of the inclusion complex (196 mg/mL) and hence increase the bio availability of the drug. It will also be studied that whether the inclusion complex show sustained release or not. In this aspect, fluorescence spectroscopy will be involved as the measurement.

## 2. Materials and methods

### 2.1. Materials

Trigonelline hydrochloride (Molecular weight = 173.60 g/mol, Purity> 98%) used in this work was purchased from Sigma Aldrich. 2-Hydroxypropyl-β-cyclodextrin (HP-β-CD, average molecular weight = 1541.54 g/mol) was obtained from TCI chemicals India PVT. LTD and used without further purification. Other reagents and chemicals were of analytical reagent grade. All experiments were done using double distilled water.

### 2.2. Methods

#### 2.2.1. Preparation of TgC/HP-β-CD inclusion complex

An inclusion complex of TgC/HP-β-CD was prepared in 1:1 M ratio by simple co-precipitation method [16]. First, TgC (25 mg) and HP-β-CD (225.89 mg) were dissolved in minimum volume of pure distilled water, then the two solutions were mixed in a 50 mL beaker and kept at 50 °C with stirring of 350 rpm/min for 24 h. Finally, the sample was evaporated under reduced pressure in a rotary evaporator at 40 °C to produce a solid inclusion complex.

#### 2.2.2. Preparation of physical mixture

A physical mixture of TgC and HP-β-CD with a 1:1 M ratio was also prepared by mixing solid TgC and HP-β-CD thoroughly for 10 min in a ceramic mortar unless a homogeneous mixture was obtained [17].

### 2.3. Inclusion complex characterization

#### 2.3.1. UV measurement

UV spectra of the inclusion complex, TgC and HP-β-CD were obtained by Agilent 8453 UV–vis spectrophotometer with uncertainty ±2 nm. A conventional 1 cm path (1 cm × 1 cm × 4 cm) quartz cell has been used. UV instrument was attached with a digital thermostat. The scans were taken within range from 190 to 1200 nm.

As the compound TgC was water soluble, double distilled $H_2O$ had been used for the spectral measurements [18].

#### 2.3.2. Conductance

Conductance measurements were taken in SYSTRONICS CONDUCTIVITY-TDS METER 308 instrument [19]. Prior to the experiment, cell constant and specific conductance of the solvent ($H_2O$) were measured. Cell constant was found to be 0.10 $cm^{-1}$. Specific Conductance of 10 mM, 10 mL pure TgC was 18.2 $mScm^{-1}$.

#### 2.3.3. Fourier Transform Infrared spectroscopy (FT-IR)

The FT-IR analysis was performed on a Perkin Elmer Spectrum FT-IR spectrometer, using KBr pellets [20]. The samples of TgC, HP-β-CD, physical mixture, and their inclusion complex were previously ground and mixed thoroughly with KBr. The KBr disks were prepared by compressing the powder. The scans were done with a resolution of 4 $cm^{-1}$, from 4000 to 500 $cm^{-1}$. The concentration of the sample in pellets was 1 mg/100 mg KBr [20].

#### 2.3.4. $^1H$ NMR

One-dimensional $^1H$ NMR spectra were recorded at room temperature on Bruker AVANCE III 400 NMR spectrometer. TgC, HP-β-CD and the complex TgC/HP-β-CD were respectively dissolved in D2O (Aldrich). The signal at 4.67 ppm of HOD was used as an internal reference [21].

#### 2.3.5. Scanning electron microscope (SEM)

The surface morphologies of TgC, HP-β-CD, TgC/HP-β-CD physical mixture and TgC/HP-β-CD inclusion complex were determined by JEOL JSM-IT 100 scanning electron microscope [22]. The pictures were taken at an excitation voltage of 15, 20 or 30 kV and a magnification of 425, 500, 1000 or 2000×.

#### 2.3.6. Sustained release by fluorescence

Release kinetics was studied with the help of fluorescence spectroscopy to determine the variation in maximum emission intensity with time [23]. First, 100 μM solution of inclusion complex (TgC/HP-β-CD) was prepared in Double distilled water. Excitation of the fluorescence spectrometer was set at 265 nm, emission scan was adjusted in the range of 275–650 with slit width at 2 nm and spectra were recorded with time gap of 0, 10, 20, 30, 40, 60, 75, 90, 105, 150, 210 mins.

## 3. Results and discussion

### 3.1. Job-plot by UV–vis determination

The stoichiometry of inclusion complex was determined by the continuous variation Job's method [24]. First, 100 μM solution of both TgC and HP-β-CD were prepared and them they were mixed by varying the molar ratio (4 mL:0 mL, 3.6 mL:0.4 mL, 3.2 mL:0.8 mL and so on) but the total concentration of the species were kept constant (Table S1). After 1 h, the absorbance at $\lambda_{max}$ was determined for all the solutions and the difference in absorbance in the presence and in absence of HP-β-CD was plotted against R (R = [TgC]/{[TgC]+[HP-β-CD]}. The shift of $\lambda_{max}$ around 265 nm of the UV-spectrum of TgC was observed to prepare the Job's plot. The absorption peak observed at 265 nm for TgC in water was due to the Π-Π* transition of the pyridinium moiety. The Fig. 1 shows a maximum value at r = 0.50, corresponding to 1:1 (TgC: HP-β-CD) stoichiometry.

### 3.2. Association constant calculation by UV–vis measurement

Association constant and stoichiometric ratio of the inclusion complex TgC/HP-β-CD can be calculated according to the Benesi-Hindebrand double reciprocal plot assuming the formation of a 1:1 host–guest complex [25].

$$\frac{1}{\Delta A} = \frac{1}{K[TgC]\Delta\in} \times \frac{1}{[HP\beta CD]} + \frac{1}{[TgC]} \quad (1)$$

Where, ΔA is the difference of absorbance between the TgC in the absence and presence of the HP-β-CD at a particular wavelength, Δε is the difference in the molar absorptivities between guest (TgC) and inclusion complex. The Fig. 2 showed the variation in UV–vis spectral changes of TgC on addition of different strength of solution.

Plot of 1/ΔA versus 1/[HP-β-CD] for three different temperatures (293 K, 298 K, 303 K) had been taken and was found to be straight lines (Fig S1 in supporting information). Linear correlation was satisfactory ($R^2 = 0.661$ at 293 k, $R^2 = 0.891$ at 298 k, $R^2 = 0.999$ at 303 k), which is less than 1, it's also confirm that the formation of a 1:1 encapsulation complex.

From the ratio of intercept and slope of these plot, association constant ($K_a$) was found to be −141005 $M^{-1}$ at 293 K, −69976 $M^{-1}$ at 298 K, −8416 $M^{-1}$ at 303 K (Table S2). Decrease in the negative $K_a$ value with temperature was likely due to the weakening of the intermolecular forces such as van der Waals or hydrogen bonding forces and as the temperature was raising binding between guest (TgC) and host (HP-β-CD) became more powerful.

The change in Gibbs' free energy (ΔG) for the inclusion process was calculated according to the given equation.

$$\Delta G = \Delta H - T\Delta S \quad (2)$$

From the Van't Hoff equation, enthalpy Change (ΔH) and entropy Change (ΔS) can be easily obtained [26].

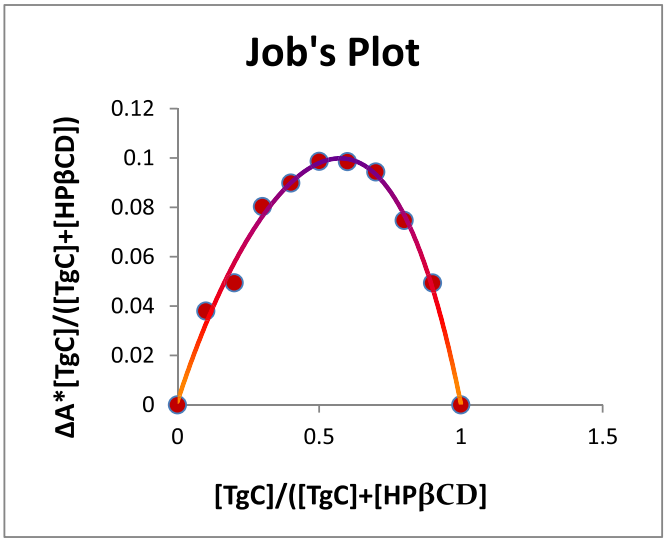


**Fig. 1.** Job's plot of TgC/HP-β-CD.

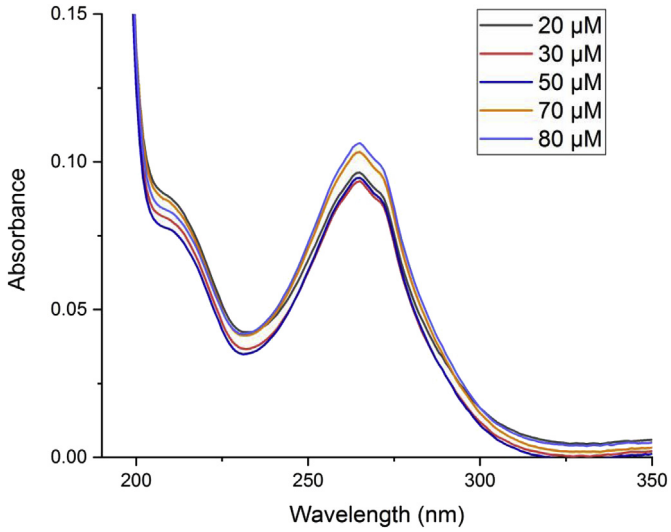


**Fig. 2.** UV–vis spectral changes on addition of HP-β-CD where, different strength of the solution having 20 μM, 30 μM, 50 μM, 60 μM, 70 μM respectively were taken at 30 °C.

$$\ln \mathbf{K} = -\frac{\mathbf{\Delta H}}{\mathbf{RT}} + \frac{\mathbf{\Delta S}}{\mathbf{R}} \quad (3)$$

Parameters have been shown in the Table 1. There are various binding forces involved during the inclusion phenomena such as hydrogen bonds, electrostatic interactions, hydrophobic forces and van der Waals interactions.

According to Ross and Subramanian [27], various thermodynamic rules can be used to interpret the type of binding mode which is summarized below:

(a) $\Delta H > 0$ and $\Delta S > 0$ i.e., hydrophobic forces;
(b) $\Delta H < 0$ and $\Delta S > 0$ i.e., electrostatic interactions;
(c) $\Delta H < 0$ and $\Delta S < 0$ i.e., van der Waals interactions and hydrogen bonds.

In our case, we got positive ΔH and ΔS suggest that inclusion process was endothermic in nature and hydrophobic forces played an important role to favour the inclusion complex, again, slight negative ΔG value suggest that interaction between TgC and HP-β-CD was spontaneous (Fig. S2) [28].

### 3.3. Association constant measurement by fluorescence measurement

The association constant can also be determined by monitoring the Changes in fluorescence emission due to the interaction between any guest and host molecules [29,30]. In case of fluorescence measurement to calculate the association constant, modified Stern–Volmer equation has been used.

**Table 1**
Data of the Van't Hoff equation for the calculation of thermodynamic parameters.

| Temp(K) | Ka/$M^{-1}$ | ΔH°(KJ $mol^{-1}$) | ΔS°(J $mol^{-1}$ $K^{-1}$) | ΔG KJ $mol^{-1}$ |
|---|---|---|---|---|
| 293 | −141005.4 | | | −0.197 |
| 298 | −69976.75 | 1.933 | 0.00727 | −0.234 |
| 303 | −8416.58 | | | −0.270 |

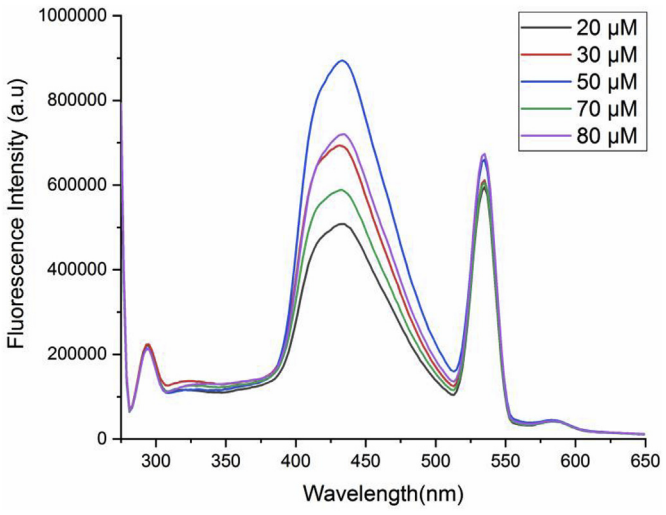


**Fig. 3.** Variation in Fluorescence emission spectra of TgC and HP-β-CD in different molar concentration.

**Table 2**
Thermodynamic parameters for TgC and HP-β-CD at 308 K.

| Temp/K | Modified Stern–Volmer method | |
|---|---|---|
| | Ka($M^{-1}$) | Correlation Coefficient ($R^2$) |
| 308 | −5000 | 0.923 |

$$\frac{\mathbf{Fo}}{\mathbf{\Delta F}} = \frac{1}{\mathbf{f{*}Ka}} \times \frac{1}{[\mathbf{Q}]} + \frac{1}{\mathbf{f}} \quad (4)$$

Where, ΔF is the difference in fluorescence in the absence and presence of the cyclodextrin at a concentration [Q], f is the fraction of accessible fluorescence, and Ka is the effective quenching constant for the accessible fluorophores, which are analogous to the associative binding constants for the host-guest system. According to the above equation, the binding constants Ka can be obtained by plotting Fo/ΔF vs. 1/[Q] and the results are shown below. TgC showed a linear fit curve when complexed with HP-β-CD that indicates 1:1 binding stoichiometry.

The variation in the fluorescence emission spectra were given in the Fig. 3 and the plot were given in Fig. S3 of supporting information. The spectra were scanned in the UV–VIS spectral range (275–650 nm) by exciting at 265 nm with scanned speed at

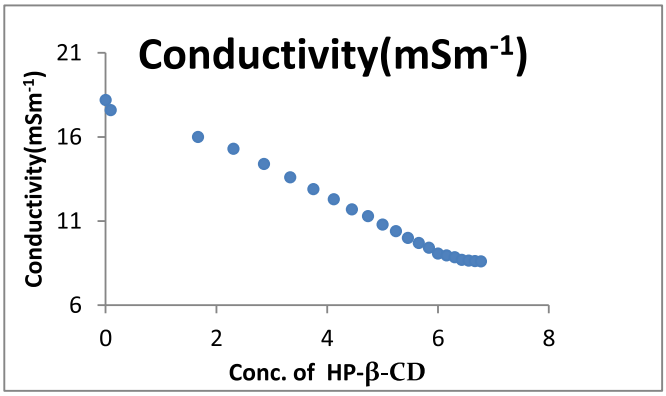


**Fig. 4.** Plot of Specific conductance vs Conc. of HP-β-CD.

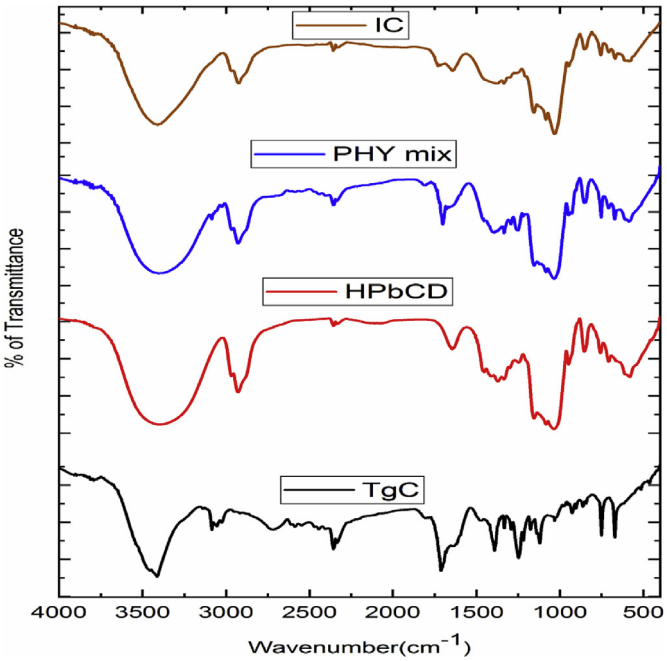


**Fig. 5.** FT-IR spectra of (a) TgC, (b) HP-β-CD (c) inclusion complex TgC/HP-β-CD (d) Physical mixture TgC/HP-β-CD.

1 nm/s (3 slits were at 2, 2 and 3 mm respectively from the end of lamp). The fluorescence emission maxima were found at four different bands located in the spectral ranges 275–300, 375–500, 515–550 and 550–600 nm. The fluorescence emission peak found at 433 nm was due to the corresponding emission of the $\pi \rightarrow \pi^*$ transition of the pyridinium moiety [31]. The other peaks were probably due to the solvent and host molecules present in the solution. The association constant have been calculated with different concentration of solution at 433 nm.

According to the Benesi-Hildebrand (B-H) method, it was found to be 1:1 stoichiometric ratio. Further, to verify the association constant values, a modified Stern–Volmer equation can be used to determine the value of Ka and it was found to be around $-5000\ M^{-1}$ which was quite comparable with the data obtained in UV–vis spectroscopy at 303 K (Table 2 and S3).

### 3.4. Conductance measurements

Conductometric method is one of the older but precious methods used to validate not only the inclusion process between guests and the host but also stoichiometry of the inclusion complex [32]. The conductivity curve has been shown in the Fig. 4 and the conductance values have been provided in Table S5 of supporting information. Prior to the experiment, 10 mM of the guest (TgC) as well as host (HP-β-CD) were prepared using $H_2O$ as solvent. Then, 10 mL pure TgC aliquot was taken and its conductivity was measured, it was found to be 18.2 $mSm^{-1}$. When, 1 mL of the HP-β-CD was added to the 10 mL of the guest solution, conductivity was found to be decreased gradually. The decreasing conductivity with adding HP-β-CD concentration, demonstrating the inclusion-complex formation between HP-β-CD and the TgC. After a certain concentration, the linearly decreasing tendency was going slow down with the addition of HP-β-CD. A distinct breakpoint was found out in the conductivity curve at a concentration of about 6 mM suggesting that the Complexation was equimolar as concentration ratio between HP-β-CD and TgC was 1.5. This indicates that either TgC was almost totally bounded in the cavity of the HP-β-CD or TgC was completely encapsulated by HP-β-CD by means of

**Table 3**
Variation of the stretching frequencies ($cm^{-1}$) of TgC and HP-β-CD protons in free and complex states determined in KBr pellet.

| TgC | HP-β-CD | TgC/HP-β-CD inclusion | TgC/HP-β-CD PHY MIX |
|---|---|---|---|
| (I)3414 $cm^{-1}$: O–H from –COOH | (I)3410 $cm^{-1}$: $\nu$(O–H) | (I)3410 $cm^{-1}$: O–H from –COOH | (I)3400 $cm^{-1}$: O–H from –COOH |
| (II)3084- 3040 $cm^{-1}$: $C^2_{sp}$-H from aromatic Ring. | (II)2928 $cm^{-1}$: $\nu(C^3_{sp}$-H) | (II)2915 $cm^{-1}$: $\nu(C^3_{sp}$–H) | (II)2927 $cm^{-1}$: $\nu(C^3_{sp}$–H) |
| (III)2357 $cm^{-1}$: C=N from aromatic ring. | (III)1635 $cm^{-1}$: The OH groups in the glucose moieties of HP-β-CD | (III)2354 $cm^{-1}$: C=N from aromatic ring. | (IV)2356 $cm^{-1}$: C=N from aromatic ring. |
| (IV)1711 $cm^{-1}$: –C=O from –COOH. | (IV)1373 $cm^{-1}$: C–H from $CH_3$ | (IV)1723 $cm^{-1}$: –C=O from –COOH. | (IV) 1701 $cm^{-1}$: –C=O from –COOH. |
| (V)1469 and 1391 $cm^{-1}$: C=C double bond from pyridine moiety. | (V)1152 $cm^{-1}$: Stretching frequency of C–O, C–C, C–O–C. | | (V)1033 $cm^{-1}$: Bending frequency of O–C–H, C–C–H, C–C–O. |
| | (VI)1033 $cm^{-1}$: Bending frequency of O–C–H, C–C–H, C–C–O. | | |

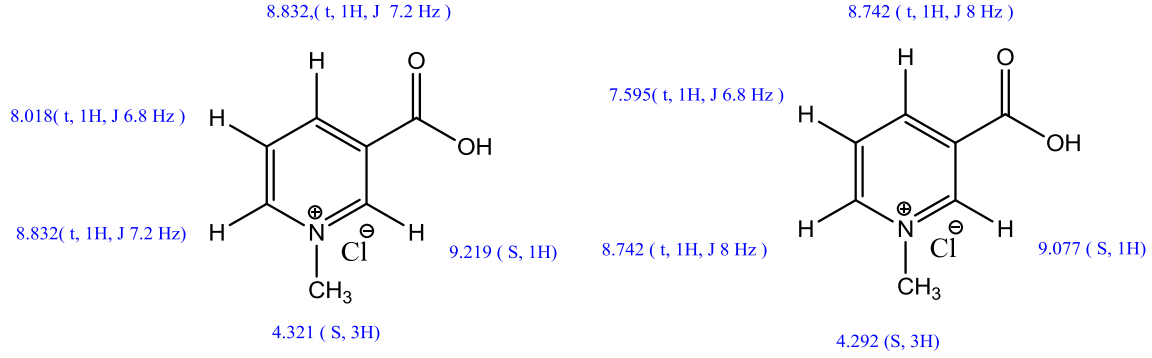


**Fig. 6.** Chemical Shift in NMR data of Free Trigonelline Hydrochloride (left) and after formation of encapsulation (right).

non-covalent interactions.

### 3.5. IR analysis

Fourier Transform Infrared spectroscopy (FT-IR) is an important method used to validate the formation of an inclusion complex [33]. The FT-IR spectra of TgC, HP-b-CD, TgC/HP-β-CD physical mixture, TgC/HP-β-CD inclusion complex are shown in Fig. 5. The variations in stretching frequency after inclusion complex formation were shown in Table 3. The FT-IR spectrum of TgC consisted of the absorption bands of O–H group of –COOH (3410 $cm^{-1}$). In the region of 3084- 3040 $cm^{-1}$, the stretching frequency of C-H from $-CH_3$ and $C^2_{sp}$-H from aromatic ring appeared. C═O group of the –COOH appears at 1711 $cm^{-1}$.

A strong absorption at 2357 $cm^{-1}$ is may be due to the presence of C═N bond in pyridinium moiety. The absorption peak in 1469 $cm^{-1}$ is corresponding to the C═C stretching vibration in the aromatic ring.

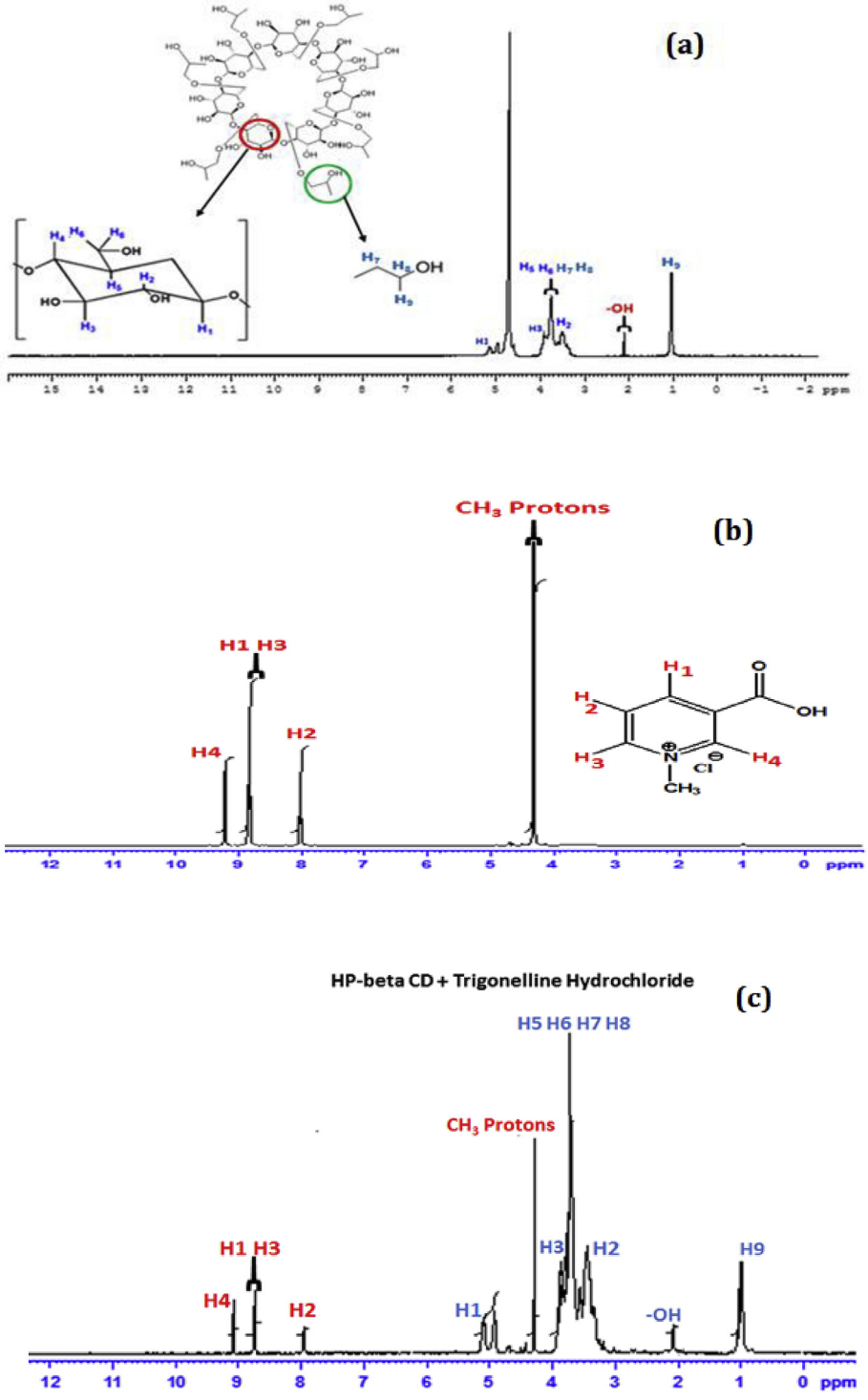


**Fig. 7.** NMR plot of (a) HP-β-CD (b) TgC (C) Inclusion complex TgC/HP-β-CD.

**Table 4**
Variation of the $^1$H NMR chemical shifts ($\delta$/ppm) of TgC and HP-β-CD protons in free and complex states determined in $D_2O$.

| Trigonelline Hydrochloride | HP-β-CD | Inclusion Complex | Shift in HP-β-CD proton |
|---|---|---|---|
| (+)N-$CH_3$: $\delta$ 4.321 **(S, 3H)** | H-1: 5.14 | H-1: 5.09 | −0.05 |
| $C_2$-H: $\delta$ 9.219 **(S, 1H)** | H-2: 3.50 | H-2: 3.56 | 0.02 |
| $C_4$-H: $\delta$ 8.857–8.814 **(t, 1H, J 7.2 Hz)** | H-3: 3.90 | H-3: 3.86 | **−0.04** |
| | H-4: 3.39 | H-4: 3.43 | −0.04 |
| $C_5$-H: $\delta$ 8.035–8.001 **(t, 1H, J 6.8 Hz)** | H-5: 3.75 | H-5: 3.76 | **0.01** |
| $C_6$-H: $\delta$ 8.857–8.814 **(t, 1H, J 7.2 Hz)** | H-6: 3.77 | H-6: 3.76 | −0.01 |
| | Me: 1.03 | Me: 1.00 | −0.03 |

Bold Values indicated the multiplicity, no of protons and coupling constant for the respective protons.

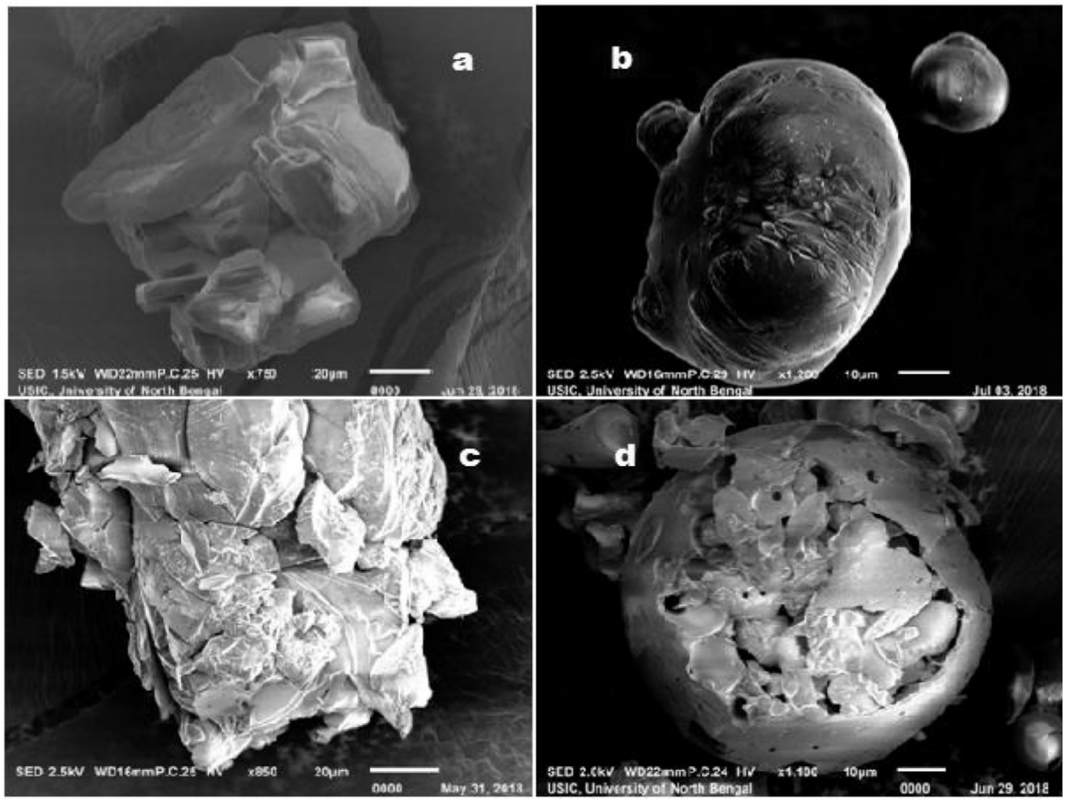


**Fig. 8.** Scanning electron photograph for (a) TgC (b) HP-β-CD (c) TgC/HP-β-CD inclusion complex (d) physical mixture.

The FT-IR spectrum of HP-β-CD showed significant absorption bands at 3410 $cm^{-1}$ (for O–H stretching vibrations), 2928 $cm^{-1}$ (for $C^3_{sp}$–H stretching vibrations) and 1373 $cm^{-1}$ (C–H stretching vibration from $CH_3$).

However, in case of both the physical mixture and inclusion complex, the absorption band between 3084 and 3040 $cm^{-1}$ disappears which indicate that C-H from –$CH_3$ and $C^2_{sp}$-H from aromatic ring may be inserted into the cavity of the cyclodextrin moiety. O-H stretching frequency from –COOH in TgC is 3414 $cm^{-1}$ which is shifted towards lower region at 3410 $cm^{-1}$ and 3400 $cm^{-1}$ for TgC/HP-β-CD inclusion complex and physical mixture respectively, this is may be due to the formation of H-bonding with host moiety. A peak appeared at 1711 cm-1 for –COOH in pure TgC had shifted to 1723 cm-1 in case of inclusion complex may be due to intermolecular hydrogen bond between OH of –COOH and terminal secondary hydroxyl group of the HP-β-CD. However, the peak appeared at 1701 $cm^{-1}$ in case of physical mixture which indicates that guest molecule was present outside the cavity of cyclodextrin molecules. The band at 1469 and 1391 $cm^{-1}$ which is generally due to C=C double bond from pyridine moiety diminished after

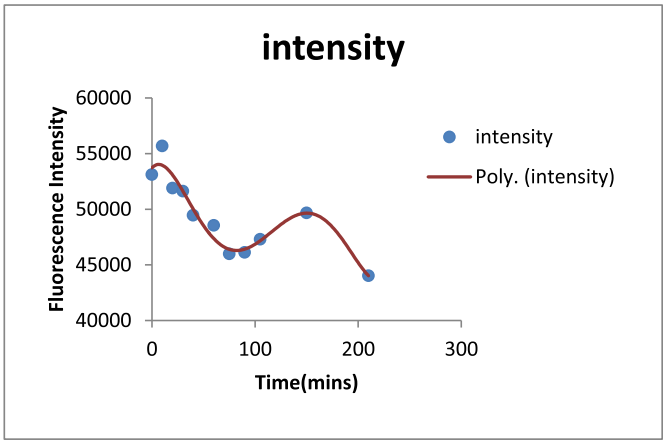


**Fig. 9.** Schematic Drug release of TgC from Hydroxy propyl-β-Cyclodextrin.

formation of the encapsulated complex. According to these changes, we might suggest that the pyridinium ring of TgC was committed.

### 3.6. $^1H$ NMR analysis

NMR (Nuclear Magnetic Resonance) is one the most powerful instrument in the study of CD complexes which provides quantitative information on spatial arrangement in case of 2D-NMR as well as detailed information on the possible inclusion mode in case of.

$^1$H NMR of CD with guest molecules [34].

Fig. 6 shows the change in chemical shift of the TgC after the formation of inclusion complex. Fig. 7 shows the chemical shifts of TgC, HP-β-CD, TgC/HP-β-CD inclusion complex and their variation in the chemical shift (Δδ) of the complex. After the formation of inclusion complex with TgC, the H-3 proton of HP-β-CD shifted 0.04 ppm and the H-5 proton of HP-β-CD shifted 0.01 ppm (Table 4). In case of the $^1$H NMR, if the guest moiety TgC enters into the cavity of the HP-β-CD molecules, electron density over the H-3, H-5 proton will be increased as both H-3 and H-5 protons are located in the inner part of the HP-β-CD cavity and consequently it will shield the protons and induce upfield shift. Again, chemical shift of the pyridinium moiety after inclusion has been shifted to lower (upfield) region that may be due to the van der Waals interaction. All these data leads to the confirmation that TgC had an interaction with the cyclodextrin cavity.

### 3.7. SEM analysis

Scanning electron microscope (SEM) is a qualitative technique used to study the change in the surface morphology of different materials like other high resolution microscopic technique [35,36]. SEM photographs of (a) TgC, (b) HP-β-CD, (c) TgC/HP-β-CD inclusion complex and (d) TgC/HP-β-CD physical mixture are shown in Fig. 8. Pure TgC appeared as irregular-shaped nanostructures with small dimensions, whereas HP-β-CD showed typical amorphous spherical particles with cavity structures. The physical mixture of TgC/HP-β-CD revealed some similarities with the Guest (TgC) and Host (HP-β-CD) molecules and both crystalline and amorphous nature are quite visible. However, for the inclusion complex, the original morphology of TgC had completely disappeared, and it was impossible to differentiate the two components of TgC and HP-β-CD, which lead to the conclusion of the formation of encapsulation complex.

### 3.8. Controlled release by fluorescence measurement

In order to investigate the controlled release behaviour of the inclusion complex of the drug molecule, fluorescence experiment was done. Prior to the experiment, exact 100 μM solution was prepared in distilled water and spectra were taken with different time. The result showed that the intensity of the solution was found to be decreasing up to 75 mins, then gradual increase in the intensity up to 150 mins. All the spectra were shown in Fig. S4 of supporting information. Fig. 9 showed a very good nature of the release profile and it suggested that HP-β-CD can be used as sustained release drug carrier.

## 4. Conclusion

In this present study, 1:1 inclusion complex of TgC and HP-β-CD was prepared and various analytical techniques such as UV, NMR, and IR had been employed to Characterized the complex. $^1$HNMR and IR showed the mode of inclusion that N-methylated part of the pyridine ring was incorporated. Association constant value of the TgC/HP-β-CD obtained by UV measurement was found to be $-8416\ M^{-1}$ at 303 K which indicate that interactions was very much negligible between guest and host and it was well matched with the value of $-5000\ M^{-1}$ that obtained by fluorescence spectroscopy. It was the hydrogen bonding that was responsible for forming the encapsulation complex. Fluorescence measurement showed a well defined curve in intensity vs time kinetics and it gave us an idea about sustained release of the drug molecule from the encapsulated complex.

## Conflict of interest

The authors declare no conflict of interest.

## Acknowledgements

This work is highly appreciated by UGC SAP (special Assistant Programme) for giving us financial support for the completion of the work. Prof. M.N. Roy is very thankful to UGC-BSR (Basic Scientific Research) for awarding 'One Time Grant'. We would like to acknowledge Mr. Gautam Sarkar, USIC, Head, In-charge for taking SEM photograph and NEHU-SAIF for the NMR 400 MHz data acquisition.

## Appendix A. Supplementary data

Supplementary data to this article can be found online at https://doi.org/10.1016/j.molstruc.2018.11.049.

## References

[1] R. Moorthy, K. Prabhu, P. Murthy, Studies on the isolation and effect of an orally active hypoglycemic principle from the seeds of fenugreek (*Trigonella foenum graecum*), Diabetes Bull 9 (1989) 69–72.
[2] J. Mishkinsky, B. Joseph, F.G. Sulman, Hypoglycaemic effect of trigonelline, Lancet 2 (1967) 1311–1312.
[3] A.E. van Dijk, M.R. Olthof, J.C. Meeuse, E. Seebus, R.J. Heine, R.M. van Dam, Acute effects of decaffeinated coffee and the major coffee components chlorogenic acid and trigonelline on glucose tolerance, Diabetes Care 32 (2009) 1023–1025.
[4] M.R. Olthof, A.E. van Dijk, C.F. Deacon, R.J. Heine, R.M. van Dam, Acute effects of decaffeinated coffee and the major coffee components chlorogenic acid and trigonelline on incretin hormones, Nutr. Metab. (Lond) 8 (2011) 10.
[5] J. Zhou, S. Zhou, Protection of trigonelline on experimental diabetic peripheral neuropathy, Evid. base Compl. Alternative Med. (2012) (2012) 164219. Article ID 8.
[6] J. Zhou, Trigonelline: a plant alkaloid with therapeutic potential for diabetes and central nervous system disease, Curr. Med. Chem. 19 (2012) 3523–3531.
[7] J. Zhou, S. Zhou, S. Zeng, Experimental diabetes treated with Trigonelline: effect on β cell and pancreatic oxidative parameters, Fund. Clin. Pharmacol. 27 (2013) 279–287.
[8] Jozsef Szejtli, Introduction and general overview of cyclodextrin chemistry, Chem. Rev. 98 (1998) 1743–1753.
[9] X. Ge, Z. Huang, S. Tian, Y. Huang, C. Zeng, Complexation of carbendazim with hydroxypropyl-β-cyclodextrin to improve solubility and fungicidal activity, Carbohydr. Polym. 89 (2012) 208–212.
[10] K. Srinivasan, K. Sivakumar, T. Stalin, 6-Dinitroaniline and β-cyclodextrin inclusion complex properties studied by different analytical methods, Carbohydr. Polym. 113 (2014) 577–587.
[11] Y. Yao, Y. Xieb, C. Hong, G. Lic, H. Shen, G. Ji, Development of a myricetin/hydroxypropyl-$i^2$-cyclodextrin inclusion complex: preparation, characterization, and evaluation, Carbohydr. Polym. 110 (2014) 329–337.
[12] G. Corti, M. Cirri, F. Maestrelli, N. Mennini, P. Mura, Sustained-release matrix tablets of metformin hydrochloride in combination with triacetyl-β-cyclodextrin, Eur. J. Pharm. Biopharm. 68 (2008) 303–309.
[13] S. Ma, W. Chen, X. Yang, N. Zhang, S. Wang, L. Liu, L. Yang, Alpinetin/hydroxypropyl-β-cyclodextrin host–guest system: preparation, characterization, inclusion mode, solubilization and stability, J. Pharmaceut. Biomed. Anal. 67–68 (2012) 193–200.
[14] L. Szente, J. Szejtli, Highly soluble cyclodextrin derivatives: chemistry, properties, and trends in development, Adv. Drug Deliv. Rev. 36 (1999) 17–28.
[15] M. e. Brewster, T. Loftsson, Cyclodextrins as pharmaceutical solubilizers, Adv. Drug Deliv. Rev. 59 (2007) 645–666.
[16] P. Tang, X. Ma, D. Wu, S. Li, K. Xu, B. Tang, H. Li, Posaconazole/hydroxypropyl-

β-cyclodextrin host–guest system: improving dissolution while maintaining antifungal activity, Carbohydr. Polym. 142 (2016) 16–23.
[17] L. Hu, H. Zhang, W. Song, D. Gu, Q. Hu, Investigation of inclusion complex of cilnidipine with hydroxypropyl-β-cyclodextrin, Carbohydr. Polym. 90 (2012) 1719–1724.
[18] L. Hu, H. Zhang, W. Song, D. Gu, Q. Hu, Investigation of inclusion complex of cilnidipine with hydroxypropyl-β-cyclodextrin, Carbohydr. Polym. 90 (2012) 1719–1724.
[19] S. Barman, D. Ekka, S. Saha, M.N. Roy, NMR, surface tension and conductance study to investigate host–guest inclusion complexes of three sequential ionic liquids with β-cyclodextrin in aqueous media, Chem. Phys. Lett. 658 (2016) 43–50.
[20] Liao, Yunhui, Zhang, Xuefei, Li Chenglin, Huang, Yanjuan, Lei Ming, Yan, Mina, Zhou, Yuefang, & Zhao, Chunshun, : Inclusion complexes of HP-β-cyclodextrin with agomelatine: Preparation, characterization, mechanism study and in vivo evaluation, Carbohydr. Polym. https://doi.org/10.1016/j.carbpol.2016.04.022.
[21] Z. Huanga, S. Tiana, X. Gea, J. Zhanga, S. Lia, M. Lia, J. Chenga, H. Zheng, Enhancing exopolysaccharide antioxidant formation and yield from *Phellinus* species through medium optimization studies, Carbohydr. Polym. 107 (2014) 241–246.
[22] Y. Yao, Y. Xie, C. Hong, G. Li, H. Shen, G. Ji, Development of a myricetin/hydroxypropyl-β-cyclodextrin inclusion complex: preparation, characterization, and evaluation, Carbohydr. Polym. 110 (2014) 329–337.
[23] P. José Salústio, Advanced technologies for oral controlled release: cyclodextrins for oral controlled release, AAPS PharmSciTech 12 (4) (December 2011).
[24] W. Misiuk, M. Zalewska, Investigation of inclusion complex of trazodone hydrochloride with hydroxypropyl-b-cyclodextrin, Carbohydr. Polym. 77 (2009) 482–488.
[25] S. Saha, A. Roy, K. Roy, M.N. Roy, Study to explore the mechanism to form inclusion complexes of $\beta$-cyclodextrin with vitamin molecules, Sci. Rep. 6 (2016) 35764.
[26] P. Tang, X. Ma, D. Wu, S. Li, K. Xu, B. Tang, H. L, Posaconazole/hydroxypropyl-β-cyclodextrin host–guest system: improving dissolution while maintaining antifungal activity, Carbohydr. Polym. 142 (2016) 16–23.
[27] P.D. Ross, S. Subramanian, Thermodynamics of protein association reactions: forces contributing to stability, Biochemistry 20 (11) (1981) 3096–3102.
[28] Y. Wei, J. Zhang, Y. Zhou, W. Bei, Y. Li, Q. Yuan, H. Liang, Characterization of glabridin/hydroxypropyl-β-cyclodextrin inclusion complex with robust solubility and enhanced bioactivity, Carbohydr. Polym. 159 (2017) 152–160.
[29] S. Jiang, H. Liu, W. Cai, A. Bai, Y. Ouyang, Y. Hu, Quasi-spherical silver nanoparticles with high dispersity and uniform sizes: preparation, characterization and bioactivity in their interaction with bovine serum albumin, Luminescence 31 (2016) 1146–1151.
[30] M. Ahumada, E. Lissi, A.M. Montagut, F.V. Henríquez, N.L. Pacioni, E.I. Alarcon, Association models for binding of molecules to nanostructures, Analyst 142 (2017) 2067–2089.
[31] H. Yisak, M.R. Abshiro, B.S. Chandravanshi, New fluorescence spectroscopic method for the simultaneous determination of alkaloids in aqueous extract of green coffee beans, Chem. Cent. J. 12 (2018) 59.
[32] M.N. Roy, M.C. Roy, K. Roy, Investigation of inclusion complex formed by ionic liquid and β-cyclodextrin through hydrophilic and hydrophobic interactions, RSC Adv. (2015), https://doi.org/10.1039/C5RA09823H.
[33] L.A. Soares, A.F. Vasconcelos Borges Leal, L.F. Fraceto, E. Rose Maia, I. Sabioni Resck, M.J. Kato, E. de Sousa Gil, A. Ribeiro de Sousa, L. Carlos da Cunha, K. Rocha Rezende, Inclusion complexes of γ-cyclodextrin and carboxyl-modified γ-cyclodextrin with C60: synthesis, characterization and controlled release application via microgels, J. Inclusion Phenom. Macrocycl. Chem. 64 (2009) 23–35.
[34] C. Yuan, Z. Jin, X. Xu, H. Zhuang, W. Shen, Inclusion complex of astaxanthin with hydroxypropyl-β-cyclodextrin: UV, FTIR, 1H NMR and molecular modeling studies, Carbohydr. Polym. 89 (2012) 492–496.
[35] J. Wang, Y. Cao, B. Sun, C. Wang, Characterisation of inclusion complex of trans-ferulic acid and hydroxypropyl-β-cyclodextrin, Food Chem. 124 (2011) 1069–1075.
[36] R. Ghosh, D. Ekka, B. Rajbanshi, A. Yasmin, M.N. Roy, Synthesis, characterization of 1-butyl-4-methylpyridinium lauryl sulfate and its inclusion phenomenon with β-cyclodextrin for enhanced applications, Colloid. Surface. Physicochem. Eng. Aspect. 548 (2018) 206–217.

Niloy Roy, Beauty Mahato, Debadrita Roy, Koyeli Das and Mahendra Nath Roy*

# Exploring inclusion complexes of cyclodextrins with quinolinone based gastro protective drug for enhancing bioavailability and sustained dischargement

https://doi.org/10.1515/zpc-2019-1500
Received June 19, 2019; accepted April 4, 2020

**Abstract:** Solid rebamipide based inclusion complexes were achieved by freeze-dry method and characterized by FTIR, UV–visible, $^1$H-NMR, 2D-ROESY, fluorescence spectroscopy, SEM and conductance. The enzyme substituted emission spectrum of the two comparative inclusion complexes with $\beta$-cyclodextrin ($\beta$-CD) and HP-$\beta$-CD in the diverse solvent systems determined the controlled release of the drug were the mid of interest. Amylase increased the stability of the inclusion complexation, proved that if it is taken together with the inclusion complex, the effectiveness and impact of the inclusion complexes will have a prolonged effect in the body. It could significantly improve the bioavailability of rebamipide.

**Keywords:** $\beta$-cyclodextrin; drug release assay; hydroxypropyl-$\beta$-cyclodextrin; molecular recognition; supramolecular chemistry.

## 1 Introduction

In recent ages, supramolecular chemistry has become a major influence in the field of macrocyclic chemistry. Although low solubility is a common issue for various drug molecules but encapsulation process makes the host-guest complexes more soluble in water. This study basically focuses on the host–guest inclusion phenomena of low water soluble rebamipide (RB) in comparison with two types of cyclodextrin for the prevention of different types of diseases like gastric cancer [1], mucosal protection against gastro duodenal

***Corresponding author: Mahendra Nath Roy**, Department of Chemistry, University of North Bengal, Darjeeling, 734013, India, E-mail: mahendraroy2002@yahoo.co.in
**Niloy Roy, Beauty Mahato, Debadrita Roy and Koyeli Das:** Department of Chemistry, University of North Bengal, Darjeeling, 734013, India

ulcers [2], treatment of gastritis [3], inflammatory disorder [4], analgesic activity, antinociceptive activity, dry eye disease, allergic conjunctival diseases, attenuated cartilage degeneration [5]. In our present exertion, we have taken rebamipide (RB) as the guest molecule, $\beta$-cyclodextrin ($\beta$-CD) and hydroxypropyl-$\beta$-cyclodextrin (HP-$\beta$-CD) as the two analogous host molecules as the articles about the study on selecting inclusion materials of mucosal drug are few (Scheme 1).

Rebamipide is chosen as the guest molecule having various impact which is still to be explored in the fields of supramolecular chemistry for it's sustain release of drug delivery in the body. Rebamipide ($C_{19}H_{15}ClN_2O_4$) belongs to the class of quinolinone family. (±)-2-(4-chlorobenzoylamino)-3-(2-oxo-1H-quinolinon-4-yl) propionic acid (MW: 370.786 g/mol) is the IUPAC name of the compound [6]. Historical facts tell that RB was known by the trade name of Mucosta, a gastro protective drug, developed in Japan, Rebagen in South Korea (Republic of Korea), China and India, Rebagit in Russia.

Cyclodextrins (CDs) are the category of cyclic oligosaccharides which have in recent times been recognized as useful matrices. Owing to its hydrophobic cavity, CD can interact with suitably sized molecules to result in the formation of inclusion complexes. This polysaccharide is a sort of novel functional macromolecule which possesses the cumulative effects of inclusion, size specificity, controlled release capability and transport properties of CD over and above the biocompatibility, non-toxicity and biodegradability of it. Recently, encapsulation of various cyclic oligosaccharides such as cyclodextrins having good cavity size with organic molecule have been carried out to validate its inclusion phenomena and it's various thermodynamic stabilities [7].

Apart from cyclodextrins, other several host molecules can also be used e. g., 18-crown-6, Calixarenes, cucurbit[n]urils such as, 18-crown-6, cucurbit[6]uril have been used as a host and drug molecules are encapsulated within their cavity to

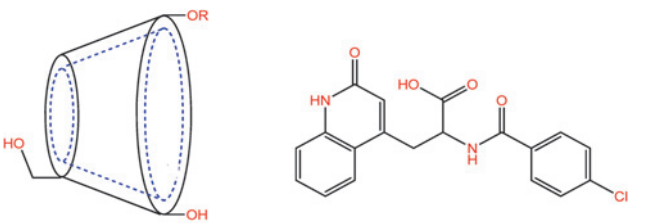


**Scheme1:** Structures of Rebamipide, $\beta$-CD and HP-$\beta$-CD.

assort various interactions and emphasize the inclusion process [8, 9]. However, in this work, among the various types of cyclodextrin, $\beta$-CD and HP-$\beta$-CD are taken as the host molecules for both the size and solubility factor matching with the model drug molecule. In support to various physicochemical, spectroscopic techniques for the two complexes in solution phase in both pure (DMSO) and mixed solvent (1:1–$C_2H_5OH$:$H_2O$) have been investigated for their potential use in controlled drug delivery applications (Scheme 2).

# 2 Experimental section

## 2.1 Materials

Rebamipide was bought from TCI Chemicals (India) Pvt. Ltd. Both the Cyclodextrins (i.e., $\beta$-CD and HP-$\beta$-CD) was bought from Sigma Aldrich Germany and used as purchased. The mass fraction purities of RB, $\beta$-CD and HP-$\beta$-CD were ≥0.99, 0.98, and 0.98, respectively.

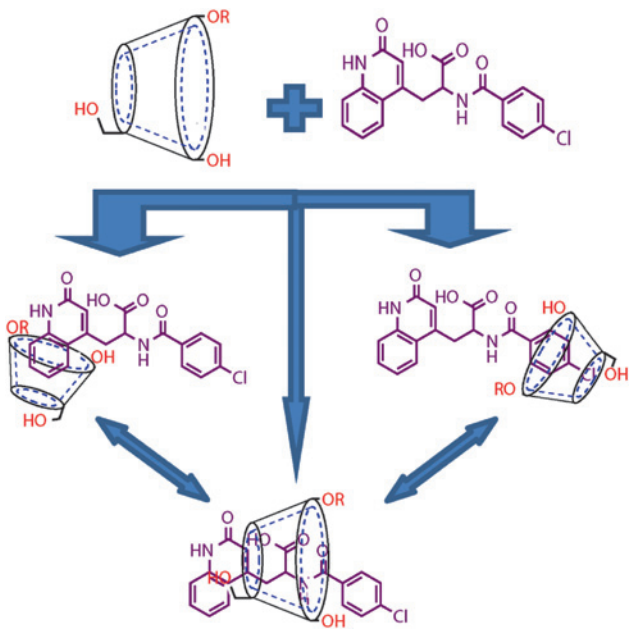


**Scheme 2:** Schematic representation of Cyclodextrin molecules forming inclusion complex with Rebamipide guest.

## 2.2 Instruments

All the Stock solutions of rebamipide, $\beta$-CD and HP-$\beta$-CD were prepared by weighing (Mettler Toledo AG-285 with uncertainty 0.0001 g) and dilution and kept in a slightly heating water bath.

Conductivities of both the solutions were studied by Mettler Toledo Seven Multi conductivity meter having uncertainty 1.0 $\mu Sm^{-1}$. It was carried out in a thermostated water bath at 298.15 K with uncertainty ±0.01 K. Double distilled water was used with specific conductance 6.0 $\mu Sm^{-1}$. Moreover, the conductivity cell was calibrated using 0.01 M aqueous KCl solution.

UV–visible spectra were recorded by Agilent 8453 Spectrophotometer. The temperatures were controlled with a digital thermostat. All the absorption spectra were recorded at 298 ± 0.1 K, 303 ± 0.1 K, 308 ± 0.1 K.

Fourier transform infrared (FT-IR) spectra were recorded on a Perkin Elmer FT-IR spectrometer by means of the KBr disk technique. Samples were prepared as KBr disks with 1 mg of solid inclusion complex and 100 mg of KBr. Fourier Transform Infrared Spectroscopy measurements were performed in the scanning range of (4000–400 $cm^{-1}$) with resolution of 4 $cm^{-1}$ at room temperature.

Differential Scanning Calorimetry (DSC) spectra were recorded by Perkin Elmer Pyris six DSC calibrated by pyris manager software. The samples were heated in the temperature range 30–300 °C in an inert nitrogen atmosphere at a heating rate of 10 °C/min. The samples were taken in an aluminum container at about 1.2 mg in all cases.

Steady state fluorescence Spectra were recorded on spectrofluorimeter from photon Technology International (PTI, U.S.). The measurements were done at an excitation of 230 nm by using quartz cuvette having 1 cm path length.

$^1$H-NMR and 2D-Rotating-frame Overhauser Effect Spectroscopy (ROESY) spectra were recorded at 400 MHz Bruker AVANCE at 298.15 K in DMSO-$d_6$ using a 5 mm probe. Signals are quoted as $\delta$ values in ppm by means of residual protonated solvent signals as an internal standard ($\delta$ 2.50 ppm). Acquisition parameters consisting of spectral width of 2000 MHz, number of scan 8, acquisition time 3.27 s. Data were reported as chemical shift.

Scanning electron microscopy (SEM) morphological images were obtained using JEOL JSM IT 100 scanning electron microscope (SEM). The images were captured at an excitation voltage of 2.5, 3.0, 5, 2.5, and 4.0 kV whereas magnification of 6000, 1400, 1400, 5500, 2700× for RB, $\beta$-CD, HP-$\beta$-CD, IC-1 and IC-2 respectively.

### 2.3 Sample preparation of solid inclusion complex of rebamipide with cyclodextrins

To prepare a complex between Cyclodextrins (i.e., $\beta$-CD and HP-$\beta$-CD) and drug, freeze drying method is the most popular method to form the inclusion complex in a solution of cyclodextrin. In this method, the guest is dissolved into a solvent solution of cyclodextrin to form the inclusion complex in a crystalline form. However, since the chosen pharmaceutical drugs have a very low solubility in water, we investigated the preparation of inclusion complexes between Cyclodextrins and the guest (RB) in organic solvent, DMSO. As reported, 1 mM solution of 25 ml RB (9.26 mg) and 1 mM of 25 ml $\beta$-CD (28.37 mg) as well as HP-$\beta$-CD (38.53 mg) were prepared. Then the solutions were mixed (added drop wise) in two different beaker and stirred for 12 h at 55 °C. Finally, the solution was freeze dried for 24 h to obtain inclusion complex.

## 3 Results and discussion

Rebamipide, the guest molecule selected in these assay is moderately soluble in organic solvent (i.e., DMSO) and partially in the binary solvent of $C_2H_5OH$ and water. As our aim is to prepare a host-guest inclusion complex which have sustain release in the body, therefore all the measurements were done by slightly increasing the temperature. Thereby increasing the temperature it was noted that all the physicochemical and spectroscopic evidences deep-rooted the formation of the various types (1:1 or 2:1 or 2:2) inclusion complexes in stable equilibrium.

Two types of solvents were used in order to show compare their stability and specificity during the formation of inclusion Complexation in various aforementioned ratios. Slightly increased temperature was used to totally dissolve both the host and the guest molecule.

Rebamipide is an insoluble drug in water and in most common organic solvents due to intermolecular electrostatic attraction between ammonium and carboxyl group. Therefore in order to increase its applicability we have tried diverse solvents to increase its solubility two fold. There are various publications based on amino acid based surfactants [10] which has increased the worth of amino acids. Here in these work we have tried an innovative way to work on derivative amino acid (i.e., rebamipide) based cyclodextrins in pure DMSO and mixed solvent of $C_2H_5OH$ and water. In various previous publications [11, 12] we found that after inclusion in cyclodextrin there is a chance of aggregation or vesicle formation with various imperative guest molecule. Here as we have taken aromatic

amino acids, therefore, there is much probability of it to behave as a surfactant. Therefore we have performed the surface tension and conductivity experiments. Different concentrations of rebamipide based cyclodextrin solutions were prepared and measured respectively.

## 3.1 Conductance study

Ion mobility increases as the temperature is raised, which leads to an increase in the limiting conductance. As the solubilization is precise at high temperature, therefore we had studied the inclusion Complexation by conductance method at the higher temperature. With the adding of cyclodextrin appears an extreme point on the dependence, which becomes more harshly when the temperature increases. At high concentrations of cyclodextrin (>1.60 mM), cyclodextrin-rebamipide–DMSO interaction becomes more intensive, which leads to the formation of bulky solvate shell affecting negatively on the ion mobility, thereby forming an inclusion complex.

From the previous publications, we have studied appearance of the extreme point on these curves indicates the presence of competing interactions in the system. We have examined two systems i.e., (HP-$\beta$-CD + RB + DMSO) and ($\beta$-CD + RB + DMSO), where the prominent results were observed. Thereby, over viewing the fact of encapsulation with the formation of break point, Sharp break point is prominent for $\beta$-CD-Rebamipide solution in DMSO (Figure 1(a)) which shows the formation of 1:1 complex and in HP-$\beta$-CD-Rebamipide-DMSO solution (Figure 1(b)), there is the uniformity in the values which shows that if we increase the cyclodextrin concentration, a linear increase in the specific conductance up to

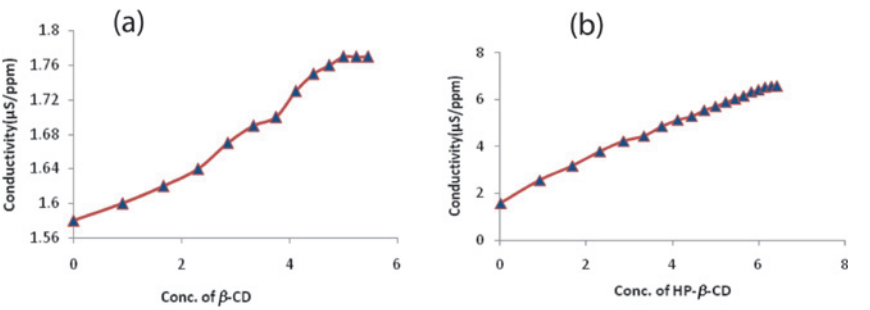


**Figure 1:** Plot of Molar Conductance (***Λ***) against concentration of (a) $\beta$-Cyclodextrin added in 10 mM for Rebamipide in DMSO solution at 308.15 K and (b) *HP-$\beta$*-Cyclodextrin in 10 mM for Rebamipide in DMSO at 308.15 K.

the HP-$\beta$-CD concentration at which "micelle like" formation began, i.e., up to the break point (i.e., CAC in case of surfactant) (Table S1 and S2 of supporting information). After the CAC was attained, conductance further increased linearly, but with a lower slope than before the CAC and the break in the conductance-concentration titration curve provides the CAC of the HP-$\beta$-CD [13–19].

## 3.2 Job plot: elucidation of stoichiometry behavior of cyclodextrins: rebamipide inclusion complex

Job's method, commonly known as the continuous variation method, is a very proficient and successful method to determine stoichiometry of any host-guest inclusion complexes. So, due to this reason this method was applied here by using UV–visible spectroscopy [20]. Here, two sets of solutions were prepared of RB with $\beta$-CD and HP-$\beta$-CD in 50% ethanolic solution, respectively, by varying the mole fractions of the guest (RB) in the range 0–1 (Tables S3–S6, supplementary data). Job's plots of the mentioned sets were plotted of using $\Delta A \times R$ against R, where $\Delta A$ means the difference in absorbance of RB without and with CD and R = [RB]/[RB] + [CD]).The whole process of taking absorbance values was done at respective $\lambda_{max}$ by maintaining 298.15 K temperature. The stoichiometry of an IC is obtained by taking the value of R at the maximum point on the curve, for example, if the ratio of guest to host is 1:2 for R ∽ 0.33, 1:1 for R ∽ 0.5, 2:1 for R ∽ 0.66 and so on. Here, in this work we got R∽0.5 as maximum in each plot, indicating a 1:1 stoichiometry of the corresponding inclusion complexes (Figure 2).

## 3.3 Determination of binding constant of RB/$\beta$-CD in aqueous ethanol by UV–Vis spectroscopy

The binding constant between $\beta$-CD, HP-$\beta$-CD and each RB has been evaluated via UV–Vis spectroscopy [21]. The Benesi–Hildebrand technique represents one of the most common strategies to determine binding constants based on absorption spectra for inclusion complex. In order to have an accurate estimation of binding constants of the inclusion complexes under investigation, changes in the absorption intensity of the RB at different wavelength, were monitored as a function of the CD's concentration and non-linear regression estimation of the $K_a$ (Figure 3(a)) was chosen.

From the UV–Vis titration, Association constant value for RB/$\beta$-CD was found to be $2.03 \times 10^4\ M^{-1}$, $3.34 \times 10^4\ M^{-1}$, $1.39 \times 10^4\ M^{-1}$, at 298.15 K, 303.15 K, and 308.15 K, respectively (Table S7 & Figure S1). The increase in association constant values ($K_a$)

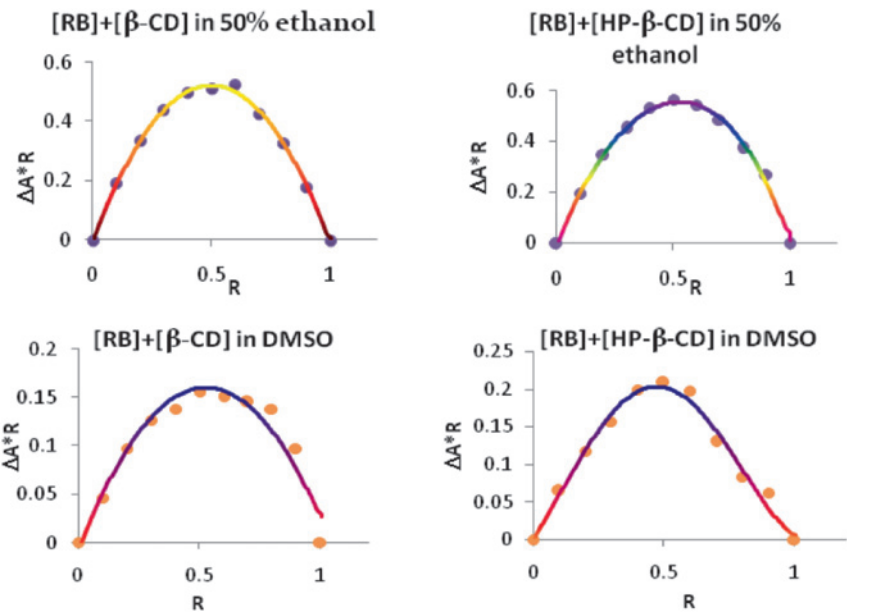


**Figure 2:** Job plot of RB/$\beta$-CD and RB/HP-$\beta$-CD systems in 50% ethanol at 298.15 K (above) RB/$\beta$-CD and RB/HP-$\beta$-CD systems in pure DMSO at 298.15 K (below).

with increasing temperature indicated the increasing nature of interaction for inclusion complexation but then again association constant value went to decrease sharply indicating weakest interaction between guest and host [22].

## 3.4 Determination of binding constant of RB/HP-$\beta$-CD in aqueous ethanol solution by UV–Vis spectroscopy

The evaluation of $K_a$ by direct spectroscopic methods relies on analytical differences between the free and complexed amino acid. The binding constant between HP-$\beta$-CD and RB also has been evaluated via UV–Vis spectroscopy. The Benesi–Hildebrand technique represents one of the most common strategies to determine binding constants based on absorption spectra for inclusion complex. In order to have an accurate estimation of binding constants of the inclusion complexes under investigation, changes in the absorption intensity of the RB at different wavelength, were monitored as a function of the CD's concentration and non-linear regression estimation of the $K_a$ (Figure 3(b)) was chosen.

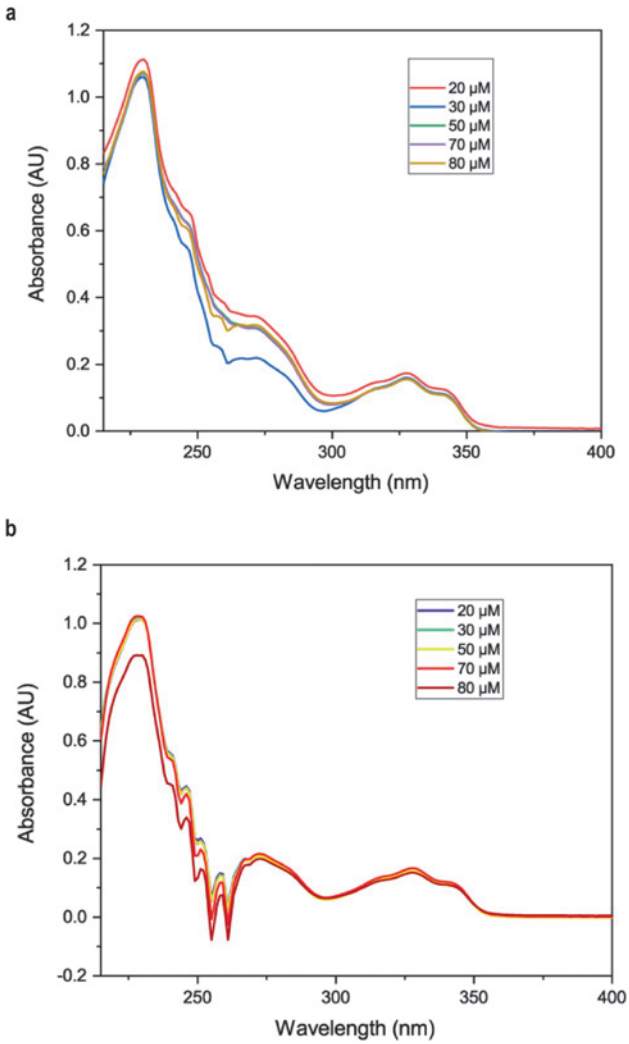


**Figure 3:** (a) Variation of UV–Vis spectra in different micromolar concentration of $\beta$-CD and RB in 50% ethanolic solution at 298.15 K. (b) Variation of UV–Vis spectra in different micromolar concentration of HP-$\beta$-CD and RB in 50% ethanolic solution at 298.15 K.

Here, the association constant was found to be $2.73 \times 10^4$ $M^{-1}$, $5.72 \times 10^4$ $M^{-1}$, $1.18 \times 10^4$ $M^{-1}$, at 298.15 K, 303.15 K, and 308.15 K, respectively (Table S8 & Figure S2). However, similar nature of association constant value is observed in case of RB/HP-$\beta$-CD system but interesting fact is that interaction between RB and HP-$\beta$-CD is greater than RB and $\beta$-CD system (Figure 4).

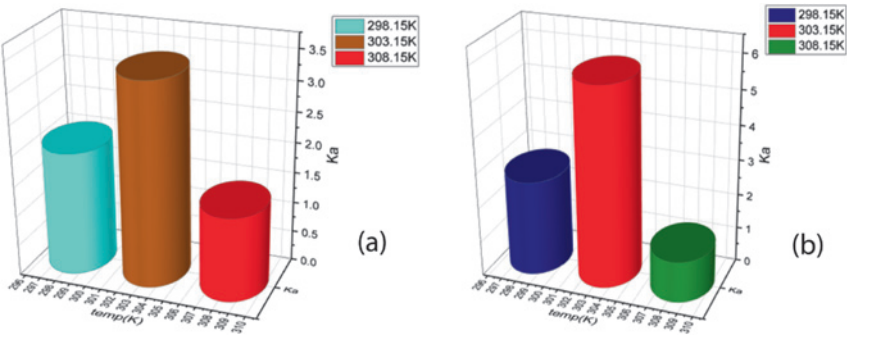


**Figure 4:** 3D graphical representation of association constant value of (a) RB/$\beta$-CD and (b) RB/HP-$\beta$-CD in aqueous ethanolic solution at three different temperatures.

## 3.5 Evaluation of thermodynamic parameters

The thermodynamic and structural characteristics during Complexation could be used to estimate the solubilizing and mode of action of cyclodextrin. To calculate the basic thermodynamic parameters, the enthalpy and entropy values, we have used the van't Hoff's equation as follows [23],

$$\ln Ka = -\frac{\Delta H^\circ}{RT} + \frac{\Delta S^\circ}{R}$$

Where $H^0$ and $S^0$ are the enthalpy and entropy during complex formation, respectively, T is the temperature, and R is the gas constant.

The Gibbs energy change was calculated by equation given below [24],

$$\Delta G^\circ = -RT\ln Ka$$

The thermodynamic parameters obtained from the van't Hoff plot using the above-mentioned equations were shown in Table 1a and b. From the given tables, the negative values in the Gibbs energy change (ΔG) and the enthalpy change (ΔH) indicated that the interaction of RB and $\beta$-CD, HP-$\beta$-CD were spontaneous and exothermic. Greater negative enthalpy change (ΔH) for RB/HP-$\beta$-CD was usually an indication of quite strong molecular interactions caused by both van der Waals forces and formation of hydrogen bonds between host and guest than that of RB/$\beta$-CD system. These interactions were may be due to incorporation hydrophobic guest into the cyclodextrin cavity host [25]. Similarly, higher negative entropy change (ΔS) for RB/HP-$\beta$-CD indicates that inclusion process is more entropy favored for RB/HP-$\beta$-CD than that of RB/$\beta$-CD system.

**Table 1a:** Energy values of RB/$\beta$-CD inclusion complexation.

| Complex | T(K) | ΔG KJ mol$^{-1}$ | ΔH$^0$/kJ mol$^{-1}$ | ΔS$^0$/J mol-1 K$^{-1}$ |
|---|---|---|---|---|
| RB/$\beta$-CD | 298.15 | −25.141 | | |
| | 303.15 | −25.087 | −28.344 | −10.742 |
| | 308.15 | −25.033 | | |

**Table 1b:** Energy values of RB/HP-$\beta$-CD inclusion complexation.

| Complex | T(K) | ΔG kJ mol$^{-1}$ | ΔH$^0$/kJ mol$^{-1}$ | ΔS$^0$/J mol$^{-1}$ K$^{-1}$ |
|---|---|---|---|---|
| RB/HP-$\beta$-CD | 298.15 | −26.277 | | |
| | 303.15 | −25.660 | −63.09 | −123.47 |
| | 308.15 | −25.043 | | |

## 3.6 Fourier transform infrared spectroscopy (FTIR) study

FT-IR is a prominent technique used to confirm the formation of an inclusion complex as there will be variation of the shape, shift and intensity of the FT-IR absorption peak before and after the formation of inclusion complex [26]. The FT-IR spectra of RB, $\beta$-CD, HP-$\beta$-CD, IC-1, IC-2 are presented in Figure 5. The FT-IR spectrum of RB consisted of the sharp absorption bands appear in the 3416 cm$^{-1}$ for O−H stretching from −COOH, 3269 cm$^{-1}$ (N-H) stretching of CONH group stretch, (−C=O) stretching of CONH appear in the region 1646 cm$^{-1}$ and aromatic ring appear in the region 1539 cm$^{-1}$. In both cases of $\beta$-CD and HP-$\beta$-CD, the IR spectra can be characterized by the intense band at 3397 and 3410 cm$^{-1}$ for O−H stretching frequencies and C−H stretching appears at 2922 and 2928 cm$^{-1}$ respectively. No characteristic peak is observed from 1500 cm$^{-1}$ to 400 cm$^{-1}$ for the two Host molecules. After the formation of the inclusion complex, in both cases of $\beta$-CD and HP-$\beta$-CD, the peak assigned for absorption of N-H stretching of CONH group has been disappeared. However, the spectra of the IC-1 i.e., inclusion complex of RB and $\beta$-CD correspond simply to the superposition of the spectra of the $\beta$-CD. All these phenomena indicate that only amide group and the acid group attached with tertiary carbon atom has been inserted into the cavity of cyclodextrin ring.

## 3.7 Differential scanning calorimetry (DSC) analysis

The pure drug RB and its Inclusion complexes with $\beta$-CD and HP-$\beta$-CD i.e., IC-1 and IC-2 were analyzed by DSC method as it can be used as recognition tool. According

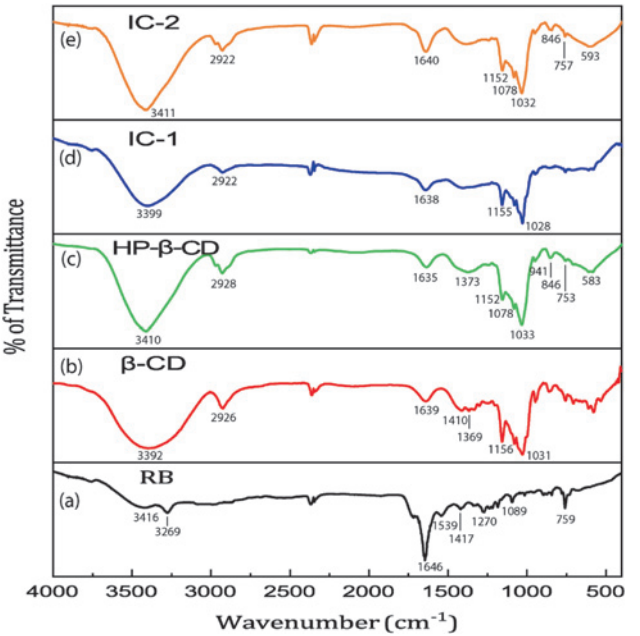


**Figure 5:** FT-IR spectra of (a) RB, (b) $\beta$-CD, (c) HP-$\beta$-CD, (d) inclusion complex of RB/ $\beta$-CD and (e) inclusion complex of RB/HP-$\beta$-CD.

to the theory, if guest molecules are encapsulated into the cyclodextrin host cavities, their physical characteristics such as melting point, boiling point should be shifted to a different temperature or may get disappeared [27]. As shown in Figure 6, RB showed a sharp characteristic endothermic melting peak at 305 °C, according to the previous literature. $\beta$-CD and HP-$\beta$-CD showed a single endothermic peak at about 88 and 60 °C which is due to the release of water from the $\beta$-CD and HP-$\beta$-CD respectively. However, when the guest molecules formed inclusion complex with $\beta$-CD i.e., IC-1, the endothermic peaks were shifted to 271 °C (RB) and 81 °C ($\beta$-CD). In case of IC-2, endothermic peaks were shifted to 259 °C (RB) and 70 °C (HP-$\beta$-CD). This Phenomena gave a strong evidence that inclusion complex has been formed.

## 3.8 $^{1}$H-NMR and 2D-NMR study

The formation of IC can be explained on the light of the $^{1}$H NMR spectroscopy study. This method based on the changes of chemical shifts of protons due to encapsulation of guest molecule into the Cyclodextrin cavity [28]. In both $\beta$-CD and HP-$\beta$-

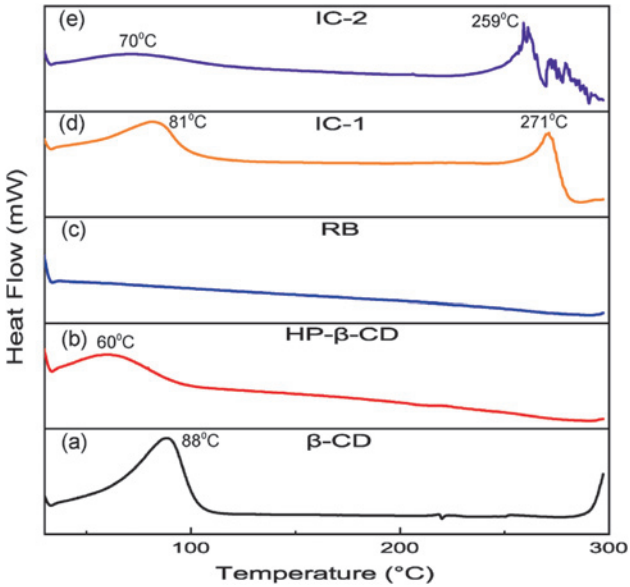


**Figure 6:** DSC thermograms of (a) $\beta$-CD, (b) HP-$\beta$-CD, (c) RB, (d) IC-1 and (e) IC-2.

CD structure, the H3 (near to wider opening side) and H5 (close to narrow rim side) are located inner part of the Cyclodextrin cavity and it is expected that when a hydrophobic moiety entered into the cyclodextrin cavity, there will be an upfield shift for those protons. It is clearly observed from Table 2a and b (in case of HP-$\beta$-CD) that for H3 and H5, a large upfield shift has been occurred than that of $\beta$-CD. The considerable changes of chemical shifts ($\Delta\delta$) suggested that the RB monomer entered into the nano hydrophobic hole of CD. Spectra are shown in Figure 7(a) and (b), For HP-$\beta$-CD, The upfield shift of H3 ($\Delta\delta = -0.07\ ppm$) is much greater than the H5 shifting ($\Delta\delta = -0.04\ ppm$) whereas, in case of $\beta$-CD, downfield shift in both cases of H3 ($\Delta\delta = 0.09\ ppm$) and the H5 ($\Delta\delta = 0.04\ ppm$) was observed, where, $\Delta\delta = \delta_{complex} - \delta_{free}$. On the other hand, minor chemical shifts are observed for H1, H2, H4, H6, and H7 that are not part of the interior hydrophobic hole of $\beta$-CD and HP-$\beta$-CD. This observation also confirmed that encapsulation of the guest moiety into hydroxypropyl derivative of cyclodextrin moiety was more prominent than that of the beta-cyclodextrin and the association constant values in solution phase for both the cases agreed with this report.

Similarly, further support for Complexation, $^1$H NMR of RB has also been performed in Complexed form (Table 2c). A significant upfield shift of Quinolone moiety rather than aromatic (holding –Cl) Protons has been observed in case of IC-2 as most of the aromatic peaks got disappeared which tells that Quinolone part are

**Table 2a:** [1]H-NMR Chemical shift data of free $\beta$-CD and its variation in complex with RB.

| $\beta$-CD protons | Free $\beta$-CD $\delta$ (ppm) | IC-1$\delta$ (ppm) | $\Delta\delta$(ppm) |
|---|---|---|---|
| H1 | 5.71–5.78 | 5.71–5.78 | 0.00 |
| H2 | 3.29–3.32 | 3.34 | – |
| H3 | 3.65 | 3.74 | 0.09 |
| H4 | 3.33–3.37 | 3.29–3.31 | – |
| H5 | 3.61 | 3.65 | 0.04 |
| H6 | 3.63 | 3.62 | –0.01 |

**Table 2b:** [1]H-NMR Chemical shift data of free HP-$\beta$-CD and its variation in complex with RB.

| HP-$\beta$-CD protons | Free HP-$\beta$-CD $\delta$ (ppm) | IC-2$\delta$(ppm) | $\Delta\delta$(ppm) |
|---|---|---|---|
| H1 | 5.01 | 4.93 | 0.08 |
| H2 | 3.23 | – | – |
| H3 | 3.78 | 3.71 | –0.07 |
| H4 | 3.13 | – | – |
| H5 | 3.55 | 3.51 | –0.04 |
| H6 | 3.49 | 3.48 | 0.01 |
| Me | 0.99 | 1.12 | –0.13 |

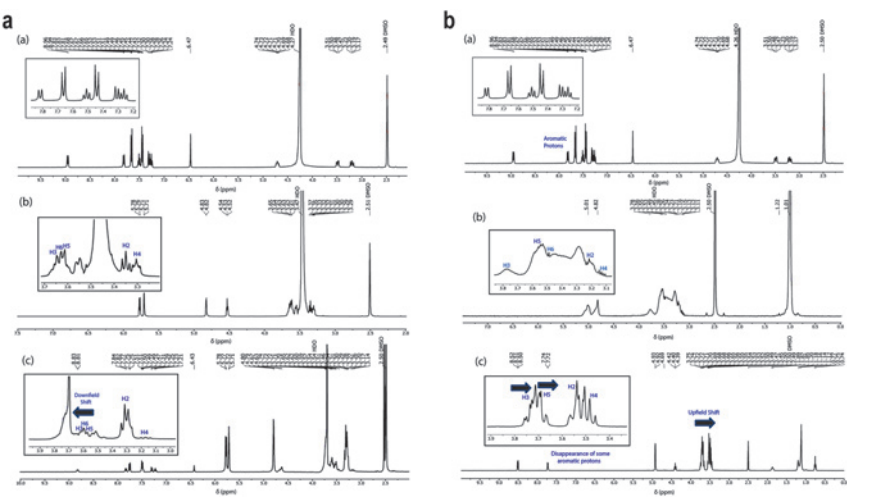


**Figure 7:** (a): [1]H-NMR spectra of (a) RB (b) $\beta$-CD and (c) RB/ $\beta$-CD (IC-1) inclusion complex. (b): [1]H-NMR spectra of (a) RB (b) HP-$\beta$-CD and (c) RB/HP-$\beta$-CD (IC-2) inclusion complex.

situated in hydrophobic hollow space. However, In case of IC-1, Here also upfield shift of Quinolone moiety rather than aromatic ring (holding –Cl) Protons has been observed but not that extent as in IC-2. Considering all these experimental data, one can conclude that the extent of formation of IC using RB is much more prominent in case of HP-$\beta$-CD over $\beta$-CD.

Two-dimensional (2D) NMR spectroscopy now-a-days has been extensively used to get some important information about the spatial proximity between host and guest molecule since two protons located closer than 4 Å in space are expected to produce cross-peaks in ROESY spectra [29]. The 2D ROESY spectrum for the inclusion complex RB/$\beta$-CD (Figure 8) showed the aromatic protons of RB have cross peaks to the H-3, and H-5 protons of $\beta$-CD, indicating the deep insertion of the benzene ring into the host cavity. Similarly, in case of RB/HP-$\beta$-CD also (Figure 8), a cross peak has been observed between aromatic protons of RB and H-3 and H-5 proton of the HP-$\beta$-CD as well as two distinct cross peaks with methine proton at $\delta$ 4.92–4.93 (ppm) and methylene proton appeared at $\delta$ 4.39–4.43 (ppm) which indicate the insertion of aromatic ring and interaction of those protons with H-3 and H-5 proton of the host molecules.

**Table 2c:** $^1$H-NMR Chemical shift data of free RB and its variation in complex.

| Pure Rebamipide | RB In IC-1 | RB in IC-2 |
|---|---|---|
| 8.94–8.96 (d, 1H, J = 8 Hz, aliphatic –N*H*–CO) | 8.81–8.83 (d, 2H, J = 8 Hz, aliphatic –N*H*–CO) | 8.50–8.52 (d, 2H, J = 8 Hz, aliphatic N*H*–CO) |
| 7.80–7.82 (d, J = 8 Hz, 2H, Arm H of benzene moiety) | 7.82–7.84 (2H, J = 8 Hz, Arm H of benzene moiety) | 7.72–7.74 (d, 2H, J = 8 Hz, Arm H of benzene moiety) |
| 7.65–7.67 (d, J = 8 Hz, 2H, Arm H of benzene moiety) | 7.75–7.77 (2H, J = 8 Hz, Arm H of benzene moiety) | – |
| 7.43–7.46 (d, 2H, Arm *H* of quinolone moiety) | 7.47–7.51 (2H, Arm *H* of quinolone moiety) | – |
| 7.49–7.53 (t, Arm *H* of quinolone moiety) | 7.31–7.29(d, Arm *H* of quinolone moiety) | – |
| 7.24–7.32 (m, 2H, Arm *H* of quinolone moiety) | 7.21–7.25 (2H, Arm *H* of quinolone moiety) | – |
| 6.47 (d, 1H, *H* adjacent to C=O group) | 6.43 (1H, *H* adjacent to C=O group) | – |
| 4.68–4.74 (m, methine H) | 4.63 (S, methine H) | 4.92–4.93 (m, methine H) |
| 4.24 (S, 1H, $-CH_2-$) | – | 4.39–4.43 (S, 1H, $-CH_2-$) |
| 3.47–3.51 (d, 1H, –C*H*(H)-, geminal) | – | – |
| 3.17–3.23 (t, 1H, –CH(*H*)-, geminal) | – | – |

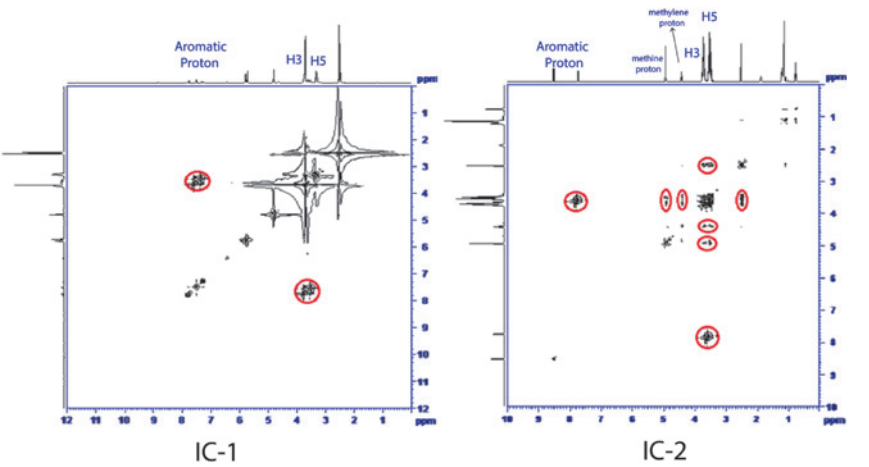


**Figure 8:** 2D ROESY spectra of IC-1 (left) & IC-2 (Right).

## 3.9 Scanning electron microscope (SEM) study

SEM is an ideal method to visualize significant changes in the surface morphology of various substances such as host, guest as well as inclusion complex [30]. The SEM images of the samples are presented in Figure 9. Pure Rebamipide appeared as needle shape crystal with small dimensions. The morphology revealed that $\beta$-CD appeared as rectangular shaped whereas HP-$\beta$-CD was appeared as spherical particles. After the formation of the RB/$\beta$-CD inclusion complex i.e., IC-1, surface morphology had been changed in different irregular shape in which the original morphology of both components disappeared and this comparison indicate the formation of the inclusion complex. However, when RB/HP-$\beta$-CD inclusion complex i.e., IC-2 was formed, some of the characteristic RB crystals were still present in the surface but shape of the surface morphology has been changed which indicate that inclusion complex was formed.

## 3.10 Release behavior in different solvents and an enzyme

In case of IC-1, as simple hydrophobic interaction rather inclusion phenomena took place, fluorescence intensity was relatively high than IC-2 in Figure 10(a). And it was largest when EtOH + $H_2O$ used as a solvent may be due to formation of hydrogen bond between EtOH + $H_2O$ with $\beta$-CD and Guest (RB) was relatively free. But upon addition of enzyme, it started to interact with guest and consequently intensity got weaker (red line). However, when DMSO was used as a solvent, intensity went to decrease which possibly due to polar aprotic nature of the solvent

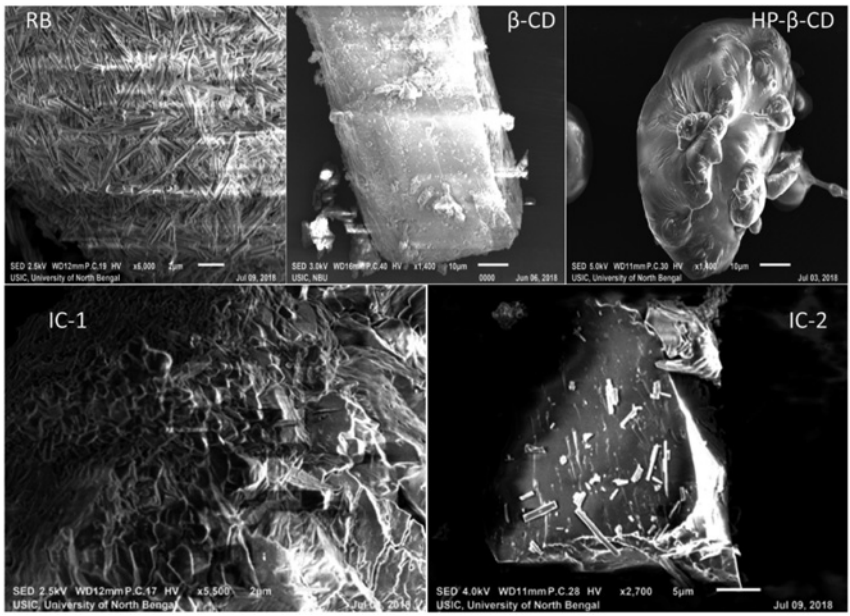


**Figure 9:** SEM microphotograph of RB, $\beta$-CD, HP-$\beta$-CD, IC-1 and IC-2 respectively.

(green line) as DMSO is not hydrogen bond donor. Again it was decrease more when enzyme was used in the solution mixture.

Another important observation was that solvent as well as enzyme had a great impact on the binding capacity between host and guest in inclusion complex. When DMSO was used in case of IC-2 showing in Figure 10(b), it has the largest fluorescence intensity (blue line) but when enzyme was added intensity got decreased. It may be due to binding of the enzyme with HP-$\beta$-CD so that guest molecule was unable to come out of the cavity (orange line). However, when same IC-2 was taken in EtOH + $H_2O$ co-solvent, intensity was also lower than that using DMSO solvent (gray line). Fluorescent intensity was lowest when enzyme was added in the same co-solvent (yellow line).Therefore, in all cases, it was found that DMSO was much more effective solvent that EtOH + $H_2O$ co-solvent. For higher soluble guest such as HP-$\beta$-CD, enzyme can be used for better binding availability.

## 3.11 Sustained release nature of inclusion complexes

Just like other experiment in this research work, biological assessment has also been done in two different solvent. One is ethanol-water mixture (1:1) and the other

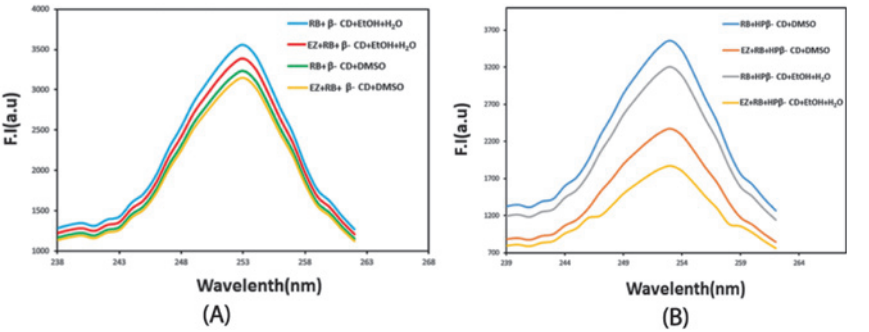


**Figure 10:** Variation in fluorescence intensity of (a) RB in $\beta$-CD in EtOH + $H_2O$ without enzyme (blue) and with enzyme (red) and in DMSO without enzyme (green) and with enzyme (yellow). (b) RB in HP-$\beta$-CD in EtOH + $H_2O$ without enzyme (blue) and with enzyme (red) and in DMSO without enzyme (green) and with enzyme (yellow).

one is DMSO. This work has been carried out with human salivary which contains $\alpha$-amylase as an enzyme. It has been reported that $\alpha$-amylase has the ability to hydrolyze water-soluble beta cyclodextrin at a slower rate compared with the corresponding unsubstituted beta cyclodextrin [31].

The release of RB from the inclusion complexes were determined by fluorescence emission spectroscopy where excitation was done at 230 nm [32]. IC-1 i.e., inclusion complex of RB/$\beta$-CD when dissolved in DMSO, its fluorescence intensity shown in Figure 11, was gradually decreasing up to 3 h but 3–4 h there was a sharp increase which indicate that the guest molecule was released very quickly. However, with increase in time, intensity was again decreasing gradually. When enzyme was used in the same solution, similar nature of fluorescence curve was obtained but here intensity in that time gap 3–4 h was quite lower which may be due to interaction between enzyme and the host cyclodextrin molecules that inhibits to release from the host cavity.

Similarly, when IC-1 dissolved in EtOH and water solvent mixture, there was a gradual decrease in the fluorescence intensity shown in Figure 11, which probably due to the non release of the part of the guest molecule. All the spectra were shown in Figure 3 of supporting information. It should be noted that solvent is highly polar in nature whereas aromatic part of the guest molecule is hydrophobic in nature. Hence, it preferred to stay inside the host. Again, same process had been carried out with ethanol-water with enzyme mixture. Result showed that there was a steep rise in the first hr but then intensity went down gradually which indicate that part of the RB guest molecule was still in the cavity of $\beta$-CD. So, all these facts suggest that RB/$\beta$-CD inclusion complex showed controlled release nature in

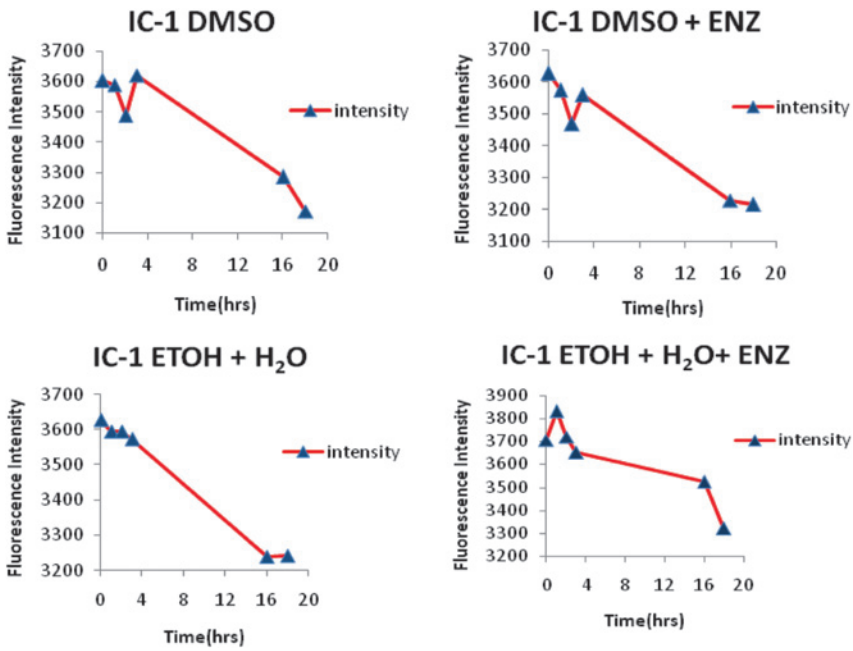


**Figure 11:** Variation in fluorescence intensity versus time of IC-1 in various solvent systems.

DMSO solvent and DMSO with enzyme as well ethanol-water mixture with enzyme but not in case of ethanol-water mixture alone.

In case of IC-2 i.e., inclusion complex of RB/HP-$\beta$-CD when dissolved in DMSO, somewhat similar release profile was observed as in case of IC-1. When enzyme was used in the same solution, similar nature of fluorescence curve was obtained which indicate that enzyme did not affect its release nature.

Similarly, when IC-2 dissolved in EtOH and water solvent mixture, there was a gradual increase in the fluorescence intensity which probably due to the high release of the part of the guest molecule (Figure 12). The spectra were shown in Figure 4 of supporting information. Although It should be noted that solvent is highly polar in nature whereas aromatic part of the guest molecule is hydrophobic in nature but it may happen that when inclusion complex was adding in co-solvent, EtOH and $H_2O$ molecules got attached with Hydroxypropyl chain of the HP-$\beta$-CD and it open up its wider part of HP-$\beta$-CD. Hence, it preferred to go outside the host. Again, same process had been carried out with ethanol-water with enzyme mixture. Result showed that there was no change in intensity which indicates that part of the RB guest molecule was still in the cavity of $\beta$-CD. So, all these facts suggest that RB/HP-$\beta$-CD inclusion complex showed controlled release

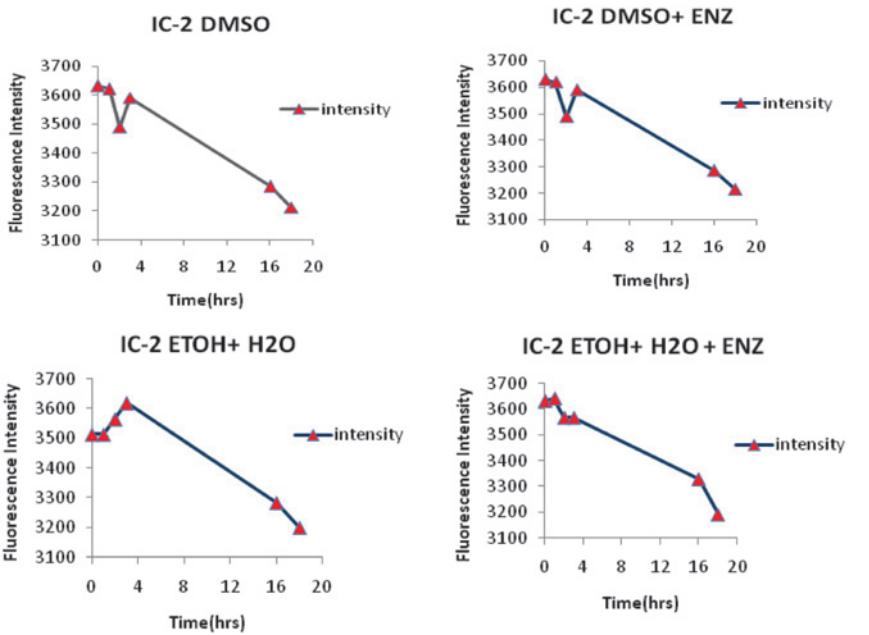


**Figure 12:** Variation in fluorescence intensity versus time of IC-1 in various solvent systems.

nature in DMSO solvent and DMSO with enzyme as well ethanol-water mixture but not in case of ethanol-water mixture with enzyme.

# 4 Conclusions

In the present work, RB/$\beta$-CD and RB/HP-$\beta$-CD complexes with greater water solubility were successfully prepared. The FT-IR, DSC, $^{1}$H NMR, and SEM results confirmed the formation of the RB/$\beta$-CD and RB/HP-$\beta$-CD inclusion complexes. Job's plot confirmed the 1:1 stoichiometry of the guest and host molecules. The high association constant ($K_a$) value obtained by RB/HP-$\beta$-CD complex suggests that the inclusion complexes formed between RB and HP-$\beta$-CD showed greater interaction than RB/$\beta$-CD inclusion complex. $^{1}$H-NMR confirmed the above statement by revealing the greater upfield shift of H3 & H5 proton in case of HP-$\beta$-CD. Conductance study revealed that Rebamipide molecules tend to aggregate in presence of $\beta$-CD and HP-$\beta$-CD in different solvents. 2D-NMR indicates that aromatic nucleus has been inserted into the cavity of $\beta$-CD and aromatic rings as well as methine and methylene group have been inserted into the cavity of HP-$\beta$-CD molecules. Finally,

from the released kinetics study, it revealed that both $\beta$-CD and HP-$\beta$-CD inclusion complexes are a promising strategy for making it sustained release of the guest molecule. This study enriches the field the supramolecular construct and may find various applications in biology as well as therapeutic and analytical chemistry.

**Acknowledgments:** This work was supported by the University of North Bengal, Department of Chemistry. The authors are grateful to UGC SAP, INDIA as well as State fellowship, Ref. No. 600/R-2018 for funding support. We would also like to acknowledge Mr. Gautam Sarkar, Head, In-charge, USIC, NBU for taking SEM photograph.
**Competing interest:** The authors declare no conflict of interest.

## References

1. Tanigawa T., Pai R., Arakawa T., Tarnawski A. S. *Dig. Dis. Sci.* 2007, *52*, 240–247; https://doi.org/10.1007/s10620-006-9226-x.
2. Moon S. J, Woo Y. J., Jeong J. H., Park M. K., Oh H. J., Park J. S., Kim E. K., Cho M. L., Park S. H., Kim H. Y., *Osteoarthritis Cartilage* 2012, *20*, 1426–1438; https://doi.org/10.1016/j.joca.2012.08.002.
3. Izawa T., Hutami I. R., Tanaka E. *Curr. Rheumatol. Rev.* 2018, *14*, 62–69; https://doi.org/10.2174/1573397113666171017113441.
4. Arakawa T., Higuchi K., Fujiwara Y., Watanabe T., Tominaga K., Sasaki E., Oshitani N., Yoshikawa T., Tarnawski A. S. *Dig. Dis. Sci.* 2005, *50*, S3–S11; https://doi.org/10.1007/s10620-005-2800-9.
5. Kinoshita S., Awamura S., Oshiden K., Nakamichi N., Suzuki H., Yokoi N. *Ophthalmology* 2012, *119*, 2471–2478; https://doi.org/10.1016/j.ophtha.2012.06.052.
6. Babu P. K., Bodireddy M. R., Puttaraju R. C., Vagare D., Nimmakayala R., Surineni N., Gajula M. R., Kumar P. *Org. Process Res. Dev.* 2018, *22*, 773–779; https://doi.org/10.1021/acs.oprd.7b00382.
7. Barman B. K., Roy K., Roy M. N. *Z. Phys. Chem*. 2019, *233*, 1109–1127; https://doi.org/10.1515/zpch-2017-1020.
8. Roy M. N., Barman S., Saha S. *Z. Phys. Chem.* 2017, *231*, 1111; https://doi.org/10.1515/zpch-2016-0804.
9. Roy K., Saha S., Datta B., Sarkar L., Roy M. N. *Z. Phys. Chem.* 2018, *232*, 281–293; https://doi.org/10.1515/zpch-2017-0003.
10. Infante M. R., Perez L., Pinazo A., Clapes P., Moran M. C., Holmberg K., Edited. Surfactant science series 114; Marcel Dekker, Inc.: New York, 2003, 193–216.
11. Loh X. J. *Materials Horizons* 2014, *1-2*, 185–195; https://doi.org/10.1039/C3MH00057E.
12. Sebestyén Z., Barcza A. B., Rohonczy J. *J. Inclusion Phenom. Macrocycl. Chem.* 2012, *73*, 199–210.
13. Sharma K. S., Patil S. R., Rakshit A. K., Glenn K., Doiron M., Palepu R. M., Hassan P. A. *J. Phys. Chem.* 2004, *108*, 12804; https://doi.org/10.1021/jp048294o.
14. Prasad M., Moulic S. P., Palepu R. *J. Colloid Interface Sci.* 2005, *284*, 658–666; https://doi.org/10.1016/j.jcis.2004.10.063.

15. Das C., Chakraborty T., Gosh S., Das B. *Colloid Polym. Sci.* 2008, *286*, 1143; https://doi.org/10.1007/s00396-008-1876-0.
16. Gosh S., Moulik S. P. *J. Colloid Interface Sci.* 1998, *208*, 357; https://doi.org/10.1006/jcis.1998.5752.
17. Ikeda S., Fujio K. *Colloid Polym. Sci.* 1992, *270*, 1009; https://doi.org/10.1007/BF00655970.
18. Backlund S., Hoiland H., Kvammea O. J., Ljosland E. *Acta Chem. Scand.* 1982, *36A*, 697; https://doi.org/10.3891/acta.chem.scand.36a-0698.
19. Bolkhus A. M., Høiland H., Gilje E., Backlund S. *J. Colloid Interface Sci.* 1988, *124*, 125–129; https://doi.org/10.1016/0021-9797(88)90332-3.
20. Job P. *Ann Chim* 1928, *9*, 113–203.
21. Liao Y., Zhang X., Li C., Huang Y., Lei M., Yan M., Zhou Y., Zhao C. *Carbohydr. Polym.* 2016, *147*, 415–425; https://doi.org/10.1016/j.carbpol.2016.04.022.
22. Tasneem S. *Zeitschrift fur Physikalische Chemie* 2017, *231*, 1831–1847; https://doi.org/10.1515/zpch-2016-0895.
23. Rajbanshi B., Saha S., Das K., Barman B. K., Sengupta S., Bhattacharjee A., Roy M. N. *Sci. Rep.* 2018, *8*, 13031; https://doi.org/10.1038/s41598-018-31373-x.
24. Yao Y., Xie Y., Hong C., Li G., Shen H., Ji G. *Carbohydr. Polym.* 2014, *110*, 329–337; https://doi.org/10.1016/j.carbpol.2014.04.006.
25. Chakraborty S., Basu S., Lahiri A., Basak S. *J. Mol. Struct.* 2010, *977*, 180–188; https://doi.org/10.1016/j.molstruc.2010.05.030.
26. Wei Y., Zhang J., Zhou Y., Bei W., Li Y., Yuan Q., Liang H. *Carbohydr. Polym.* 2017, *159*, 152–160; https://doi.org/10.1016/j.carbpol.2016.11.093.
27. Abarca R. L., Rodríguez F. L., Guarda A., Galotto M., Bruna J. E. *Food Chem.* 2016, *196*, 968–975; https://doi.org/10.1016/j.foodchem.2015.10.023.
28. Yuan C., Jin Z., Xu X. *Carbohydr. Polym.* 2012, *89*, 492–496; https://doi.org/10.1016/j.carbpol.2012.03.033.
29. Ma S., Chen W., Yang X., Zhang N., Wang S., Liu L., Yang L. *J. Pharmaceut. Biomed. Anal.* 2012, *67-68*, 193–200; https://doi.org/10.1016/j.jpba.2012.04.038.
30. Tang P., Li S., Wang L., Yang H., Yan J., Li H. *Carbohydr. Polym.* 2015, *131*, 297–305; https://doi.org/10.1016/j.carbpol.2015.05.055.
31. Szente L., Szejtli J. *Adv. Drug Deliv. Rev.* 1999, *36*, 17–28; https://doi.org/10.1016/S0169-409X(98)00092-1.
32. Qu H., Yang L., Yu J., Dong T., Rong M., Zhang J., Xing H., Wang, Pan L., Liu H. *RSC Adv.* 2017, *7-57*, 35704–35710; https://doi.org/10.1039/C7RA04444E.

**Supplementary Material:** The online version of this article offers supplementary material (https://doi.org/10.1515/zpch_2019-1500).

Journal of Molecular Liquids 329 (2021) 115481

Contents lists available at ScienceDirect

Journal of Molecular Liquids

journal homepage: www.elsevier.com/locate/molliq

# Exploring β-CD grafted GO nanocomposites with an encapsulated fluorescent dye duly optimized by molecular docking for better applications

Niloy Roy, Pranish Bomzan, Debadrita Roy, Biswajit Ghosh, Mahendra Nath Roy *

*Department of Chemistry, University of North Bengal, Darjeeling 734013, India*

ARTICLE INFO

*Article history:*
Received 23 October 2020
Received in revised form 20 January 2021
Accepted 22 January 2021
Available online 27 January 2021

*Keywords:*
Graphene oxide
β-cyclodextrin
Supramolecular complex
Fluorescent probe
Encapsulation

ABSTRACT

Here, we have designed and synthesized β-cyclodextrin grafted Graphene Oxide based fluorescent probe with encapsulated fluorescent dye. The nanocomposites were characterized by several spectroscopic methods such as FTIR, DLS, zeta potential, UV–vis and fluorescence spectroscopy. Thermal gravimetric analysis (TGA) was employed to account for thermal stability of β-CD grafted graphene oxide nanocomposites. Nile blue molecules are well encapsulated into the cyclodextrin cavity and embedded on the surface of Graphene Oxide sheet. Molecular Docking study helps us to understand the feasibility of encapsulation process of fluorescent dye inside our synthesized nanocomposites. Various physicochemical properties like UV–vis and fluorescence spectra of composite in different solvent and photophysical properties like fluorescence quantum yield, molar extinction coefficient, stokes shift have been calculated.



## 1. Introduction

Now-a-days, cancer has become a major issue throughout the world, although, there are numerous diagnostic methods such as magnetic resonance imaging (MRI), ultrasound, positron emission tomography (PET) imaging, X-ray imaging and single-photon emission computed tomography (SPECT) are available [1]. Recently, fluorescent probes are widely used for cancer cell imaging in cell biology. When photosensitizing dye is being given to a cancer patient, it localizes in the cancerous tissue and when light of appropriate wavelength is placed, it is activated and evolves strong fluorescent colour [2]. Recently, Polymer nanoparticles as well nanocomposites are used extensively in biomedical applications [3].

However, one has to be very selective when choosing the photosensitizers [4]. An efficient fluorescent probe is based on dye where emission maximum is found to be in the far-red end of the visible spectrum i.e., above 600–700 nm to minimize background interference [5,6]. In our study, we have chosen Nile blue chloride (NB) as our fluorescent dye. It is a cationic dye and is readily soluble in water. It is a photostable organic dye from the benzo[*a*]phenoxazine family, which shows strong fluorescence. It has redshifted absorbance spectra and its emission maximum falls in the NIR region with high fluorescent quantum yields, making it a potential fluorescent probe for biological imaging and photodynamic action [7,8].

Graphene oxide (GO), the precursor of graphene, being water-soluble has attracted tremendous interest in the field of biomedicine in past few years [9]. It consists of several functional groups (hydroxyl, epoxy, carbonyl, carboxylic groups) and high surface area which makes it potential nano-carriers for drug and gene delivery [10]. It has been reported that GO having enormous oxygen rich functional group can be modified by many non-toxic functional group to extend biological application [11,12].

Cyclodextrins (CDs) are generally cyclic oligosaccharides of six to eight D-glucose monomers linked by α-1, 4-glucose bonds [13]. They have the ability to encapsulate various drug molecules forming supramolecular host-guest complex [14]. They are extensively used as drug carrier [15], enzyme mimics [16], and photochemical sensors [17]. They can be used as catalyst [18], separating agent [19] and chemosensing [20].

In a recent study, Banerjee et al. [21], showed that fluorescent guest encapsulated βCD complexes are embedded or adsorbed on the surface of GO nanosheet to understand the electron transfer mechanism from complex to GO. Whereas, Ray et al. [22], worked with analogous dye Nile red with β-cyclodextrin to investigate various spectroscopic properties. In our present study, supramolecular assembly of Nile blue (NB) with β-cyclodextrin and Graphene oxide (GO), i.e., GO-βCD-NB nanocomposites, was designed and synthesized (Scheme 1). In this work, we have been able to prepare NB and GO nanocomposites with

* Corresponding author.
*E-mail address:* mahendraroy2002@yahoo.co.in (M.N. Roy).

https://doi.org/10.1016/j.molliq.2021.115481
0167-7322/

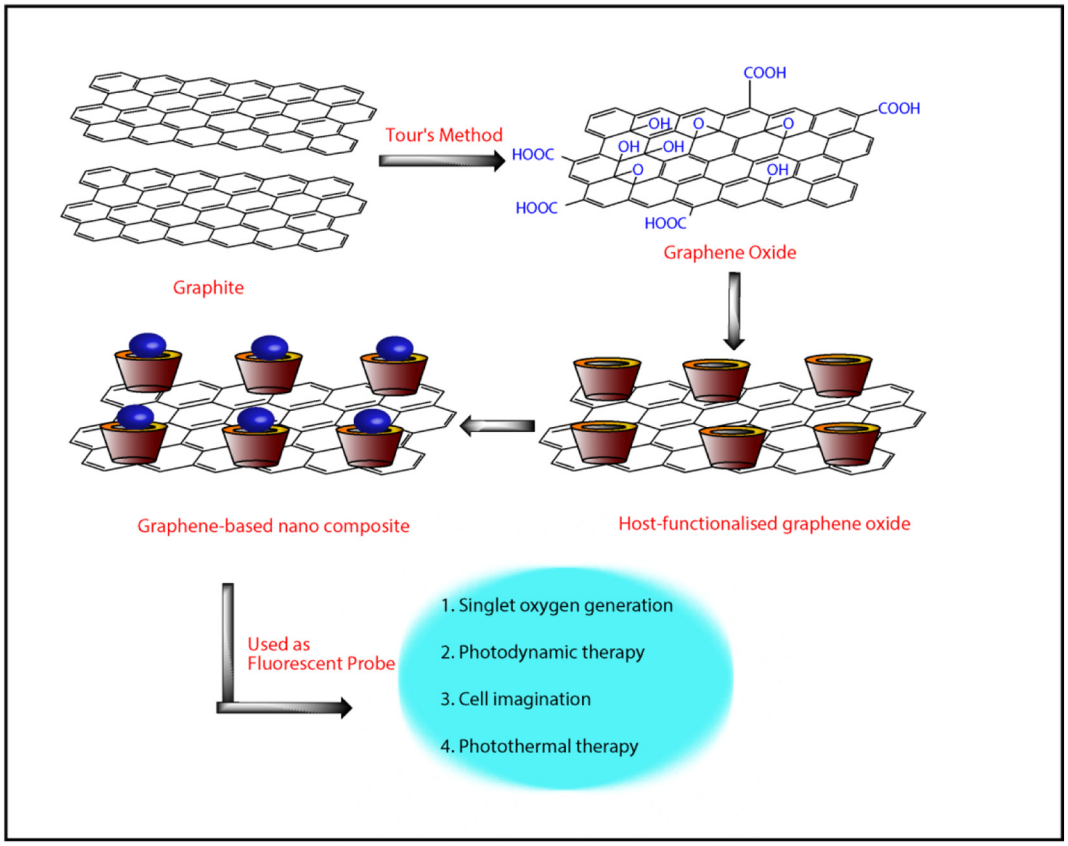


**Scheme 1.** Schematic diagram for the synthesis of rGO-βCD composites and the interaction between the guest (Nile blue) and the host (βCD) moiety linked up to rGO nanosheet.

βCD host molecules for enhancing applicability in showing fluorescence imaging.

## 2. Methods and experimental section

### *2.1. Chemicals and materials*

All the materials such as graphite flake, βCD and Nile blue were obtained from Sigma Aldrich India PVT. LTD. Deionized water (DW, 18 MΩ cm) was used for preparing aqueous solutions.

### *2.2. Instruments*

UV–Vis spectra and Fluorescence spectra were recorded by an Agilent 8453 spectrophotometer and a PTI Quanta Master fluorescence spectrophotometer (Quantamaster-40, USA) respectively. The SEM micrographs of nanocomposites were obtained by JEOL JSM-IT 100 Microscope. The zeta potentials and size of nanocomposites were measured by a Malvern Nanosizer. Infrared spectra of the samples were recorded by a Fourier transform infrared spectrometer (Perkin Elmer FT-IR). All TGA spectra were recorded by TA Instrument Q-50 TGA.

### *2.3. Preparation of GO*

GO was synthesized using modified Hummers method from purified natural graphite flakes as reported earlier [23]. According to the method, a mixture of graphite flakes (3.0 g, 1 wt equiv) and $KMnO_4$ (18.0 g, 6 wt equiv) were added to 9:1 mixture of concentrated $H_2SO_4$/$H_3PO_4$ (360:40 mL), the mixture get warmed upto 40 °C showed exothermic nature. The reaction was kept at 55 °C and stirred with magnetic stirring for 12 h. After cooling at room temperature, the reaction mixture was poured into crust ice (~400 mL) with 30% $H_2O_2$ (3 mL). The solid material obtained after filtration was then wash twice successively with 200 mL of water, 200 mL of 30% HCl and 200 mL of ethanol. After that, solution was centrifuged at 4000 rpm for 10 min and again washed with distilled water so that various chlorides, sulphate ions got free. Finally, the solution was dried by rotary evaporator under reduced pressure and obtained 1.7 g of product.

### *2.4. Preparation of GO-βCD*

To prepare rGO-βCD composite, a relatively greener approach was chosen rather than using highly toxic hydrazine as reducing agent [24]. Prior to the experiment, GO was ultrasonicated in distilled water for 10 min for getting a homogenous solution. Then, 200 mL of 1 mg/mL βCD aqueous solution was mixed with 200 mL of 0.5 mg/mL GO aqueous suspension. The mixture was stirred at room temperature for 12 h. Then the pH of the mixture was adjusted to 12 by adding aqueous solution of NaOH (1.0 M). Finally, the solution was heated at 75 °C and stirred at 370 rpm for 6 h. After the reaction, the stable black dispersion of the rGO-βCD mixture was centrifuged at a relative centrifugal force 4000 rpm so that unreacted βCD got removed from the solution followed by washing with distilled water for three times. After that a solid rGO-βCD nanocomposites was obtained by using rotary evaporator under reduced pressure.

### *2.5. Preparation of GO-βCD-NB*

Once, CD was attached on the surface of GO via chemical reaction between hydroxyl groups of CD and epoxide groups of GO, rGO-βCD

nanocomposites was prepared. Then, 1 mM of NB was dissolved in 20 mL of water and it was added in 20 mL of prepared rGO-βCD nanocomposites. The solution was heated at 55 °C and stirred at 370 rpm for 12 h for evaporation.

### 2.6. Preparation of modified for GO-βCD molecular docking

The crystal structure of β-cyclodextrin was taken from Chembridge Crystal data centre (CCDC) as CIF file (ID: 762697). The two-dimensional structure of graphene oxide (PubChem CID: 124202900) was used in the canonical smiles format from https://pubchem.ncbi.nlm.nih.gov. The flat 2D structure then converted into a three dimensional arrangement using an online server at https://www.mn-am.com/online_demos/corina_demo. The structures of graphene oxide and cyclodextrin reduced graphene oxide have been modified according to our need and hydrogen bonds and formal charges were added to the ligand before optimizing the whole structures. Finally, we performed molecular docking studies in MOE 2015 software to better understand the interaction of NB with the different surface modified GO-βCD conjugates.

## 3. Results and discussion

### 3.1. UV-vis spectroscopic study

UV–vis spectroscopic study was used to investigate the interaction between pure NB with GO-βCD nanocomposites. Although GO exhibits a peak around at 231 nm which may be due to the π-π* transition of C=C double bond [25] but in our case, according to the spectra shown in Fig. S1, GO dispersion showed the maximum absorption at the wavelength of 264 nm which is somewhat about 30 nm longer. After the formation of GO-βCD nanocomposites, the peak got shifted to 258 nm, which indicate the grafting of βCD on the Graphene oxide nanosheets. When UV–vis spectrum of pure Nile blue was studied, two distinct peaks at 279 nm in far-ultraviolet region due to long wavelength π-π* transitions of aromatic ring and 634 nm in visible light region due to n-π* transitions of C=N were observed. But when NB was encapsulated inside the GO-βCD nanocomposites, the intensity got reduced which indicate that encapsulation was taking place during the synthesis [26]. The Fig. S2 shows the digital photograph of GO, GO-βCD, GO-βCD-NB and NB. Typically, GO exhibits pale yellow colour whereas GO-βCD dispersion appears dark black colour. However, GO-βCD-NB composite showed very good dispersion stability for few months.

### 3.2. Steady state fluorescence spectroscopic study

Cushing et al. [27], showed that GO was able to show excellent fluorescence due to electronic energy transition as well as excitation wavelength dependence possibly due to "giant red-edge effect". GO generally consist of aromatic rings (C=C) and various oxygen-containing functional groups such as hydroxyl groups (-OH), carboxyl groups (COOH), carbonyl (C=O) and epoxy (C-O-C). The fluorescence emission spectra of GO is very broad around 400–700 nm. The GO sheets exhibited three different fluorescence emission peaks at 455 nm, 567 nm and 635 nm as shown in Fig. 1 and all the three peaks have different relative intensities [28]. Upon 260 nm excitation, graphene oxide showed three emission peaks at 455 nm, 567 nm and 635 nm due to $\sigma^* \rightarrow n$ electronic transition of C-OH, $\pi \rightarrow \pi^*$ transition of the graphitic C=C double bond and $\pi^* \rightarrow n$ transition of the C=O associated groups respectively, thereby, confirming that GO has been formed which is also quite similar as in the previous literatures [29,30]. After the formation of GO-βCD nanocomposites, the emission peak have been shifted towards the lower region i.e., at 450 nm. During the reaction course, βCD molecules were grafted on the surface of the graphene oxide.

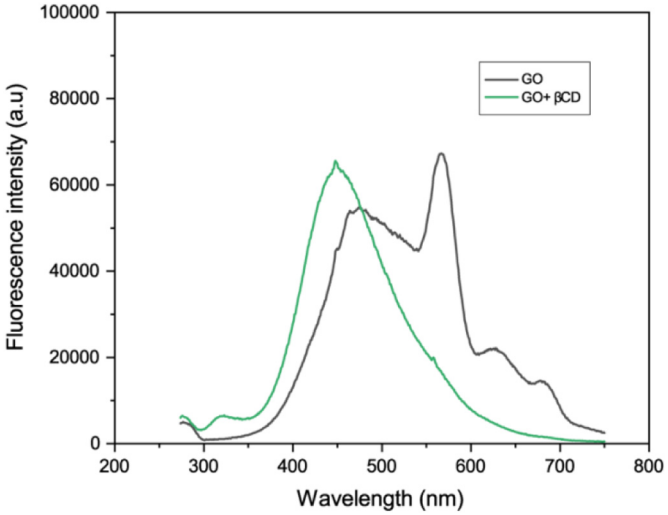


**Fig. 1.** Fluorescence emission spectra of GO, GO-βCD composites.

### 3.3. Infrared spectroscopic study

GO spectrum shows a peak at around 1723 $cm^{-1}$ which is basically due to the presence of several C=O functional group like aldehyde (-CHO), ketone(-C=O) etc. linked on the surface of GO structure. Fig. 2 showed all the different components. The peaks at 1616 $cm^{-1}$ and 1118 $cm^{-1}$ of the GO spectrum were ascribed to the functional groups of aromatic C=C and C–O, respectively, whereas peak at 1376 $cm^{-1}$ might be due to the C-OH stretching vibrations [31,32]. After the functionalisation by βCD on GO nanosheets, the disappearance of a peak at 1723 $cm^{-1}$ and the appearance of C-O/C-C stretching vibrations at 1018 $cm^{-1}$ and 1125 $cm^{-1}$, O-H/C-H bending vibrations at 1410 $cm^{-1}$ and aromatic C=C stretching around 1573 $cm^{-1}$ ensures

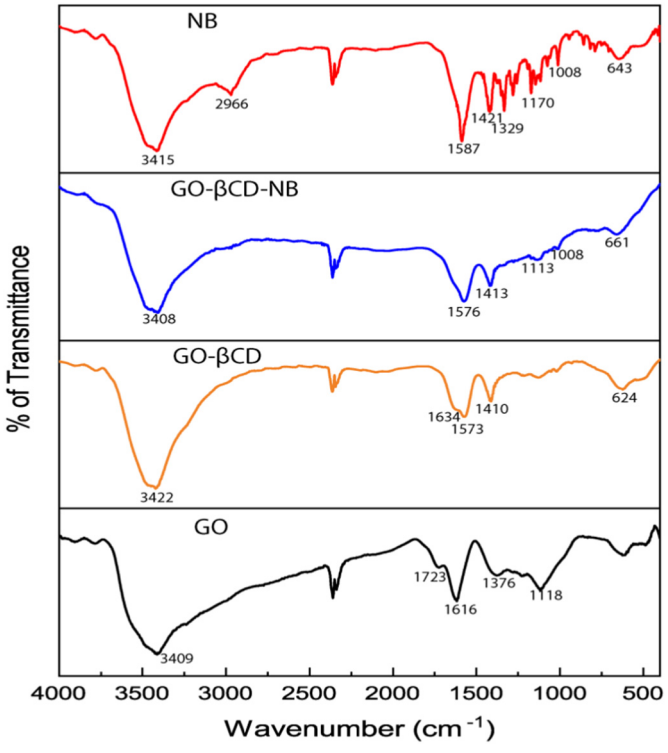


**Fig. 2.** Infrared spectra of GO, GO-βCD, GO-βCD-NB, NB.

that graphene oxide has been reduced resulting in the formation of GO-βCD composite [33,34].

In the spectrum of NB, the C–H stretching frequency of $CH/CH_2$ groups and N–H bending vibration were observed at 2915 $cm^{-1}$ and 1587 $cm^{-1}$ respectively. But after the formation of GO-βCD-NB composites, there was disappearance of a peak at 2915 $cm^{-1}$ and the characteristic peak at 1587 $cm^{-1}$ was found to be shifted to lower region around 1576 $cm^{-1}$ which suggest that Nile blue was encapsulated and stabilized onto the GO-βCD composite.

### 3.4. Scanning electron microscope (SEM) study

The surface morphology of GO, GO-βCD, GO-βCD-NB and NB are shown in Fig. S3. It is clearly observed that the GO surface appeared wrinkled, sharp edged and irregularly shaped. In GO-βCD nanocomposites, the particles were viewed as an aggregated form [35,36]. Free NB appeared to have small ball like shape, while after GO-βCD-NB formation, there was an alteration in its size and shape. All these observations provide a qualitative idea about the surface morphology of NB encapsulated GO-βCD.

### 3.5. DLS size measurement study (particle size distribution)

The size distribution of aqueous dispersion of GO, GO-βCD and GO-βCD-NB were studied by DLS technique where the standard spherical particle models were used. The hydrodynamic diameter of GO, GO-βCD and GO-βCD-NB were found to be 0.576 μm, 0.739 μm and 1.532 μm respectively as shown in supporting information (Fig. S4). According to Liu et al. [37], the effective size of particles in GO and rGO are 0.56 μm and 2.93 μm respectively, which very well matches the values of our experimental data [38].

### 3.6. DLS zeta potential measurement

Zeta (ξ) potential is also an important parameter to characterize the different graphene based materials. It gives the knowledge about the stability of colloidal dispersions with valuable information about magnitude and effective surface charge around the colloidal particle [39]. According to literature, only those composites are considered to be stable whose zeta potential values are either more positive than +30 mV zeta values or more negative than −30 mV [40]. According to Konkena et al., zeta potential of reduced graphene oxide drops down below −30 mV having pH > 8 [41]. In our study, we found that GO suspension had ξ = −49.1 mV. This is due to the presence of hydroxyl and other oxygenated functionalisation on the surface of GO (Fig. S5). In case of GO-βCD, the particle showed a negative zeta potential of −32.7 mV which indicates its fair stability in solution. However, in case of GO-βCD-NB, the surface potential significantly decreased to −25.4 mV and the decrease of negative zeta potential indicates the reduction of graphene oxide via grafting of cyclodextrin on the surface of GO and the nanocomposites becomes quite aggregated as can be seen from fig. S2. However, having low dispersion stability of the nanocomposites, thermal stability obtained by TGA analysis makes the nanocomposites more efficient as a guest surface coated nanocomposites.

### 3.7. Thermal gravimetric analysis (TGA)

Functionalisation of βCD molecules on the surface of graphene oxide was determined by thermal gravimetric analysis. The TGA curves for GO, βCD and GO-βCD are shown in Fig. 3. As per the literature, GO has low thermal stability around 100 °C with a moderate weight loss caused due to the removal of adsorbed water. The oxygen-containing functional groups such as epoxides, carboxyl and hydroxyl groups were decomposed between 100 and 200 °C, and more than 99% of GO had been reduced when the temperature was raised upto 600 °C [42]. βCD showed a rapid weight loss at 100 °C and tends to decompose at about 320 °C, but with the rise of temperature to 350 °C it almost decomposes to about 68%.

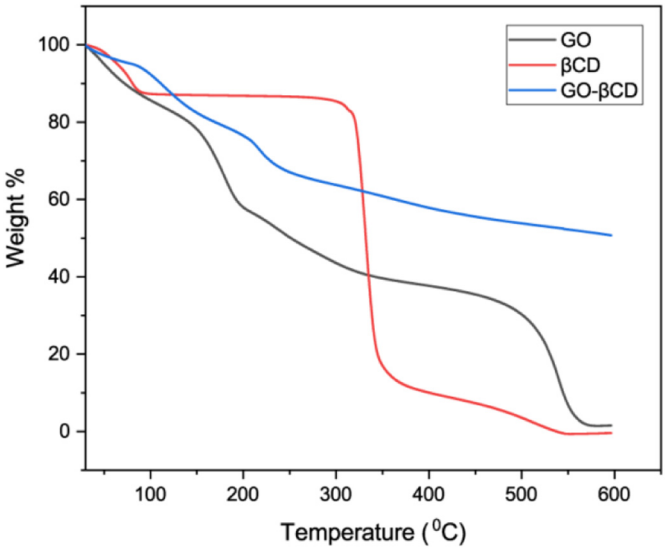


**Fig. 3.** TGA of GO, βCD and GO-βCD.

The decomposition curve of GO-βCD was found to exhibit the combination of the curves of GO and raw βCD. The weight loss of 10% at around 100-150 °C may be attributed to the decomposition of βCD while at around 150-250 °C a weight loss of 15% emerged. When the temperature was raised upto 600 °C, only 50% weight percentage was reduced indicating that βCD molecules could be functionalized at the edges of the reduced GO sheets. These observations showed that functionalized graphene oxide showed much higher thermal stability [43].

### 3.8. Encapsulation capacity of GO-βCD composites by fluorescence spectroscopic study

To investigate the encapsulating power of GO-βCD composite with Nile blue, fluorescence spectroscopic technique has been used. In this study, for three different sets were prepared where, 10 μM of NB was used as pure in each case, in the second set, 10 μM βCD was added and finally in the third set, 0.05 mg/mL GO-βCD composites were added and shaken for an hour. It can be seen from Fig. 4 that the

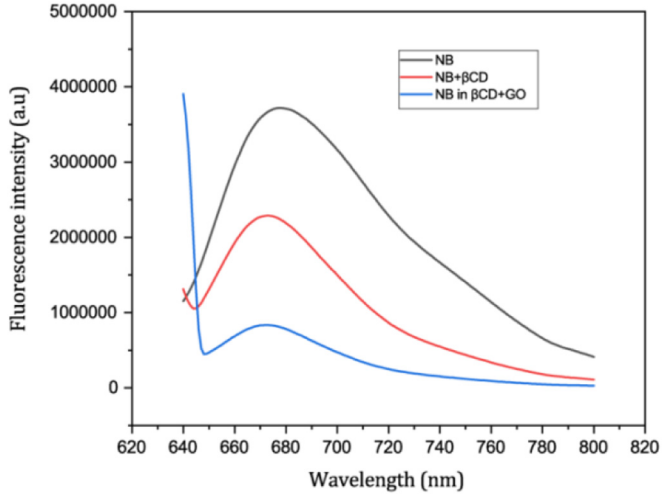


**Fig. 4.** Fluorescence intensity of 10 μM NB (black), 10 μM NB + 10 μM β-CD (red) and 10 μM NB + 0.05 mg/mL βCD-GO nanocomposites (blue).

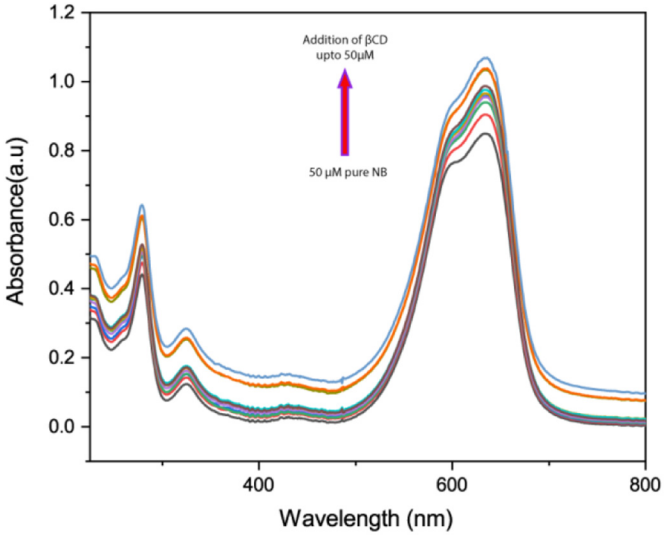


**Fig. 5.** Spectral titration of NB with βCD solution to calculate association constant.

fluorescence intensity of NB was quenched by βCD to approximately 38.4%. While the quenching of NB by GO-βCD composite was enhanced to about 77.5% which was possibly due to the energy transfer from dye to graphene oxide and adsorption of some dye on the surface of GO [44].

### 3.9. Association constant determination by UV-vis method

A knowledge regarding the binding constant is also significant in terms of drug delivery issues. In order to get the value of binding constant, Benesi-Hildebrand method was employed and titration curve were shown in Fig. 5. The double reciprocal plot of $1/(A_0–A)$ versus $1/[\beta CD]$ was obtained on titration of NB with different concentrations of βCD (Table S1). A good linear relationship between $1/(A_0–A)$ and $1/[\beta CD]$ suggest the 1:1 stoichiometry of inclusion complexes (Fig. S6) [45]. The binding constant ($K_a$) of the 1:1 NB-βCD complexes were calculated to be $2.1 \times 10^4\ M^{-1}$. According to the previous literature, NB has better binding constant value for its interaction with various enzymes, proteins, and such high binding constant facilates the release of Nile blue molecules from CD cavity to the specific tumor sites in cancer cells [46].

### 3.10. Molecular docking study

To understand the encapsulation mechanism, binding of NB + βCD and NB + GO-βCD inclusion complex were studied by molecular docking study [47]. Generally, if the binding energy is more negative, the interaction between the host and guest will be stronger. Before docking all the structures were optimized. From all the optimized structures shown in Fig. 6, it can be seen that the phenoxazine moiety of Nile blue molecule is localized into the cavity with its $–N(C_2H_5)_2$ group near the narrow rim, oxazine ring near the wider rim and benzene ring inside the hydrophobic hollow space of βCD. The Gibbs free energies of the docked optimized structures of NB + βCD, two NB with GO grafted one βCD, NB with GO grafted two βCD and two NB with GO grafted two βCD were found to be −5.36 kcal/mol,

−5.53 kcal/mol, −5.82 kcal/mol and − 4.88 kcal/mol respectively. The negative Gibbs free energy values indicate the encapsulation process to be thermodynamically favourable. This gives us a strong idea that there is usually strong binding of the molecule with GO-βCD nanocomposites rather than pure βCD [48].

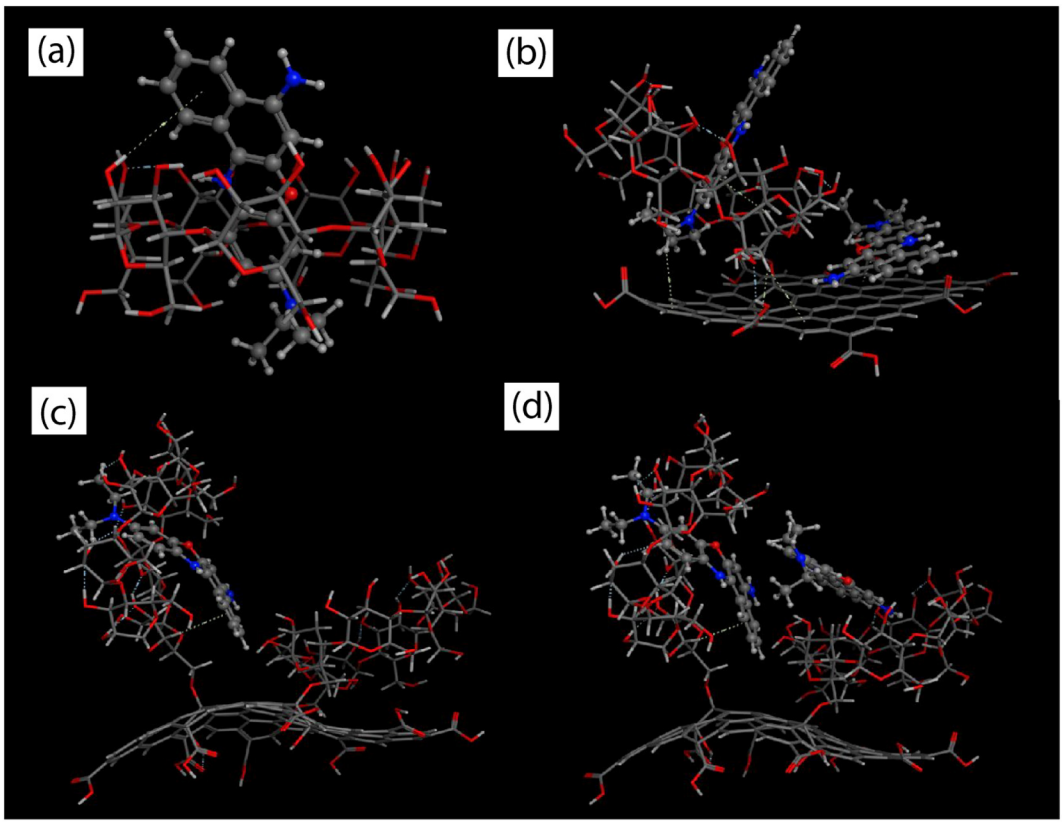


**Fig. 6.** Molecular docking images of (a) NB + βCD (b) two NB with GO grafted one βCD (c) NB with GO grafted two βCD (d) two NB with GO grafted two βCD.

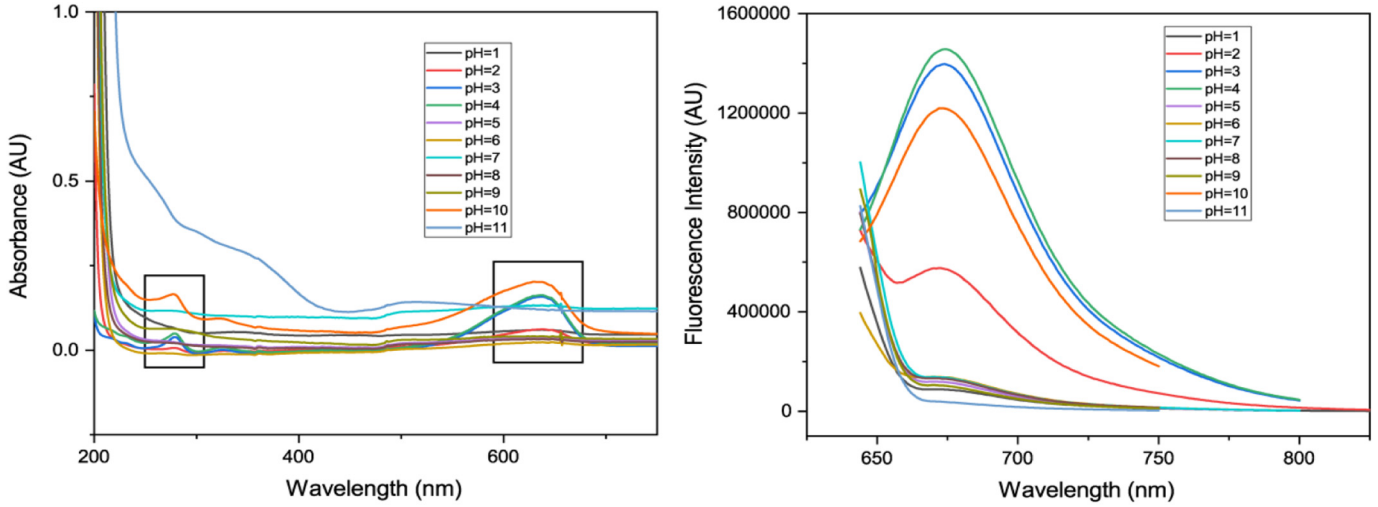


**Fig. 7.** UV-vis and fluorescence spectra of 0.5 mg/mL NB-βCD-GO nanocomposites at different pH from 1 to 11.

## 4. Different photophysical properties

### *4.1. Physicochemical properties of NB-βCD-GO Nanocomposites*

Fig. 7 shows the variation of absorption maximum and fluorescence of GO-βCD-NB nanocomposites with pH. In strong acidic medium, pH ≤ 2, the absorption maximum got diminished. However, absorption peak was observed at 638 nm with ε ~ $1.58 \times 10^4$ $M^{-1}$ $cm^{-1}$ and ~ $1.63 \times 10^4$ $M^{-1}$ $cm^{-1}$ respectively at pH = 3 and 4. Then again at pH = 5 and 6, such absorption peak got diminished. At neutral region pH = 7, a peak at 638 nm dramatically enhanced with ε ~ $1.32 \times 10^4$ $M^{-1}$ $cm^{-1}$.

At moderate alkaline medium, pH = 8 & 9, further no absorption peak was found to appear, but in highly alkaline medium, new absorption peaks at 237 nm appeared with ε ~ $2.02 \times 10^4$ $M^{-1}$ $cm^{-1}$ and ~ $1.20 \times 10^4$ $M^{-1}$ $cm^{-1}$ at pH = 10 and 11 respectively [49,50].

In the similar way, when 0.5 mg/mL of GO-βCD-NB composites were taken in different pH solutions, fluorescence intensity reached maximum in case of pH at 4. Then, a gradual decrease in fluorescence intensity for different pH medium was observed. This is possibly due to aggregation of Nile blue loaded inside GO-βCD cavity in neutral medium. These kinds of aggregations are most probably due to hydrophobic interactions. Generally, Pure NB can act as pH probe due to its high pH sensitivity. According to Martinez et al., in aqueous solution the acidic form of Nile blue molecules results in H-aggregation which causes disappearance of its fluorescence and thereby, effecting photophysical behaviour of Nile blue [51]]. In our study, it was observed that the GO-βCD-NB nanocomposites showed considerable fluorescence in highly acidic medium, pH = 2, 3, 4 and in highly basic medium, pH = 10.

### *4.2. Photophysical properties of the composites in different solvents: UV-vis absorption and fluorescence emission behaviour*

In order to characterize the spectral properties of the nanocomposites, we first studied its solvent dependency [52]. Out of six different solvents, three polar protic and three polar aprotic solvents have been used. As shown in Fig. 8, the probe exhibits single absorption and emission bands mainly contributed by NB moieties and the peaks due to reduced GO have been totally diminished. The peaks centred at around 630 nm correspond to the maximum absorption and emission wavelengths of NB [53]. The maximum absorption and emission wavelengths

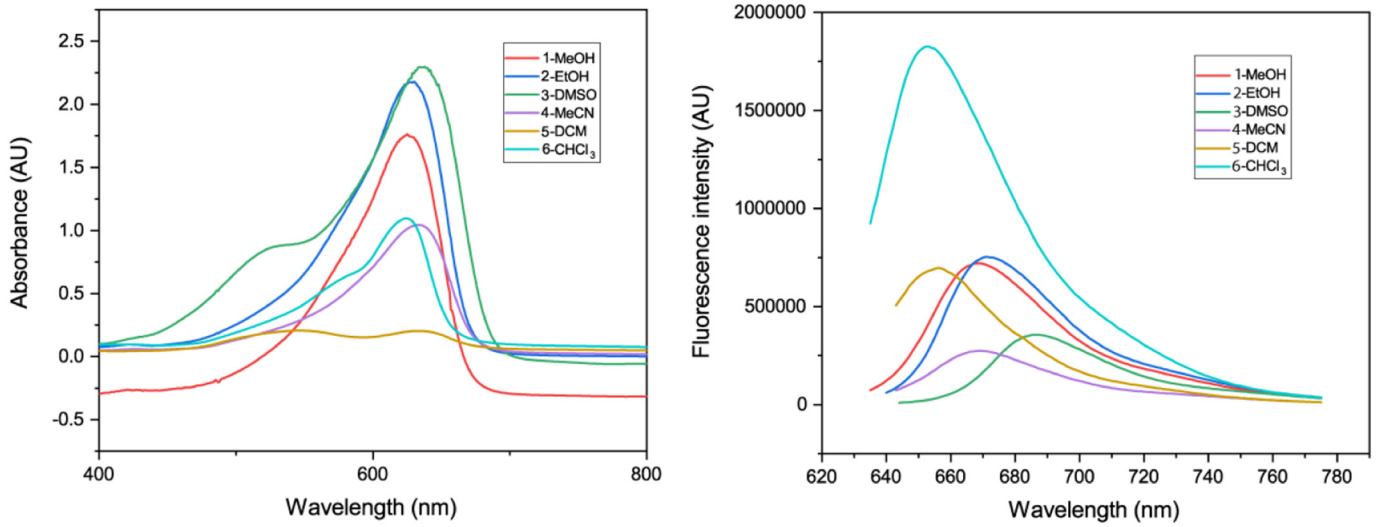


**Fig. 8.** UV–Vis spectra (left) and fluorescence emission spectra (right) in different solvents.

**Table 1**
Photophysical properties of the composites where 50 μM of NB solution were taken in 0.5 mg/mL of GO-βCD was taken in different solvent.

| No | Solvent | Absorbance | | Fluorescence | | Stokes Shift (nm) | ε Values ($M^{-1}$ $cm^{-1}$) |
|---|---|---|---|---|---|---|---|
| | | Wavelength (nm) | A.U | Wavelength (nm) | A.U | | |
| 1. | MeOH | 625 | 1.76410 | 669 | 720,345 | 44 | 35,282 |
| 2. | EtOH | 630 | 2.17974 | 671 | 752,811 | 41 | 43,184 |
| 3. | DMSO | 634 | 2.297323 | 688 | 355,092 | 54 | 45,946 |
| 4. | MeCN | 633 | 1.044811 | 669 | 274,006 | 36 | 20,896 |
| 5. | DCM | 633 | 0.203392 | 656 | 696,870 | 23 | 4000 |
| 6. | $CHCl_3$ | 624 | 1.096071 | 652 | 1,826,493 | 28 | 21,921 |

**Table 2**
Relative fluorescence quantum yield calculation of GO-βCD-NB and after three days.

| Sample | Integrated emission intensity (I) | Absorbance at ~ 636 nm (A) | Refractive Index of solvent (η) | PLQY (ϕ) |
|---|---|---|---|---|
| GO-βCD-NB | 187,918 | 1.60213565 | 1.3605 | 0.19683 |
| GO-βCD-NB After Three days | 32,724 | 1.57810974 | 1.3606 | 0.03480 |

of nanocomposites have been shown in Table 1 ($\lambda_{abs}$, 625–634 nm and $\lambda_{em}$, 652–688 nm for MeOH to $CHCl_3$). The absorption maxima of our GO-βCD-NB nanocomposites have been found to increase linearly. While, the fluorescence intensity gradually decreases upto acetonitrile with increasing solvent polarity (owing to the ICT process that enables this dye to respond to environmental polarity) and then again tends to increase upto chloroform [54].

The additional red shift of NB in protic solvents, such as alcohols and probably chloroform, is associated with the hydrogen-bond formation with the carbonyl group of the dye. According to the previous literature [55], NB in MeOH showed its absorption maximum at 625 nm, and emission maximum at 655 nm with molar extinction coefficient 80,800 $M^{-1}$ $cm^{-1}$. However, for our NB encapsulated nanocomposites, the emission maximum, $\lambda_{em}$, was shifted to 669 nm with highest stokes shift of 44 nm followed by reduction of molar extinction coefficient to 35,282 $M^{-1}$ $cm^{-1}$.

In case of polar aprotic solvents like dichloromethane, irradiation with 624 nm wavelength showed strong fluorescence with least stokes shift of 28 nm. According to previous literature [56], in DMSO, Nile blue showed stokes shift of about 33 nm, however, absorption peak of NB in GO-βCD nanocomposites was observed at 634 nm and emission maximum at around 688 nm but stokes shift increases to 54 nm. This study helps us to know that DMSO is more effective polar aprotic solvent for our nanocomposites. Therefore, solvent-dependent spectral properties of nanocomposites make them ideal scaffolds for the development of improved biological indicators.

### *4.3. Relative fluorescence quantum yield calculation of the composites*

Considering the absorbance (A) and integrated fluorescence intensity (I) at a specific concentration and the excitation wavelength at 636 nm, fluorescence quantum yields (ϕ) were calculated using the following equation:

$$QY_x = QY_{ref} \times \frac{\eta_x^2}{\eta_{ref}^2} \times \frac{I_x}{A_x} \times \frac{A_{ref}}{I_{ref}}$$

where, the subscript **x** and **ref** stands for sample and reference dye respectively, **η** is the refractive index of the solvent. Anthracene is taken as the reference dye whose quantum yield is 0.27 in ethanol [57,58].

Fluorescence quantum yield for fluorescent dye as well as fluorescent nanocomposites is very vital. It measures the efficiency of the conversion of absorbed photons into emission photon. A typical fluorescence spectrometer is used for the measurement of relative fluorescence quantum yield. For pure NB molecules, φ was found to be 0.27 in ethanol as reported in literature [59]. However, in case of our nanocomposites, relative fluorescence quantum yield of NB decreased to 0.19 and when the same experiment were carried out after three days with the same solution, it got reduced to 0.03. So, there is an obvious decrease in relative fluorescence quantum yield (Table 2).

## 5. Conclusion

For cyclodextrin grafted graphene-based nanocomposites, graphene oxide was mainly considered to have common as well as important functions, such as, trapping and shielding of dye from degradation, enhancing both pH response of dye and pollutant adsorptivity. In this work, a unique process of encapsulation of NB molecules by βCD grafted reduced graphene oxide (GO) in the aqueous medium has been synthesized and established emphatically through vivid spectroscopic investigations. The experimental results are rationalized by molecular docking studies and showed the encapsulation of NB molecules inside free βCD as well as reduced GO-βCD sheets. Exploiting the host-guest chemistry of NB with GO-βCD, it was demonstrated that encapsulation power of GO-βCD nanocomposites revealed that NB molecules are entering inside the cavity of GO-βCD nanocomposites twice than that of pure βCD. Graphene functionalized with cyclodextrin coated nanocomposites can be used as bio mimic for Nile blue fluorescent probe for various cell imaging experiments. This study also suggested that how specific cyclodextrin functionalities can help to increase biodegradability of GO leading to the design of efficient biodegradable carriers based on graphene nanomaterials, and the thermal stability of nanocomposites have been increased. The result demonstrated that the pH responsive characteristic of graphene-based nanocomposites is vital in case of fluorescence imaging, designing a nanocomposites with improved photophysical performance and better delivery system to release the loaded NB molecules to acquire highly efficient biological activity.

## Authors contributions

N.R., P.B., D.R., B.G. and M.N.R contributed to the design and analysis of experiments. N.R., P.B., D.R., and B.G. performed the experiments in this manuscript. N.R., P.B., wrote the manuscript. N.R., P.B., and M.N.R critically reviewed the manuscript.

## Declaration of Competing Interest

The authors declare no competing financial interest.

## Acknowledgments

This work was supported by the UGC-NFSC {Ref. No. 2219/(CSIR-UGC NET JUNE 2019)} to N.R. and UGC-JRF {Ref No. 222/(CSIR-UGC NET DEC. 2017)} to P.B. and CSIR-JRF (Ref. No. 17/12/2017(ii) EU-V) to B.G in order to carry out research work and M. N. Roy acknowledges the financial support from Basic Scientific Research, UGC, Govt. of

India for giving one time grant (Ref. No. F.4-10/2010) augmenting the research works in the field of chemical science.

## Appendix A. Supplementary data

UV-vis spectra, Photograph of different composites, DLS, Zeta potential measurements, SEM microphotograph, Table for Benesi-Hildebrand plot for association constant, Linear plot of $1/\Delta A$ vs $1/[\beta CD]$ ($M^{-1}$). Supplementary data to this article can be found online at [https://doi.org/10.1016/j.molliq.2021.115481].

## References


[1] J. Pan, Y. Yang, W. Fang, W. Liu, K. Le, D. Xu, X. Li, Fluorescent phthalocyanine −graphene conjugate with enhanced NIR absorbance for imaging and multimodality therapy, ACS Appl. Nano Mater. 1 (6) (2018) 2785–2795, https://doi.org/10.1021/acsanm.8b00449.

[2] Z. Tong, G. Singh, A.J. Rainbow, Extreme dark cytotoxicity of Nile blue a in normal human fibroblasts, Photochem. Photobiol. 74 (5) (2001) 707–711, https://doi.org/10.1562/0031-8655(2001)0740707EDCONB2.0.CO2.

[3] J. Madsen, I. Canton, N.J. Warren, E. Themistou, A. Blanazs, B. Ustbas, X. Tian, R. Pearson, G. Battaglia, A.L. Lewis, Steven P. Armes, S. P., Nile blue-based nanosized pH sensors for simultaneous far-red and near-infrared live bioimaging, J. Am. Chem. Soc. 135 (39) (2013) 14863–14870, https://doi.org/10.1021/ja407380t.

[4] B. Wang, J. Fan, X. Wang, H. Zhu, J. Wang, H. Mu, X. Peng, A Nile blue based infrared fluorescent probe: imaging tumors that over-express cyclooxygenase-2, Chem. Commun. 51 (2015) 792–795, https://doi.org/10.1039/C4CC08915D.

[5] A.L. Bastos, D. Marques, Nile blue inducible fluorescence of tumour cells, Zeitschrift für Naturforschung B 27 (11) (1992) 1395–1398, https://doi.org/10.1515/znb-1972-1123.

[6] M. Wainwright, Non-porphyrin photosensitizers in biomedicine, Chem. Soc. Rev. 25 (5) (1996) 351–359, https://doi.org/10.1039/CS9962500351.

[7] H.J. Van Staveren, O.C. Speelman, M.J.H. Witjes, L. Louis Cincotta, W.M. Star, Fluorescence imaging and spectroscopy of ethyl nile blue a in animal models of (pre) malignancies, Photochem. Photobiol. 73 (1) (2001) 32–38, https://doi.org/10.1562/0031-8655(2001)0730032FIASOE2.0.CO2.

[8] X.D. Liu, C. Fan, R. Sun, Y.J. Xu, J.F. Ge, Nile-red and Nile-blue-based near-infrared fluorescent probes for in-cellulo imaging of hydrogen sulfide, Anal. Bioanal. Chem. 406 (2014) 7059–7070, https://doi.org/10.1007/s00216-014-8131-y.

[9] H.R. Thomas, S.P. Day, W.E. Woodruff, C. Valles, R.J. Young, I.A. Kinloch, G.W. Morley, J.V. Hanna, N.R. Wilson, J.P. Rourke, Deoxygenation of graphene oxide: reduction or cleaning? Chem. Mater. 25 (18) (2013) 3580–3588, https://doi.org/10.1021/cm401922e.

[10] G.P. Kotchey, B.L. Allen, H. Vedala, N. Yanamala, A.A. Kapralov, Y.Y. Tyurina, J. Klein-Seetharaman, V.E. Kagan, A. Star, The enzymatic oxidation of graphene oxide, ACS Nano 5 (3) (2011) 2098–2108, https://doi.org/10.1021/nn103265h.

[11] D.Y. Zhang, Y. Zheng, C.P. Tan, J.H. Sun, W. Zhang, L.N. Ji, Z.W. Mao, Graphene oxide decorated with Ru(II)−polyethylene glycol complex for lysosome-targeted imaging and photodynamic/photothermal therapy, ACS Appl. Mater. Interfaces 9 (8) (2020) 6761–6771, https://doi.org/10.1021/acsami.6b13808.

[12] P. Zheng, N. Wu, Fluorescence and sensing applications of graphene oxide and graphene quantum dots: a review, Chem. Asian J. 12 (18) (2017) 2343–2353, https://doi.org/10.1002/asia.201700814.

[13] B. Rajbansi, S. Saha, K. Das, B.K. Barman, S. Sengupta, A. Bhattacharjee, M.N. Roy, Study to probe subsistence of host-guest inclusion complexes of α and β-cyclodextrins with biologically potent drugs for safety regulatory dischargement, Sci. Rep. 8 (1) (2018) 1–20, https://doi.org/10.1038/s41598-018-31373-x.

[14] N. Roy, B. Ghosh, D. Roy, B. Bhaumik, M.N. Roy, Exploring the inclusion complex of a drug (Umbelliferone) with α-cyclodextrin optimized by molecular docking and increasing bioavailability with minimizing the doses in human body, ACS Omega 5 (56) (2020) 30243–30251, https://doi.org/10.1021/acsomega.0c04716.

[15] N. Roy, B. Mahato, D. Roy, K. Das, M.N. Roy, Exploring inclusion complexes of cyclodextrins with quinolinone based gastro protective drug for enhancing bioavailability and sustained dischargement, Z. Phys. Chem. 1 (2020)https://doi.org/10.1515/zpch-2019-1500 (ahead-of-print).

[16] T.H. Fenger, J. Bjerre, M. Bols, Cyclodextrin aldehydes are oxidase mimics, Chem. Bio Chem. 10 (15) (2009) 2494–2503, https://doi.org/10.1002/cbic.200900448.

[17] Y. Liu, Y. Song, Y. Chen, X.Q. Li, F. Ding, R.Q. Zhong, Biquinolino-modified b-cyclodextrin dimers and their metal complexes as efficient fluorescent sensors for the molecular recognition of steroids, Chem. Eur. J. 10 (15) (2004) 3685–3696, https://doi.org/10.1002/chem.200305724.

[18] K. Kanagaraj, K. Pitchumani, Per-6-amino-β-cyclodextrin as a chiral base catalyst promoting onepot asymmetric synthesis of 2-Aryl-2, 3-dihydro-4-quinolones, J. Organomet. Chem. 78 (2) (2013) 744–751, https://doi.org/10.1021/jo302173a.

[19] F. O'Keeffe, S.A. Shamsi, R. Darcy, P. Schwinté, I.M. Warner, A persubstituted cationic β-cyclodextrin for chiral separations, Anal. Chem. 69 (23) (1997) 4773–4782, https://doi.org/10.1021/ac970370e.

[20] P. Liu, S. Sun, X. Guo, X. Yang, J. Huang, K. Wang, Q. Wang, J. Liu, L. He, Competitive host–guest interaction between β-cyclodextrin polymer and pyrene-labeled probes for fluorescence analyses, Anal. Chem. 87 (5) (2015) 2665–2671, https://doi.org/10.1021/ac503301q.

[21] R. Banerjee, R. Riya Sinha, P. Purkayastha, β-cyclodextrin encapsulated coumarin 6 on graphene oxide nanosheets: impact on ground-state electron transfer and excited-state energy transfer, ACS Omega 4 (14) (2019) 16153–16158, https://doi.org/10.1021/acsomega.9b02335.

[22] A. Ray, S. Das, N. Nitin Chattopadhyay, Aggregation of nile red in water: prevention through encapsulation in β-cyclodextrin, ACS Omega 4 (1) (2019) 15–24, https://doi.org/10.1021/acsomega.9b02335.

[23] D.C. Marcano, D.V. Kosynkin, J.M. Berlin, A. Sinitskii, Z. Sun, A. Slesarev, L.B. Alemany, W. Lu, J.M. Tour, Improved synthesis of graphene oxide, ACS Nano 4 (8) (2010) 4806–4814, https://doi.org/10.1021/nn1006368.

[24] H. Zhao, L. Yang, Y. Li, X. Ran, H. Ye, G. Zhao, Y. Zhang, F. Liu, C.A. Li, A comparison study of macrocyclic hosts functionalized reduced graphene oxide for electro chemical recognition of tadalafil, Biosens. Bioelectron. 89 (2017) 361–369, https://doi.org/10.1016/j.bios.2016.07.016.

[25] M. Khandelwal, A. Anil Kumar, One-step chemically controlled wet synthesis of graphene nanoribbons from graphene oxide for high performance supercapacitor applications, J. Mater. Chem. A 3 (45) (2015) 22975–22988, https://doi.org/10.1039/C5TA07603J.

[26] T.S.H. Pham, L. Fu, P. Mahon, G. Lai, A. Yu, Fabrication of β-cyclodextrin-functionalized reduced graphene oxide and its application for electrocatalytic detection of carbendazim, Electrocatalysis 7 (5) (2016) 411–419, https://doi.org/10.1007/s12678-016-0320-3.

[27] S.K. Cushing, M. Li, F. Huang, N. Wu, Origin of strong excitation wavelength dependent fluorescence of graphene oxide, ACS Nano 8 (1) (2014) 1002–1013, https://doi.org/10.1021/nn405843d.

[28] M. Li, S.K. Cushing, X. Zhou, S. Guo, N. Wu, Fingerprinting photoluminescence of functional groups in graphene oxide, J. Mater. Chem. 22 (44) (2012) 23374–23379, https://doi.org/10.1039/C2JM35417A.

[29] P. Zheng, N. Wu, Fluorescence and sensing applications of graphene oxide and graphene quantum dots: a review, Chem. Asian J. 12 (18) (2017) 2343–2353, https://doi.org/10.1002/asia.201700814.

[30] D. Kozawa, Y. Miyauchi, S. Mouri, K. Matsuda, Exploring the origin of blue and ultraviolet fluorescence in graphene oxide, J. Phys. Chem. Lett. 4 (12) (2013) 2035–2040, https://doi.org/10.1021/jz400930f.

[31] S. Wang, Y. Li, X. Fan, F. Zhang, G. Zhang, β-cyclodextrin functionalized graphene oxide: an efficient and recyclable adsorbent for the removal of dye pollutants, Front. Chem. Sci. Eng. 9 (1) (2015) 77–83, https://doi.org/10.1007/s11705-014-1450-x.

[32] J.P. Rourke, P.A. Pandey, J.J. Moore, M. Bates, I.A. Kinloch, R.J. Young, N.R. Wilson, The real graphene oxide revealed: stripping the oxidative debris from the graphene-like sheets, Angew. Chem. Int. Ed. 50 (14) (2011) 3173–3177, https://doi.org/10.1002/ange.201007520.

[33] C. Xu, J. Wang, L. Wan, J. Lin, X. Wang, Microwave-assisted covalent modification of graphene nanosheets with hydroxypropyl-b-cyclodextrin and its electrochemical detection of phenolic organic pollutants, J. Mater. Chem. 21 (28) (2011) 10463–10471, https://doi.org/10.1039/C1JM10478K.

[34] S.R. Pour, M. Dinari, A. Abdolmaleki, Monochlorotriazinyl-β-cyclodextrin grafted on graphene oxide as an attractive green heterogeneous nanoreactor for selective oxidation reaction with NBS in wate, Chem. Select 4 (20) (2019) 6390–6396, https://doi.org/10.1002/slct.201900962.

[35] F. Liu, S. Chung, G. Oh, T.S. Seo, Three-dimensional graphene oxide nanostructure for fast and efficient water-soluble dye removal, ACS Appl. Mater. Interfaces 4 (2) (2012) 922–927, https://doi.org/10.1021/am201590z.

[36] A. Heydariab, H. Sheiban, Facile polymerization of b-cyclodextrin functionalized graphene or graphene oxide nanosheets using citric acid crosslinker by in situ melt polycondensation for enhanced electrochemical performance, RSC Adv. 6 (12) (2016) 9760–9771, https://doi.org/10.1039/C5RA24685G.

[37] S. Liu, T.H. Zeng, M. Hofmann, E. Burcombe, J. Wei, R. Jiang, J. Kong, Y. Chen, Antibacterial activity of graphite, graphite oxide, graphene oxide, and reduced graphene oxide, Membr. Oxid. Stress ACS Nano 5 (9) (2011) 6971–6980, https://doi.org/10.1021/nn202451x.

[38] B.R. Coleman, T. Knight, V. Gies, Z.J. Jakubek, S. Zou, Manipulation and quantification of Graphene oxide flake size: photoluminescence and cytotoxicity, ACS Appl. Mater. Interfaces 9 (34) (2017) 28911–28921, https://doi.org/10.1021/acsami.7b08585.

[39] A. Mallick, A. Nandi, S. Basu, Polyethylenimine coated graphene oxide nanoparticles for targeting mitochondria in cancer cells, ACS Appl. Bio. Mater. 2 (1) (2018) 14–19, https://doi.org/10.1021/acsabm.8b00519.

[40] J.M. Tijerina, D. Venkataramani, C.P. Aichele, C.S. Tiwary, J.E. Smay, A. Mathkar, P. Chang, P.M. Ajayan, Quantifi cation of the particle size and stability of graphene oxide in a variety of solvents, Part. Part. Syst. Charact. 32 (3) (2015) 334–339, https://doi.org/10.1002/ppsc.201400099.

[41] B. Konkena, S. Vasudevan, Covalently linked, water-dispersible, cyclodextrin: reduced-graphene oxide sheets, Langmuir 28 (34) (2012) 12432–12437, https://doi.org/10.1021/la3020783.

[42] C.K. Chun Kiang Chua, M. Pumera, Monothiolation and reduction of graphene oxide via one-pot synthesis: hybrid catalyst for oxygen reduction, ACS Nano 9 (4) (2015) 4193–4199, https://doi.org/10.1021/acsnano.5b00438.

[43] C. Xu, X. Wang, J. Wang, H. Hu, L. Wan, Synthesis and photoelectrical properties of b-cyclodextrin functionalized graphene materials with high bio-recognition capability, Chem. Phys. Lett. 498 (1–3) (2010) 162–167, https://doi.org/10.1016/j.cplett.2010.08.060.

[44] L. Yang, H. Zhao, Y. Li, X. Ran, G. Deng, X. Xie, C.P. Li, Fluorescent detection of Tadalafil based on competitive host−guest interaction using p-sulfonated calix[6] arene functionalized graphene, ACS Appl. Mater. Interfaces 7 (48) (2015) 26557–26565, https://doi.org/10.1021/acsami.5b07833.

[45] N. Roy, P. Bomzan, M.N. Roy, Probing host-guest inclusion complexes of ambroxol hydrochloride with α- & β-cyclodextrins by physicochemical contrivance subsequently optimized by molecular modeling simulations, Chem. Phys. Lett. 748 (2020) 137372, https://doi.org/10.1016/j.cplett.2020.137372.
[46] K. Pal, S. Mallick, A.L. Koner, Complexation induced fluorescence and acid–base properties of dapoxyl dye with c-cyclodextrin: a drug-binding application using displacement assays, Phys. Chem. Chem. Phys. 17 (24) (2015) 16015–16022, https://doi.org/10.1039/C5CP01696G.
[47] S. Mohandoss, T. Stalin, Photochemical and computational studies of inclusion complexes between β-cyclodextrin and 1,2-dihydroxyanthraquinones, Photochem. Photobiol. Sci. 16 (4) (2017) 476–488, https://doi.org/10.1039/C6PP00285D.
[48] R. Kurapati, F. Bonachera, J. Russier, A.R. Sureshbabu, C. Ménard-Moyon, K. Kostarelos, A. Bianco, Covalent chemical functionalization enhances the biodegradation of graphene oxide, 2D Materials 5 (1) (2017) 015020, https://doi.org/10.1088/2053-1583/aa8f0a.
[49] X.L. Wang, R. Sun, W.J. Zhu, X.L. Sha, J.F. Ge, Reversible absorption and emission responses of nile blue and azure a derivatives in extreme acidic and basic conditions, J. Fluoresc. 27 (3) (2017) 819–827, https://doi.org/10.1007/s10895-016-2017-7.
[50] J. Jose, Y. Ueno, K. Burgess, Water-soluble nile blue derivatives: syntheses and photophysical properties, Chem. Eur. J. 15 (2) (2009) 418–423, https://doi.org/10.1002/chem.200801104.
[51] J. Fan, H. Dong, M. Hu, J. Wang, H. Zhang, H. Zhu, W. Suna, X. Peng, Fluorescence imaging lysosomal changes during cell division and apoptosis observed using nile blue based near-infrared emission, Chem. Commun. 50 (7) (2013) 882–884, https://doi.org/10.1039/C3CC48043G.
[52] V.H. Frade, M.S.T. Goncalves, P.J. Coutinho, J.C. Moura, Synthesis and spectral properties of long-wavelength fluorescent dyes, J. Photochem. Photobiol. A Chem. 185 (2–3) (2007) 220–230, https://doi.org/10.1016/j.jphotochem.2006.06.013.
[53] V. Martinez, M. Henary, Nile red and nile blue: applications and syntheses of structural analogues, Chem. Eur. J. 22 (39) (2016) 13764–13782, https://doi.org/10.1002/chem.201601570.
[54] Z. Yang, Y. He, J.H. Lee, W.S. Chae, W.X. Ren, J.H. Lee, C. Kang, J.S. Kim, A nile red/BODIPY-based bimodal probe sensitive to changes in the micropolarity and microviscosity of the endoplasmic reticulum, Chem. Commun. 50 (79) (2014) 11672–11675, https://doi.org/10.1039/C4CC04915B.
[55] M. Kubinyi, J. Brátán, A. Grofcsik, L. Biczók, B. Poór, I. Bitter, A. Grün, B. Bogáti, K. Tóth, Proton transfer and supramolecular complex formation between nile blue and tetraundecylcalix[4]resorcinarene—a fluorescence spectroscopic study, J. Chem. Soc. Perkin Trans. 2 (10) (2002) 1784–1789https://doi.org/10.1039/B202637F.
[56] A. Yadigarli, Q. Song, S.I. Druzhinin, H. Schönherr, Probing of local polarity in poly (methyl methacrylate) with the charge transfer transition in Nile red, Beilstein J. Org. Chem. 15 (1) (2019) 2552–2562, https://doi.org/10.3762/bjoc.15.248.
[57] W. Li, L. Li, H. Xiao, R. Qi, Y. Huang, Z. Xie, H. Zhang, Iodo-BODIPY: a visible-light-driven, highly efficient and photostable metal-free organic photocatalyst, RSC Adv. 3 (32) (2013) 13417–13421, https://doi.org/10.1039/C3RA40932E.
[58] J. Jose, K. Kevin Burgess, Syntheses and properties of water-soluble nile red derivatives, J. Organomet. Chem. 71 (20) (2006) 7835–7839, https://doi.org/10.1021/jo061369v.
[59] A.M. Brouwer, Standards for photoluminescence quantum yield measurements in solution (IUPAC technical report), Pure Appl. Chem. 83 (12) (2011) 2213–2228, https://doi.org/10.1351/PAC-REP-10-09-31.